



DOCTORAL THESIS NO. 2023:48
FACULTY OF NATURAL RESOURCES AND AGRICULTURAL SCIENCES

Faba bean foods: Structure and texture

Evaluation of faba bean component behaviours in
different product matrices

KLARA NILSSON



Faba bean foods: Structure and texture

Evaluation of faba bean component behaviours in different product matrices

Klara Nilsson

Faculty of Natural Resources and Agricultural Sciences (NJ)

Department of Molecular Sciences

Uppsala



SWEDISH UNIVERSITY
OF AGRICULTURAL
SCIENCES

DOCTORAL THESIS

Uppsala 2023

Acta Universitatis Agriculturae Sueciae
2023:48

Cover: components (starch, protein and fibre) extracted from faba bean are combined in different food matrices in single-system (starch), mixed-system (starch & protein) and food model studies. The structure-texture relationship was evaluated for all systems.

ISSN 1652-6880

ISBN (print version) 978-91-8046-148-1

ISBN (electronic version) 978-91-8046-149-8

<https://doi.org/10.54612/a.31n0p7ijfc>

© 2023 Klara Nilsson, <https://orcid.org/0000-0001-7548-321X>

Swedish University of Agricultural Sciences, Department of Molecular Sciences, Uppsala, Sweden

The summary chapter of this thesis is licensed under CC BY 4.0, other licences or copyright may apply to illustrations and attached articles.

Print: SLU Grafisk Service, Uppsala 2023

Faba bean foods: Structure and texture. Evaluation of faba bean component behaviours in different product matrices

Abstract

Faba bean (*Vicia faba minor*) is a cool-climate crop that could serve as a locally sourced sustainable ingredient in transition towards a more plant-based diet in temperate regions. Poor texture is one of the main aversion factors of plant-based foods, so this thesis characterised the functionality of faba bean components and their effect on structure and texture in different food matrices. The main aim in this thesis was to increase the knowledge on structure-texture relationship in increasingly complex faba bean food products.

Isolated faba bean fractions (starch, protein and fibre) were studied. Faba bean starch was physiochemically characterised and microscopic and macroscopic properties were correlated. Different ratios of starch and protein were then combined to create mixed gels. Faba bean starch formed a relatively viscous paste due to long branch-chains, high amylose content and larger granule size. Addition of protein perturbed starch network formation, delaying and reducing associated pasting and gel viscosities in mixed systems. For food model systems, two prototypes were designed: i) a combination of faba bean starch, protein and fibre to produce edible ink for 3D-printed foods and ii) faba bean protein films reinforced with cellulose nanocrystals (CNC) for use as bio-degradable edible packaging. For the 3D samples, fibre appeared to have a stabilising effect on structure, improving ink printability while also ensuring that 3D-printed objects retained their shape. Carbohydrate-rich 3D-printed objects had a more porous structure that required less force to compress than structurally more compact protein-rich objects. Addition of CNC resulted in stronger, stiffer and more opaque films with improved barrier properties.

Thus faba bean fractions in different combinations and processing approaches yield different textures. Using the basic knowledge of component functionalities in simple systems obtained in this thesis, intra- and intermolecular factors influencing product texture in more complex systems can be assessed.

Keywords: Faba bean, starch, texture, structure, rheology, pasting, gel.

Åkerbönmat: Struktur och konsistens. Utvärdering av åkerbönkomponents beteenden i olika produktmatriser

Abstrakt

Åkerbönan (*Vicia faba minor*) är en näringsriks gröda som skulle kunna nyttjas som närproducerad ingrediens, i växtbaserade produkter, i kalltempererade regioner. Ett av de främsta skälen till att en konsument inte väljer att övergå till en mer växtbaserad kost är dess ofördelaktiga konsistens. Därför handlar denna avhandling om att karakterisera funktionaliteten hos isolerade åkerbönkomponenter (stärkelse, protein och fibrer) och deras effekt på struktur och textur i olika typer av livsmedel. Huvudsyftet med projektet var att öka kunskapen om sambanden mellan struktur-textur i åkerbönlivsmedelsprodukter med olika grader komplexitet.

Först karakteriserades åkerbönstärkelsen fysiokemiskt och dess mikroskopiska och makroskopiska egenskaper korrelerades. Sedan kombinerades olika mängder av stärkelse och protein för att skapa blandade geler. Åkerbönstärkelse bildar en relativt tjock pasta på grund av långa glukoskedjor, hög amyloshalt och granulstorlek. Tillsatsen av protein störde bildandet av stärkelsenätverk vilket bidrog till att förklistringsprocessen fördröjde och att gelviskositeten blev lägre i dem blandade systemen. Två livsmedelsprototyper designades: i) ätbart bläck för 3D-printad mat som bestod av en kombination av åkerbön; stärkelse, protein och fiber och ii) åkerbönproteinfilmer förstärkta med cellulosa nanokristaller (CNC) för användning som nedbrytbar/ätbar förpackning. För 3D-proverna verkade fibrer ha en stabiliserande effekt på strukturen, vilket förbättrade printbarheten av bläcket samtidigt som de 3D-utskrivna objekten kunde behålla sin form. De kolhydratrika 3D-printade föremålen hade en mer porös struktur som krävde mindre kraft för att komprimera än de strukturellt mer kompakta proteinrika föremålen. Tillsatsen av CNC resulterade i att filmerna blev starkare, styvare, grumligare och med förbättrade barriäregenskaper.

Olika mängder och bearbetningsmetoder av åkerbönsfraktioner i livsmedel påverkar en produkts konsistens. Genom kunskap om grundläggande komponentfunktioner i olika livsmedelssystem som studeras i denna avhandling, kan man förstå intra- och intermolekylära faktorer påverkan i produkttextur i mer komplexa system.

Nyckelord: åkerböna, stärkelse, textur, struktur, reologi, förklistring, gel.

Dedication

Till Xerxes, min första bebis

Contents

List of Publications	9
Graphical abstract	12
1. Introduction	13
2. Background.....	15
2.1 Characterisation of faba bean components	15
2.1.1 Faba bean starch.....	16
2.1.2 Faba bean protein.....	17
2.1.3 Faba bean fibre.....	18
2.1.4 Other components	19
2.2 Ingredient functionality.....	20
2.2.1 Component interaction with water	21
2.2.2 Pasting (starch thickening)	23
2.2.3 Gel formation	25
2.3 Faba bean components as texturising agents	27
2.4 Correlating microstructure and texture.....	30
3. Aims and Objectives	33
4. Consideration of Methods.....	35
4.1 Material	35
4.1.1 Sample description	37
4.2 Method overview.....	39
4.2.1 Chemical composition and structure of faba bean starch ...	39
4.2.2 Ingredient functionality and physical behaviour	39

4.2.3	Evaluation of food model systems	40
5.	Results and Discussion (Papers I-IV)	47
5.1	Chemical composition and structure of faba bean starch	47
5.1.1	Starch composition and molecular structure.....	47
5.2	Ingredient functionality and physical behaviour	49
5.2.1	Hydration-related properties	49
5.2.2	Starch gelatinisation and granular swelling	50
5.2.3	Pasting.....	54
5.2.4	High temperature pasting	56
5.2.5	Rheological properties of systems.....	57
5.2.6	Large deformation: Compression testing.....	59
5.3	Food model products	62
5.3.1	Faba bean starch.....	62
5.3.2	Starch:protein faba bean gels.....	63
5.3.3	3D-food products	63
5.3.4	Protein films	65
6.	Conclusions	67
7.	Future perspectives	69
8.	What is a sustainable faba bean product?.....	71
	References.....	75
	Popular science summary	89
	Populärvetenskaplig sammanfattning	91
	Acknowledgements	93

List of Publications

This thesis is based on the work contained in the following papers, referred to by Roman numerals in the text:

- I. Klara Nilsson, Corine Sandström, Hüsamettin Deniz Özeren, Francisco Vilaplana, Mikael Hedenqvist & Maud Langton (2022). Physiochemical and thermal characterisation of faba bean starch. *Journal of Food Measurement and Characterization* 16 (6),4470-4485.
- II. Klara Nilsson, Mathias Johansson, Corine Sandström, Hanna Eriksson Röhnisch, Mikael S. Hedenqvist, Maud Langton (2023). Pasting and gelation of faba bean starch-protein mixtures, Gelation and stability of protein-starch composite for food products. *Food Hydrocolloids* 138 (108494).
- III. Mathias Johansson, Klara Nilsson, Fanny Knab and Maud Langton (2022). Faba bean fractions for 3D printing of protein-, starch- and fibre-rich foods. *Processes* 10 (466).
- IV. Sandra Rojas-Lema, Klara Nilsson, Jon Trifol, Maud Langton, Jaume Gomez-Caturla, Rafael Balart , Daniel Garcia-Garcia & Rosana Moriana (2021). Faba bean protein films reinforced with cellulose nanocrystals as edible food packaging material. *Food Hydrocolloids* 121 (107019).

Papers I-IV are reproduced with the permission of the publishers.

The contribution of Klara Nilsson to the papers included in this thesis was as follows:

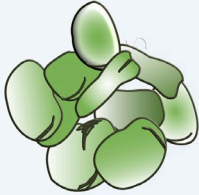
- I. Designed the experiment with the supervisors, performed the experiments and statistical evaluation, and wrote the manuscript.
- II. Contributed equally with Mathias Johansson. Designed the experiment with the co-authors, performed the experiments and statistical evaluation, and wrote the manuscript.
- III. Contributed equally with Mathias Johansson. Designed the experiment with the co-authors, performed the experiments and statistical evaluation, and wrote the manuscript.
- IV. Performed the experiments and reviewed the manuscript.

The following papers were published during the timeframe of the doctoral education but are not part of this thesis

- i. Mathias Johansson, Daniel Johansson, Anna Ström, Jesper Rydén, Klara Nilsson, Jakob Karlsson, Rosana Moriana & Maud Langton (2022). Effect of starch and fibre on faba bean protein gel characteristics. *Food Hydrocolloids* 131 (107741).
- ii. Sandra Rojas-Lema, Klara Nilsson, Maud Langton, Jon Trifol, Jaume Gomez-Caturla, Rafael Balart, Daniel Garcia-Garcia & Rosana Moriana (2023). The effect of pine cone lignin on mechanical, thermal and barrier properties of faba bean protein films for packaging applications. *Journal of Food Engineering* 339 (111282).

Faba bean structure & texture

1: Starting material:



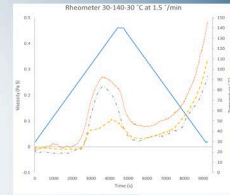
2: Single system

Faba bean Starch

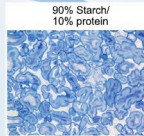
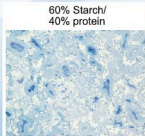
Thermal behaviour



Physio-chemical characterisation



3: Mixed system



Faba bean Starch + Protein composite



4: Food model system

Faba bean protein

&



Biodegradable & biobased films

Packaging development

Product development



Faba bean Starch + Protein + Fibre

Graphical abstract visualising project outline and articles referred to in this thesis

1. Introduction

Climate change, COVID-19 and the war in Ukraine are all factors placing global food security, safety and production at risk. To achieve the climate targets in the Paris Agreement, such as staying below a 1.5 °C mean temperature rise, while also supplying the growing global population with food, the fragile food system needs to become more resilient and sustainable.

The food industry accounts for about one-third of global greenhouse gas emissions and 70% of global water use (Graça *et al.*, 2014; Willett *et al.*, 2019). The major stressors connected with European food production include production of animal-based foods, production of synthetic fertilisers and food transport (Cusworth *et al.*, 2021; Filho *et al.*, 2022; Rööös *et al.*, 2020; Tidåker *et al.*, 2021). According to Rööös *et al.* (2020), the climate impact of the Swedish diet could be reduced by 20% if Swedish meat consumption were to be halved and instead replaced by domestically grown grain legumes.

Faba bean (*Vicia faba minor*) is a cool-climate legume crop primarily used for animal feed in Sweden. However, based on its nutrient profile, faba bean could be a healthy, sustainable plant-based food for human consumption (Guillon & Champ, 2002). Faba bean plants can biologically fix atmospheric nitrogen, which can reduce the need for artificial fertiliser, thereby contributing to a more sustainable cropping rotation (Fouad *et al.*, 2013).

In Sweden, the vegetarian and plant-based product sector is one of the fastest-growing markets, increasing by 16% in recent years (Macklean, 2020). The most prominent influences for consumers choosing plant-based products are curiosity, health, sustainability and animal welfare (Gebhardt & Hadwiger, 2020). Consumers are now demanding a wide array of plant-based products made using simple ingredients with good organoleptic properties. In 2020, soybean, wheat and pea were the most common texturising ingredients in plant-based foods available on the Swedish market (Macklean, 2020). However, these ingredients are often imported from

distant countries such as China, USA, Canada and Italy (Tidåker *et al.*, 2021).

Soybean is a particularly versatile ingredient owing to its gelling properties, ability to form anisotropic fibre structures and emulsification abilities (Vatansever *et al.*, 2020). A disadvantage of soybean and wheat is that both are major food allergens for susceptible individuals (FDA, 2023). Despite the high level of interest and strong incentives for transition to more plant-based diets, plant-based products are still considered a niche market segment (Giacalone *et al.*, 2022).

The functional properties of legume ingredients make them suitable as a replacement for proteins from other sources and for incorporation into cereal-based products such as breads, pastas and gluten-free alternatives (Affrifah *et al.*, 2023; Sozer *et al.*, 2017). Documented applications of faba bean include bread, other baked goods, extruded snacks, meat (extenders/alternatives) and pasta (Affrifah *et al.*, 2023).

The sensory quality of plant-based products has been identified as one of the main aversion factors (Giacalone *et al.*, 2022; Hassoun *et al.*, 2022; McClements & Grossmann, 2021; Nasrabadi *et al.*, 2021). Creating an appealing texture is in fact one of the major challenges in the development of plant-based foods. Texturally, pulse proteins have been described as having lower cutting strength and less chewiness than soybean- or gluten-based products, due to their different gel-forming properties and amino acid composition (Webb *et al.*, 2023). Legume starches are reported to form firm gels (Hoover *et al.*, 2010), although gel rigidity is dependent on factors such as starch purity, concentration and processing temperature. The high fibre content of legumes can be nutritionally beneficial and is a common reason for incorporation of legumes into various products (Farooq & Boye, 2011; Guillon & Champ, 2002). Fibre behaviour and its influence on food texture are highly dependent on fibre solubility (Keskin *et al.*, 2021). To expand utilisation of faba bean as a textural ingredient in food products, a clear understanding of the physicochemical characteristics and textural properties of faba bean components is required.

Therefore the structure-texture relationship of faba bean components in different food matrices was evaluated in this thesis by examining the synergistic functionality effect of the faba bean components in different food matrices

2. Background

This chapter describes the main components found in faba bean and their functional properties

2.1 Characterisation of faba bean components

In food production, a common processing practice is to separate the cotyledon from the hull, with the cotyledon being used in the main products and the hull representing a side-stream (Krenz *et al.*, 2023). The faba bean cotyledon and hull studied in this thesis differed in chemical composition as shown in the paper by Johansson *et al.*, 2022. For example, the cotyledon had a higher content of starch and protein than the fibre-rich hull (Figure 1). When describing components based on other studies in the remainder of this chapter, components extracted from cotyledon are referred to unless otherwise stated.

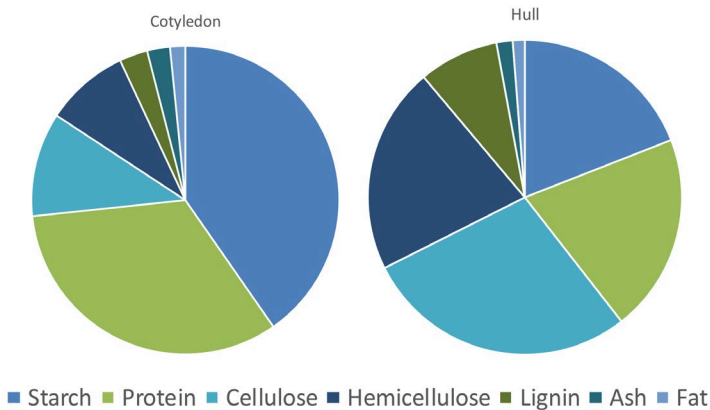


Figure 1. Composition of faba bean cotyledon and hull. Cellulose, hemicellulose and lignin make up the fibre fraction. Source: (Johansson *et al.*, 2022)

2.1.1 Faba bean starch

The properties of starch and how it reacts in different food products are highly dependent on composition, configuration and granular morphology. A thorough description of faba bean starch composition, structure and behaviour is provided in Paper I. To summarise, up to 45% of faba bean biomass consists of starch (Hoover *et al.*, 2010; Johansson *et al.*, 2022; Punia *et al.*, 2019), with the amylose content of faba bean starch ranging from 29 to 40% (Ambigaipalan *et al.*, 2011; Li *et al.*, 2019; Zhang *et al.*, 2019). Most cereal starch granules consist of 15-30% amylose, with the exception of waxy starches that contain very little or no amylose (<10%) while other types are truly amylose-rich (>40%) (Bertoft, 2017; Tester *et al.*, 2004). For faba bean starch, the reported degree of polymerisation (DP) for almost linear amylose is 1400 (Hoover *et al.*, 2010), while for highly branched amylopectin DP is 20.4 (Li *et al.*, 2019). The polymorphic pattern corresponds to the crystalline arrangement of starch. Faba beans, like most other legume starches, are characterised by a C-polymorphic pattern (Ambigaipalan *et al.*, 2011; Hoover *et al.*, 2010; Li *et al.*, 2019; Zhang *et al.*, 2019) which consists of both more compact A-type and looser B-type starch, commonly found in cereals and tubers, respectively (Bertoft, 2017; Buléon *et al.*, 1998).

The starch granule consists of alternating semi-crystalline and amorphous growth rings. The more numerous, but also shorter, amylopectin chains form double helices, which crystallise and make up the ordered semi-crystalline lamella. The amorphous lamella contains amylose, some of the longer amylopectin chains and the amylopectin branching points. Faba bean starch has been found to have cracked granular surfaces (Ambigaipalan *et al.*, 2011; Li *et al.*, 2019; Zhang *et al.*, 2019). According to Glaring *et al.* (2006), granular cracking may occur because of strain imposed on the granules as they grow owing to weak chain interactions, resulting in sub-optimal amylopectin packaging.

Starch is a major side-stream product from isolation of pulse protein (Guillon & Champ, 2002; Ren *et al.*, 2021). Glycaemic index (GI) is lower for legume starches than for cereal and tuber starches, which partly relates to higher amylose and resistant starch content in legumes (Tayade *et al.*, 2019). Resistant starch is defined as the portion of starch that is not digested and 11% of faba starch is reported to consist of resistant starch (Ambigaipalan *et*

al., 2011). Resistant starch can be added to a product to increase the dietary fibre content, without changing the taste and texture (Champ, 2004).

Starch is a versatile ingredient that is often included in foods for a variety of purposes, *e.g.* thickening, gelling, adding stability and replacing or extending more costly ingredients (Mason, 2009; Zhang *et al.*, 2021).

2.1.2 Faba bean protein

Approximately one-third of the faba bean consists of protein (Johansson *et al.*, 2022; Mayer Labba *et al.*, 2021). Most of these proteins comprise globulins (70-78%), followed by glutelins (12-18%), prolamins (1.8-3.6%) and albumins (1.4-3.0%) (Alghamdi, 2009; Martineau-Côté *et al.*, 2022). Classification of the proteins depends on their solubility. Globulins are soluble in low-salt solutions, albumins in water, prolamins in 70% alcohol, and glutelins in alkaline solutions (Farooq & Boye, 2011; Martineau-Côté *et al.*, 2022; Osborne, 1907; Sharan *et al.*, 2021). Faba bean proteins tend to be least soluble around the isoelectric point at pH 5-5.5 (Danielsson, 1950; Langton *et al.*, 2020).

Depending on their sedimentation coefficient, faba bean globulins are categorised into 11s (legumin) and 7s (vicilin) types (Farooq & Boye, 2011; Herneke *et al.*, 2021; Ma *et al.*, 2022), with legumin commonly being the most abundant (55%) (Sharan *et al.*, 2021). Plant globular proteins tend to be compact hydrophobic structures that can form gels upon heating (McClements & Grossmann, 2022). Faba bean proteins have been found to be rich in the amino acids leucine and lycine and lacking in the sulphur-containing amino acids methionine and cysteine (Ma *et al.*, 2022; Mayer Labba *et al.*, 2021).

Legumes have a different amino acid composition than cereals, and have therefore been suggested as a complementary ingredient to improve the overall nutrition of cereal products (Farooq & Boye, 2011; Mayer Labba *et al.*, 2021).

Depending on concentration, protein fractions are categorised as concentrate (48-65%) or isolate ($\geq 75\%$) (Vatansever *et al.*, 2020). The functionality of a protein in a food product, such as solubility, emulsification, foaming ability and gelling characteristics, is not only influenced by botanical origin and extraction procedure, but is also very sensitive to different environmental conditions, such as pH, temperature and ionic

strength (Herneke *et al.*, 2021; Langton *et al.*, 2020; Ma *et al.*, 2022; McClements & Grossmann, 2021, 2022; Totosaus *et al.*, 2002).

2.1.3 Faba bean fibre

Dietary fibre refers to the group of carbohydrates that are not digested or absorbed by the human small intestine, with complete or partial fermentation in the large intestine (Tiwari & Cummins, 2020). This is a broad group with a range of functionalities and includes the fractions cellulose, hemicellulose and lignin. Resistant starch is also classified as a fibre (Champ, 2004), but as this fraction is extracted during starch isolation, it can also be considered with the starch fraction. The fibre content of the hull is significantly higher than that of the cotyledon (Johansson *et al.*, 2022; Karataş *et al.*, 2017; Krenz *et al.*, 2023). Karataş *et al.*, 2017 reported the fibre content of the whole faba bean seed to be 27.5%, which included the hull that consisted of 82% fibre. When the fractions cotyledon and hull were separated using a dehulling-machine, the reported the fibre content was 22% and 56% respectively (Johansson *et al.*, 2022). The significantly lower fibre content of the hull (56% vs. 82%), was likely caused by the machine separated hull fraction containing higher amounts of starch- and protein-rich cotyledon, which would have a “diluting” effect on the overall fibre content.

Cellulose is an insoluble polymer of glucose that is widely found in cell walls (Tiwari & Cummins, 2020). In faba bean, the cellulose content has been found to be 27% for the hull and 10% for the cotyledon (Johansson *et al.*, 2022). Cellulose nanocrystals can be isolated from cellulose and incorporated into biodegradable plant-based products to strengthen their mechanical properties (Moriana *et al.*, 2016). Hemicellulose is a heteropolymer consisting of monomers of arabinose, mannose, galactose, glucose and xylose (Benaïmeche *et al.*, 2020). Lignin consists of indigestible complex aromatic polymers that impart strength and stiffness to plant cell walls (Frei, 2013).

Because of the beneficial health effects, fibre is often used as a functional ingredient. The water and oil absorption abilities of fibre can have a significant impact on the rheological properties of products to which it is added. In addition, fibre has the ability to develop complexes, particularly with proteins, which can improve the structural integrity of foods (Farooq & Boye, 2011; Guillon & Champ, 2002; Tiwari & Cummins, 2020).

2.1.4 Other components

Faba bean lipid

The lipid content in faba bean is low and research on faba bean lipids is scarce. The lipid content in a common Swedish faba bean variety has been found to be lower (1.2-1.6%) (Johansson *et al.*, 2022) than that in an Italian faba bean variety (3.1-3.2%) (Caprioli *et al.*, 2016). Faba bean is rich in polyunsaturated fatty acids (46-50%), particularly in the essential linoleic fatty acid (C18:2, *n*-6) (43-45%) with a corresponding low percentage of linolenic fatty acid (C18:3, *n*-3) (2.8-3.4%) (Caprioli *et al.*, 2016).

Anti-nutrients

Legumes may contain a number of bioactive compounds that are conventionally classified as anti-nutrients, including phytates, saponins, lectins and protease inhibitors (Mayer Labba *et al.*, 2021; Sandberg, 2018). Phytates can form insoluble and indigestible mineral complexes, which may reduce the bioavailability of iron and zinc (Sandberg, 2018). Of 15 faba bean cultivars evaluated by Mayer Labba *et al.* (2021), only one was estimated to have high bioavailability of iron and zinc, which coincided with low phytate levels. The digestibility of certain legume-based proteins may decrease if trypsin or proteases inhibitors are present (Sharma & Sehgal, 1992; Herreman *et al.*, 2020).

Two prevalent faba bean pyrimidine glycosides, vicine and convicine, are also considered anti-nutrients (Dhull *et al.*, 2021; Khazaei *et al.*, 2019) and high consumption of these may cause favism, a severe form of haemolytic anaemia, in susceptible individuals. The ratio of convicine to vicine appears to vary between cultivars, but to reduce the risk of favism selecting a cultivar with low levels of the components may be preferable.

Thus, faba bean may contain a range of anti-nutrients in different proportions that depend on the cultivar, but also on cultivation conditions.

Minerals & vitamins

The minerals present in the highest levels in faba bean are potassium and phosphorus, but most of the phosphorus is unavailable as it is present in the form of phytates (Dhull *et al.*, 2021). Bioavailability of iron and zinc can be reduced by the presence of phytates (Mayer Labba *et al.*, 2021; Sandberg, 2018), due to the formation of insoluble and indigestible phytate-mineral

complexes. Regarding vitamins, faba bean has a higher content of water-soluble vitamins than fat-soluble vitamins. The vitamin content in faba bean decreases during cooking, as a result of decomposition and increased leaching rates (Dhull *et al.*, 2021; Revilla, 2015).

2.2 Ingredient functionality

Food products rarely consist of just one component and an agglomeration of ingredients is generally present. The design of the food matrix and ingredient processing influence ingredient functionality, which in turn affects the physicochemical, sensorial and gastrointestinal properties of the final food product. Figure 2 shows a simplified version of a food matrix, with the main components found in faba beans in the centre of the diagram, and the different ingredient functionalities influencing the textural properties in the resulting food products around the edge. These functionalities depend on the proportions and interactions between the different components, and may change depending on processing parameters.

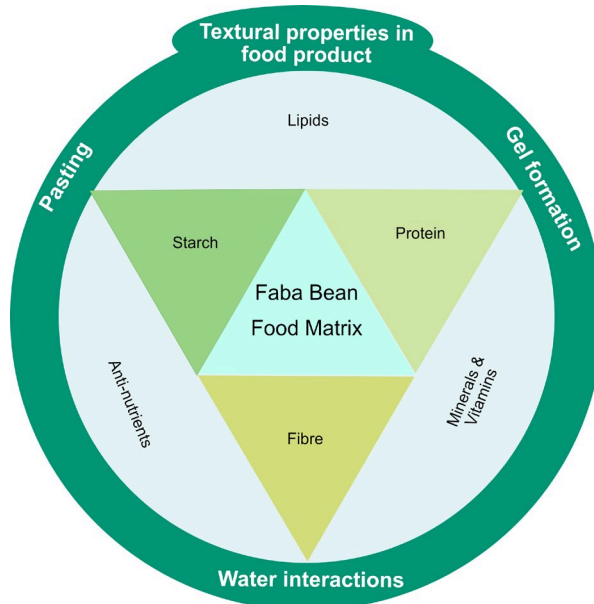


Figure 2. Characteristics of a faba bean food matrix, with the main fractions in faba bean that provide different textures to the matrix (depending on composition and processing) in the centre of the diagram. Functionalities specifically important to understand the work presented in this thesis are listed on the outer rim.

2.2.1 Component interaction with water

Solubility

The solubility of a molecule and how it binds to water influences its ability to thicken solutions, form gels and stabilise emulsions. Biopolymer solubility is governed by molecular features such as molar mass, surface hydrophobicity and electrical characteristics (McClements & Grossmann, 2022). Low-soluble macromolecules are more prone to aggregate and form hydrophobic crosslinks (McClements & Grossmann, 2022).

Starch is insoluble in cold water. The proportions of crystalline and amorphous components govern granule swelling and solubility properties (Wani *et al.*, 2016). The swelling power and water solubility of faba bean starch in solution increase as the temperature increases, partly due to an increment in starch molecular mobility. However, in comparison with other bean starches, the solubility of faba bean starch remains relatively low at higher temperatures (90 °C), likely due to stronger hydrogen bonds and higher amylose content, which restricts swelling and results in improved granular integrity (Zhang *et al.*, 2019).

The solubility of proteins is pH-dependent and for legume proteins tends to be lowest at around pH 4-6, because of reduced electrostatic repulsion occurring at the isoelectric point (Ma *et al.*, 2022). Faba bean protein has its lowest solubility at around pH 5, which is also a common pH for foodstuffs, but the solubility can be increased by adding table salt (Langton *et al.*, 2020). The solubility of faba bean protein decreases from 0.5 g/g to 0.3 g/g after being heated to 150 °C, presumably because of structural degradation (Bühler *et al.*, 2020).

The techno-functionality of dietary fibre is influenced by its origin (Guillon & Champ, 2002). Most of the fibre found in the cotyledon of pulses tends to be soluble dietary fibre (Farooq & Boye, 2011; Tiwari & Cummins, 2020). The insoluble fibre fraction is mainly found in the hull (Farooq & Boye, 2011). In whole faba beans, a major part of the fibre fraction is insoluble fibre (10-16.0%), while it contains minor amounts of soluble fibre (0.6-1.1%) (Mayer Labba *et al.*, 2021). According to Mayer Labba *et al.* (2021), the soluble fibre fraction in faba bean has the highest content of arabinose, rhamnose and soluble uronic acids. Soluble dietary fibre is widely used as a food additive (thickener, stabiliser, emulsifier and gelling agent), because it can dissolve in water to form a gel and, compared with insoluble

fibre, is lighter in colour and flavour (Guillon & Champ, 2002). Because of the coarser texture, insoluble fibre is suitable for use in extruded and bakery products (Guillon & Champ, 2002)

Hydration and water retention properties

The texture and mouthfeel of a food product are strongly influenced by the presence of fluids and the water retention capacity of the ingredients (Boye *et al.*, 2010; McClements & Grossmann, 2022). Water binding is accompanied by particle swelling. Within the food matrix, water may be retained through the formation of porous three-dimensional (3D) networks, but as the crosslinking density increases within the network, swelling of the matrix decreases (Cornet *et al.*, 2021).

Starch granules are in general insoluble in cold water, but when heated the granules swell as water is absorbed, resulting in the starch granule losing its crystallinity, a process called gelatinisation (for more details of starch gelatinisation, see section 2.2.2 of this thesis).

The water-holding capacity of faba bean protein has been reported to increase by 86% when heated to above 150 °C, an effect associated with the increase in insoluble fractions at higher temperatures (Bühler *et al.*, 2020).

Fibre can bind water in numerous ways, such as polar and hydrophobic interactions, hydrogen bonding and enclosure (Chaplin, 2003). The water-binding capacity of insoluble fibre tends to be relatively high (Tiwari & Cummins, 2020). The polar groups in cellulose, hemicellulose and lignin increase water uptake by lignocellulosic fibres (Zabihzadeh, 2010). However, there are conflicting reports on how the size of the fibre particles influences their water-holding capacity (Tosh & Yada, 2010). For pea hulls, water retention increases as mean particle size decreases (Auffret *et al.*, 1994), an effect attributed to increased surface area and pore volume, while for navy bean hulls the opposite occurs, with water retention improving as the fibre particles become coarser (Daubenmire *et al.*, 1993).

Water binding can be determined through different methods such as centrifugation, filtration or freeze-drying, which may generate different results. Therefore results should not be generalised, but considered as an indicative factor of the particle behaviour according to the methodology used (Chaplin, 2003). The amount of mobile and immobile fractions within a mixture, a property associated with hydration capacity, can be measured by

solid-state ^{13}C nuclear magnetic resonance (NMR) spectroscopy (Morgan *et al.*, 1995; Tang & Hills, 2003; Zhu, 2017).

Thickening

Polysaccharides can be added to foods as a functional ingredient with the purpose of increasing the viscosity in order to generate desirable textural or mouthfeel attributes or reduce the rate of gravitational separation of particulate matter (McClements & Grossmann, 2022). The thickening power relates to how much ingredient is required to effectively increase viscosity. Typically, the thickening power increases as the particle volume ratio increases (Bai, 2017). Insoluble fibre tends to have higher swelling power than soluble fibre (Tiwari & Cummins, 2020).

2.2.2 Pasting (starch thickening)

The starch incorporated in nearly all food products is thermally pre-treated, which induces a range of structural changes that impact upon the product texture. Figure 3 shows a typical pasting curve of starch and provides an understanding of the mechanistic changes that starch undergoes during heating and cooling.

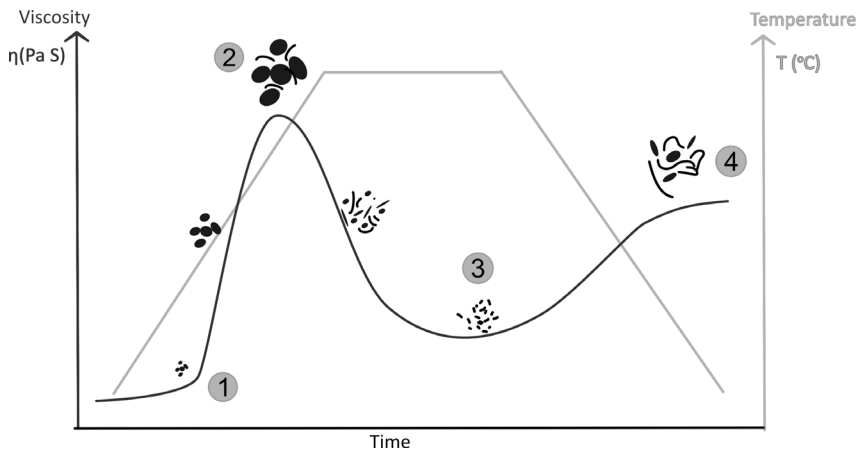


Figure 3. Starch pasting curve where: pasting initiates as the granules start to swell (1). The granules continue swelling until peak viscosity (2), at which granular disintegration causes viscosity to decrease to minimum viscosity (3), where the difference between minimum viscosity and maximum viscosity is called breakdown viscosity. During cooling the starch gels, final viscosity (4). The difference between final viscosity and maximum viscosity is called set-back. Diagram interpreted from Schirmer *et al.*, 2015 .

Gelatinisation

Starch gelatinisation, when starch goes from an ordered to a disordered state, can be considered as the initial stage of the pasting curve (Figure 3, step 1) and is the irreversible dissociation of the crystallites that can be seen as loss of birefringence (Gernat *et al.*, 1990; Muñoz *et al.*, 2015; Schirmer *et al.*, 2015). The resulting swelling initiates in regions where the intramolecular bonds are weakest, penetrating the more amorphous layer of the granules (Vamadevan & Bertoft, 2015, 2020). Gelatinisation temperature for faba bean starches is reported to lie between 57 and 75 °C (Ambigaipalan *et al.*, 2011; Lee, 2007; Li *et al.*, 2019; Zhang *et al.*, 2019).

According to Tester and Morrison (1990), gelatinisation temperature reflects the perfectness of crystallites, where starches with higher crystalline order and more stable crystals have a high gelatinisation temperature and narrower endothermic peak. In comparison with other bean starches, faba bean starches display significantly lower temperatures and enthalpies for gelatinisation with a high swelling factor, possibly as a consequence of a less well-ordered crystalline structure and granular cracks facilitating the entry of water (Ambigaipalan *et al.*, 2011). Faba bean also has a relatively broad gelatinisation range compared with other bean starches (Zhang *et al.*, 2019), which may imply crystalline structures with varying stability. There are conflicting findings on how granular size influences gelatinisation, *e.g.* Haase & Shi (1991) found that smaller faba bean starch granules had lower gelatinisation enthalpy, while Wang *et al.* (2011) found the opposite for field pea starches. The gelatinisation parameters of starches can be determined using differential scanning calorimetry (DSC) (Hoover *et al.*, 2010).

Pasting

Pasting refers to the changes in dissolution of starch upon further heating after gelatinisation. The pasting temperature is when the viscosity begins to rise (Figure 3, step 1) caused by granular swelling and by the leaching out of low-molecular-weight components. For faba bean, amylose leaching is already detectable at temperatures of 75 °C, reflecting the weaker interactions between amylose-amylose and/or amylose-amylopectin (Ambigaipalan *et al.*, 2011).

The peak viscosity represents the highest viscosity attained (Figure 3, step 2). The curve then starts to flatten or decrease as the starch crystals melt and swollen granules rupture/collapse, resulting in more rapid water movement

into the granules (Balet *et al.*, 2019). Peak viscosity tends to be lower for faba bean than for other legumes, a factor associated with the amylose content (Li *et al.*, 2019; Zhang *et al.*, 2019).

The breakdown viscosity of faba bean starches (Figure 3, step 3) is also comparatively low (Li *et al.*, 2019; Zhang *et al.*, 2019). Leached amylose reduces the breakdown viscosity by maintaining granular integrity and preventing collapse (Li *et al.*, 2019). Upon cooling, starch gelation occurs as, the leached amylose forms a network and amylopectin tends to recrystallise (Li *et al.*, 2019; Zhang *et al.*, 2019), resulting in higher final viscosity (Figure 3, step 4). Legume starches are commonly characterised by high pasting temperature, absence of peak viscosity, increasing viscosity during the holding period and high set-back (Hoover *et al.*, 2010).

Instruments commonly used to measure pasting behaviour include the rapid viscoanalyser (RVA), rheometer and Brabender Viscograph. In the RVA and rheometer, starch is heated in excess water under constant rotation and the force required to maintain the rotation corresponds to the change in viscosity. This constant shearing prevents the starch from sedimenting.

2.2.3 Gel formation

Gels are semi-solid viscoelastic polymeric materials that incorporate large amounts of water (hydrogels), air (aerogels) or oil (oleogels) within the three-dimensional network (Cao & Mezzenga, 2020).

Starch gels are heat-set irreversible and formed through hydrophobic interactions (see the preceding sub-section on starch pasting for more details). Li *et al.* (2019), suggested that faba bean starch could be used in the production of noodles because of its strong gelling ability.

Globular proteins, including faba bean proteins, form heat-set irreversible gels (McClements & Grossmann, 2022). During gel formation the protein denatures, thereby exposing non-polar surface groups that can associate with each other through hydrophobic interactions (Cao & Mezzenga, 2020). Denaturation for faba bean protein isolate occurs at 94 °C (Nivala *et al.*, 2017), which corresponds well to the denaturation temperature of the protein subunits legumin (95 °C) and vicilin (84 °C) (Kimura *et al.*, 2008). The reported minimum gelling concentration for faba bean protein-rich flour is 7% and that for protein isolate, which has a lower carbohydrate content, is 12% (Vogelsang-O'Dwyer *et al.*, 2020). According to Fernández-Quintela

et al. (1997), the lowest gelling concentration of faba bean protein is somewhat higher (14%).

A recent study by Johansson *et al.* (2022) found that faba bean protein-dominated mixed systems start forming gels at between 75 and 80 °C. Mixtures with higher starch and/or fibre content formed firm gels, presumably because of higher water retention by the carbohydrate fractions effectively increasing the protein concentration in the remaining aqueous area (Johansson *et al.*, 2022). Decreasing the pH from 7 to 5 has also been found to be an effective way to improve protein gelling ability (Langton *et al.*, 2020). The gels in that study were coarser at pH 5, which may relate to the protein solubility.

Viscoelasticity

Most food products are viscoelastic, meaning that they exhibit a combination of liquid-like (viscous) and solid-like (elastic) behaviour. Small-amplitude oscillatory rheometry is the primary technique used to measure viscoelastic properties as a function of time, temperature, strain or frequency (Liepsch, 2016). In the case of plate-plate/plate-cone geometry, the sample is loaded between two plates with a known gap (h). The bottom plate is kept stationary while the top plate oscillates at a given stress and/or strain amplitude and/or frequency, and the material's response to the motion in terms of stress and strain is monitored (Figure 4a). For purely elastic materials, maximum stress and strain occur simultaneously, and thus these parameters are in phase. For purely viscous material, stress and strain are out of phase by 90°. For viscoelastic materials, the resulting stress can be quantified somewhere between these two extreme components, *i.e.* in-phase (0°) and out-of-phase (90°) (Kasapis & Bannikova, 2016; Liepsch, 2016).

Some standard rheological parameters for viscoelastic materials and how these parameters relate to each other are shown in Figure 4b. Storage modulus (elastic modulus, G') is the ratio of in-phase stress to applied strain and the magnitude of storage modulus is proportional to the number of permanent interactions and the strength of the interactions present in the sample (Kasapis & Bannikova, 2016). The corresponding parameter for the out-of-phase response is loss modulus (viscous modulus, G''), measuring the sample's flow properties. The loss tangent ($\tan \delta$) represents the ratio between loss modulus and storage modulus, *i.e.* $\tan \delta = G''/G'$, summarising the viscoelastic character of a material. High $\tan \delta$ values indicate samples

with a more viscous-like nature, while low $\tan \delta$ values indicate more solid-like material. Complex modulus (G^*) is the overall response of a material and can be described as the material's total stiffness. It is calculated as: $G^* = \sqrt{(G')^2 + (G'')^2}$ (Kasapis & Bannikova, 2016; Liepsch, 2016).

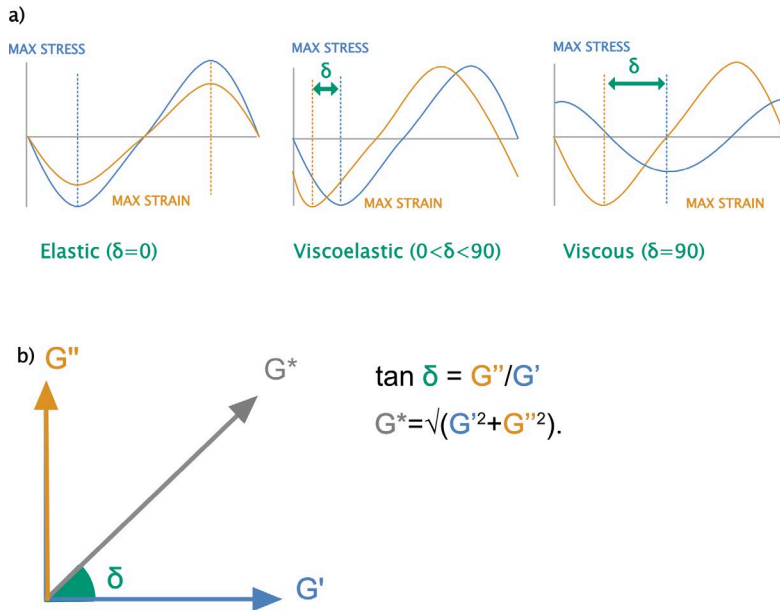


Figure 4. a) Figurative sinusoidal wave representation of viscoelastic products and b) relationship between complex modulus G^* , $\tan \delta$, storage modulus G' and loss modulus G'' . Diagram interpreted from Liepsch (2016)

2.3 Faba bean components as texturising agents

Faba bean has been added to various food products with the aim of improving the nutritional profile of the product and/or reducing the environmental impact. For example, addition of pulses to wheat products can improve the fibre content and amino acid profile (Farooq & Boye, 2011). It is important that adding faba bean to a food product does not impair/compromise product quality.

Numerous studies have researched the effect of fortifying pasta-like products with faba bean (Giménez *et al.*, 2012; Kaya *et al.*, 2018; Laleg *et al.*, 2016, 2017; Petitot *et al.*, 2010; Rizzello *et al.*, 2017; Rosa-Sibakov *et*

al., 2016). Replacing some of the wheat/semolina flour in pasta with faba bean has been found to decrease some quality attributes of the pasta product. Gluten gives wheat unique properties such as elasticity and cohesiveness, while addition of the non-glutenous, more fibre-rich faba bean flour reduces the gluten network strength by diluting the gluten (Petitot *et al.*, 2010; Laleg *et al.*, 2017). The higher fibre proportion in faba bean flour also weakens the gluten through fibre particles physically disrupting protein network formation (Petitot *et al.*, 2010; Laleg *et al.*, 2016, 2017). Drying at high temperatures strengthens the protein structure of pasta by promoting protein aggregation, resulting in increased integrity and product resilience (Petitot *et al.*, 2010; Laleg *et al.*, 2017). As mentioned previously, the globular proteins in faba bean are heat-induced gel proteins. Up to 30% of wheat flour could be replaced with faba bean flour without having too negative an impact on pasta quality while still maintaining optimum protein quality in nutritional terms (Giménez *et al.*, 2012; Rizzello *et al.*, 2017).

Because of its higher fibre content, replacing wheat flour with faba bean flour (Giménez *et al.*, 2012) or hull flour (Kaya *et al.*, 2018) increases the water absorption of pasta dough. Interestingly, the greater hardness of cooked faba bean-fortified pasta has been attributed to the overall higher protein content and lower water uptake during cooking (Petitot *et al.*, 2010). In production of gluten-free pasta, Rosa-Sibakov *et al.* (2016) found that addition of fermented faba bean flour resulted in a more porous structure and rupture of the starch granules, which reduced water absorption, causing increased hardness.

In production of wheat bread, addition of faba bean flour has a positive impact on the nutritional properties, but may slightly reduce loaf volume (Coda *et al.*, 2017), possibly due to some alterations in gluten network development. Daliani *et al.* (2019) found that bread fortified with faba bean hull had increased postprandial satiety, which was correlated with the overall higher fibre content.

In a recent study, addition of faba bean hull to beef patties was found to reduce cooking losses because of the thickening ability of the fibre, which created a network that held both fat and water (Elsebaie *et al.*, 2022). In an earlier study, Vaisey *et al.* (1975) found that faba bean could be added to beef patties as an extender, increasing both fat and moisture retention, but with a decrease in apparent juiciness because the faba bean-bound water was not released during chewing. In production of extruded meat analogues using

pulses, the texture properties most affected are reported to be caused by ash, fibre, fat and protein content and water-holding capacity of the protein isolate/concentrate (Ferawati *et al.*, 2021b). Products consisting of commercial faba bean protein isolate in those studies were harder and chewier than the other pulse samples, an effect correlated with the lower protein content and higher content of fat, fibre and carbohydrate. A lower extrusion temperature was used for non-commercial faba bean proteins, because of lower protein denaturation temperature, and this resulted in the analogues having fibre more aligned in a crosswise direction (Ferawati *et al.*, 2021b). This was a desirable effect as it created analogues that texturally resembled meat products more than when fibres were aligned lengthwise (Ferawati, *et al.*, 2021b).

In the production of vegan cheese analogues, it has been found that faba bean cheeses are harder and chewier than yellow pea analogues, relating to the higher protein content in faba bean (Ferawati, *et al.*, 2021a). Moreover, cheese analogues produced from roasted faba bean had higher chewiness and hardness than those produced from boiled faba bean (Ferawati, *et al.*, 2021a). It was hypothesised that because the roasting process was of shorter duration and used hot air circulation, starch gelatinisation and denaturation of the protein were less complete than in the hydrothermal treatment (Ferawati, *et al.*, 2021a). Thus during production of the cheese analogues, the ungelatinised starch and undenatured protein in the roasted faba bean flours started to gelatinise, denature and build a gel network, thereby forming a harder gel texture.

Faba bean (flour or protein) has been used as an emulsifying ingredient in some much softer food products, *e.g.* tofu, yoghurt (Jiang *et al.*, 2020) and mayonnaise (Armaforte *et al.*, 2021; Ouraji *et al.*, 2020). Jiang *et al.* (2020) identified high starch content and low lipid content as limiting factors in the development of emulsion gels. Starch gelation was prevented either through hydrolysis or by removal of the starch. For the yoghurts, viscosity was higher in products containing hydrolysate starch, because of its ability to form hydrogen bonds (Jiang *et al.*, 2020). For the tofu, starch-free analogues were firmer than starch hydrolysate analogues, as the hydrolysate starch hindered protein gelation and reduced water-holding capacity (Jiang *et al.*, 2020). In production of faba bean protein-based mayonnaise, xanthan gum had to be added as a stabiliser (Armaforte *et al.*, 2021) or the faba bean protein had to be pre-treated (Ouraji *et al.*, 2020).

The protein composition, high fibre content and strong starch gelling ability are all properties of faba bean that influence the functionality and use of faba bean in different sorts of food products.

2.4 Correlating microstructure and texture

The texture of food consists of several different physical sensations, attributes that are perceived through mastication. The textural quality of food is derived from the structural organisation at the molecular, microscopic and macroscopic level (Bourne, 2002). By combining microscopy with complementary data, the effect of morphological changes on product texture can be identified. Foods are complex multicomponent systems where the microstructure parameters and interactions are affected by processing and product properties.

The composition of a product provides limited information on the structure (Aguilera, 2005). The texture of a food is not static, but evolves in line with changes in structure (Bourne, 2002). An example of this is how the texture of starch solution changes during pasting, because of heating, despite the composition remaining unchanged.

Textural analysis may only provide information on one structural aspect of the food, as different structures within the matrix may respond to a specific measuring method. For whey gels, Langton *et al.* (1996) found that destructive large deformation tests provided information on the overall gel network structure, while non-destructive textural analysis provided information on the gel strands. From the destructive textural analysis, those authors concluded that larger pore and particle size of the whey gels contributed to a more grainy and gritty texture that increased the sensation of the gel falling apart. In the non-destructive tests, softer texture of the gels was correlated with a more conglomerated structure. For highly stranded networks, the gels were instead perceived as springy (Langton *et al.*, 1996). It was shown by He *et al.* (2016) that the predictive power of perceived mouthfeel for thickened solutions increased when the evaluation protocol used a combination of rheological methods, rather than relying solely on one type of method. In that study, shear rheology values corresponded to thickness and extensional rheology values to overall stickiness and mouth coating.

Studies on how product structure and texture change under different conditions can help predict product behaviour. Microscope analysis has revealed that the higher cooking losses for legume pasta compared with normal pasta are caused by the protein network not enveloping the starch granules in the legume pasta, which causes the starch to leak out (Laleg *et al.*, 2016; Rosa-Sibakov *et al.*, 2016). In a study by Rizzello *et al.* (2017), higher cooking losses in faba bean-fortified pasta were correlated with a less homogenous network and larger porosity, and those authors speculated that the higher cooking losses also resulted in reduced nutritional value. Wheat products fortified with fermented faba bean flour, compared with non-fermented, have been found to have a firmer, more stable and cohesive structure, which can be related to a thicker and more cohesive protein network (Coda *et al.*, 2017; Rosa-Sibakov *et al.*, 2016).

Knowledge of the relationship between structure and texture is thus key for effectively optimising food production processes and for developing new products with desired sensory qualities.

3. Aims and Objectives

Transition towards a more plant-based diet involving locally grown legumes has been suggested as an effective method by which the Swedish food system can become more resilient and sustainable (Röös *et al.*, 2020; Tidåker *et al.*, 2021). However, the sensory quality of plant-based foods has been identified as a barrier to consumer acceptance (Alcorta *et al.*, 2021; Giacalone *et al.*, 2022; Hassoun *et al.*, 2022), with the development of appealing texture being a particular challenge. Faba bean is a cool-climate crop with a good nutritional profile that has high potential as an ingredient in healthy and sustainable plant-based products. To broaden the utilisation of faba bean in food products, a deeper knowledge of the different faba bean components (starch, protein and fibre), their functionalities and their synergetic effect on product texture is required.

The overall aim in this thesis was to compare the functionality of faba bean components and their effect on texture by analysing the synergetic functionalities of different components in different types of food matrices and food model prototypes. Specific objectives of the work were to:

- Physiochemically characterise and compare faba bean starch from cotyledon and hull with wheat starch, and assess how external heating factors, such as heating rate and temperature ranges, affected the thermal behaviour of the starches (Paper I)
- Identify different factors influencing the pasting properties of faba bean starch (Papers I-II)
- Evaluate the effect of addition of protein and protein/fibre extracted from faba bean on the texture of faba bean starch, by measuring system behaviour under small and large deformations (Papers II-III)

- Compare the gel-forming behaviour and microstructure of differently proportioned starch:protein composite gels, to determine factors affecting gel properties (Paper II)
- Design different food models, 3D-printed products and edible protein films, and evaluate their suitability in food products by determining the relationship between composition and functionality (resulting properties) (Papers III- IV)

4. Consideration of Methods

First, the samples were chemically, structurally and physically characterised. Next, ingredient functionalities were analysed and the data were compared against the molecular properties. Finally, the food-model-systems were assessed to evaluate the suitability of these potential prototype products for their end-use. The different methods used for characterisation can serve as a foundation when trying to understand, explain and compare the different product properties from the simple to the more complex food-matrix systems.

4.1 Material

Faba bean (*Vicia faba minor*, variety ‘Gloria’) was kindly supplied by RISE, Uppsala, Sweden. The beans were cultivated in 2016 in central Sweden and stored dry until use.

In all papers (I-IV), the fractionation method for a particular type of component was very similar and is described in detail in each paper. In brief, the proteins were extracted using isoelectric point extraction and the starch by mild alkaline treatment. The most efficient fractionation sequence, with the best yield and minimal changes to the isolated components, was to start fractionating the protein, followed by starch and fibre. The yields obtained were then protein 56%, starch 91% and fibre 29%.

An outline of the fractionation procedure is shown in Figure 5, together with the components used in each study. In Paper I, only the starch was isolated, while in Paper IV only the protein was extracted from the faba bean. In Papers II and III, multiple fractions were recovered and used.

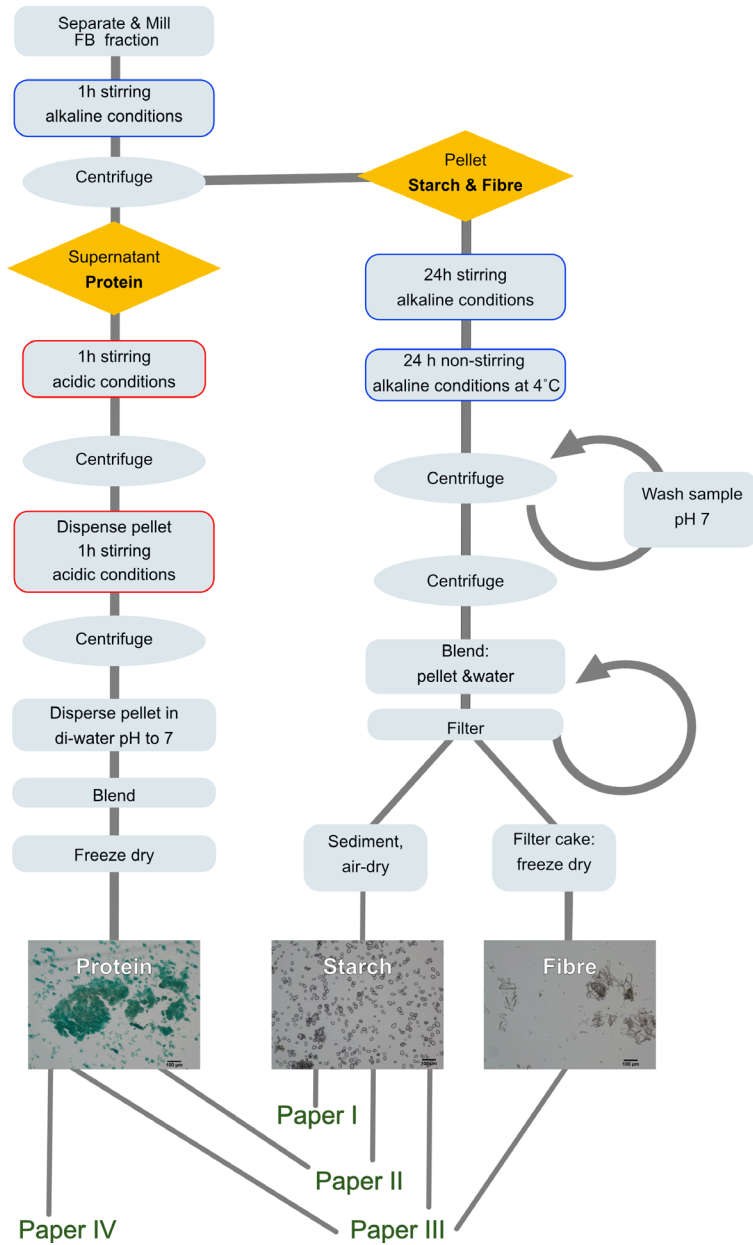


Figure 5. Outline of faba bean fraction (protein, starch, fibre) and isolation methods used in Paper I (starch), Paper II (starch and protein), Paper III (starch, fibre and protein) and Paper IV (protein) Scale bar= 100 μ m.

4.1.1 Sample description

Paper I

Faba bean starches from cotyledon and hull were characterised and compared with commercial wheat starch supplied by Lantmännen Reppe AB, Linköping, Sweden. The starch samples used were cotyledon and hull of faba bean and wheat (including both A and B granules).

Paper II

Different ratio faba bean starch and protein were combined to make composite gels with 12% solids content. Figure 6 shows the composition of the solid components of the different gels.

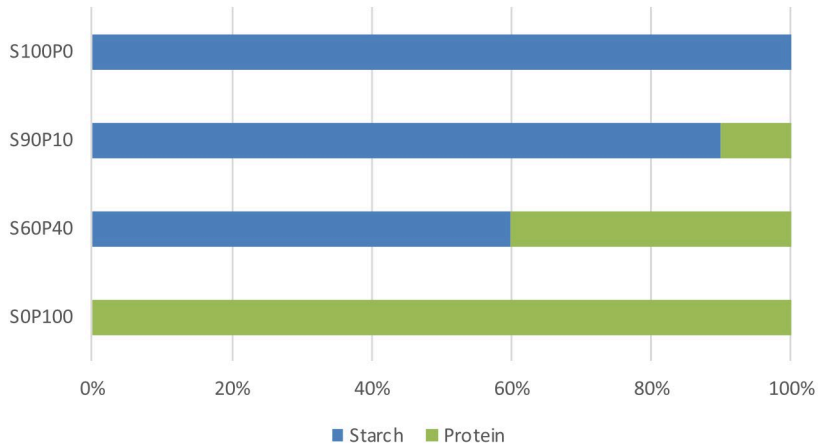


Figure 6. Dry weight distribution of the faba bean components starch (S) and protein (P) in the gels studied in Paper II.

The gels were prepared by mixing the starch and protein with water for 40 min to ensure homogeneity. The mixtures were then heated under continuous stirring in a water bath at 65 °C to prevent starch sedimentation. For gel formation, the samples were heated to 95 °C and then cooled to 25 °C at 1.5 °C/min.

Paper III

Different ratios of faba bean starch, protein and fibre were combined to create edible inks suitable for 3D-printing (Figure 7).

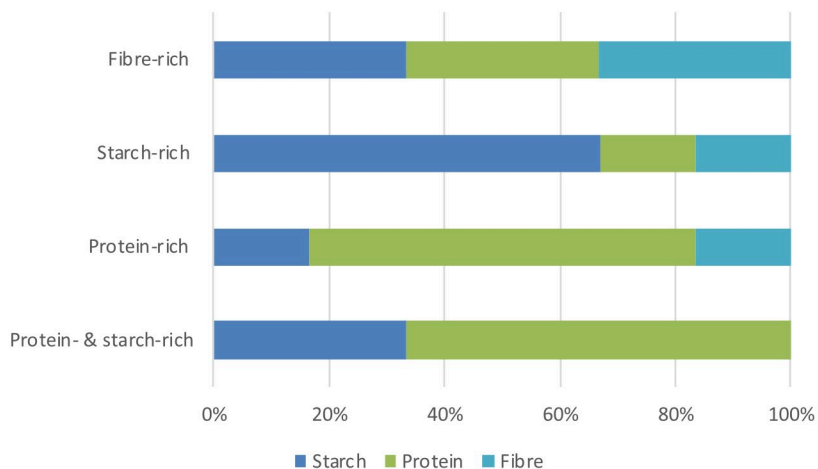


Figure 7. Dry weight distribution of faba bean components in the inks studied in Paper III.

To make the inks for 3D-printing, the starch was mixed with 70% of the total quantity of water. The total quantity of water was adjusted to each type of ink, ensuring that the inks had a good printable viscosity that could form a free-standing 3D object during printing. The starch solution was heated to 60 °C before addition of the protein, fibre and remaining 30% of water. To remove air bubbles, the ink pastes were extruded through a syringe three times before finally being added to the 3-mL cartridge used for printing. The samples were printed as cubes ($14 \times 14 \times 14 \text{ mm}^3$) using a BIO X bioprinter, frozen at -18 °C and then freeze-dried.

Paper IV

Edible films for use in food packaging were created by combining faba bean protein, glycerol and different doses of pine cone cellulose nano-crystals (CNC) (Table 1). To produce the CNCs, ground-up pine cone particles were first subjected to alkaline treatment and then bleached to remove the hemicellulose and lignin. The bleached samples were hydrolysed under

acidic conditions, with the excess acid removed through centrifugation and dialysis. The CNC suspensions were then sonicated and hydrolysed again. The CNC samples were stored in the fridge until further use.

Table 1. *Composition (dry weight basis) of the faba bean protein (FBP) films reinforced with Cellulose nano-crystals (CNC) produced in Paper IV*

Sample	FBP	FBP:CNC-1%	FBP:CNC-3%	FBP:CNC-5%	FBP:CNC-7%
Protein (g)	5	5	5	5	5
Glycerol (g)	2.5	2.5	2.5	2.5	2.5
CNC, wt-% of dry protein	0	1	3	5	7

To prepare the films, the protein was dissolved in glycerol and water. The pH of the solution was adjusted to 10.5 and it was stirred for 1 h before heating to 85 °C to denature the protein. The CNC was added to the films after the denaturation step. The resulting solutions were cast into films and dried before being conditioned at 52% humidity for 48 h.

4.2 Method overview

A schematic overview of the different types of analysis applied Papers I-IV is shown in Figure 8. A more detailed description of the different methods applied in the papers is provided in Table 2.

4.2.1 Chemical composition and structure of faba bean starch

In Paper I, a range of methods were used to characterise the chemical and structural composition of faba bean, with the aim of understanding how composition affects the thermal behaviour of the starch.

4.2.2 Ingredient functionality and physical behaviour

Functional properties such as water absorption, swelling, pasting behaviour and gelation affect the sensory characteristics of food products and play an important role in the physical behaviour of a food and its ingredients. In this thesis, the functionality of faba bean fractions was assessed in mono-

component systems and increasingly complex multi-component systems, to evaluate the synergetic functional properties of the components (Papers I-IV). This approach was intended to help in predicting the development of different food textures depending on the combination of systems and processing parameters.

4.2.3 Evaluation of food model systems

The food products created and evaluated were:

- 3D-printed cracker products (Paper III).
- Edible faba bean protein films (Paper IV).

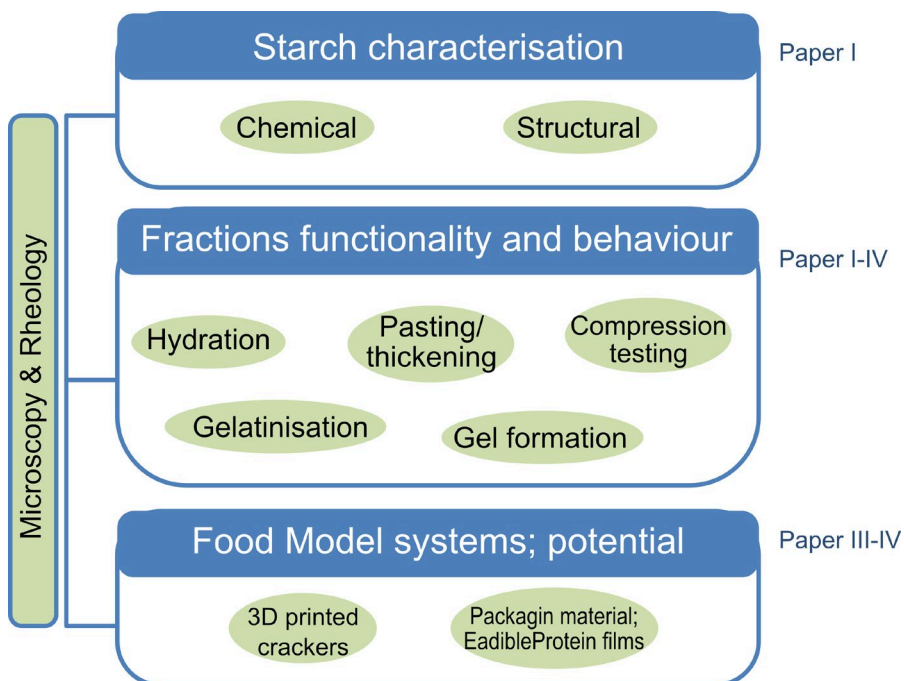


Figure 8. Overview of the different types of analysis performed in this thesis. The different findings were compared and theories were developed based on a synthesis of the data.

Table 2. Description of the different analyses performed in this thesis

Analysis	Description	References	Paper
Starch characterisation			
<i>Chemical composition</i>			
Total starch & resistant starch (RS)	α -amylase & amyloglucosidase (AMG) solubilises non-RS to glucose. The RS-rich pellet was washed in alcohol before being dissolved in KOH. The solution was neutralised and starch was hydrolysed to glucose with AMG. The RS and solubilised starch content were measured with glucose oxidase/peroxidase reagent (GOPOD) in a spectrophotometer.	Megazyme, K-RSTAR 05/19	I
Amylose content	The proportion of amylose to total starch was quantified. Starch was completely dispersed by heating in dimethyl sulphoxide (DMSO), for total starch the sample was at this stage hydrolysed to D-glucose. To determine the amylose content, amylopectin was precipitated by addition of Con A. The supernatant (amylose fraction) was hydrolysed to D-glucose. Both D glucose fractions were analysed using GOPOD.	Megazyme, K-AMYL 06/18	I
Protein	Protein content was calculated from the nitrogen content ($N \times 6.25$) measured by the Kjeldahl method using a 2520 digester, Kjeltec 8400 analyser unit and 8460 sampler unit.	NMKL-6	I
Fat	Acid hydrolysis in Hydrotec 8000 and solvent extraction of fat using petroleum ether in a Soxtec 8000 extraction unit.	Commission Regulation (EC) No 152/2009	I
Ash	Samples were incinerated at 650 °C, with the mass of the remaining sample representing the ash content.	AOAC, 2000	I
<i>Starch structure</i>			
Degree of branching	¹ H NMR spectroscopy was performed on starch samples mixed with DMSO in 5-mm NMR tubes. The ¹ H spectra was recorded (Bruker Avance III 600 MHz NMR spectrometer). The	Nilsson <i>et al.</i> , 1996	I

Analysis	Description	References	Paper
Molecular weight	anomeric proton at the $\alpha(1 \rightarrow 6)$ -linkage of the branching point, which has a different chemical shift than other anomeric protons, was used for quantification of DB.	Vilaplana & Gilbert, 2010	I
Degree of polymerisation	Weight distribution (w(log Vh)) and size dependence of the weight average molecular weight (Mw(Vh)) were obtained using size exclusion chromatography (SEC).	Vilaplana & Gilbert, 2010	I
Diffraction pattern	Samples were enzymatically debranched. Size exclusion chromatography (SEC) was carried out and, using mathematical models, branch chain length distribution (w(log Xde)) was calculated. Two different methods were used: XRD : With Panalytical X'pert Pro operating at 45 kV and 44 mA, with Cu K α radiation. Diffraction patterns were recorded using a radiation wavelength of 1.54 Å. The runs were duplicated for each sample. ¹³ C CPMAS NMR Starch samples (~ 80 mg) were packed into 4 mm ZrO ₂ rotors and the CPMAS spectra were recorded at 25 °C, using a spinning frequency of 12 kHz, a contact time of 1-2 ms and a repetition delay of 2.5-5 s	Hermans & Weidinger, 1948; Özeren et al., 2020	I
Crystallinity	The crystallinity ratio was determined by the Rietveld method. Crystalline peaks were resolved from the amorphous halo and relative crystallinity was obtained as the area of the crystalline peaks divided by the total intensity area within 2 θ of 3-40°.	Rietveld, 1969	I
<i>Microstructure/morphology</i>			
Light microscopy	Using light microscope (Nikon Eclipse Ni-SSR 930151, Tokyo, Japan) for right field microscopy, DIC and polarised light. Starch granules/areas were dyed using Logulus/water solution (50% v/v). Prior to microscopy analysis, the gels were fixed with glutaraldehyde and ethanol washing.		I & II

Analysis	Description	References	Paper
Scanning electron microscopy (SEM)	SEM (Hitachi TM-1000, Tokyo, Japan) at an accelerating voltage 15 kW, with an image size of 2560 × 1920 pixels. Carbon tape with evenly distributed samples was mounted on an SEM stub and sputter coated with Au. In paper IV the cryofracture surface of films were coated with a thin layer of platinum and were examined using field emission scanning electron microscope (FESEM) ZEISS model ULTRA55 (Eindhoven, The Netherlands)		I, II, III & IV
Ingredient Functionality			
<i>Hydration</i>			
Water mobility	¹³ CPMAS and SPMAS flour mixtures with starch:protein ratio 60:40 and 90:10 were weighed out and packed into 4 mm ZrO ₂ rotors. Spinning (CPMAS) and single-pulse excitation magic angle spinning (SPMAS) were obtained using a Bruker Avance III 600 MHz spectrometer equipped with a double-resonance 4 mm (1H&19F)/(15N-31P) CPMAS probe. The CPMAS spectra were recorded with a contact time of 1-2 ms and a repetition delay of 2.5-5 s. The NMR measurements were performed at a spinning frequency of 8 kHz and at three different temperatures; first at 25 °C before heating, then at 85 °C and finally at 25 °C after cooling. The maximum temperature was set to 85 °C, due to the limits of the instrument.	Larsen <i>et al.</i> , 2013	II
Water binding capacity (g/g)	The amount of water retained by samples before heating was determined by making 12% (w/v) flour mixture-water solutions. The samples were mixed, then centrifuged, the excess water was removed and the remaining hydrated solids were weighed.	Bravo-Núñez & Gómez, 2019	II & III
Water absorption index (g/g)	Samples were weighed out and heated to different temperatures before centrifugation. The pellet was weighed and the supernatant was dried and weighed. Solid contents (Paper II 12%, Paper III 5%) Water Absorption Index (g/g) = (Pellet mass)/(Original sample mass)	(Bravo-Núñez & Gómez, 2019)	II & III
Water solubility index (g/100g)	Water solubility index (g/100g) = ((Dried supernatant)/(Original sample mass))*100	Bravo-Núñez & Gómez, 2019	II & III

Analysis	Description	References	Paper
<i>Gelatinisation</i>			
Hot-stage microscopy	A tensile-stage Linkam with heating capacity was attached to the light microscope. Samples were observed under both polarised and brightfield light. The heating rate was 5 °C/min within the range 25-95 °C.		I & II
Gelatinisation	Gelatinisation characteristics of starch thermal properties were measured using a DSC.		I
<i>Pasting</i>			
Pasting-RVA	In the RVA the pasting properties were determined at two different heating rates, 12 °C/min and 1.5 °C/min at temperature ranges 50-95-50 °C. For microscopy analysis, smears of the pastes were made on microscope slides immediately after each run.		I
Pasting-rheometer	A rheometer equipped with a Peltier pressure cell and steel starch paddle. Heating cycles, 50-95-50 °C (Paper I) and 20-95-25 °C (Paper II), heating rate 1.5 °C/min, were applied in triplicate to each starch type.		I & II
High-temperature pasting	Rheometer equipped with a Peltier pressure cell and steel starch paddle. Temperature range: 30-140-30 °C with heating rate of 1.5 °C/min (Paper I) and 20-150-25 °C with heating rate 5 °C/min (Paper II),		I & II
<i>Small-oscillation amplitude sweeps</i>			
Temperature ramp	Using a rheometer equipped with a 40-mm aluminium plate. The gelation process was monitored at constant strain and amplitude during a temperature ramp consisting of heating from 65 to 95-25 °C at a rate of 1.5 °C/min and 30 min holding time at 95 °C followed by an additional holding time of 30 min.		II

Analysis	Description	References	Paper
Frequency sweep	Increasing frequency at constant temperature and amplitude. Measures the frequency dependence of a material and predict structure	Zhang <i>et al.</i> , 2017	II
Amplitude sweep	Constant frequency and temperature with increasing amplitude to determine the linear viscoelastic region (LVR), which corresponds to the robustness of a material.	Zhang <i>et al.</i> , 2017	II & III
<i>Large deformation</i>			
Compression testing	The gels samples were compressed to 70% of their original height and freeze-dried cubes to 60% at a rate of 1 mm/s using a texture analyser (Stable Micro Systems, TA-HDi, Surrey, UK) equipped with a 500 N load cell and a 36 mm cylindrical aluminium probe. A trigger force of 0.05 N was used to initiate measurement and data collection. Due to the weak nature of the 60:40 gels, a trigger force of 0.01 N was used to reduce the compression of these gels occurring before data collection started. For freeze-dried 3D-printed samples, the compression tests were performed in two directions, with the infill pattern facing upwards and sideways.	Johansson <i>et al.</i> , 2021	II & III
<i>Analysis of food model properties</i>			
Colour	Cube and film colour was measured with L*a*b colour space using a colorimeter.		III & IV
Solubility	The films were dried at 105 °C to constant weight. Dried film was placed in a test-tube with 10 mL distilled water, with the tubes and contents periodically stirred for 24 h at 25 °C. The non-solubilised matter was dried and solubility was calculated.	Masamba <i>et al.</i> , 2016	IV
Film thickness	The thickness of the FBP films was determined at 10 random points around each film sample, using a manual micrometre with 0.001 mm sensitivity.		IV

Analysis	Description	References	Paper
Thermogravimetric analysis	Samples with a total weight between 8 and 10 mg were placed in an alumina crucible (70 μ L) and heated from 30 to 800 $^{\circ}$ C at a constant heating rate of 10 $^{\circ}$ C/min under nitrogen atmosphere (flow rate 50 mL min/L)		IV
Tensile stretching	Preconditioned FBP films were cut into rectangular strips (30 \times 4 mm ²) and placed between the tensile grips. The initial grip distance was set at 15 mm and the crosshead speed at 5 mm min/L. At least five specimens of each film were tested at room temperature and the average results were obtained.	ASTM D882-02,	IV
Transparency	Preconditioned film specimens were cut into rectangles and directly placed in the spectrophotometer cell, transmittance of light at 600 nm	ASTM D1746	IV
Oxygen transmission rate	The area of measurement of the samples was 5 cm ² and the OTR measurements were performed at 23 $^{\circ}$ C and 50% RH using an OTR Permeation Analyzer Mocon. Before the analysis, the samples were conditioned for 2 days at 23 $^{\circ}$ C and 50% RH.	ASTM F1307-20	IV
Water vapour permeability	Conditioned circular films were sealed on permeability cups containing 2 g of CaCl ₂ (0% RH) with an exposed area of 10 cm ² . The cups were placed in a desiccator at 25 \pm 1 $^{\circ}$ C containing a saturated Mg(NO ₃) \cdot 6H ₂ O solution to reach a relative humidity of 54% \pm 3%. The cups were weighed each hour for a total period of 8 h using an analytical balance. The changes in cup weight were plotted as a function of time and the slope was calculated by linear regression.	ASTM E96-95	IV
ATR-FTIR	Each sample was subjected to 20 scans between 4000 and 600 cm/L with resolution of 4 cm/L by attenuated total reflection method (ATR) in an infrared spectrometer. After attenuation of total reflectance and baseline correction, spectra were normalised with a limit ordinate of 1.5 absorbance units.		IV

5. Results and Discussion (Papers I-IV)

In the work presented in this thesis, different fractions isolated from faba bean were combined to create different food matrices that could be used to produce different food textures.

The simpler food systems are discussed first in this chapter, and then the samples with increasing level of compositional complexity. This sequence of results provides a fundamental understanding of physiochemical and structural factors influencing the functional properties of the materials produced and the mechanism/s. As the complexity of samples increased, the number of factors that could influence the behaviour, structure and texture of the resulting food matrix also increased.

5.1 Chemical composition and structure of faba bean starch

Purity, molecular structure, swelling intensity and concentration of starch were identified as key factors influencing the structural effect of starch in different matrices.

5.1.1 Starch composition and molecular structure

In Paper I, starches from faba bean cotyledon and hull were compared with commercial wheat starch. The isolated hull starch was actually not from the hull, but from the outer layers of the cotyledon that were only peeled away during machine de-hulling. This was verified by the hull starch content being 0% when hand-peeled and 19% when machine-peeled. The chemical composition was the main difference between the cotyledon and hull rich-

starch fraction that influenced the starch behaviour during gelatinisation and pasting.

Chemical composition

The faba bean hull starch-rich fraction was the least pure, containing the highest proportions of protein, fat and ash. The amylose and resistant starch content were both significantly higher for the hull (amylose 36%, resistant starch 13%) followed by the cotyledon (amylose 32%, resistant starch 6.7%) and lastly the wheat (amylose 21%, resistant starch 0.5%). The chemical composition of the different starches is summarised in Table 1 in Paper I.

Structure

Differences between the botanically different starches (faba bean and wheat) were largely attributable to differences in their molecular structure and granular morphology.

The chain length distribution of amylopectin and amylose (cut-off at 100) is shown in Figure 3 in Paper I. The degree of polymerisation (DP) distribution was very similar for the faba bean starches isolated from the cotyledon and hull, both for the shorter-chain amylopectin and longer-chain amylose. In comparison, wheat starch had a higher prevalence of very short-chain and short-chain amylopectin. The faba bean starches had a bimodal branch chain distribution for amylopectin, with two populations centred around DP 700 and DP 2500, with longer branch chains being slightly more abundant. Amylose chain distribution in the wheat starch had a larger abundance of shorter chains.

Starch granules from faba bean starch cotyledon, hull and wheat are depicted in Figure 9. The faba bean starches were relatively similar, with a homogenous population with an oval shape and average length of ~21-23 μm , as measured using image analysis. The wheat starch granules were more heterogeneous, with two sizes for the disc-shaped populations with average length of 20 μm (A granules) and 7 μm (B granules).

5.2 Ingredient functionality and physical behaviour

5.2.1 Hydration-related properties

Although water is not a component extracted from faba bean, it was an important ingredient incorporated into all the different food matrices studied in this thesis. Water often acts as a plasticiser, influencing many of the mechanical properties of the food matrix (Blahovec, 2007). The effect of the water is dependent on how it binds with the components.

Table 3 shows the combined calculated hydration values from Papers II and III. What was referred to as swelling power in Paper III was calculated in the same manner as the water absorption index in Paper II. Using the raw data from Paper III, the different hydration values were recalculated using the same equations as in Paper II (equations 1 and 2). Although the hydration analysis was performed using different solids contents and methodology, a trend for improved water-binding ability with increasing temperature was observed for all samples. Negative water-binding capacity of the protein was observed at 20 °C, presumably because the protein dissolved in the water and was decanted with the supernatant. At all temperatures, the water solubility index of the protein was higher for starch than for fibre.

For starch, water binding/absorption was highest at 95 °C and lowest at room temperature. The enhanced water absorption abilities of the starch at higher temperatures could be because of starch gelatinisation, which started at 67 °C. At 60 °C, fibre was the component that bound most water and would presumably also have bound most water if heated to 95 °C as in Paper II.

The relatively high water-binding ability of faba bean fibre may be related to the relatively high proportion of hydrophilic polysaccharides (28%) (Johansson *et al.*, 2022) in relation to the hydrophobic lignin fraction (1%) (Johansson *et al.*, 2022; Bell & Shires, 1982). Other factors improving the water-binding abilities of legume fibres are high amounts of insoluble fibre and increased surface area and pore size of the fibre (Tiwari & Cummins, 2020). The ability of fibres to trap, *i.e.* consequentially bind, water has been correlated with an increase in particle size (Chaplin, 2003).

Table 3. Calculated hydration values obtained in Papers II and III for different faba bean components at different temperatures

Temperature	20 °C		60 °C		95 °C	
Paper	II		III		II	
Measurement	WBC (g/g) ¹	WAI (g/g) ²	WSI (100g/g) ³	WAI (g/g) ²	WSI (100g/g) ³	
Flour	NA	2.3±0.0	31.8±0.1	NA	NA	
Starch	1.4±0.0	3.7±0.0	2.0±0.1	11.7±0.4	2.5±0.1	
Protein	-0.4±0.1	1.1±0.1	84.1±0.1	2.5±0.2	73.6±1.8	
Fibre	NA	12.1±1.2	0.5±0.1	NA	NA	

¹Water-binding capacity, ²water absorption index, ³water solubility index.

5.2.2 Starch gelatinisation and granular swelling

During gelatinisation, starch goes from an ordered to a disordered state. In Paper I, it was observed that gelatinisation temperature, as determined by DSC (Table 3 in Paper I) coincided well with granule swelling, as estimated by hot-stage microscopy (Figure 7 in Paper I). Temperatures at which gelatinisation started were as follows: cotyledon 67 °C, Hull 70 °C and wheat 58 °C. Figure 9 shows the progressive swelling of starch granules at 30 °C, 67 °C (onset of cotyledon starch gelatinisation), 73 °C (end-set of cotyledon starch gelatinisation) and 90 °C. Figure 10 shows the length and width population distribution of the starch granules at 30 °C and at temperatures around the gelatinisation point of cotyledon starch (60, 65 and 70 °C). At higher temperatures (>75 °C), the average size of granules could not be calculated because of particles overlapping.

Hull starch, with the highest amylose content, was most heat-stable, followed by cotyledon and finally wheat. There was a strong correlation between gelatinisation temperature and amylose content ($r = 0.99$; $p < 0.01$). Amylose is known to have a stabilising effect on granules, which retards swelling and thereby delays gelatinisation (Tester & Morrison, 1990).

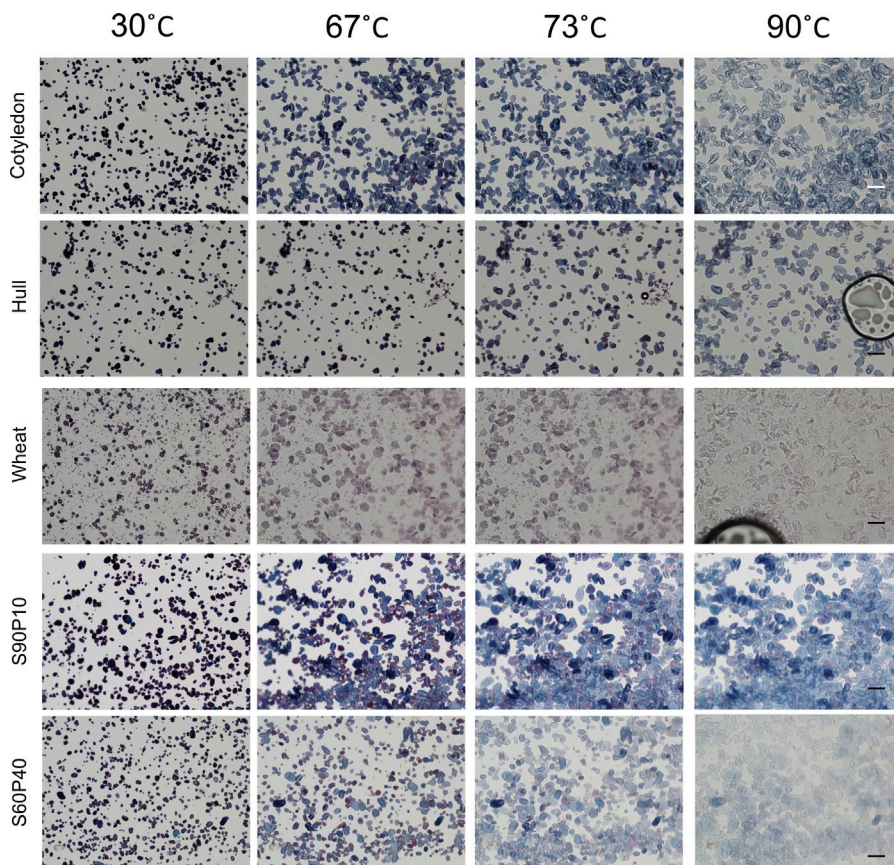


Figure 9. Starch granules at different temperatures in Paper I (cotyledon, hull, wheat) and Paper II (S90P10, S60P40). In Paper I, hull starch had the lowest degree of swelling, associated with the amylose content and long starch chains. In Paper II, samples with higher protein content (S60P40) showed tendencies for retarded swelling and more iodine discolouration. Scale bar = 100 μ m.

A high prevalence of short-chain amylopectin was negatively correlated with gelatinisation temperature ($r = -0.97$; $p < 0.01$). The high abundance of very short-chain amylopectin in the wheat starch may have lowered the gelatinisation temperature, as this type of amylopectin causes crystalline defects. Crystallite quality is reflected in the gelatinisation temperature of starch (Cai *et al.*, 2014; Tester & Morrison, 1990). In addition, the narrower temperature and enthalpy range for the faba bean starches (see table 3, Paper I) in comparison with wheat starch could have been due to the more

homogenous size distribution of the faba bean starch granules (Singh *et al.*, 2003).

Comparison of granular swelling of the different starch/protein mixtures in Paper II indicated a reduced rate of swelling of the starch granules in the more protein-rich samples (Figure 10). More pronounced colour loss was observed for the sample with a higher protein content (S60P40, see micrographs in Figure 9). Possible explanations for the discolouration of the starch mixtures in Paper II are that the protein prevented the iodine from re-forming iodine-starch complexes after gelatinisation, either by binding to the iodine, making it unavailable, or by physically blocking the iodine from forming complexes with the starch. The discolouration observed for the wheat starch in Paper I at 90 °C was likely not caused by competition for iodine, as no protein was added to the mixture and the protein content of the wheat was 0.2%. It is possible that the colour loss was caused by the iodine-starch complex decomposing at higher temperatures (Fonslick & Khan, 1989).

Water mobility

In Paper II, water mobility and hydration of starch at 25 °C before heating, at 85 °C, and at 25 °C after heating were compared using ¹³C CPMAS NMR. The gelatinisation values of the starch and granular swelling curve had already indicated that structural and morphological changes occurred in the starch during heating in excess water. The NMR data showed that hydration was slightly less efficient in the higher-protein samples (S60P40 vs S90P10) (see Figure 3 in Paper II). Less efficient hydration of the samples with higher protein content could perhaps explain why there was reduced granular swelling and iodine affinity for these samples. In Paper I, the higher presence of protein in the hull starch (2.8%) compared with cotyledon starch (0.6%) could be an additional factor that delayed gelatinisation and granular swelling.

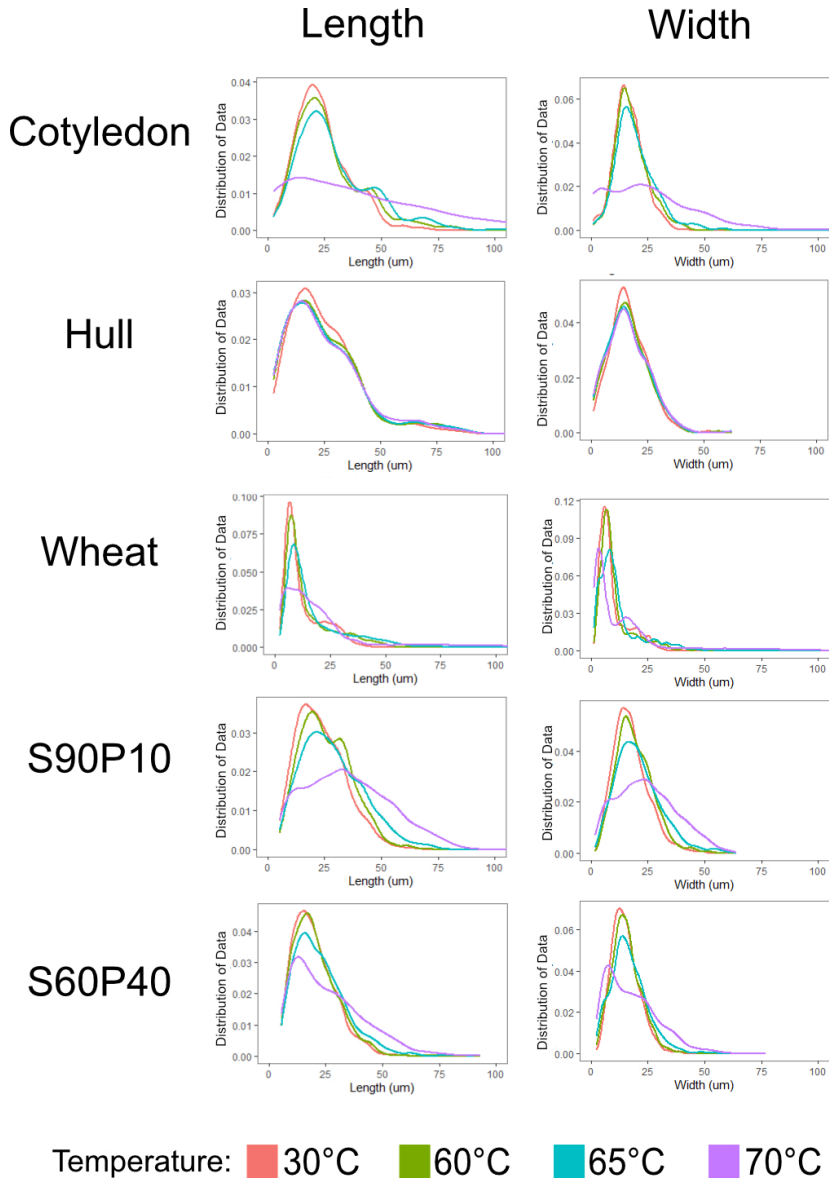


Figure 10. Density diagrams of starch granular swelling at different temperatures 30, 60, 65 and 70 °C, where the x-axis shows measured length/width and the y-axis the population distribution of the granules. The cotyledon, hull and wheat samples are from Paper I, samples S90P10 and S60P40 are from Paper II. For all samples, granules increased in length and width as the temperature increased.

5.2.3 Pasting

Pasting at 95 °C

The results of pasting (Papers I and II) showed that heating the samples to 95 °C was not sufficient to achieve peak viscosity (Figure 11). In Paper I (Figure 11a) cotyledon starch had the highest final viscosity, followed by hull starch, and wheat starch had the lowest final viscosity. Factors influencing pasting properties were the size of the granules, amylose/amylopectin ratio, degree of polymerisation, heating rate and temperature range. The higher viscosity of the faba bean starch compared with the botanically different wheat can be attributed to the longer amylose and amylopectin chains present in the faba bean starches (Li *et al.*, 2020). High abundance of very short amylopectin chains (DP <6) was negatively correlated with relative viscosity ($r = -0.97$; $p < 0.01$). Higher degree of polymerisation has been found to increase aggregation viscosity because of increased interaction between the chains (Li *et al.*, 2020).

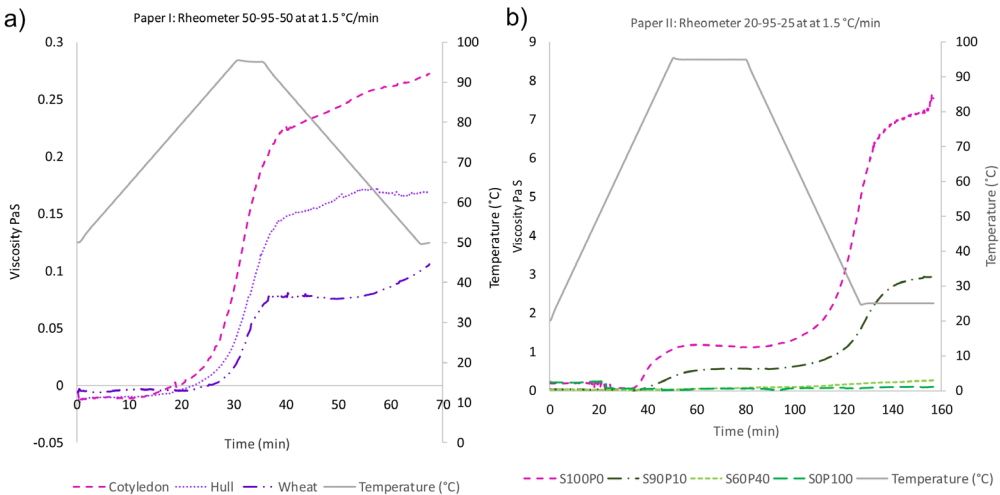


Figure 11. Pasting graph (measured by rheometer) from Paper I (a) and Paper II (b). Note that the slightly different temperature ranges and concentrations may have influenced the pasting curves. Cotyledon and S100P0 are pure cotyledon starch pastes with 8% solids content (final viscosity 0.27 PaS) and 12% solids content (final viscosity 7.3 PaS), respectively (pink line). Peak viscosity was not detected for any sample.

The larger average size of the swollen faba bean granules compared with wheat (see Figure 9) was another factor which could partly explain the higher viscosity, showing a strong correlation ($r = 0.73$; $p < 0.03$) (Bajaj *et al.*, 2018; Cornejo-Ramírez *et al.*, 2018; Sandeep *et al.*, 2010). Heating the same starch type at 12 °C/min in the RVA produced granules that were on average 1.3 times larger than when the heating rate was 1.5 °C/min (see Figure 9 in Paper I). The final viscosity with high-temperature heating was on average 2.2 times greater than with low-temperature heating in the RVA and 5.9 times greater than with low-temperature heating in the rheometer (see Figure 8 in Paper I).

The overall higher starch content in the fraction extracted from the cotyledon (96%) compared with the hull (94%) could be another reason for the higher viscosity. In Paper II, samples with a higher starch content were the most viscous (see Figure 11b). Samples with a higher starch content started to thicken at lower temperatures than samples with a higher protein content. The pure starch sample in Paper II had a pasting temperature of 73 °C. When the starch:protein ratio was 90:10, the pasting temperature increased to 78 °C and for samples with a ratio of 60:40 the pasting temperature was 90 °C. Higher protein content in starch:protein gels has previously been associated with augmented pasting temperature and reduced gel firmness (Bravo-Núñez *et al.*, 2019; Joshi *et al.*, 2014; Núñez-Santiago *et al.*, 2004; Oñate Narciso & Brennan, 2018; Onwulata *et al.*, 2014; Ribotta *et al.*, 2007; Yang *et al.*, 2004). In lentil starch:protein mixtures, delayed pasting associated with protein incorporation has been related to the overall higher denaturation temperature of the protein, which is essential for heat-induced gelation (Joshi *et al.*, 2014). For the pure protein samples in Paper II, no pasting temperature was detected (during heating and stirring), which may have been because the solids content (12%) was below the minimum gelling concentration of faba bean protein (14%) (Fernández-Quintela *et al.*, 1997). In addition, the constant stirring may have disrupted the protein network required for gel formation.

Interestingly, the solids content of pure starch samples also influenced the initial pasting temperature. In Paper I, when the solids content was 8% pasting of the cotyledon starch was initiated at 77 °C, while in Paper II the equivalent pure starch mixture with a higher solids content of 12% had a lower pasting temperature of 73 °C (see pink line in Figure 11).

The initial increase in viscosity during pasting is mainly caused by starch granules swelling, resulting in close packing of the granules (Dhillon & Seetharaman, 2011; Eliasson, 1986). At a higher solids content, the swollen granules come in contact earlier, increasing the viscosity and thereby effectively decreasing the pasting temperature.

5.2.4 High temperature pasting

Figure 12 shows the high-temperature pasting curves for the three different starches studied in Paper I (a) and the starch protein mixtures studied in Paper II (b). In Paper I, cotyledon starch had the highest peak viscosity, which was achieved at 119 °C. Peak viscosity of the slightly less pure hull starch was somewhat lower, but was attained at a slightly higher temperature (121 °C). There were two peaks for the wheat starch, with the first at 104 °C, reflecting melting of the amylopectin, and the second at 132 °C, reflecting melting of the amylose-lipid complex (Ahuja *et al.*, 2020; Richardson *et al.*, 2004).

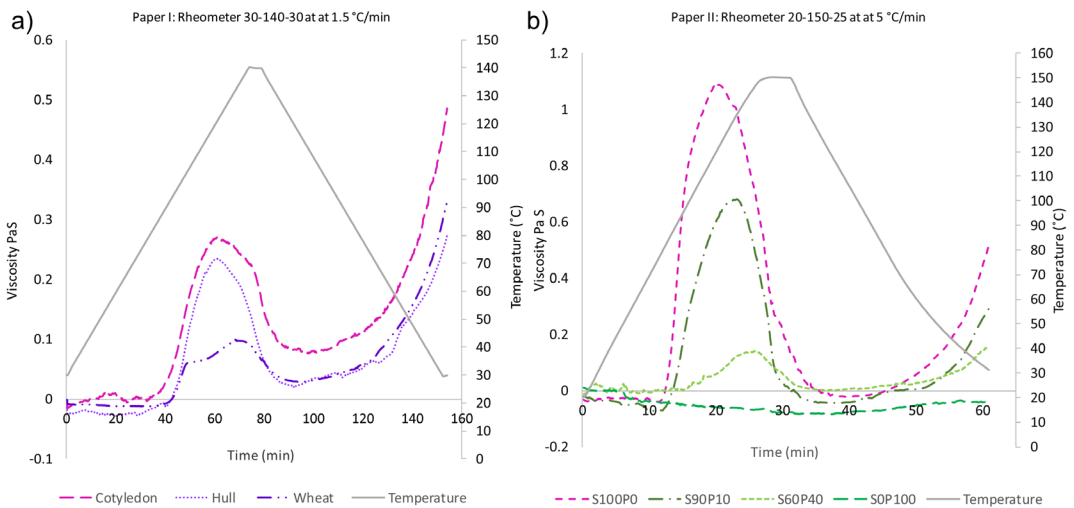


Figure 12. High-temperature pasting curves from Paper I (a) and Paper II (b). Note that the slightly different temperature ranges, heating rates and concentrations may have influenced the pasting curves. Pink line is cotyledon and S100P0 are essentially both pure cotyledon starch pastes, with 8% and 12% solids content, respectively. Peak viscosity was achieved for all samples.

In Paper II, the mixtures containing more starch had a higher peak viscosity, achieved at lower temperatures. In Paper I, the peak viscosity for the cotyledon starch was 0.27 PaS and in Paper II the peak viscosity for the equivalent pure starch mixture was 1.11 PaS. Both the higher solids content (12% vs. 8%) and the slightly higher heating rate (5 °C/min vs. 1.5 °C/min) in the analysis in Paper II could be the reason for the higher peak viscosity.

During pasting, peak viscosity reflects maximum granular swelling and viscosity decreases as the granules rupture. The difference between maximum viscosity and minimum peak viscosity is called viscosity breakdown. In Paper II (Figure 12b), minimum viscosity was similar for the samples, regardless of starch:protein ratio, resulting in breakdown viscosity being higher overall for samples with the highest peak viscosity values. In contrast, in Paper I (Figure 12a), minimum viscosity occurred at a slightly higher value (*i.e.* at a higher viscosity) for the cotyledon starch compared with the hull and wheat starch. Better maintained viscosity during heating and cooling may suggest more molecular entanglements of the paste (Onwulata *et al.*, 2014). Another possible explanation for the somewhat higher minimum viscosity of the cotyledon starch in Paper I compared with Paper II could be the lower solids content, and therefore less granular contact, which may have reduced the prevalence of the granules rupturing. The slightly lower maximum temperature (140 °C vs. 150 °C) in Paper I might also have caused less granular rupture. Better-maintained starch granules in the cotyledon starch in Paper I could potentially explain why the final viscosity for the two pure starch samples was similar (0.48 PaS vs. 0.5 PaS for the pure starch paste in Papers I and II, respectively) despite different starch concentrations (8% and 12%, respectively).

5.2.5 Rheological properties of systems

Small deformations: gelation and frequency sweep

For the starch protein composite gels examined in Paper II, viscosity of the system increased in line with the starch content (Figure 7a in Paper II). The softening effect of the protein on the starch system could be due to changes in gel microstructure and differing hydration properties, as discussed earlier. The mixtures with a higher ratio of protein were also more frequency-dependent, indicating a weakened gel structure with more viscous properties

(Figure 8 in Paper II). Similar behaviour was observed by Joshi *et al.* (2014) for lentil starch:protein gels.

Amplitude sweep

The gels studied in Paper II and the inks studied in Paper III can both be classed as soft solids. The results from the amplitude sweeps in both studies are shown in Figure 13.

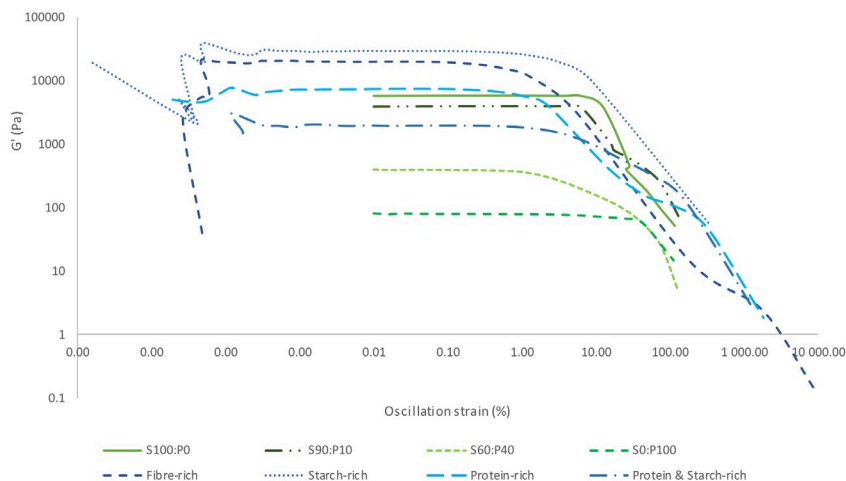


Figure 13. Amplitude sweeps of the different starch:protein mixtures in Paper II (green lines) and the inks in Paper III (blue lines).

By measuring the length of the linear viscoelastic region (LVR), amplitude sweeps show the robustness of a material. The overall higher solids content of the inks in Paper III (23-38%) compared with the gels in Paper II (12%) is a likely reason for the higher storage modulus. For solutions with xanthan gum and scleroglucan, increasing hydrocolloid concentration also increases both moduli in amplitude and frequency sweeps (Li *et al.*, 2022). During ink production in Paper III, the samples were heated to 60 °C, which is a temperature below that of both starch gelatinisation and pasting and protein gelation. The G' of the samples might have been even higher if the inks had been heated to 95 °C during production, as this could induce gel formation of the starch, fibre and protein fractions. Johansson *et al.* (2022) found that mixed faba bean protein continuous gels only started to gel at temperatures above 75-80 °C.

In both Papers II and III, the samples with the highest starch content in relation to other samples within the same study had the highest G' , indicating that they were most solid-like. The abrupt endpoint for the LVR in the pure starch gels in Paper II indicates that the starch formed a stable but brittle gel (see Figure 13) and observations during the printing in the lab. Despite the pure protein gels having the lowest G' , the LVR was relatively long and narrow, which could indicate more stable gel (Hodder, 2021). This long LVR may be the result of the more homogenous particle size distribution within pure protein composite gels (Hodder, 2021). If the solids content of the gels had been higher, the viscosity would presumably have been higher and the LVR even longer, because of a more close-knit network (Dhillon & Seetharaman, 2011).

In Paper III, the ink without any fibre (protein- & starch-rich) was the most viscous-like, with the highest $\tan \delta$ values (see Table 3 in Paper III). The sloping LVR curve of the protein- & starch-rich samples further supports the suggestion that protein may have a softening effect that weakened the overall viscoelastic structure. The protein-rich ink contained a similar amount of protein, but the carbohydrate portion comprised a mixture of starch and fibre. Compared with the protein- & starch-rich ink, the protein-rich ink was more solid-like, with higher G' and lower $\tan \delta$ value, showing the important stabilising effect of fibre on the inks. The protein-rich ink had a lower yield stress with a more abrupt ending, indicating a more brittle gel. It is possible that incorporation of fibre in the starch:protein gels studied in Paper II could also have increased gel stability in gels with a higher protein content.

5.2.6 Large deformation: Compression testing

The structure stability of faba bean products was evaluated using compression tests (see Figure 14). Large deformation compression tests using a texture analyser were performed in Papers II (Figure 14a) and III (Figure 14b). The samples studied in Paper II were gels, classed as soft solids, while those in Paper III were much harder, as they had been freeze-dried.

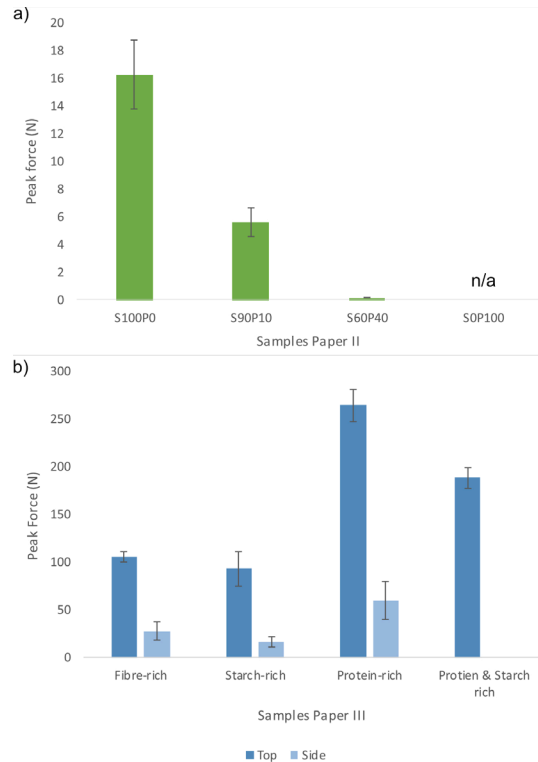


Figure 14. Peak force required in compression testing of soft solids gels in Paper II (a) (green bars) and hard solids 3D-printed cubes in Paper III (b) (blue bars). Due to sample discrepancies measurement data is missing in both graphs; in Paper II no free standing gel was created for sample S0P100 and in Paper III the cubes Protein & starch rich had concaved walls so samples were not compressed on the side because of compression surface not being flat.

The gels followed the rheological pattern of more starch inducing a more stable and harder gel (Figure 14a). This stabilising effect of the starch could be because of the more closely packed starch system, as observed in light micrographs, and a more developed and fibrous network, as seen in scanning electron micrographs (SEM) (Figure 15). In the light microscopy images, the starch appeared to be the continuous phase for all gels. However, when the protein content was 30-40%, areas within the gels appear to contain clusters of amylose and/or protein aggregation, creating inhomogeneities within the gel (Figure 15). Thus, it is possible that the higher content of protein perturbed gel network development of the starch. Because of incompatibility,

polysaccharide-protein mixtures are known to create water-in-water emulsions (Wolf, 2013). The immiscibility of the components may increase due to factors such as increased molecular weight, ordering/ aggregation, increased ionic strength, cooling and/or pH (Wolf, 2013).

Proteins have previously been suggested to interfere with network development and limit the hydrogen bonding between starch chains, which could result in a less fibrous and more compact network (Ribotta *et al.*, 2007; Tanger *et al.*, 2022). In SEM images, the fibrous starch network appeared less developed with increasing protein content. Johansson *et al.* (2022) found that for faba bean gels with protein as the continuous phase, addition of starch and/or fibre to the system weakened the gel, presumably because of more structural inhomogeneity.

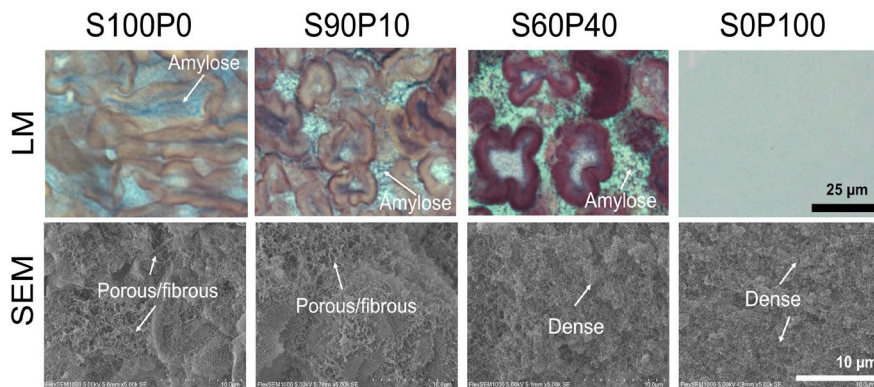


Figure 15. Light microscopy (LM) and scanning electron microscopy (SEM) images of starch:protein gels in Paper II. Examples of regions with porous and dense network structures are highlighted with arrows.

Interestingly, for the freeze-dried samples in Paper III, samples with a higher protein content were the hardest, indicated by compression testing (Figure 14b). During amplitude sweeps of the corresponding inks, those with higher protein content appeared to be less stable indicated by the LVR (Figure 13). The porous and more fibrous network of the carbohydrate-rich samples when dried (Figure 16) may be the reason for the lighter, airier texture, requiring less force during compression (see Figure 14b). Similarly, Lille *et al.* (2018) observed that the hardness of 3D-printed crackers decreased when some of the semi-skimmed milk powder used was replaced with cellulose nano-fibres.

Another indication that sample porosity influences perceived hardness is that compressing samples from the side required less force than when samples were compressed from the top (Figure 14b). During top compression, the different layers were directly stacked on top, further indicating that a more compact structure for hard solids results in a harder texture.

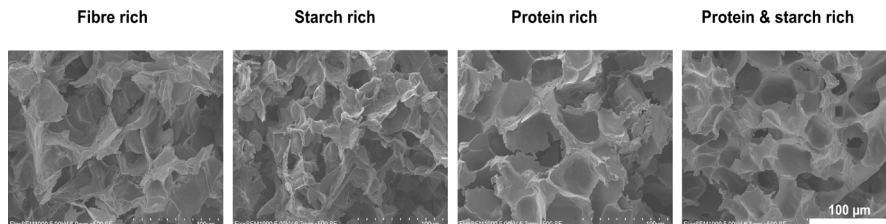


Figure 16. Scanning electron micrographs of the fracture surface of the freeze-dried cubes in Paper III. The fibre-rich and starch-rich samples appeared to have a more perforated irregular structure compared with the protein and protein- & starch-rich samples.

5.3 Food model products

In Papers III and IV, two potential food products were developed; a 3D-printed freeze-dried cracker-like product and an edible protein film. However, it can be argued that in all four papers in this thesis, the use of the faba bean-rich component fractions in potential food products was investigated. Depending on the end-product, different product properties will be desirable and prioritised.

5.3.1 Faba bean starch

Faba bean starch formed very viscous pastes with a much higher final viscosity than wheat starch pastes. The higher prevalence of long starch chains, larger granules and relatively high amylose content were contributing factors to the higher viscosity shown by the faba bean starch. Gelatinisation for faba bean starch occurred at slightly higher temperatures than in wheat starch, due to the higher amylose content. These results show that faba bean starch has good potential for use as a thickener. If faba bean replaces cereal starch in a product, the amount of starch and temperature during processing may need to be adjusted to minimise textural differences because of the higher thickening power of legume starch.

5.3.2 Starch:protein faba bean gels

Gels with a higher ratio of starch were firmer and more brittle. According to Yang *et al.* (2004), the softening effect of protein in mixed gels could be reduced by increasing the overall solids content. Much of the stability of faba bean starch-rich gels is believed to come from the closely packed granules and amylose layers between the granules, both of which are perturbed by aggregating pockets of protein.

The desirable properties of a gel are dependent on the type of food into which they are incorporated and the texture consumers expect. If a product requires a firm, stable gel, then a starch-rich gel may be desirable. However, if the gelled product should be pourable, thus having lower yield stress, more protein in the gel may be preferred.

5.3.3 3D-food products

The different cracker prototypes (cubes) created in Paper III were easily distinguishable depending on product composition (Figure 17). In terms of appearance, the carbohydrate-rich cubes were lighter in colour, more uniform and had distinct layers. The carbohydrate-rich cubes required less force to compress (Figure 14b) than the cubes with a higher protein content, which could be attributed to the more porous network seen in the micrographs (Figure 16). A finding further supporting this structure-texture relationship is that compressing the cubes with the infill pattern facing the side (*i.e.* along the porous pattern) required less force than compressing the cubes with the pattern infill pattern facing the top, so the printing layers were directly stacked (see Figure 14b and Figure 17).

The samples without fibre (protein- & starch-rich cubes) were the most challenging to print, with around 25% of the printed cubes having to be discarded due to faults. In contrast, the fibre-rich cubes were the easiest to print, as none needed to be discarded. For the other two sample types (protein-rich cubes and starch-rich cubes), 5% of the cubes needed to be discarded due to faults. Therefore, fibre appeared to impart structural stability to the cubes, facilitating 3D-printing. Having high wastage because of inconsistencies in products would be inefficient and costly for a food product developer.

In taste tests on the 3D-printed cubes in the laboratory, the carbohydrate-rich cubes were preferred because of their more neutral flavour and lighter

texture. A more structured and rigorous sensory and consumer study evaluating the different cubes would be needed to determine which cube type is most liked and which attributes are the greatest contributing factors.

It could be argued that the protein- & starch-rich cubes had the smallest potential to be a successful food product, due to inconsistencies in printing and the overall less preferred texture and flavour of the cubes with higher protein. The positive nutritional effects of legume fibre, such as improving glycaemic index, lowering blood lipids and improving gut health (Tiwari & Cummins, 2020) can further strengthen the argument for fibre incorporation into food products.

Through 3D-printing, a range of products tailored to specific consumer groups can be achieved. However, the relatively high price and slow production of 3D-printed foods may hinder the development and production process. In addition, freeze-drying is one of the costliest methods to dehydrate products, so investigating the effect of alternative dehydration methods on product texture could be interesting. However, if good quality, nutritious, tailor-made, well-liked products with minimal production waste can be produced, 3D-printing of food is definitely a production method for the future.

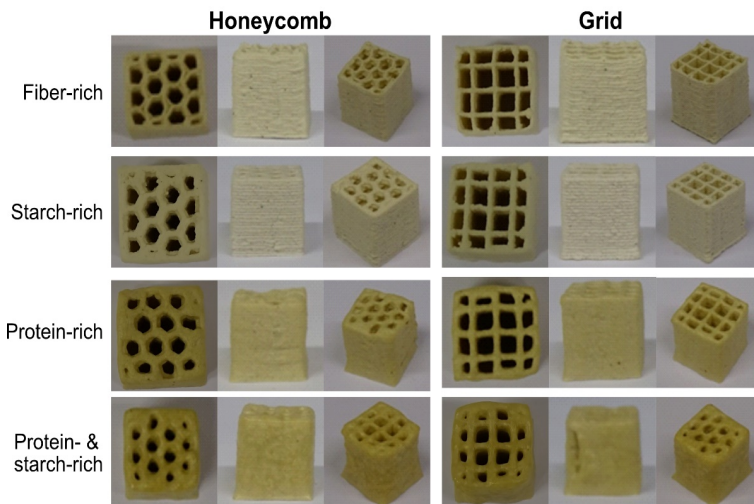


Figure 17. Different types of 3D-printed cubes obtained in Paper III, cubes are shown from different directions. The first column of each pattern type shows infill pattern facing the side and the second column with infill pattern facing the top of the cube. The cube placements correspond to the placement-direction of the cubes in the texture analyzer for the compression testing, i.e. side and top

5.3.4 Protein films

In Paper IV, edible faba bean protein-based films reinforced with different amounts of pine cone cellulose nanocrystals (CNC) were produced (Figure 18). The spectra obtained in FTIR analysis (Figure 3 in Paper IV) suggested that films with a higher content of CNC added had more intramolecular interactions, consisting mainly of hydrogen bonds between the amino and carboxyl groups of the protein and the hydroxyl groups of the CNCs. This resulted in more compact films, with reduced chain mobility (Shabanpour *et al.*, 2018). The increase in hydrogen bonding within the film matrix can also be attributable to higher thermal stability (Osorio-Ruiz *et al.*, 2019) of the CNC-rich films (Qazanfarzadeh & Kadivar, 2016), which effectively reduced the water solubility.



Figure 18. Macroscopic aspects of edible faba bean protein-based films with different amounts of pinecone cellulose nanocrystals (CNC).

As the CNC concentration increased in the films, the cross-sectional roughness also increased (Figure 4 in Paper IV). In addition, the size and number of surface pores declined with CNC incorporation, providing further evidence of a higher number of intramolecular bonds (Osorio-Ruiz *et al.*, 2019). The formation of CNC aggregates within the films led to a reduction in lightness and slight increase in brown colour. Both the transparency and the transmittance also declined with increasing CNC incorporation,

presumably as a result of formation of CNC aggregates (Qazanfarzadeh & Kadivar, 2016; Shabanpour *et al.*, 2018).

Higher structural density of the high-CNC film matrix could partly explain the improved barrier properties (oxygen and water transmission) of the films with higher incorporation of CNC, as the permeability decreased. The control film was the most ductile, and even at only 1% and 3% CNC incorporation the ductility of the films decreased. The higher stiffness in the CNC film could be explained by increased hydrogen bonding, as reported by others (Gonzalez & Igarzabal, 2015; Shabanpour *et al.*, 2018; Sukyai *et al.*, 2018). The tensile strength of the films improved when 5% or 7% CNC was incorporated.

The films produced in Paper IV were intended as prototypes for food packaging. The main task of food packaging is to protect and preserve the food encased by the packaging material. Plastic made from fossil fuels is a commonly used food packaging material, thanks to its good barrier properties to oxygen and aroma compounds and high tensile strength and tear strength (Jabeen *et al.*, 2015). Drawbacks of plastic packaging include very low water vapour transmission rate and the major disadvantage that it is non-biodegradable. When using renewable resources to produce biodegradable packaging material, it is important that the protective and preservative properties are maintained. The results in Paper IV showed that reinforcing faba bean films with CNC can successfully produce a film or coating that could be used as a biodegradable packaging material. Higher incorporation rates of CNC, of around 7%, would be most desirable because of the increased barrier properties and tensile strength and reduction in UV-transmittance. To adhere to government incentives, meet consumer demands and reduce climate impacts, Swedish food companies are already choosing to replace transparent plastic with paper packaging with a picture of the product instead (Jari Kotiaho, personal communication, May 6, 2022). Thus, with consumer attitude shifting towards prioritising biodegradability over packaging transparency, the drawbacks of the darker, more opaque and browner colour of the CNC-rich films may be overlooked.

6. Conclusions

This thesis examined the functionality of faba bean components (starch, proteins and fibre) and their effect on texture in different types of food matrices, as a critical step in the development of novel plant-based foods. The key findings were that:

- Higher starch purity, amylose content, degree of polymerisation, granule size and concentration appeared to increase overall pasting viscosity and lower associated pasting temperature.
- Higher protein content in continuous starch gels caused the amylose and protein to aggregate into separate clusters. Higher heterogeneity of gels with a higher protein content seemed to be a weakening factor.
- Fibre appeared to have a stabilising effect in mixed faba bean paste-like systems, most likely due to the water retention properties of fibre.
- The structural role of faba bean components and their effect on texture depended on the water content of the products. The components influence on perceived hardness differed between soft and hard solids.
- Faba bean fractions can be combined to produce bio-inks suitable for 3D-printing. Equal amounts of the starch, protein and fibre components produced the most stable inks with the most successful printability.
- Addition of CNC to edible protein films created from faba bean made the films stronger, less ductile, more thermally resistant, better barrier properties and more opaque.

These results show that texture of faba bean products can be tailored by controlling the amount of specific components in the food system, emphasising the importance of knowledge of the functionality and synergetic properties of faba bean components when seeking to develop texturised food products.

7. Future perspectives

This thesis showed that faba bean components have different functionalities which change depending on the structure and composition of the food matrix. To use faba bean as a textural ingredient and develop novel faba bean-based products, more knowledge on the structure-texture relationship is required.

In the work described in this thesis, the extraction sequence protein, starch, fibre was chosen, because this gave the highest yield of the components without causing apparent alterations to isolates. When protein was the last component isolated in multicomponent extractions, it turned black. Future studies should investigate the reasons why faba bean protein turns black during certain isolation methods and how the fractionation methods used for components influence their functionality. To increase the efficiency of the bio-refinery process, the effects of fractionation methods on component yield and purity should also be investigated

A surprising finding in this thesis was that addition of protein increased the discolouration of starch dyed with iodine upon heating. Further research into how protein affects the iodine-starch complex could perhaps help describe the interaction between starch and protein in mixed systems. It could be interesting to study whether fibre has an effect on the iodine affinity of faba bean starch.

Compression test results showed that proteins had a softening effect in soft solids and a hardening effect in hard dried 3D-cubes. Better knowledge of the structural and textural role of components depending on the water content of the system is needed for the development of novel food products with specific textures. The effect of the drying process, *i.e.* hot-air drying and freeze-drying, on product texture could also be compared, as the dry products would have a similar moisture content, but a different structure.

Flavour and nutrition are two very important parameters of food, and thus investigating on the correlation between product structure/texture and flavour release and nutrient bioavailability could be interesting. Off-flavours and anti-nutrients are limiting factors for the development of faba bean products, so tracking these undesirable components throughout the development/production of a faba bean product could be useful in identifying processing procedures and structures that promote or mitigate the undesirable components.

In Paper IV in this thesis, cellulose nanocrystals were extracted from pine cones, but faba bean hull is also rich in cellulose. Therefore, it could be interesting to isolate CNC from the hull and incorporate it into faba bean products. This could add value to the hull fraction and reduce waste, as more of the faba bean would be used.

Only one variety of faba bean (var. 'Gloria') was investigated in this thesis. A comparison of the composition and functional properties of the components in common varieties of faba bean could be useful for developing a better overview of use of this crop as a texturising ingredient.

There are multitude of directions that future research could choose mirroring the complexity of multicomponent systems.

8. What is a sustainable faba bean product?

The UN definition of sustainability is “meeting the needs of the present without compromising the ability of future generations to meet their own needs” (Keeble, 1988).

Faba bean, a rotational cool-climate protein crop, is often proposed as a sustainable alternative to both soybean and animal-based products. Throughout this thesis work, I found myself considering characteristics that faba bean food products themselves should possess in order to be sustainable. Sustainability is usually categorised into three dimensions (environmental, economic and social). With food being of both emotional and cultural (social) significance, implementing change can be challenging. According to the food ethnologist Richard Tellström (personal communication August 31, 2022), changes in dietary habits and in food systems are driven by changes in economic, political and societal values.

For a product to be sustainable, it should be produced with minimal environmental impact, but it should also be commercially successful. Figure 19 summarises some of the properties that may be most important when developing a sustainable food product. For any food product to be sustainable, it should be both tasty and healthy. Taste is the primary factor determining whether a consumer likes a product or not, and is also the main re-purchase driver (International Food Information Council, 2020). Inferior sensory quality of plant-based products has been identified as a barrier to consumer acceptance and preference (Giacalone *et al.*, 2022). Animal-based products are often rich in umami, salty and fatty tastes, for which humans have a preference. In contrast pulses and pulse-derived ingredients have been described as having off-flavours, which is a major barrier to consumption (Roland *et al.*, 2017), however, different processing techniques and additional ingredients may reduce or mask the off-flavours. For faba beans,

the presence of free phenolics, vicine, and convicine has been linked to strong taste and aftertaste, bitterness, and a drying sensation of the mouth, while lipid oxidation products were related to pea, cereal, and off-odours and flavours (Tuccillo *et al.*, 2022). Texture attributes such as “juiciness” associated with meat are caused by the water-holding capacity of meat protein and its ability to encapsulate fat (Giacalone *et al.*, 2022).

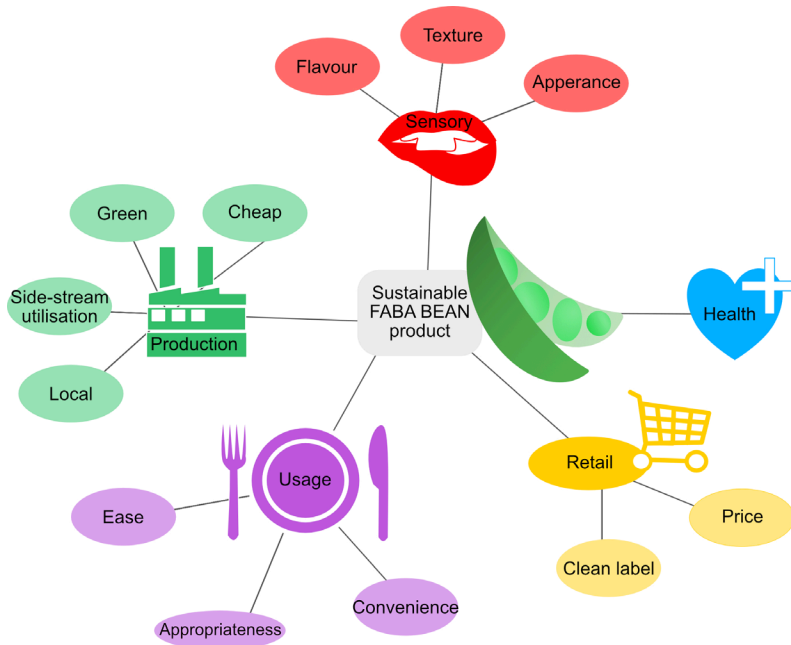


Figure 19. Important properties to consider for a product based on faba bean to be sustainable.

For a faba bean product to be deemed sustainable, it should also be healthy. Faba bean has a higher protein content than many other legumes, but also contains anti-nutritional factors which can reduce the bioavailability of nutrients and protein uptake (Dhull *et al.*, 2021; Martineau-Côté *et al.*, 2022). Various processing techniques, such as cooking, drying and fermenting, have been shown to lower the anti-nutrient content (Crépon *et al.*, 2010; Martineau-Côté *et al.*, 2022). By combining faba bean and cereal flour, products with superior nutritional quality can be achieved, because of an overall improved amino-acid profile. The relatively high fibre and

resistant starch concentrations in faba bean are an additional benefit, as they can reduce the glycaemic index of products. In Sweden, around 50% of adults are overweight (Nyman, 2018), so there is a need for nutritious food product alternatives. Faba bean products should be developed in such a way that nutrients are promoted and anti-nutrients are suppressed.

Faba bean products must also achieve market success. After taste, product price is the second most important factor determining whether a consumer will buy a product or not (International Food Information Council, 2020). High product costs have been identified as a major barrier to transition towards a more plant-based diet, as 50% of flexitarians perceive plant-based alternatives to be too expensive (European Union, 2021). It is probable that consumers may become more price-sensitive in the near future, as food prices increased by 21% for an average Swedish family between December 2021 and December 2022 (Matpriskollen, 2022). The price of products can be kept low if the production costs remain relatively low through the use of affordable ingredients, cheap production processes and access to a large consumer base (ProVeg International, 2020). The methods applied in this thesis, such as freeze drying and 3D-printing, are relatively expensive and for commercialisation of products less costly methods are required. The need to add stabilisers and preservatives could also be avoided by having more knowledge on the structure-processing relationship and by developing effective packaging materials.

Between 2019 and 2021, legume-based snacks were the legume product category that increased most, with *e.g.* an increase of 169% on the Australian market, emphasising the interest in convenience (Bielefeld *et al.*, 2021). The difficulty and time required for preparing legumes have resulted in declining intake over the past century (Cusworth *et al.*, 2021; Messina, 1999). Sweden is the European country with the highest intake of ultra-processed foods (Mertens *et al.*, 2022). Ultra-processed foods are often designed to have extended shelf-life and be profitable, palatable, attractive and easy to consume. However, to achieve these desirable traits ingredients that make the foods sub-optimal in nutritional quality may be added. Ideally, newly developed faba bean products should be convenient, *i.e.* easy to prepare and eat.

Finally, production of faba bean products should be local, ideally at minimal cost with minimal environmental impact. Side-streams from the production of the faba bean product should be utilised and, if unfit for human

consumption, perhaps transformed into packaging material or animal feed. Recent events such as the Covid-19 pandemic and the war in Ukraine have highlighted how heavily affected the food system is by external factors. In Sweden, there has been great discussion recently on the need for the country's food system to become more self-sustaining and resilient. On average, transport of legumes contributes half of their CO₂ emissions in climate impact calculations, so keeping the whole production chain local could minimise the climate impact (Tidåker *et al.*, 2021). However, food trade is also positive and when conditions are stable it could be an effective measure for global cooperation towards a more sustainable future.

To summarise, a sustainable faba bean food product needs to be appealing to the consumer by having the right sensory properties, and it should also be healthy. Textural analysis should be performed in combination with sensory and consumer evaluations to deepen knowledge of how different processes affect sensory perceptions. For consumers to choose a faba bean product at the point of sale, it should be priced appropriately and fulfil consumer expectations. Through effective marketing and clear instructions on how the novel faba bean product can be used and consumed, it can hopefully become a staple household food item.

References

- Affrifah, N. S., Uebersax, M. A., & Amin, S. (2023). Nutritional significance, value-added applications, and consumer perceptions of food legumes: A review. *Legume Science*, 1–16. <https://doi.org/DOI: 10.1002/leg3.192>
- Ahuja, A., Lee, R., Latshaw, A., & Foster, P. (2020). Rheology of starch dispersions at high temperatures. *Journal of Texture Studies*, 51(4), 575–584. <https://doi.org/10.1111/jtxs.12517>
- Alcorta, A., Porta, A., & Amparo, T. (2021). *Foods for Plant-Based Diets : Challenges and Innovations*. 1–23.
- Alghamdi, S. S. (2009). Chemical Composition of Faba Bean (*Vicia faba* L.) Genotypes under Various Water Regimes.pdf. *Pakistan Journal of Nutrition*, 8(4), 477–482.
- Ambigaipalan, P., Hoover, R., Donner, E., Liu, Q., Jaiswal, S., Chibbar, R., Nantanga, K. K. M., & Seetharaman, K. (2011). Structure of faba bean, black bean and pinto bean starches at different levels of granule organization and their physicochemical properties. *Food Research International*, 44(9), 2962–2974. <https://doi.org/10.1016/j.foodres.2011.07.006>
- AOAC. (2000). Ash of Animal Feed. AOAC Official Methods 942.05. In *Journal of AOAC International* (Vol. 857, Issue 1942).
- Armaforte, E., Hopper, L., & Stevenson, G. (2021). Preliminary investigation on the effect of proteins of different leguminous species (*Cicer arietinum*, *Vicia faba* and *Lens culinaris*) on the texture and sensory properties of egg-free mayonnaise. *Lwt*, 136(October 2020). <https://doi.org/10.1016/j.lwt.2020.110341>
- ASTM D1746. (2016). *Standard Test Method for Transparency of Plastic Sheeting: Vol. 08.01*. <https://doi.org/10.1520/D1746-15>
- ASTM D882-02. (2010). *Standard Test Method for Tensile Properties of Thin Plastic Sheeting: Vol. 08.01*. <https://doi.org/10.1520/D0882-02>
- ASTM F1307-20. (2020). *Standard Test Method for Oxygen Transmission Rate Through Dry Packages Using a Coulometric Sensor: Vol. 15.10*. <https://doi.org/10.1520/F1307-20>
- Auffret, A., Ralet, M. C., Guillon, F., Barry, J. L., & Thibault, J. F. (1994). Effect of grinding and experimental conditions on the measurement of hydration properties of dietary fibres. In *LWT - Food Science and Technology* (Vol. 27, Issue 2, pp. 166–172). <https://doi.org/10.1006/fstl.1994.1033>
- Bajaj, R., Singh, N., Kaur, A., & Inouchi, N. (2018). Structural, morphological, functional and digestibility properties of starches from cereals, tubers and legumes: a comparative study. *Journal of Food Science and Technology*, 55(9), 3799–3808. <https://doi.org/10.1007/s13197-018-3342-4>
- Balet, S., Guelpa, A., Fox, G., & Manley, M. (2019). Rapid Visco Analyser (RVA) as a Tool

- for Measuring Starch-Related Physicochemical Properties in Cereals: a Review. *Food Analytical Methods*, 12(10), 2344–2360. <https://doi.org/10.1007/s12161-019-01581-w>
- Bell, J. M., & Shires, A. (1982). Composition and Digestibility By Pigs of Hull Fractions From Rapeseed Cultivars With Yellow or Brown Seed Coats. *Canadian Journal of Animal Science*, 62(2), 557–565. <https://doi.org/10.4141/cjas82-065>
- Benaïmeche, O., Seghir, N. T., Sadowski, L., & Mellas, M. (2020). The Utilization of Vegetable Fibers in Cementitious Materials. In *Encyclopedia of Renewable and Sustainable Materials* (Issue 2013). Elsevier Ltd. <https://doi.org/10.1016/b978-0-12-803581-8.11596-6>
- Bertoft, E. (2017). Understanding starch structure: Recent progress. *Agronomy*, 7(3). <https://doi.org/10.3390/agronomy7030056>
- Bielefeld, D., Hughes, J., & Grafenauer, S. (2021). The Changing Landscape of Legume Products Available in Australian Supermarkets. *Nutrients*, 13(3226), 1–10. <https://doi.org/10.3390/nu13093226>
- Blahovec, J. (2007). Role of water content in food and product texture. *International Agrophysics*, 21(3), 209–215.
- Bourne, M. (2002). *Food Texture and Viscosity (Second Edition)*.
- Boye, J., Zare, F., & Pletch, A. (2010). Pulse proteins: Processing, characterization, functional properties and applications in food and feed. *Food Research International*, 43(2), 414–431. <https://doi.org/10.1016/j.foodres.2009.09.003>
- Bravo-Núñez, Á., Garzón, R., Rosell, C. M., & Gómez, M. (2019). Evaluation of starch-protein interactions as a function of pH. *Foods*, 8(5), 2–11. <https://doi.org/10.3390/foods8050155>
- Bravo-Núñez, Á., & Gómez, M. (2019). Physicochemical properties of native and extruded maize flours in the presence of animal proteins. *Journal of Food Engineering*, 243(August 2018), 49–56. <https://doi.org/10.1016/j.jfoodeng.2018.09.005>
- Bühler, J. M., Dekkers, B. L., Bruins, M. E., & Van Der Goot, A. J. (2020). Modifying faba bean protein concentrate using dry heat to increase water holding capacity. *Foods*, 9(8), 1–16. <https://doi.org/10.3390/foods9081077>
- Buléon, A., Colonna, P., Planchot, V., & Ball, S. (1998). Starch granules: Structure and biosynthesis. *International Journal of Biological Macromolecules*, 23(2), 85–112. [https://doi.org/10.1016/S0141-8130\(98\)00040-3](https://doi.org/10.1016/S0141-8130(98)00040-3)
- Cai, J., Cai, C., Man, J., Zhou, W., & Wei, C. (2014). *Structural and functional properties of C-type starches*. 101, 289–300.
- Cao, Y., & Mezzenga, R. (2020). Design principles of food gels. *Nature Food*, 1(2), 106–118. <https://doi.org/10.1038/s43016-019-0009-x>
- Caprioli, G., Giusti, F., Ballini, R., Sagratini, G., Vila-Donat, P., Vittori, S., & Fiorini, D. (2016). Lipid nutritional value of legumes: Evaluation of different extraction methods and determination of fatty acid composition. *Food Chemistry*, 192, 965–971. <https://doi.org/10.1016/j.foodchem.2015.07.102>
- Champ, M. (2004). Resistant starch. In Anne-Charlotte Eliasson (Ed.), *Starch in Food Structure, function and application* (Vol. 1, Issue 1, pp. 560–574). Woodhead Publishing Limited. <https://doi.org/10.1108/00346659610105842>

- Chaplin, M. F. (2003). Fibre and water binding. *Proceedings of the Nutrition Society*, 62(1), 223–227. <https://doi.org/10.1079/pns2002203>
- Coda, R., Varis, J., Verni, M., Rizzello, C. G., & Katina, K. (2017). Improvement of the protein quality of wheat bread through faba bean sourdough addition. *Lwt*, 82, 296–302. <https://doi.org/10.1016/j.lwt.2017.04.062>
- Commission Regulation (EC) No 152/2009. (2009). *European Commission: Determination of crude oils and fat*. Official Journal of the European Communities.
- Cornejo-Ramírez, Y. I., Martínez-Cruz, O., Del Toro-Sánchez, C. L., Wong-Corral, F. J., Borboa-Flores, J., & Cinco-Moroyoqui, F. J. (2018). The structural characteristics of starches and their functional properties. *CYTA - Journal of Food*, 16(1), 1003–1017. <https://doi.org/10.1080/19476337.2018.1518343>
- Cornet, S. H. V., Snel, S. J. E., Lesschen, J., Jan, A., Goot, V. Der, & Sman, R. G. M. Van Der. (2021). Enhancing the water holding capacity of model meat analogues through marinade composition. *Journal of Food Engineering*, 290, 110283. <https://doi.org/10.1016/j.jfoodeng.2020.110283>
- Crépon, K., Marget, P., Peyronnet, C., Carrouée, B., Arese, P., & Duc, G. (2010). Nutritional value of faba bean (*Vicia faba* L.) seeds for feed and food. *Field Crops Research*, 115(3), 329–339. <https://doi.org/10.1016/j.fcr.2009.09.016>
- Cusworth, G., Garnett, T., & Lorimer, J. (2021). Legume dreams: The contested futures of sustainable plant-based food systems in Europe. *Global Environmental Change*, 69(February), 102321. <https://doi.org/10.1016/j.gloenvcha.2021.102321>
- Danielsson, C.-E. (1950). An Electrophoretic Investigation of Vicilin and Legumin from Seeds of Peas. *Acta Cheice Scandinavica*, 4, 762–771.
- Daubenmire, S. W., Zabik, M. E., & Setser, C. . (1993). Development of lowfat, cholesterol-free, high-fiber muffins. 1. Fiber source and particle size effects on quality characteristics. *School Food Service Research Review*, 17(1), 15–20.
- Dhillon, S., & Seetharaman, K. (2011). Rheology and texture of starch gels containing iodine. *Journal of Cereal Science*, 54(3), 374–379. <https://doi.org/10.1016/j.jcs.2011.07.005>
- Dhull, S. B., Kidwai, M. K., Noor, R., Chawla, P., & Rose, P. K. (2021). A review of nutritional profile and processing of faba bean (*Vicia faba* L.). *Legume Science*, 4(3), 1–13. <https://doi.org/10.1002/leg3.129>
- Eliasson, A-C. (1986). Viscoelastic Behaviour During the Gelatinization of Starch. *Journal of Texture Studies*, 17, 253–265.
- European Union. (2021). *What consumers want : a survey on European consumer attitudes towards plant-based foods with a focus on flexitarians* (Issue 862957).
- Farooq, Z., & Boye, J. I. (2011). Novel Food and Industrial Applications of Pulse Flours and Fractions. In *Pulse Foods*. Elsevier Ltd. <https://doi.org/10.1016/B978-0-12-382018-1.00011-3>
- FDA. (2023). *Food Allergies*. <https://www.fda.gov/food/food-labeling-nutrition/food-allergies>
- Ferawati, F. (2021). *The development of novel foods from Swedish pulses - Raw material composition and processing effects* (Issue 421) [Linnaeus University, Kalmar]. <http://www.diva-portal.org/smash/get/diva2:1593810/FULLTEXT01.pdf>

- Ferawati, F., Hefni, M., Östbring, K., & Witthöft, C. (2021a). The Application of Pulse Flours in the Development of Plant-Based Cheese Analogues: Proximate Composition, Color, and Texture Properties. *Foods*, *10*(2208), 1–11. <https://doi.org/10.3390/foods10092208>
- Ferawati, F., Zahari, I., Barman, M., Hefni, M., Ahlström, C., Witthöft, C., & Östbring, K. (2021b). High-moisture meat analogues produced from yellow pea and faba bean protein isolates/concentrate: Effect of raw material composition and extrusion parameters on texture properties. *Foods*, *10*(4). <https://doi.org/10.3390/foods10040843>
- Fernández-quintela, A., Macarulla, M. T., Barrio, A. S. D. E. L., & Mart, J. A. (1997). *Composition and functional properties of protein isolates obtained from commercial legumes grown in northern Spain*. 331–342.
- Filho, W. L., Setti, A. F. F., Azeiteiro, U. M., Lokupitiya, E., Donkor, F. K., Etim, N. A. N. A., Matandirotya, N., Olooto, F. M., Sharifi, A., Nagy, G. J., & Djekic, I. (2022). An overview of the interactions between food production and climate change. *Science of the Total Environment*, *838*(June). <https://doi.org/10.1016/j.scitotenv.2022.156438>
- Fonslick, J., & Khan, A. (1989). Thermal Stability and Composition of the Amylose-Iodine Complex. *Journal of Polymer Science*, *27*, 4161–4167.
- Fouad, M., Mohammed, N., Aladdin, H., Ahmed, A., Xuxiao, Z., Shiyang, B., & Tao, Y. (2013). Faba Bean. *Genetic and Genomic Resources of Grain Legume Improvement*, 113–136. <https://doi.org/10.1016/B978-0-12-397935-3.00005-0>
- Frei, M. (2013). Lignin : Characterization of a Multifaceted Crop Component. *The Scientific World Journal*, *2013*, 25. <http://dx.doi.org/10.1155/2013/436517>
- Gebhardt, B., & Hadwiger, K. (2020). *PLANT-BASED FOR THE FUTURE Insights on European consumer Scope of This Study*. Vegency.
- Gernat, C., Radosta, S., Damaschun, G., & Schierbaum, F. (1990). Supramolecular Structure of Legume Starches Revealed by X-Ray Scattering. *Starch - Stärke*, *42*(5), 175–178. <https://doi.org/10.1002/star.19900420504>
- Giacalone, D., Clausen, M. P., & Jaeger, S. R. (2022). Understanding barriers to consumption of plant-based foods and beverages: insights from sensory and consumer science. *Current Opinion in Food Science*, *48*, 100919. <https://doi.org/10.1016/j.cofs.2022.100919>
- Giménez, M. A., Drago, S. R., Greef, D. De, Gonzalez, R. J., Lobo, M. O., & Samman, N. C. (2012). *Rheological , functional and nutritional properties of wheat / broad bean (Vicia faba) flour blends for pasta formulation*. *134*, 200–206. <https://doi.org/10.1016/j.foodchem.2012.02.093>
- Glaring, M. A., Koch, C. B., & Blennow, A. (2006). Genotype-specific spatial distribution of starch molecules in the starch granule: A combined CLSM and SEM approach. *Biomacromolecules*, *7*(8), 2310–2320. <https://doi.org/10.1021/bm060216e>
- Gonzalez, A., & Igarzabal, C. I. A. (2015). Nanocrystal-reinforced soy protein films and their application as active packaging. *Food Hydrocolloids*, *43*, 777–784. <https://doi.org/10.1016/j.foodhyd.2014.08.008>
- Graça, J., Calheiros, M. M., & Oliveira, A. (2014). Moral Disengagement in Harmful but Cherished Food Practices? An Exploration into the Case of Meat. *Journal of*

- Agricultural and Environmental Ethics*, 27(5), 749–765.
<https://doi.org/10.1007/s10806-014-9488-9>
- Guillon, F., & Champ, M. M.-J. (2002). Carbohydrate fractions of legumes: uses in human nutrition and potential for health. *British Journal of Nutrition*, 88(S3), 293–306.
<https://doi.org/10.1079/bjn2002720>
- Haase, N. U., & Shi, H. L. (1991). A Characterization of Faba Bean Starch (*Vicia faba* L.). *Starch - Stärke*, 43(6), 205–208. <https://doi.org/10.1002/star.19910430602>
- Hassoun, A., Cropotova, J., Trif, M., Rusu, A. V., Bobiş, O., Nayik, G. A., Jagdale, Y. D., Saeed, F., Afzaal, M., Mostashari, P., Khaneghah, A. M., & Regenstein, J. M. (2022). Consumer acceptance of new food trends resulting from the fourth industrial revolution technologies: A narrative review of literature and future perspectives. *Frontiers in Nutrition*, 9. <https://doi.org/10.3389/fnut.2022.972154>
- He, Q., Hort, J., & Wolf, B. (2016). *Food Hydrocolloids Predicting sensory perceptions of thickened solutions based on rheological analysis*. 61, 221–232.
<https://doi.org/10.1016/j.foodhyd.2016.05.010>
- Hermans, P. H., & Weidinger, A. (1948). Quantitative x-ray investigations on the crystallinity of cellulose fibers. A background analysis. *Journal of Applied Physics*, 19(5), 491–506.
<https://doi.org/10.1063/1.1698162>
- Herneke, A., Lendel, C., Johansson, D., Newson, W., Hedenqvist, M., Karkehabadi, S., Jonsson, D., & Langton, M. (2021). Protein Nanofibrils for Sustainable Food–Characterization and Comparison of Fibrils from a Broad Range of Plant Protein Isolates. *ACS Food Science & Technology*, 1(5), 854–864.
<https://doi.org/10.1021/acsfoodscitech.1c00034>
- Herreman, L., Nommensen, P., Pennings, B., & Laus, M. C. (2020). Comprehensive overview of the quality of plant- And animal-sourced proteins based on the digestible indispensable amino acid score. *Food Science and Nutrition*, 8(10), 5379–5391.
<https://doi.org/10.1002/fsn3.1809>
- Hodder, P. (2021). *Introduction to Rheology and Measurement Techniques – Part 2*. Uppsala.
- Hoover, R., Hughes, T., Chung, H. J., & Liu, Q. (2010). Composition, molecular structure, properties, and modification of pulse starches: A review. *Food Research International*, 43(2), 399–413. <https://doi.org/10.1016/j.foodres.2009.09.001>
- International Food Information Council. (2020). Food & Health Survey 2020. *Ific*.
<https://foodinsight.org/wp-content/uploads/2020/06/IFIC-Food-and-Health-Survey-2020.pdf>
- Jabeen, N., Majid, I., Nayik, G. A., Jabeen, N., Majid, I., & Nayik, G. A. (2015). Bioplastics and food packaging : A review Bioplastics and food packaging : A review. *Cogent Food & Agriculture*, 42(1). <https://doi.org/10.1080/23311932.2015.1117749>
- Johansson, M., Johansson, D., Ström, A., Rydén, J., Nilsson, K., Karlsson, J., Moriana, R., & Langton, M. (2022). Effect of starch and fibre on faba bean protein gel characteristics. *Food Hydrocolloids*, 131(April). <https://doi.org/10.1016/j.foodhyd.2022.107741>
- Johansson, M., Xanthakis, E., Langton, M., Menzel, C., Vilaplana, F., Johansson, D. P., & Lopez-Sanchez, P. (2021). Mixed legume systems of pea protein and unrefined lentil fraction: Textural properties and microstructure. *Lwt*, 144(November 2020), 111212.

<https://doi.org/10.1016/j.lwt.2021.111212>

- Joshi, M., Aldred, P., Panozzo, J. F., Kasapis, S., & Adhikari, B. (2014). Rheological and microstructural characteristics of lentil starch-lentil protein composite pastes and gels. *Food Hydrocolloids*, *35*, 226–237. <https://doi.org/10.1016/j.foodhyd.2013.05.016>
- Karataş, S. Ç., Günay, D., & Sayar, S. (2017). In vitro evaluation of whole faba bean and its seed coat as a potential source of functional food components. *Food Chemistry*, *230*, 182–188. <https://doi.org/10.1016/j.foodchem.2017.03.037>
- Kasapis, S., & Bannikova, A. (2016). Rheology and Food Microstructure. In J. Ahmed, P. Ptaszek, & S. Basu (Eds.), *Advances in Food Rheology and its Applications* (1st ed., pp. 7–46). Elsevier Ltd. <https://doi.org/10.1016/B978-0-08-100431-9/00002-4>
- Kaya, E., Tunçel, N. Y., & Tunçel, N. B. (2018). Utilization of lentil, pea, and faba bean hulls in Turkish noodle production. *Journal of Food Science and Technology*, *55*(5), 1734–1745. <https://doi.org/10.1007/s13197-018-3086-1>
- Keeble, B. R. (1988). The Brundtland Report: “Our Common Future.” *Medicine and War*, *4*(1), 17–25. <https://doi.org/10.1080/07488008808408783>
- Keskin, S. O., Ali, T. M., Ahmed, J., Shaikh, M., Siddiq, M., & Uebersax, M. A. (2021). Physico-chemical and functional properties of legume protein, starch, and dietary fiber—A review. *Legume Science*, *4*(117), 1–15. <https://doi.org/10.1002/leg3.117%0Awileyonlinelibrary.com/journal/legumescience>
- Khazaei, H., Purves, R. W., Hughes, J., Link, W., O’Sullivan, D. M., Schulman, A. H., Björnsdotter, E., Geu-Flores, F., Nadzieja, M., Andersen, S. U., Stougaard, J., Vandenberg, A., & Stoddard, F. L. (2019). Eliminating vicine and convicine, the main anti-nutritional factors restricting faba bean usage. *Trends in Food Science and Technology*, *91*(March), 549–556. <https://doi.org/10.1016/j.tifs.2019.07.051>
- Krenz, L. M. M., Grebenteuch, S., Zocher, K., Rohn, S., & Pleissner, D. (2023). Valorization of faba bean (*Vicia faba*) by-products.pdf. *Biomass Conversion and Biorefinery*. <https://doi.org/10.1007/s13399-023-03779-9>
- Laleg, K., Barron, C., Cordelle, S., Schlich, P., Walrand, S., & Micard, V. (2017). How the structure, nutritional and sensory attributes of pasta made from legume flour is affected by the proportion of legume protein. *Lwt*, *79*, 471–478. <https://doi.org/10.1016/j.lwt.2017.01.069>
- Laleg, K., Cassan, D., Barron, C., Prabhasankar, P., & Micard, V. (2016). Structural, culinary, nutritional and anti-nutritional properties of high protein, gluten free, 100% legume pasta. *PLoS ONE*, *11*(9), 1–19. <https://doi.org/10.1371/journal.pone.0160721>
- Langton, M., Astrdm, A., & Hermansson, A. (1996). Texture as a reflection of microstructure. *Food Quality and Preference*, *7*(3/4), 185–191.
- Langton, M., Ehsanzamir, S., Karkehabadi, S., Feng, X., Johansson, M., & Johansson, D. P. (2020). Gelation of faba bean proteins - Effect of extraction method, pH and NaCl. *Food Hydrocolloids*, *103*. <https://doi.org/10.1016/j.foodhyd.2019.105622>
- Larsen, F. H., Kasprzak, M. M., Larke, H. N., Knudsen, K. E. B., Pedersen, S., Jorgensen, A. S., & Blennow, A. (2013). Hydration properties and phosphorous speciation in native, gelatinized and enzymatically modified potato starch analyzed by solid-state MAS NMR. *Carbohydrate Polymers*, *97*(2), 502–511.

- <https://doi.org/10.1016/j.carbpol.2013.05.014>
- Lee, H. J. (2007). *The isolation and characterisation of starches from legume grains and their application in food formulations*. February, 22.
- Li, C., Wu, A., Yu, W., Hu, Y., Li, E., Zhang, C., & Liu, Q. (2020). Parameterizing starch chain-length distributions for structure-property relations. *Carbohydrate Polymers*, 241(March). <https://doi.org/10.1016/j.carbpol.2020.116390>
- Li, L., Yuan, T. Z., Setia, R., Raja, R. B., Zhang, B., & Ai, Y. (2019). Characteristics of pea, lentil and faba bean starches isolated from air-classified flours in comparison with commercial starches. *Food Chemistry*, 276(October 2018), 599–607. <https://doi.org/10.1016/j.foodchem.2018.10.064>
- Li, X., Harding, S. E., Wolf, B., & Yakubov, G. E. (2022). Instrumental characterization of xanthan gum and scleroglucan solutions: Comparison of rotational rheometry, capillary breakup extensional rheometry and soft-contact tribology. *Food Hydrocolloids*, 130(April), 107681. <https://doi.org/10.1016/j.foodhyd.2022.107681>
- Liepsch, D. (2016). A Basic Introduction to Rheology Shear Flow. *J Biomech*, 35(4), 415–435. <https://cdn.technologynetworks.com/TN/Resources/PDF/WP160620BasicIntroRheology.pdf>
- Lille, M., Nurmela, A., Nordlund, E., Metsä-Kortelainen, S., & Sozer, N. (2018). Applicability of protein and fiber-rich food materials in extrusion-based 3D printing. *Journal of Food Engineering*, 220, 20–27. <https://doi.org/https://doi.org/10.1016/j.jfoodeng.2017.04.034>
- Ma, K. K., Greis, M., Lu, J., Nolden, A. A., McClements, D. J., & Kinchla, A. J. (2022). Functional Performance of Plant Proteins. *Foods*, 11(4), 1–23. <https://doi.org/10.3390/foods11040594>
- Macklean. (2020). *Marknadsanalys och potential för växtbaserade proteiner- Rapport till AFuru, Mikaelna Pers och Amanda Andersson, LRF: Vol. Januari*. www.lrf.se/globalassets/dokument/mitt-lrf/nyheter/2020/marknadsanalys-och-potential-for-vaxtbaserade-proteiner.pdf
- Martineau-Côté, D., Achouri, A., Karboune, S., & L'Hocine, L. (2022). Faba Bean: An Untapped Source of Quality Plant Proteins and Bioactives. *Nutrients*, 14(8), 1–27. <https://doi.org/10.3390/nu14081541>
- Masamba, K., Li, Y., Hategekimana, J., Liu, F., Ma, J., & Zhong, F. (2016). Effect of Gallic acid on mechanical and water barrier properties of zein-oleic acid composite films. *Journal of Food Science and Technology*, 53(5), 2227–2235. <https://doi.org/10.1007/s13197-015-2167-7>
- Mason, W. R. (2009). Starch Use in Foods. In *Starch* (Third Edit). Elsevier Inc. <https://doi.org/10.1016/B978-0-12-746275-2.00020-3>
- Matpriskollen. (2022). *Så här mycket dyrare är din matkasse i år*. <https://matpriskollen.se/2022/12/sahar-mycket-dyrare-ar-din-matkasse-i-ar/>
- Mayer Labba, I. C., Frøkiær, H., & Sandberg, A. S. (2021). Nutritional and antinutritional composition of fava bean (*Vicia faba* L., var. minor) cultivars. *Food Research International*, 140(August 2020). <https://doi.org/10.1016/j.foodres.2020.110038>

- McClements, D. J., & Grossmann, L. (2021). The science of plant-based foods: Constructing next-generation meat, fish, milk, and egg analogs. *Comprehensive Reviews in Food Science and Food Safety*, 20(4), 4049–4100. <https://doi.org/10.1111/1541-4337.12771>
- McClements, D. J., & Grossmann, L. (2022). Next-Generation Plant-based Foods. In *Next-Generation Plant-based Foods*. <https://doi.org/10.1007/978-3-030-96764-2>
- Megazyme. (2018). Amylose/Amylopectin: Assay Procedure K-AMYL 06/18. In *Megazyme Data Booklet* (Vol. 6). <https://www.megazyme.com/amylose-amylopectin-assay-kit?sSearch=amylose>
- Megazyme. (2019). *RESISTANT STARCH, ASSAY PROCEDURE, K-RSTAR 05/19* (Vol. 19).
- Mertens, E., Colizzi, C., & Peñalvo, J. L. (2022). Ultra-processed food consumption in adults across Europe. *European Journal of Nutrition*, 61(3), 1521–1539. <https://doi.org/10.1007/s00394-021-02733-7>
- Messina, M. J. (1999). Legumes and soybeans: overview of their nutritional profiles and. *Am J Clin Nutr*, 70(February), 439–450.
- Morgan, K. R., Furneaux, R. H., & Larsen, N. G. (1995). Solid-state NMR studies on the structure of starch granules. *Carbohydrate Research*, 276(2), 387–399. [https://doi.org/10.1016/0008-6215\(95\)00173-Q](https://doi.org/10.1016/0008-6215(95)00173-Q)
- Moriana, R., Vilaplana, F., & Ek, M. (2016). Cellulose Nanocrystals from Forest Residues as Reinforcing Agents for Composites: A Study from Macro- to Nano-Dimensions. *Carbohydrate Polymers*, 139, 139–149. <https://doi.org/10.1016/j.carbpol.2015.12.020>
- Muñoz, L. A., Pedreschi, F., Leiva, A., & Aguilera, J. M. (2015). Loss of birefringence and swelling behavior in native starch granules: Microstructural and thermal properties. *Journal of Food Engineering*, 152, 65–71.
- Nasrabadi, M. N., Doost, A. S., & Mezzenga, R. (2021). Modification approaches of plant-based proteins to improve their techno-functionality and use in food products. *Food Hydrocolloids*, 118(January), 106789. <https://doi.org/10.1016/j.foodhyd.2021.106789>
- Nilsson, G. S., Bergquist, K. E., Nilsson, U., & Gorton, L. (1996). Determination of the degree of branching in normal and amylopectin type potato starch with ¹H-NMR spectroscopy: Improved resolution and two-dimensional spectroscopy. *Starch/Staerke*, 48(10), 352–357. <https://doi.org/10.1002/star.19960481003>
- Nivala, O., Mäkinen, O. E., Kruus, K., Nordlund, E., & Ercili-Cura, D. (2017). Structuring colloidal oat and faba bean protein particles via enzymatic modification. *Food Chemistry*, 231, 87–95. <https://doi.org/10.1016/j.foodchem.2017.03.114>
- NMKL-6. (1976). *Nitrogen. Determination On, in food and feed according to Kjeldahl*. Nordic Committee on Food Analysis.
- Núñez-Santiago, M. C., Bello-Pérez, L. A., & Tecante, A. (2004). Swelling-solubility characteristics, granule size distribution and rheological behavior of banana (*Musa paradisiaca*) starch. *Carbohydrate Polymers*, 56(1), 65–75. <https://doi.org/10.1016/j.carbpol.2003.12.003>
- Nyman, A. (2018). *Varannan svensk har övervikt eller fetma*No Title. SCB. <https://www.scb.se/hitta-statistik/artiklar/2018/varannan-svensk-har-overvikt-eller-fetma/>
- Oñate Narciso, J., & Brennan, C. (2018). Whey and Pea Protein Fortification of Rice Starches:

- Effects on Protein and Starch Digestibility and Starch Pasting Properties. *Starch/Staerke*, 70(9–10), 1–6. <https://doi.org/10.1002/star.201700315>
- Onwulata, C. I., Tunick, M. H., & Thomas-Gahring, A. E. (2014). Pasting and extrusion properties of mixed carbohydrate and whey protein isolate matrices. *Journal of Food Processing and Preservation*, 38(4), 1577–1591. <https://doi.org/10.1111/jfpp.12118>
- Osborne, T. B. (1907). *The Proteins of The Wheat Kernel* (p. 119). Carnegie institution of Washington;
- Osorio-Ruiz, A., Avena-Bustillos, R. J., Chiou, B.-S., Rodríguez-González, F., & Martínez-Ayala, A.-L. (2019). Mechanical and Thermal Behavior of Canola Protein Isolate Films As Improved by Cellulose Nanocrystals. *ACS Omega*, 4, 19172–19176.
- Ouraji, M., Alimi, M., Motamedzadegan, A., & Shokoohi, S. (2020). Faba bean protein in reduced fat/cholesterol mayonnaise: extraction and physico-chemical modification process. *Journal of Food Science and Technology*, 57(5), 1774–1785. <https://doi.org/10.1007/S13197-019-04211-9/FIGURES/4>
- Özeren, H. D., Olsson, R. T., Nilsson, F., & Hedenqvist, M. S. (2020). Prediction of plasticization in a real biopolymer system (starch) using molecular dynamics simulations. *Materials & Design*, 187, 108387. <https://doi.org/10.1016/j.matdes.2019.108387>
- Petitot, M., Boyer, L., Minier, C., & Micard, V. (2010). Fortification of pasta with split pea and faba bean flours: Pasta processing and quality evaluation. *Food Research International*, 43(2), 634–641. <https://doi.org/10.1016/j.foodres.2009.07.020>
- ProVeg International. (2020). *European Consumer Survey on Plant-based Foods – Describing the product landscape and uncovering priorities for product development and improvement*.
- Punia, S., Dhull, S. B., Sandhu, K. S., & Kaur, M. (2019). Faba bean (*Vicia faba*) starch: Structure, properties, and in vitro digestibility—A review . *Legume Science*, 1(1), 3–7. <https://doi.org/10.1002/leg3.18>
- Qazanfarzadeh, Z., & Kadivar, M. (2016). International Journal of Biological Macromolecules Properties of whey protein isolate nanocomposite films reinforced with nanocellulose isolated from oat husk. *International Journal of Biological Macromolecules*, 91, 1134–1140. <https://doi.org/10.1016/j.ijbiomac.2016.06.077>
- Ren, Y., Yuan, T. Z., Chigwedere, C. M., & Ai, Y. (2021). A current review of structure, functional properties, and industrial applications of pulse starches for value-added utilization. *Comprehensive Reviews in Food Science and Food Safety*, 20(3), 3061–3092. <https://doi.org/10.1111/1541-4337.12735>
- Revilla, I. (2015). Impact of Thermal Processing on Faba Bean (*Vicia faba*) Composition. In *Processing and Impact on Active Components in Food*. Elsevier Inc. <https://doi.org/10.1016/B978-0-12-404699-3.00040-8>
- Ribotta, P. D., Colombo, A., León, A. E., & Cristina Añón, M. (2007). Effects of soy protein on physical and rheological properties of wheat starch. *Starch/Staerke*, 59(12), 614–623. <https://doi.org/10.1002/star.200700650>
- Richardson, G., Kidman, S., Langton, M., & Hermansson, A. M. (2004). Differences in amylose aggregation and starch gel formation with emulsifiers. *Carbohydrate*

- Polymers*, 58(1), 7–13. <https://doi.org/10.1016/j.carbpol.2004.06.013>
- Rietveld, H. M. (1969). A profile refinement method for nuclear and magnetic structures. *Journal of Applied Crystallography*, 2(2), 65–71. <https://doi.org/10.1107/s0021889869006558>
- Rizzello, C. G., Verni, M., Koivula, H., Montemurro, M., Seppa, L., Kemell, M., Katina, K., Coda, R., & Gobetti, M. (2017). Influence of fermented faba bean flour on the nutritional, technological and sensory quality of fortified pasta. *Food and Function*, 8(2), 860–871. <https://doi.org/10.1039/c6fo01808d>
- Roland, W. S. U., Pouvreau, L., Curran, J., Van De Velde, F., & De Kok, P. M. T. (2017). Flavor aspects of pulse ingredients. *Cereal Chemistry*, 94(1), 58–65. <https://doi.org/10.1094/CCHEM-06-16-0161-FI>
- Röös, E., Carlsson, G., Ferawati, F., Hefni, M., Stephan, A., Tidåker, P., & Witthöft, C. (2020). Less meat, more legumes: Prospects and challenges in the transition toward sustainable diets in Sweden. *Renewable Agriculture and Food Systems*, 35(2), 192–205. <https://doi.org/10.1017/S1742170518000443>
- Rosa-Sibakov, N., Heiniö, R. L., Cassan, D., Holopainen-Mantila, U., Micard, V., Lantto, R., & Sozer, N. (2016). Effect of bioprocessing and fractionation on the structural, textural and sensory properties of gluten-free faba bean pasta. *Lwt*, 67, 27–36. <https://doi.org/10.1016/j.lwt.2015.11.032>
- Sandberg, A. (2018). *Bioavailability of minerals in legumes*. 2002, 281–285. <https://doi.org/10.1079/BJN/2002718>
- Sandeep, S., Singh, N., Isono, N., & Noda, T. (2010). Relationship of granule size distribution and amylopectin structure with pasting, thermal, and retrogradation properties in wheat starch. *Journal of Agricultural and Food Chemistry*, 58(2), 1180–1188. <https://doi.org/10.1021/jf902753f>
- Schirmer, M., Jekle, M., & Becker, T. (2015). Starch gelatinization and its complexity for analysis. *Starch/Stärke*, 67(1–2), 30–41. <https://doi.org/10.1002/star.201400071>
- Shabanpour, B., Kazemi, M., Ojagh, S. M., & Pourashouri, P. (2018). *International Journal of Biological Macromolecules Bacterial cellulose nano fibers as reinforce in edible fish myofibrillar protein nanocomposite films*. 117, 742–751. <https://doi.org/10.1016/j.ijbiomac.2018.05.038>
- Sharan, S., Zanghelini, G., Zotzel, J., Bonerz, D., Aschoff, J., Saint-Eve, A., & Maillard, M.-N. (2021). Fava bean (*Vicia faba* L.) for food applications: From seed to ingredient processing and its effect on functional properties, antinutritional factors, flavor, and color. *Comprehensive Reviews in Food Science and Food Safety*, 20(1), 401–428. <https://doi.org/https://doi.org/10.1111/1541-4337.12687>
- Sharma, A., & Sehgal, S. (1992). Effect of processing and cooking on the antinutritional factors of faba bean (*Vicia faba*). *Food Chemistry*, 43(5), 383–385. [https://doi.org/10.1016/0308-8146\(92\)90311-O](https://doi.org/10.1016/0308-8146(92)90311-O)
- Singh, N., Singh, J., Kaur, L., Sodhi, N. S., & Gill, B. S. (2003). Morphological, thermal and rheological properties of starches from different botanical sources. *Food Chemistry*, 81(2), 219–231. [https://doi.org/10.1016/S0308-8146\(02\)00416-8](https://doi.org/10.1016/S0308-8146(02)00416-8)
- Sozer, N., Holopainen-Mantila, U., & Poutanen, K. (2017). Traditional and new food uses of

- pulses. *Cereal Chemistry*, 94(1), 66–73. <https://doi.org/10.1094/CCHEM-04-16-0082-FI>
- Sukyai, P., Anongjanya, P., Bunyahwuthakul, N., Kongsin, K., Harnkarnsujarit, N., Sukatta, U., Sothornvit, R., & Chollakup, R. (2018). *Effect of cellulose nanocrystals from sugarcane bagasse on whey protein isolate-based films*. 107(February), 528–535. <https://doi.org/10.1016/j.foodres.2018.02.052>
- Tang, H., & Hills, B. P. (2003). Use of ¹³C MAS NMR to study domain structure and dynamics of polysaccharides in the native starch granules. *Biomacromolecules*, 4(5), 1269–1276. <https://doi.org/10.1021/bm0340772>
- Tanger, C., Müller, M., Andlinger, D., & Kulozik, U. (2022). Influence of pH and ionic strength on the thermal gelation behaviour of pea protein. *Food Hydrocolloids*, 123(May 2021), 106903. <https://doi.org/10.1016/j.foodhyd.2021.106903>
- Tayade, R., Kulkarni, K. P., Jo, H., Song, J. T., & Lee, J. D. (2019). Insight Into the Prospects for the Improvement of Seed Starch in Legume—A Review. *Frontiers in Plant Science*, 10(October), 1–17. <https://doi.org/10.3389/fpls.2019.01213>
- Tester, R. F., Karkalas, J., & Qi, X. (2004). Starch - Composition, fine structure and architecture. *Journal of Cereal Science*, 39(2), 151–165. <https://doi.org/10.1016/j.jcs.2003.12.001>
- Tester, R. F., & Morrison, W. R. (1990). Swelling and Gelatinisation of cereal starches I. Effect of Amylopectin, Amylose and Lipids. *Cereal Chemistry*, 65(6), 551–557.
- Tidåker, P., Karlsson Potter, H., Carlsson, G., & Rööds, E. (2021). Towards sustainable consumption of legumes: How origin, processing and transport affect the environmental impact of pulses. *Sustainable Production and Consumption*, 27, 496–508. <https://doi.org/10.1016/j.sp.2021.01.017>
- Tiwari, U., & Cummins, E. (2020). Legume fiber characterization, functionality, and process effects. In *Pulse Foods: Processing, Quality and Nutraceutical Applications*. Elsevier Inc. <https://doi.org/10.1016/B978-0-12-818184-3.00007-6>
- Tosh, S. M., & Yada, S. (2010). Dietary fibres in pulse seeds and fractions: Characterization, functional attributes, and applications. *Food Research International*, 43(2), 450–460. <https://doi.org/10.1016/j.foodres.2009.09.005>
- Totosaus, A., Montejano, J. G., Salazar, J. A., & Guerrero, I. (2002). A review of physical and chemical protein-gel induction. *International Journal of Food Science and Technology*, 37(6), 589–601. <https://doi.org/10.1046/j.1365-2621.2002.00623.x>
- Tuccillo, F., Kantanen, K., Wang, Y., Martin Ramos Diaz, J., Pulkkinen, M., Edelman, M., Knaapila, A., Jouppila, K., Piironen, V., Lampi, A. M., Sandell, M., & Katina, K. (2022). The flavor of faba bean ingredients and extrudates: Chemical and sensory properties. *Food Research International*, 162(PA), 112036. <https://doi.org/10.1016/j.foodres.2022.112036>
- Vamadevan, V., & Bertoft, E. (2015). Structure-function relationships of starch components. *Starch/Stärke*, 67(1–2), 55–68. <https://doi.org/10.1002/star.201400188>
- Vamadevan, V., & Bertoft, E. (2020). Observations on the impact of amylopectin and amylose structure on the swelling of starch granules. *Food Hydrocolloids*, 103(October 2019), 105663. <https://doi.org/10.1016/j.foodhyd.2020.105663>

- Vatansver, S., Tulbek, M. C., & Riaz, M. N. (2020). Low- and High-Moisture Extrusion of Pulse Proteins as Plant-Based Meat Ingredients: A Review. *Cereal Foods World*, 65(4). <https://doi.org/10.1094/cfw-65-4-0038>
- Vilaplana, F., & Gilbert, R. G. (2010). Two-dimensional size/branch length distributions of a branched polymer. *Macromolecules*, 43(17), 7321–7329. <https://doi.org/10.1021/ma101349t>
- Vogelsang-O'Dwyer, M., Petersen, I. L., Joehnke, M. S., Sørensen, J. C., Bez, J., Detzel, A., Busch, M., Krueger, M., O'Mahony, J. A., Arendt, E. K., & Zannini, E. (2020). Comparison of Faba Bean Protein Ingredients Produced Using Dry Fractionation and Isoelectric Precipitation: Techno-Functional, Nutritional and Environmental Performance. *Foods* 2020, Vol. 9, Page 322, 9(3), 322. <https://doi.org/10.3390/FOODS9030322>
- Wang, S., Sharp, P., & Copeland, L. (2011). Structural and functional properties of starches from field peas. *Food Chemistry*, 126(4), 1546–1552. <https://doi.org/10.1016/j.foodchem.2010.11.154>
- Wani, I. A., Sogi, D. S., Hamdani, A. M., Gani, A., Bhat, N. A., & Shah, A. (2016). Isolation, composition, and physicochemical properties of starch from legumes: A review. *Starch/Stärke*, 68(9–10), 834–845. <https://doi.org/10.1002/star.201600007>
- Webb, D., Li, Y., & Alavi, S. (2023). Chemical and physicochemical features of common plant proteins and their extrudates for use in plant-based meat. *Trends in Food Science and Technology*, 131(March 2021), 129–138. <https://doi.org/10.1016/j.tifs.2022.11.006>
- Willett, W., Rockström, J., Loken, B., Springmann, M., Lang, T., Vermeulen, S., Garnett, T., Tilman, D., DeClerck, F., Wood, A., Jonell, M., Clark, M., Gordon, L. J., Fanzo, J., Hawkes, C., Zurayk, R., Rivera, J. A., De Vries, W., Majele Sibanda, L., ... Murray, C. J. L. (2019). Food in the Anthropocene: the EAT–Lancet Commission on healthy diets from sustainable food systems. *The Lancet*, 393(10170), 447–492. [https://doi.org/10.1016/S0140-6736\(18\)31788-4](https://doi.org/10.1016/S0140-6736(18)31788-4)
- Wolf, B. (2013). Designed Food Structures Based on Hydrocolloids. In Jennifer E. Norton, P. J. Fryer, & I. T. Norton (Eds.), *Formulation Engineering of Foods* (1st ed., pp. 59–81). John Wiley & Sons, Ltd.
- Yang, H., Irudayaraj, J., Otgongchimeg, S., & Walsh, M. (2004). Rheological study of starch and dairy ingredient-based food systems. *Food Chemistry*, 86(4), 571–578. <https://doi.org/10.1016/j.foodchem.2003.10.004>
- Zabihzadeh, S. M. (2010). Water uptake and flexural properties of natural filler/HDPE composites. *BioResources*, 5(1), 316–323.
- Zhang, B., Qiao, D., Zhao, S., Lin, Q., Wang, J., & Xie, F. (2021). *Trends in Food Science & Technology Starch-based food matrices containing protein : Recent understanding of morphology , structure , and properties*. 114(June), 212–231.
- Zhang, D., Mu, T., & Sun, H. (2017). Calorimetric, rheological, and structural properties of potato protein and potato starch composites and gels. *Starch/Stärke*, 69(7–8), 1–12. <https://doi.org/10.1002/star.201600329>
- Zhang, Z., Tian, X., Wang, P., Jiang, H., & Li, W. (2019). Compositional, morphological, and

physicochemical properties of starches from red adzuki bean, chickpea, faba bean, and baiyue bean grown in China. *Food Science and Nutrition*, 7(8), 2485–2494. <https://doi.org/10.1002/fsn3.865>

Zhu, F. (2017). NMR spectroscopy of starch systems. *Food Hydrocolloids*, 63, 611–624. <https://doi.org/10.1016/j.foodhyd.2016.10.015>

Popular science summary

Increased consumption of locally produced legumes has both dietary and environmental benefits. The carbon footprint of 1 kg of legumes is 0.8 kg CO₂-equivalent compared with 28 kg CO₂-equivalent food for beef. It has been suggested that the environmental impact of the Swedish diet could be reduced by 20% if 50% of meat consumed were replaced with locally sourced legumes, such as faba bean.

Faba bean and other legumes have excellent nutritive qualities, as they are low in fat, relatively high in protein and dietary fibre and contain a variety of micronutrients and phytochemicals.

In Sweden, the range of plant-based products available on the market has increased by 16% in recent years. However, the proportion of products containing Swedish-sourced ingredients is still small and imported soybean dominates, with long transport distances contributing considerably to energy use and climate impact. Faba bean is a cool-climate crop with a good nutrient profile that could be used as a locally-sourced texturising ingredient for plant-based food products on the Swedish market.

Creating an appealing texture is one of the main challenges when developing plant-based foods, and poor sensory quality is one of the main aversion factors for such foods. To achieve desirable textures, plant-based products often require extensive processing and addition of stabilising ingredients, contravening consumer demand for minimally processed and clean-label products.

This thesis investigated the functionalities of faba bean components (starch, protein and fibre) in different types of food systems. First, faba bean starch was characterised in terms of composition, structure and behaviour. Next, faba starch and protein were combined to produce gels, a common structure found in many foods from yogurts to sausages. The mixed gel

results were correlated with the results of analysis of the single-system starch. Finally, two food models were designed; a 3D-printed cracker-like product consisting of faba bean starch, protein and fibre, and edible faba bean protein films, aimed for bio-degradable packaging, reinforced with pine cone cellulose.

The faba bean starch formed firm pastes, thanks to long molecular chains and a well-developed paste network. Addition of protein weakened the rigidity of the starch network and produced a denser gel. However, in the 3D-printed crackers, addition of fibre resulted in a more stable product with an airier and lighter texture. Addition of cellulose to the faba bean films improved film strength, barrier properties and heat resistance, but unfortunately the reinforced films also became stiffer and more opaque.

The functionality of faba bean ingredients depended on the food matrix. By controlling the amount and processing of the components, faba bean products with specific texture can be developed, which could avoid the need for stabilisers and enable production of more desirable textures.

Faba bean, Sweden's oldest bean crop, may be the solution to a very topical problem. Faba bean and other bean types should perhaps no longer be referred to as the "poor man's meat", but instead as the "prosperous man's meal", as a future with faba bean may indeed be green.

Populärvetenskaplig sammanfattning

Att öka konsumtionen av lokalt producerade baljväxter har både kost- och miljöfördelar. Koldioxidavtrycket för 1 kg baljväxter är 0,8 kg CO₂-ekvivalenter kontra 28 kg CO₂-ekvivalenter för nötkött. Den svenska kostens miljöpåverkan skulle minska med 20 procent om hälften av köttkonsumtionen ersattes av lokala baljväxter, såsom åkerbönor.

Åkerbönor har utmärkta näringsegenskaper eftersom de är låga i fetthalt och har ett relativt högt proteininnehåll, kostfiber och olika mikronäringsämnen

I Sverige har kategorin växtbaserade produkter de senaste åren ökat med 16%. Men andelen av produkter som innehåller svenska råvaror är liten på marknaden. Istället dominerar importerad soja, där de långa transportsträckorna bidrar till en avsevärd energianvändning och klimatpåverkan. Åkerböna är en gröda anpassad för det svenska klimatet med en bra näringsprofil som potentiellt skulle kunna användas som en lokalt framställd texturerande ingrediens för den svenska marknaden.

Att skapa en tilltalande konsistens är en av de största utmaningarna när man utvecklar växtbaserade livsmedel och är ett av skälen till att konsumenten väljer bort dem. För att uppnå önskvärda texturer kräver växtbaserade produkter ofta omfattande bearbetning och tillsats av stabiliserande ingredienser, vilket strider mot konsumenternas efterfrågan på minimalt bearbetade och ”kravmärkta” etikettprodukter.

I detta projekt undersöktes funktionerna för åkerbönsfraktionerna stärkelse, protein och fiber i olika typer av livsmedelssystem. För det första karakteriserades åkerbönsstärkelsen med avseende på sammansättning, struktur och beteende. Därefter kombinerades stärkelse och protein för att producera geler. Det är en vanlig struktur som finns i många livsmedel allt i

från yoghurt till korv. De blandade gelresultaten korrelerades med analysen av det enklare stärkelsen-systemet. Slutligen designades två livsmedelsmodeller; 3D-printad kexprodukt bestående av stärkelse, protein och fibrer från åkerböna och ätbara proteinfilmerna, förstärkta med tallkottecellulosa, avsedda för biologiskt nedbrytbara förpackningar. Vidare har åkerbönskomponentens påverkan i de olika studierna analyserats.

Åkerbönsstärkelsen bildar fasta geler tack vare långa molekylkedjor och ett välutvecklat gelnätverk. Tillsatsen av protein försvagade gelens styvhet och gav den mer lös konsistens med ett gelnätverk som strukturellt var mera kompakt. I de 3D-printade kexen såg man dock att genom tillsats av fiber bildades en stabilare produkt med en luftigare och mer utvecklat nätverk med lättare textur. Tillsatsen av cellulosa i åkerbönsfilmerna resulterade i en förbättring av filmstyrka, barriäregenskaper och värmebeständighet, men tyvärr på bekostnad av att filmerna blev mer bräckliga och ogenomskinliga. Funktionsdugligheten hos åkerbönskomponenter beror på matmatrisen. Genom att kontrollera mängden och bearbetningen av komponenterna kan åkerbönsprodukter med specifik textur utvecklas i framtiden, vilket kan minska behovet av stabiliseringsmedel och möjliggöra produktion av mer önskvärda texturer.

Åkerbönan, Sveriges äldsta bönsort, kan vara lösningen på ett högaktuellt problem. Kanske borde åkerbönan eller bönor inte längre kallas "den fattigas kött" utan i stället som "den välmående mannens måltid" eftersom de genom sina egenskaper brett kan berika en grön framtid.

Acknowledgements

Late autumn 2022 I had my first baby Xerxes. My thesis late spring 2023, feels like my second baby. I would not have been able to fulfil this PhD project without the support and encouragement from my colleagues, friends and family.

The first person I would like to thank is my main supervisor **Maud**, thank you for selecting me to do this PhD, I have learnt incredibly much and met amazing people through the project. Being a member of your research group has been really enjoyable. Big thanks to my co-supervisors, thank you **Corine** for your help with NMR and all you kind supporting words, **Mikael** thank you for support in both tricky scientific questions and writing of manuscripts and **Rosana** thank you for your help at the start and end om my PhD.

My pre-evaluator of this thesis was **Kati** , thank you for reading my thesis and all the comments. Thank you **Mary** for doing the language corrections.

There are many people at SLU I would like to thank, starting with the members of my research group STEG. **Mathias**, the co-author of two of my papers, thank you so much for your help and guidance in the lab and support when writing the manuscripts. I would not be graduating if I had not had you collaboration. Next to my other office mates **Anja** and **Solja**, than you for your friendships, laughter, stories and advice on various topics. You two have made coming to work such an enjoyable experience. To my fellow foodie **Jaqueline** thanks you for your funny compilations and life queries. To **Johanna** and **Alejandra** thank you for reviewing my thesis and best of luck with your studies! **Hanna**, although you are no longer a PhD I include you in this category, thank you for your kind word that you especially need to hear whilst writing a thesis! **Galia**, my co-course leader in the introduction course, thank you for making an amazing course with me, for making our

research available to the public and LiFT. Finally thank you **Henrik** for sharing you beer and enthusiasm, **Jing** for all the baby clothes and encouragement during my studies and **Saeid** for genuine interest in my research.

Next I would like to thank everyone who also spent much of their break time in the small fika room of the D-corridor. Thank you **Elin, Yan , Troy, Marijana, Björn, Filip , Oksana** and **Ani**, the small lunch room was at times very crowded but full of interesting discussions. To the few who have left SLU but are missed **Johnny, Fredric, Christina, Frida, Maria, Daniel, Lena** and **Mathilde**. To **Vadim** and **Gaulime**, thank you for the different celebrations that you organised for us in the corridor, thank you **Anders** for help on teaching questions. Thank you PhD co-ordinator **Monika**, thank you for standing up for us, supporting me through different issues at SLU. I would also like to thank **all my fellow PhD students** for being there.

I did not do any of the projects in these thesis on my own and would like to thank all my co-authors. Thank you **Fran** and **Özmatin** for your help with the structural characterisation of the starch. **Fanny** for developing the 3D print inks. **Daniel** for your few months at SLU, showing me how to make the films and **Jon** for showing me around the KTH lab. During my time at SLU I was involved in a lot of teaching which I thoroughly enjoyed, I would like to thank all the students I met through the introduction course and the food technology course for giving my PhD another meaning.

Thank you to **all my friends** for supporting and rooting for me.

Till **mamma** och **pappa**, tack så mycket för ert stöd, att ni hejat på mig och låtit mig ta mina egna beslut. Ni har alltid funnits där för mig och ställt upp i vått och torrt och uppmanat mig att följamin drömmar. Tack **Adam** för att jag fick låna kontoret, jag hade aldrig hunnit bli klar annars och tack **Nisse** för att var den sötast taxen som finns. Tack **Pia** för hjälpen med Xerxes, det var tur att farmor bodde så nära.

Sist men definitivt inte minst **Douglas**. Utan din humor, kärlek, tålmod och stöd hade detta aldrig varit möjligt. Ett särskilt tack för ditt stöd de senaste månaderna då du passat **Xerxes** så att jag kan bli klar med min avhandling trots att du själv också pluggar, jag vet inte vad jag skulle ha gjort utan dig.



Physiochemical and thermal characterisation of faba bean starch

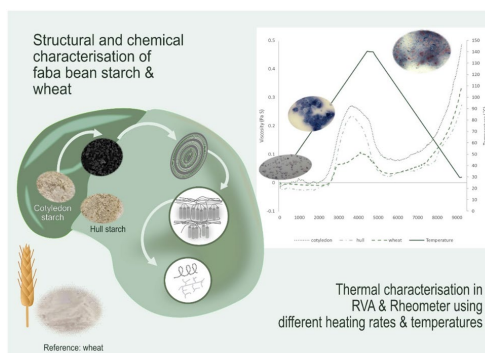
Klara Nilsson¹ · Corine Sandström¹ · Hüsamettin Deniz Özeren^{2,3} · Francisco Vilaplana³ · Mikael Hedenqvist² · Maud Langton¹

Received: 26 April 2022 / Accepted: 14 July 2022
© The Author(s) 2022

Abstract

The structure and physicochemical properties of starch isolated from the cotyledon and hull of faba beans and from wheat (as reference) were examined using 16 different methods. The amylose content in faba bean cotyledon and hull starch was 32% and 36%, respectively, and that in wheat starch was 21%. The faba bean cotyledon and hull starch were structurally alike both displaying C-polymorphic pattern, a similar degree of branching and similar branch chain length distributions. Wheat starch had a significantly greater prevalence of short amylopectin chains (DP < 12) and a higher degree of branching. Granules in both faba bean starches exhibited surface cracks and were more homogenous in size than the smoother wheat starch granules. Gelatinisation temperature was higher for the faba bean starches, likely as an effect of high amylose content and longer starch chains delaying granular swelling. Cotyledon starch produced pastes with the highest viscosities in all rheological measurements, probably owing to larger granules. Higher prevalence of lipids and resistant starch reduced the viscosity values for hull starch. For all starches, viscosity increased at faster heating rates. During the rheological analyses, the samples were exposed to different instruments, heating rates and temperatures ranges, differing from standard rheological procedures, which could help predict how different processing techniques effect the final starch textures.

Graphical abstract



Keywords Amylose · Amylopectin · Degree of polymerisation · Gelatinisation · Rheology · High temperature pasting

Introduction

The food sector accounts for approximately 30% of the world's total energy consumption and 22% of total greenhouse gas emissions [1]. To sustain the growing global

✉ Klara Nilsson
klara.nilsson@slu.se

Extended author information available on the last page of the article

population while combating climate change, a shift towards plant-based dietary patterns is required [2, 3].

Wheat is Sweden's most cultivated crop and [4] has a relatively high soil nutrient requirement thereby increasing demand for mineral fertiliser. Correlation between years with high yields of wheat and sales of mineral fertilisers exists [5]. Negative environmental impact of mineral fertiliser are associated with nutrient leaching which can cause eutrophication and greenhouse gas emissions. In contrast faba beans (*Vicia faba* L.) a cool climate legume that is cultivated in several countries including Sweden [4], contributes to sustainable crop rotations because they can biologically fix atmospheric nitrogen (N₂), thereby diversifying production systems [6]. In Sweden faba beans are currently primarily used as animal feed but the excellent nutritive qualities [7, 8] render them suitable for human consumption. Globally, faba bean is one of the leading crops used for producing pulse protein isolate [9], where starch represents a major side-stream component [3, 8]. To minimise the climate impact of faba bean production, all components of the beans should be utilised.

The physicochemical properties influencing food applications of starch are determined by chemical composition, molecular structure, crystallinity and granular morphology [10–12]. Starch, a glucose polymer, is composed of two types of polysaccharides, almost linear chain amylose and hyperbranched amylopectin [13]. The amylose content in faba bean starch ranges from 29 to 40% [14–16]. The relatively high amylose content gives legume starches characteristic thermal properties such as restricted swelling capacity, high gelation temperature, more prominent aggregation and high final viscosity of gels [10, 12, 17]. Functional and physicochemical properties of pulse starches have been further explained by Singh [12].

The numerous chains in amylopectin are much smaller than the major chains found in amylose [18]. For faba bean amylose the degree of polymerisation (DP) is in the region of 1400 [17] and for amylopectin DP is 20.4 [16]. The amylose forms the amorphous and the amylopectin semi-crystalline granular regions. The radial arrangement of the crystalline amylopectin is believed to cause the birefringence patterns of starch under polarised light. The birefringence pattern for faba bean starch has been reported to be both strong and weak indicating disorganised amylopectin within the crystalline lamella [14, 15]. To further support this theory, scanning electron microscopy (SEM) imaging studies have revealed that faba bean starches are prone to cracking [14, 15] due to sub-optimal packing of starch chains, resulting in more fragile granules [14, 19].

Starch granules swell when heated in excess water because water molecules become linked by hydrogen bonding to the exposed hydroxyl groups of amylose and amylopectin and the crystalline structure is disrupted [12]. The

reported swelling patterns of faba bean starch are somewhat contradicting. Zhang, Tian, Wang, Jiang and Li [15] found that the swelling capacity of faba bean starches increased dramatically at temperatures surpassing 70 °C and progressively increased with temperature, likely due to increased molecular mobility. In another study swelling factor of faba bean starches progressively increased between 60 and 80 °C before declining beyond 85 °C [14]. Initially the presence of granular cracks facilitated the entry of water and increased amylose leaching. However, at temperatures beyond 85 °C the cracks reduced granular integrity therefore retarding the swelling. Compared to other pulse starches, solubility of faba bean starch was comparatively lower at 90 °C, also attributed to the granular integrity where restricted swelling and solubility were present [15].

The presence of granular cracks does not seem to have influenced the measured relative crystallinity of the faba bean starch (18–22%) [12, 13], which is within the reported crystallinity range (17–34%) of pulse starches [17]. Faba bean starches are classified to having the C-type polymorphic pattern; a combination of the more compact A-type pattern and more loosely packed B-type [20], which causes the B-type polymorphs melt at lower temperature than the A-type [21].

During gelatinisation, starch undergoes from order to disorder phase transitions [17]. An observation from multiple studies [14–16] was that the enthalpy of gelatinisation (ΔH) for faba bean starch was in the lower end of the spectrum compared to other legumes. The gelatinisation temperatures ranged from 59 to 75 °C [11, 14–16] which was within the temperature gelatinisation spans reported for other legumes [17]. Li et al. [16] found that starches with a C-polymorphic pattern had lower ΔH than A-type polymorphs. In the study by Ambigaipalan et al. [14] comparing C-type starches, the proportion of B-polymorphic content was not considered a factor influencing the gelatinisation properties. Instead, they [14] ratiocinated that the weakened crystalline structure of faba bean starch lowered the required ΔH . Haase and Shi [22] who compared two varieties Chinese faba bean starches to a German one and found that the smaller German variety had a lower gelatinisation enthalpy.

For pasting to commence, starch granules need to be completely gelatinised [23]. During pasting the starch granules continue to swell with polysaccharides leaching out from the granules resulting in an increase of viscosity occurring during the shearing [12, 24]. Faba bean starch is reported to have high setback and final viscosity [11, 15, 16]. It is hypothesised that aggregation of leached amylose contributes to a strong-gelled network, which can reduce granular breakdown and maintain viscous gels. It is important to note that in each study [10, 13, 14] the heating profile of the rheological measurements was limited to heating the samples to the standard 95 °C. The shape of the obtained pasting curves

indicate that peak viscosity was not attained which could be contributing reason for the high setback and final viscosity. Amylose leaching has been reported to be much higher in faba beans (22%) compared to other bean sorts (black bean (15.5%) and pinto bean (16%)) [25]. The stability of starches is reflected in changes in viscosity during the heating process, while the changes occurring during cooling can predict the texture of the final products [11, 26]. Faba bean starches forming significantly stronger gels than other pulse starches lead Li et al. [16] to suggest that faba bean starch should be used for firm starch gel products such as glass noodles and jello-desserts.

In comparison to cereal starches, pulse starches tend to have a lower GI (glycaemic index) which can be beneficial when moderating insulin response and regulating the glucose metabolism [12]. The higher amylose content, C-type crystalline structure, resistant starch content and absence of pores on granular surfaces in pulse starches are associated with slower digestion rates, thereby improving the satiation effects of the foods [12, 27].

The aims of this study were to determine the chemical and structural composition of starches from Swedish faba bean cotyledon, faba bean hull, and to assess the influence of composition on the thermal properties. Wheat starch was used as a well-known Swedish sourced reference. Molecular size and structure were analysed by a combination of size exclusion chromatography (SEC) and nuclear magnetic resonance spectroscopy (NMR), while the polymorphic configuration of the lamella was measured using X-ray diffraction (XRD) and NMR. The granular swelling profile was visualised using microscopy and results were correlated with differential scanning calorimetry (DSC) measurements. The rheological profile was assessed using different heating profiles, up to 140 °C, and heating rates in a rapid viscosity analyser (RVA) and a rheometer. By comparing how the different heating parameters influence the measured viscosities, processes can be optimised to achieve desired products.

Materials and methods

Materials

Faba beans (*Vicia faba minor*) of the variety *Gloria* grown in central Sweden in 2016 were kindly provided by RISE in Uppsala, Sweden. The cultivar *Gloria* was chosen because it currently cultivated as a food crop due to lower tannin content [28]. The beans were dried until further use.

Prior to starch extraction, the beans were dehulled (Lu Cao Hi-tech Machinery, China). The hull and cotyledon fractions were then separately milled in a rotary mill (Barbender 880803, Duisburg, Germany) with mesh size 0.7 mm.

Starch from wheat, was used as a reference material and was kindly supplied by Lantmännen Reppe AB, Linköping W, Sweden. The reason for choosing wheat starch was because wheat is the most cultivated crop in Sweden [4], wheat starch can therefore be found in an abundance of products and has been widely studied.

Hand-peeling: real ratio of cotyledon to hull in faba beans

To compare the ratio cotyledon to hull produced by the dehulling machine to the true ratio of the fractions, triplicate batches of 100 individual whole faba beans were immersed in distilled water at room temperature for 1 h. The beans were then peeled by hand. The cotyledon and hull fractions were dried separately at 105 °C and their relative proportions in total bean mass were calculated.

Starch extraction

Starch extraction was based upon the extraction procedure of Lee [29] with some minor modifications. In brief, 200 g ± 1 g milled faba fractions cotyledons or hull were steeped in 1 L sodium hydroxide (NaOH) solution (0.02% w/v) for 24 h under continuous stirring at room temperature, and thereafter for a further 24 h without agitation at 4 °C. The bean matter was then separated from the NaOH solution by centrifugation (Thermo Scientific, Sorvall Lynx 4000, Waltham, MA, USA) at 3700×g for 5 min. The supernatant was removed and replaced with distilled water and the centrifugation process was repeated until pH 7 was reached.

After the final wash, the pellet was collected and mixed in a kitchen blender. The homogenised solution was filtered through a Büchner filter with a 70 µm nylon filter. To maximise starch extraction, these mixing and filtering steps were repeated. For starch recovery, the filtrate was left to stand without agitation overnight at 4 °C. The brown top layer of the starch was scraped off and the remaining starch was recovered and dried at 40 °C for 48 h. The dried starch was weighed and gently ground using a pestle and mortar. The starch samples were collected and stored in individual plastic bags for each extraction in a dry room until further analysis. In SEC and XRD measurements, starch from the early and late washing step were compared. However, due to scarcity of the material from the late washing, the extracted starch from each raw material was pooled for the remaining analyses.

All analysis were made in triplicate unless otherwise stated.

Chemical composition analysis of starch

Moisture content

To determine moisture content, 100 mg of samples was dried overnight at 105 °C (Heraeus UT12, Germany). The moisture content was calculated from the difference in mass before and after oven drying.

Total starch and resistant starch

Total starch and resistant starch content were determined using the commercially available resistant starch kit (K-RSTAR 05/19, Megazyme International Ireland Ltd) according to AOAC Official Method 2002.02 [30].

Amylose content

For determining the amylose content, the commercially available AM/AP assay kit (K-AMYL 06/18 by Megazyme International Ireland Ltd) was used with a method modified from Yun and Matheson [31].

Ash content

For determining ash content, the AOAC Official Method 942.05 was followed.

Protein content

Protein content was calculated from the nitrogen content ($N \times 6.25$) measured by the Kjeldahl method [32], using a 2520 digester, Kjeltac 8400 analyser unit and 8460 sampler unit (all from Foss, Denmark).

Fat content

Fat content was determined according to Commission Directive 152/2009 EC (2009) [33] using Hydrotec 8000 and Soxtec 8000 extraction units, both from Foss, Denmark.

Both the measured protein content and crude fat content for the wheat starch were calculated from single measurements, the standard deviation from the experiment control were 0.07 from raw protein and 0.14 from crude fat.

Degree of branching

Degree of branching (DB) [34–36] was determined using ^1H NMR spectroscopy. Starch samples (~10 mg) were placed in 5 mm NMR tubes, deuterated dimethyl sulfoxide ($\text{DMSO}-d_6$, 0.6 mL) was added and the mixture was kept at 80 °C overnight. To avoid spectral disturbance from hydroxyl proton signals, TFA- d_1 (10 μL) was added to the mixture just

before the NMR measurements [36]. The ^1H spectra were recorded on a Bruker Avance III 600 MHz NMR spectrometer, using a 5 mm broadband observe detection smart probe equipped with z-gradient. The ^1H spectra were acquired at 60 or 80 °C, using 128 scans with an acquisition time of 2.7 s and a relaxation delay of 12 s. The anomeric proton at the $\alpha(1 \rightarrow 6)$ -linkage of the branching point, which has a different chemical shift than other anomeric protons, was used for quantification of DB. DB was calculated as the ratio $I1 - 6 / (I1 - 6 + I1 - 4)$, where $I1 - 6$ is the integrated signal at 4.8 ppm and $I1 - 4$ is the integrated signal between 5.0 and 5.2 ppm, corresponding to H1 of glucose at the $\alpha(1 \rightarrow 6)$ and $\alpha(1 \rightarrow 4)$ -linkages, respectively.

Size exclusion chromatography (SEC)

Prior to the SEC analyses, intact branched starch samples were gelatinised and dissolved directly in SEC eluent consisting of dimethyl sulfoxide (DMSO, HPLC grade, Scharlab, Sweden) with 0.5% w/w LiBr (ReagentPlus) in a thermo-mixer at 80 °C with agitation. Enzymatic debranching of the starch molecules was performed with isoamylase (Megazyme, Ireland) in a 0.1 M acetate buffer (pH 3.5) at 37 °C for 4 h. After incubation, the samples were neutralised to pH 6.5–7.0, boiled to deactivate the enzyme, freeze-dried and redissolved in SEC eluent (DMSO with 0.5% w/w LiBr) for subsequent SEC analysis.

Separation of the intact starch samples and the debranched samples was performed in a SECurity 1260 system (Polymer Standard Services, Mainz, Germany) coupled to a multiple-angle laser light scattering detector (MALLS; BIC-MwA7000, Brookhaven Instrument Corp., New York) and a refractive index detector (SECurity 1260, Polymer Standard Services, Mainz, Germany) thermostatted at 45 °C, using a GRAM PreColumn, 30 and 3000 analytical columns (Polymer Standards Services, Mainz, Germany), with a flow rate of 0.5 mL min^{-1} at 60 °C.

Calibration of the SEC separation was performed using the Mark-Houwink relation by injection of pullulan standards provided by Polymer Standards Services (PSS, Mainz, Germany). The Mark-Houwink parameters for pullulan in DMSO/LiBr (0.5 wt%) at 80 °C are $K = 2.427 \times 10^{-4}$ dL g^{-1} and $a = 0.6804$ [37]. Data treatment and collection were performed using WinGPC software (Polymer Standards Services, Mainz, Germany) and the data were further analysed by additional mathematical procedures presented elsewhere [37]. The differential index of refraction (dn/dc) for starch in DMSO/LiBr 0.5% was taken to be 0.0544 mL g^{-1} [37]. Different molecular parameters and distributions, including SEC weight distribution ($w(\log V_h)$), branch chain-length distribution ($w(\log X_{de})$) and size dependence of the weight-average molecular weight ($M_w(V_h)$), were thus obtained. The

macromolecular size distributions are presented in terms of hydrodynamic radius (R_h), with $V_h = 4/3 \pi R_h^3$.

X-ray diffraction (XRD)

The XRD measurements were performed using a Panalytical X'pert Pro operating at 45 kV and 44 mA, with Cu K α radiation. Diffraction patterns were recorded using a radiation wavelength of 1.54 Å. The runs were duplicated for each sample. The crystallinity ratio was determined by the Rietveld method [38]. The crystalline peaks were resolved from the amorphous halo and the relative crystallinity was obtained as the area of the crystalline peaks divided by the total intensity area within 2θ of 3° – 40° [39, 40].

^{13}C CPMAS NMR

^{13}C cross-polarisation (CP) magic angle spinning (MAS) NMR spectra were obtained on a Bruker Avance III 600 MHz spectrometer using a double-resonance 4 mm (^1H & ^{19}F)/(^{15}N , ^{31}P) CP-MAS probe. Starch samples (~80 mg) were packed into 4 mm ZrO $_2$ rotors and the CPMAS spectra were recorded at 25 °C, using a spinning frequency of 12 kHz, a contact time of 1–2 ms and a repetition delay of 2.5–5 s. The amount of water in the dried starch samples was: cotyledon 7.5%, hull 8.6% and wheat 9.5%.

Light microscopy

Starch granules were suspended in 50% (v/v) glycerol/water and aliquots of the starch slurry were pipetted onto a glass slide. To emphasise contrast and granular structure for brightfield microscopy, granules were stained with dilute Logulus/water solution (50% v/v) prior to sealing with a cover slip. Samples were examined under polarized light and differential interface contrast (DIC) was prepared in the same manner as for brightfield microscopy, with the exemption of the Logulus staining. All observations were performed using a light microscope (Nikon Eclipse Ni-SSR 930151, Tokyo, Japan) with objective PlanApo 20 \times (0.75 N.A.) and PlanApo 40 \times (0.95 N.A.). Images were recorded with a Nikon Digital Sight DS-Fi2 camera (Nikon, Tokyo, Japan) with resolution of 2560 \times 1920 pixels.

For image analysis, the micrographs were thresholded in Fiji/ImageJ. To reduce noise, the limitation settings for the images were minimal size 2 μm^2 and circularity 0.2. The programme was set to exclude granules on the micrograph edges.

To calculate average length and width, an ellipse was fitted for each individual granule.

Hot-stage microscopy

A 1 mg sample of starch was suspended with 1 mL distilled water using a vortex mixer, 80 μL of the starch–water slurry were pipetted onto a cover slip and 15 μL of diluted Logulus stock solution were added to dye the starch. The specimen was then observed using brightfield microscopy. A smaller cover slip was placed on top and the sample was sealed with nail polish. For birefringence analysis using polarised light, samples were not stained with Logulus solution.

A tensile-stage Linkam (model TST350, Linkam Scientific Instruments, Surrey, UK) with heating capacity was attached to the light microscope (Nikon Eclipse Ni-SSR 930151, Tokyo, Japan). Samples were observed under both polarized and brightfield light, using objective Plan Fluoro 10 \times (0.30 N.A.). Because of the working distance of objectives, higher magnifications were not possible.

The heating rate was 5 °C/min within the range 25–95 °C. A sequence of images (2560 \times 1920 pixels) was captured with a microscope camera (Nikon, DS-Fi2, Tokyo, Japan) every 12 s, i.e. at each 1 °C temperature interval.

All the acquired images were visually analysed and compared, to pinpoint the temperature at which major granular changes were observed. From 40 to 75 °C at 5 °C intervals, the images were analysed as previously described for light microscopy, using Fiji/ImageJ.

Scanning electron microscopy (SEM)

The starch granules were also analysed by SEM (Hitachi TM-1000, Tokyo, Japan) at an accelerating voltage 15 kV, with an image size of 2560 \times 1920 pixels. Carbon tape with the evenly dispersed starch samples was mounted on an SEM stub and sputter coated with Au (Cressington Scientific Instruments, Sputter coater-108 auto, Watford, UK).

Differential scanning calorimetry (DSC)

Gelatinisation characteristics of starch thermal properties were measured using a Mettler Toledo DSC1. Starch samples 3 ± 1 mg and 12 ± 1 μL distilled water were placed in aluminium pans and sealed hermetically (MT no. 51119872). The sealed pans were allowed to stand overnight at room temperature in order to achieve uniform distribution of water before DSC analysis. The samples were scanned from 30 to 200 °C at a rate of 10 °C/min. A thermogram was recorded with an empty aluminium pan as reference and the blank pan value was subtracted from all measurements. The sample chamber was flushed with inert gas (nitrogen, purge rate 50 mL/min) during the scan.

Rheological measurements

A Rapid Visco Analyzer (RVA, Newport Scientific, Warriewood, NSW, Australia) and a rheometer (HR-3, Discovery Hybrid Rheometer, New Castle, DE, USA) were used to analyse, measure and compare the rheological properties of the different starches depending on heating rate, temperature ranges and which instrument was used.

Rapid Visco Analyzer (RVA)

In the RVA the pasting properties were determined at two different heating rates, 12 °C/min and 1.5 °C/min. For both experimental set-ups, 2 g starch were mixed with 25 mL distilled water. The paddle rotation was 960 rpm for the first 10 s, then constant at 160 rpm for the remainder of the experiment. The samples were equilibrated at 50 °C for 1 min before heating to 95 °C. With heating rate 12 °C/min, the samples were kept at maximum temperature (95 °C) for 2.5 min before cooling at 12 °C/min to 50 °C and held at the final temperature for 2 min. With heating rate 1.5 °C/min, the heated starch mixtures were kept at maximum (95 °C) temperature for 5 min and final (50 °C) temperature 2 min. The interval between viscosity and temperature readings was 4 s. For microscopy analysis, smears of the pastes were made on microscope slides immediately after each run.

Rheometer

Rheology data were obtained using the rheometer equipped with a Peltier pressure cell and steel starch paddle. Two different heating cycles, 50–95–50 °C and 30–140–30 °C, both with a heating rate of 1.5 °C/min, were applied in triplicate to each starch type. Before cooling at the same rate (1.5 °C/min), the samples were held at maximum temperature for 5 min. The rotational speed for the initial 20 s was the device's maximum, i.e. 50 rad/s (477.5 rpm), and then for the remainder of the experiment it was 16.75 rad/s (160 rpm). To mimic the concentration of the starch slurry in the RVA measurements, 2.08 g of starch were mixed with 26 mL distilled water. For microscopy analysis, smears of the pastes were made on glass slips immediately after each run.

Statistical analyses

Statistical analyses were carried out in Excel and Rstudio (Version 1.2.5033, RStudio Inc., MA, USA). One-way and two-way ANOVA with Pearson correlation coefficients and density plots using ggplot2 were created in R.

Results and discussion

Chemical composition

The ratio of cotyledon to hull and the starch content of the hull fraction differed depending on the method used for fraction separation. When the beans were peeled by hand, the cotyledon fraction represented $88.4 \pm 0.2\%$ and the hull fraction $11.6 \pm 0.2\%$ of the whole faba bean mass, and the measured starch content of the hull was negligible ($0.004 \pm 0.00\%$). However, when the beans were peeled by machine, the ratio of cotyledon to hull was estimated to be 78 to 22, and the measured starch content of the hull was $19.1 \pm 0.6\%$ [41]. Therefore, it is likely that part of the hull starch analysed in this study was actually starch from the outer layers of the cotyledon. During the machine-dehulling the embryo location was not taken into consideration.

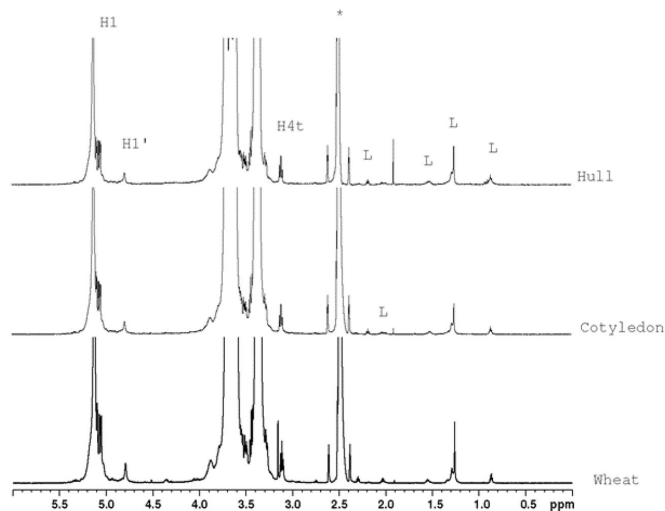
The chemical composition of starch from the cotyledon, hull and wheat samples is summarised in Table 1, the composition of the cotyledon starch was in accordance with literature values [11, 14–16, 22, 29]. The starch extracted from faba bean hull contained significantly more protein and ash as well as more fat, than the other two starches, possible due to the presence of the embryos. The wheat starch contained significantly lower amounts of amylose (21%) compared with the faba bean starches (hull 36%, cotyledon 32%) (Table 3).

The quantity of resistant starch was greatest in the hull (13.1%), followed by the cotyledon (6.7%), while wheat starch contained negligible amounts of resistant starch (0.5%). Resistant starch is defined as the starch that can resist α -amylase hydrolysis in the small intestine and is therefore available for fermentation in the large intestine [42, 43].

Degree of branching

To our knowledge, measuring the degree of branching (DB) in faba bean starch using ^1H NMR is a new feature where comparable values could not be found in literature. Based on the ^1H NMR spectra (Fig. 1), DB of cotyledon, hull and wheat starch was determined to be 4.1, 4.2 and 4.7%, respectively. The slightly higher DB of wheat starch correlates well with its lower amount of amylose. Previous studies have shown that wheat starch has a low level of branching, with α -(1,4)/ α -(1–6) ratio of around 21. Signals from lipids were clearly observed in the ^1H -NMR spectra of, hull, cotyledon and wheat starch samples (Fig. 1), with the profile being slightly different in wheat starch compared with the hull and cotyledon starches.

Fig. 1 ^1H NMR spectra of starch from wheat starch and from faba bean cotyledon and hull. Glucose H1 at the $\alpha(1 \rightarrow 4)$ -linkage (H1) and at the $\alpha(1 \rightarrow 6)$ -linkage (H1') is indicated, as is H4 of non-reducing end terminal residues (H4-t). Beside the H1 and H4 signals from glucose in starch, (L) signals corresponding to lipidic protons are also indicated. *Deuterated dimethyl sulfoxide (DMSO)



Molecular size and degree of polymerisation (DP)

Figure 2 shows the size distributions, $w(\log V_h)$ and absolute molecular weight (M_w) of intact branched starch molecules as a function of their hydrodynamic radius (R_h). A typical bimodal distribution was observed for all starch types, corresponding to the amylose (R_h 10–100 nm) and amylopectin (R_h 100–1000 nm) populations. The absolute molar mass values from light scattering (MALLS) detection were comparable, with average values for the amylose and amylopectin populations in the faba bean cotyledon and hull starches of 10–20 MDa and 60–100 MDa, respectively. These were slightly lower molar masses than in the reference wheat starch. There were no significant differences between the early and late washing faba bean samples.

In the branch chain length distributions as a function of the degree of polymerisation (DP) after enzymatic debranching (Fig. 3), there were two evident peaks for all starches, with a cut-off at around DP 100 in the SEC graphs. Others have identified DP 100 as the cut-off point for amylopectin and amylose [44].

Wheat starch contained proportionately more short-chain amylopectin (DP 6–12) and very-short-chain amylopectin (DP < 6). The branch-chain length distribution was similar for the faba bean cotyledon and hull starches, but the DP distribution for the faba bean starches differed from previously reported values [14, 16] in that they contained a smaller proportion of DP ≤ 24 . Correlation between degree of branching and high prevalence of short chain amylopectin was strong, respectively DP < 6 ($r = 0.99$; $p < 0.001$), DP 6–12 ($r = 1.00$; $p < 0.001$) and DP > 37 ($r = -1$; $p < 0.001$). No statistically significant correlation was found between

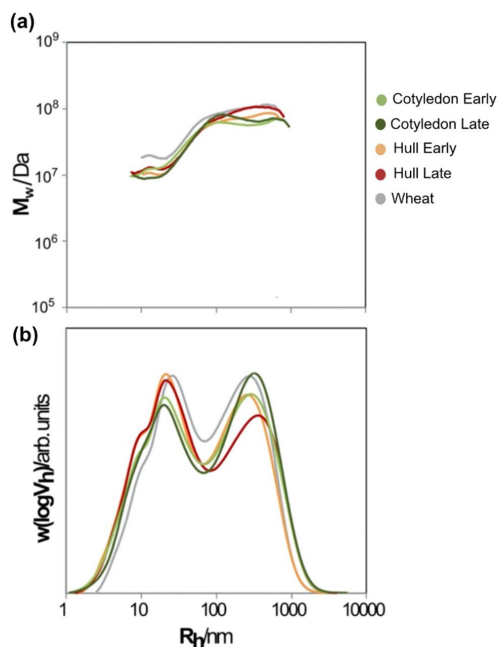


Fig. 2 Distribution of (a) absolute molecular weight [M_w /Da] and (b) size exclusion chromatography (SEC) weight [$w(\log V_h)$] of intact branched starch molecules as a function of the hydrodynamic radius [R_h /nm]. Amylose < [R_h /nm 100] < amylopectin. 'Early' and 'Late' refer to washing steps

Table 1 Chemical composition (dry weight basis) of starch extracted from faba bean cotyledon and hull and from wheat grain (mean \pm standard deviation)

Samples	Chemical composition, %					
	Total starch	Amylose *	Resistant starch*	Protein	Fat	Ash
Cotyledon	95.5 ^b \pm 0.3	32.2 ^b \pm 0.8	6.7 ^b \pm 0.3	0.55 ^a \pm 0.08	0.32 ^a \pm 0.03	0.18 ^a \pm 0.01
Hull	93.6 ^a \pm 0.8	36.0 ^c \pm 0.9	13.1 ^c \pm 1.1	2.8 ^b \pm 0.6	0.53 ^a \pm 0.04	0.46 ^b \pm 0.01
Wheat	99.0 ^c \pm 0.3	21.2 ^a \pm 0.8	0.50 ^a \pm 0.07	0.2 ^a \pm NA	0.40 ^a \pm NA	0.15 ^a \pm 0.01

NA not applicable (the SD from the experiment control were; \pm 0.07 raw protein and \pm 0.14 crude fat)

The superscript lower-case letters signify statistical significant difference compared in each column

*Percentage of total starch

amylopectin molecular weight or hydrodynamic radius with either degree of branching or prevalence of a specific DP.

The most interesting difference between the faba bean starches and the reference wheat starch was in terms of amylose branches. Both faba bean starches showed a bimodal branch chain length distribution for amylose, with two populations centred around DP 700 and DP 2500. In all faba bean samples, the larger branch population (centred around DP 2500) in amylose was more abundant than the smaller (centred around DP 700). On the contrary, wheat starch showed a larger abundance of the shorter amylose branches (centred at DP 1100) than of the longer branches (centred at DP 2500).

X-ray diffraction (XRD)

In the X-ray diffraction spectra of the different starches (Fig. 4), the faba bean cotyledon and hull starches both displayed spectra typical for C-type starches, whilst the spectra for wheat starch resembled the A-type pattern. The hull and wheat starches, but not the cotyledon starch, exhibited low intensity peak at $2\theta = 20^\circ$ (Fig. 4), indicating the presence of V-type amylose lipid complex [45].

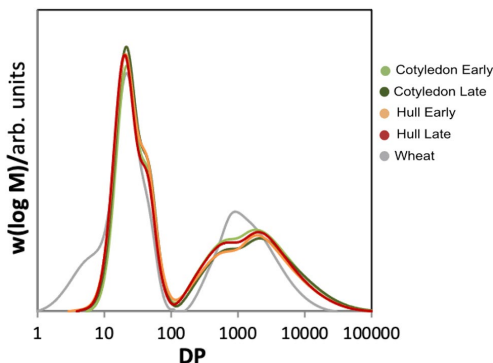


Fig. 3 Branch chain length of the starch i.e. SEC molecular weight [w(logM)] as a function of degree of polymerisation (DP) distribution amylopectin < DP 100 > amylose

The relative crystallinity was highest for wheat starch (18.6%). In both faba bean starches, the relative crystallinity was lower in samples extracted in the late washing (cotyledon 16.4%, hull 16.7%) than in the early washing (cotyledon 17.6%, hull 17.5%). For all samples the relative crystallinity was comparatively lower than previous reports i.e. for wheat (27–36%) [46] and faba 20–22% [14, 15]. Amylose content was negatively correlated ($r = -0.747$; $r < 0.05$) with relative crystallinity, which could be attributed to the fact that amylopectin makes up the semi-crystalline region, whereas amylose is present in the amorphous form [16, 18, 47, 48]. A negative correlation between relative crystallinity and amylose content has been reported previously for a range of legume starches [50].

¹³C CPMAS NMR

The ¹³C CPMAS NMR spectra for the cotyledon, hull and wheat starches are shown in Fig. 5, with the assignment of the C1 to C6 resonances of the glucose-repeating unit indicated at the top of the spectra. The C1 region commonly used to analyse the structure of different types of starch

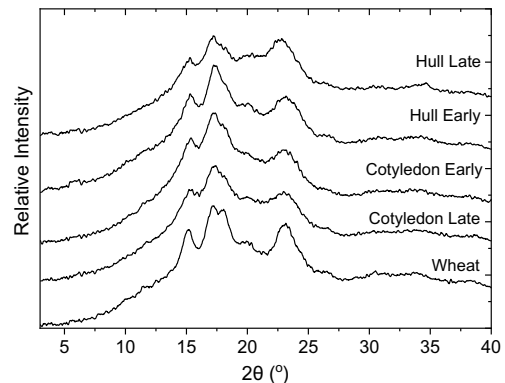


Fig. 4 Wide-angle X-ray powder diffraction spectra of hull starch, cotyledon starch and wheat starch. Strong singlet peaks at 17° and 23° 2θ indicate C-type polymorph for the faba bean starches; hull and cotyledon. Doublet peak at 17 – 18° 2θ and strong peaks at 15° and 23° 2θ in wheat indicates A-type polymorph [49, 50]

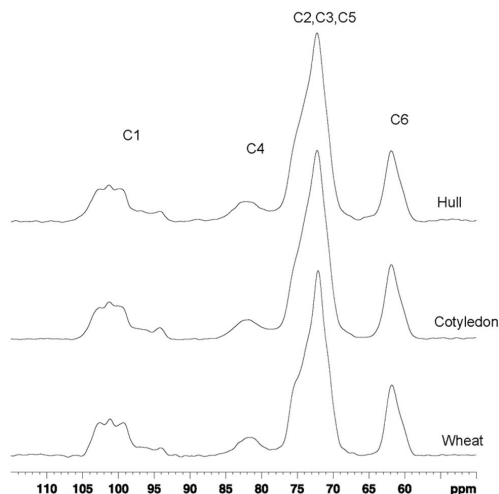


Fig. 5 ^{13}C CP/MAS NMR spectra of wheat, faba bean cotyledon and faba bean hull starches with resolution-enhanced apodization (GB=0.1, LB=-100)

[51–55] exhibits signals from amorphous and crystalline starch with chemical shifts between 93.9 and 105.2 ppm. The C1 signal in wheat starch showed the distinct three-peak pattern characteristic of crystalline A-type starch. For B-type starch, the C1 signal is a doublet, while for C-type starch it is a mixed pattern of both A- and B-types. In general, the C1 signal appears as a triplet if the A-crystalline structure is predominant and as a doublet if the B-type is predominant. Thus, the cotyledon starch had a pattern more similar to that of C-type starch with a predominance of A-type, for the hull starch the triplet pattern was even more nuanced. An interpretation of both the XRD and NMR-spectra of the hull starch could be that the hulls starch also displays the polymorphic-pattern C_A type (closer to A type), as previously observed by Cai, Cai, Man, Zhou and Wei [55]. The broad resonances in the C1 region together with the broad C-4 signal around 80–84 ppm represent amorphous starch (Fig. 4). The signal at 93.9 ppm was present in all CPMAS spectra and was not much broader than the signals from crystalline starch. This signal has been observed in CPMAS NMR spectra of many different types of starch, and has recently been tentatively attributed to constrained conformations [56].

Granular morphology

The size range of the different starch granules at room temperature is shown in Table 2. Mean length and mean width of the cotyledon starch were both larger than for the hull starch, the cotyledon starches were also more uniform in size, with a smaller standard deviation.

Table 2 Granule length and width (mean \pm standard deviation) of faba bean cotyledon starch, faba bean hull starch and wheat starch as measured by light microscopy

Sample	Length μm		Width μm	
Cotyledon	22.8 ^d \pm 6.7		17.1 ^d \pm 4.3	
Hull	21.3 ^c \pm 6.7		15.8 ^c \pm 4.7	
Wheat	A	B	A	B
	19.8 ^b \pm 6.1	7.0 ^a \pm 1.5	15.2 ^b \pm 5.1	6.7 ^a \pm 1.6

The superscript lower-case letters signify statistical significant difference

In both the cotyledon (a2–a5 in Fig. 6) and hull (b2–b5) starches, granule shape varied between ellipsoidal and irregular. In the SEM micrographs, evident cracks were present on granule surfaces for both faba bean starches. The wheat starch (panels c2–c5 in Fig. 6) was composed of both larger A ($> 10 \mu\text{m}$) and smaller B ($< 10 \mu\text{m}$) granules. The wheat starch granules were either round or ellipsoidal, with visible pits or craters on the surface (indicated by chevrons in Fig. 6c). These type of structures are reported to be caused presumably by enzymatic reactions [57].

Panels a3, b3 and c3 in Fig. 6 show the birefringence of starch granules in faba bean cotyledon, faba bean hull and wheat starch, respectively. The birefringence patterns of faba bean granules was both strong and weak, which is consistent with literature values [14]. A less defined Maltese cross was seen for the faba bean samples, presumably due to suboptimal packing of the amylopectin owing to weak interactions between the chains [11, 19] caused by large deviations in amylopectin DP preventing optimal packing of double helical segments [58]. Interestingly, granules displaying weak birefringence patterns had cracks on the surfaces (see arrows in panels a3–a5 & b3–b5 in Fig. 6).

Thermal transitions-granular swelling

Figure 7 shows the size distribution of starch granules at different temperature intervals between 30 and 70 °C measured during the hot-stage microscopy. The microscopy images were separately analysed at 1 °C intervals in order to see more precisely at which temperatures major changes were observed. The size of cotyledon starches (Fig. 7a) started to increase at 61 °C and the greatest increase in size was between 65 and 66 °C, followed by the granules becoming more translucent and merging.

The hull starch (Fig. 7b) was the most heat-tolerant of the three starches, as the granules retained their shape and resisted swelling. For the hull, the most dramatic increment in size was observed between 71 and 72 °C. At 73 °C, the granules became more translucent with jagged edges.

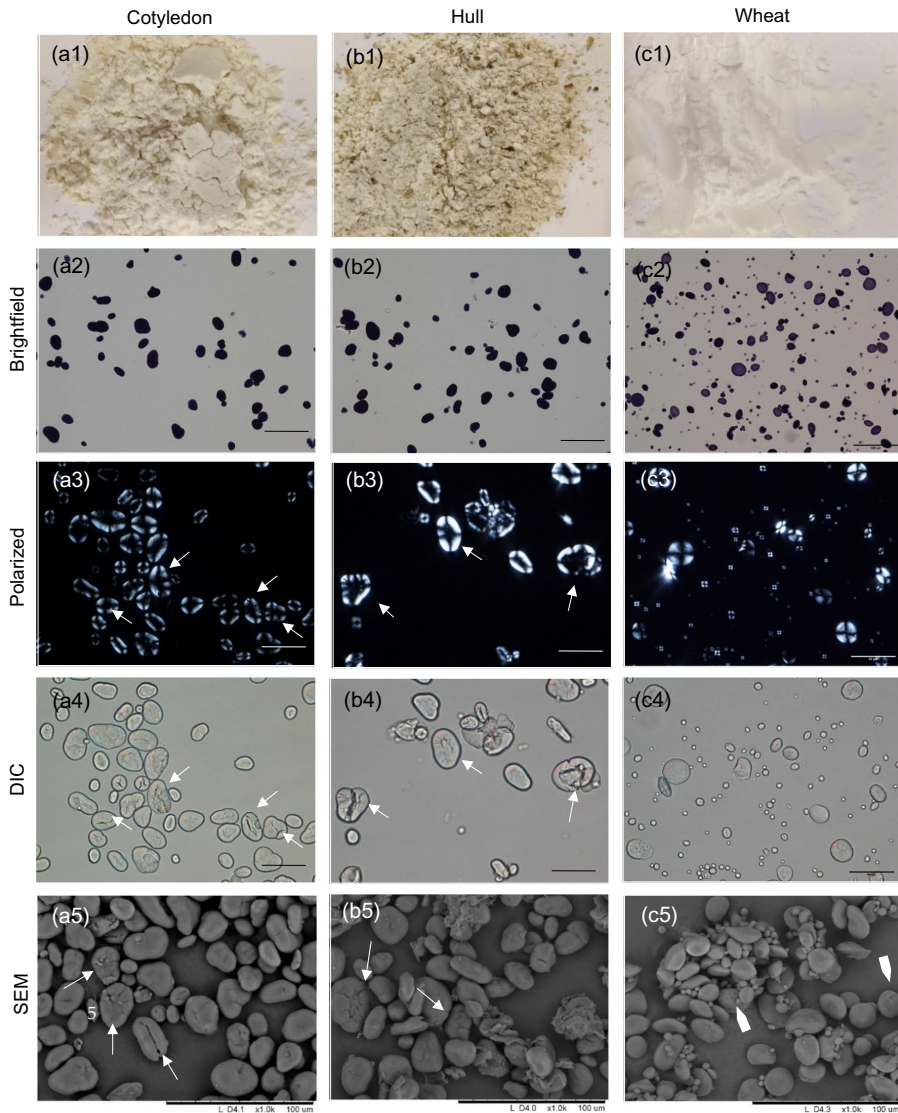


Fig. 6 (a) cotyledon starch; (b) hull starch; (c) wheat starch; (1) Normal photograph; (2) light microscope micrograph; (3) polarized light micrograph; scale bar=100 μm ; (4) differential interface con-

trast (DIC) micrograph; scale bar=50 μm (5) and scanning electron micrograph; scale bar=50 μm . Arrows indicate cracked granules; chevrons indicate surface pitting

The wheat starch (Fig. 7c) was the least heat-tolerant of the three starches. Swelling initiated at 53–54 $^{\circ}\text{C}$, while a dramatic increase in size was observed at 57 $^{\circ}\text{C}$.

Loss of birefringence can be considered as an indicator that the starch has fully gelatinised. Birefringence was

completely lost at 71 $^{\circ}\text{C}$ for the hull, 62 $^{\circ}\text{C}$ for the cotyledon and 58 $^{\circ}\text{C}$ for the wheat.

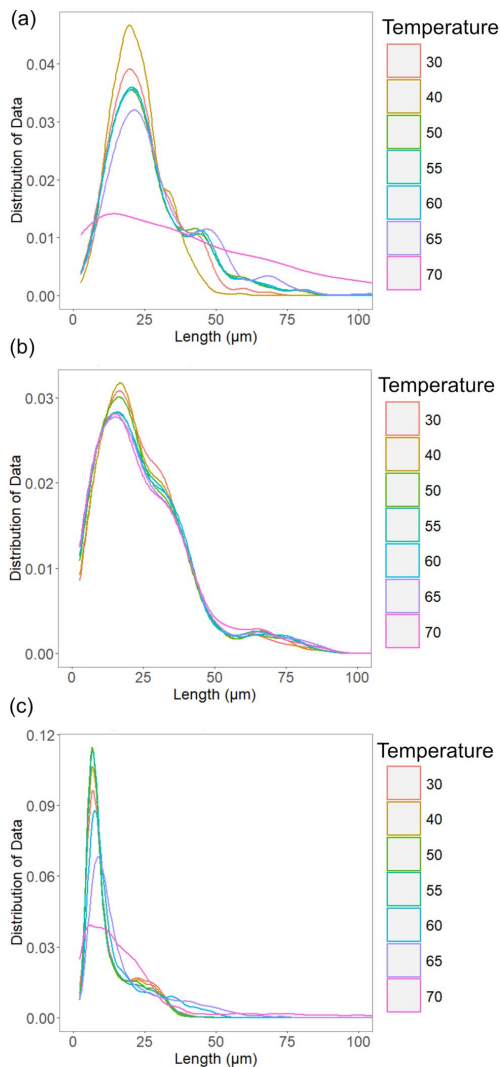


Fig. 7 Density diagrams showing along the x-axis the starch granular length and along the y-axis the distribution of granules within population at different temperatures. **a** Faba bean cotyledon starch; **b** faba bean hull starch and **c** wheat starch during progressive heating from the hot-stage microscopy

Thermal transitions- gelatinisation temperatures

Thermal transition temperatures recorded during the DSC ranked the starches in the order hull > cotyledon > wheat (Table 3). The temperatures recorded for the phase transitions in DSC were in accordance with the changes in

Table 3 Thermal transition temperatures (mean \pm standard deviation) recorded by differential scanning calorimetry (DSC)

Sample	T_o ($^{\circ}\text{C}$) ¹	T_p ($^{\circ}\text{C}$) ²	T_c ($^{\circ}\text{C}$) ³	ΔH (J/g) ⁴
Cotyledon	67.2 ^b \pm 0.1	69.4 ^b \pm 0.1	72.7 ^b \pm 0.3	7.4 ^b \pm 0.3
Hull	70.0 ^a \pm 0.1	72.4 ^a \pm 0.2	75.5 ^a \pm 0.2	7.6 ^b \pm 0.2
Wheat	57.6 ^c \pm 0.2	61.1 ^c \pm 0.1	64.9 ^c \pm 0.1	9.5 ^a \pm 0.2

The superscript lower-case letters signify statistical significant difference.

¹Onset temperature

²Peak temperature

³Endset or conclusion temperature

⁴Enthalpy change

granular structure observed by hot-stage microscopy (Fig. 7). The onset gelatinisation temperature for both faba bean starch samples was higher than in previous reported studies (range 57–65 $^{\circ}\text{C}$), but the endset temperature was more similar to that reported previously (72–75 $^{\circ}\text{C}$) [14–16, 29]. Despite the narrower gelatinisation temperature range for the faba bean samples in this study, the enthalpy of gelatinisation for the hull and cotyledon starches was within the reported range [14–16, 29].

Correlation between gelatinisation temperature and amylose content was strong ($r=0.99$; $p<0.001$). The hull starch, with the highest amylose content, had the most restricted swelling pattern and highest gelatinisation temperature, while the wheat starch, with the lowest amylose content, displayed the lowest gelatinisation temperature. Amylose retards initial swelling by imposing a stabilising effect on the granular structure [59].

The peak temperature during gelatinisation reflects the crystallite quality, while the gelatinisation enthalpy is a reflection of the overall crystallinity and an indicator of the loss of molecular order within the granule [55]. There was a strong negative correlation between gelatinisation temperature and abundance of very short amylopectin chains, ($r=-0.97$; $p=0.006$). It is possible that the higher prevalence of short-chain amylopectin in the wheat reduced the gelatinisation temperature, as the so-called “fingerprint” amylopectin chains (DP 6–8, see Fig. 3) are too short to form double helices and instead cause crystalline defects, which could facilitate the entry of water [19, 20].

The DSC curve (available in supplementary material) of wheat starch exhibited a wider peak than that of the bean samples. This coincided with a wider gelatinisation temperature range (7.3 $^{\circ}\text{C}$) for wheat starch compared with both faba bean starches (5.5 $^{\circ}\text{C}$). The enthalpy of gelatinisation was higher for wheat starch (9.5 J/g) than for cotyledon starch (7.4 J/g) and hull starch (7.6 J/g). The wheat starch contained two distinct granule populations

(see Table 2 and Fig. 6), which could be the reason for the broader gelatinisation range [60].

Pasting

Figure 8 shows pasting curves for heating profile 50–95–50 °C in: RVA with heating rate 12 °C/min (a), RVA with heating rate 1.5 °C/min (b) and rheometer with heating rate 1.5 °C/min (c) and heating profile 30–140–30 °C in rheometer with heating rate 1.5 °C/min (d). It was the striking difference between the shape of the pasting curves and viscosities values of the 12 °C/min

RVA pasting curve (Fig. 8 a) and rheometer pasting curve with heating profile 30–140–30 °C (Fig. 8d), that sparked the investigation to compare the RVA (Fig. 8b) with the rheometer (Fig. 8c) using the same parameters.

The general shape of the pasting curves with the heating profile 50–95–50 °C (Fig. 8; a-c) was similar, with cotyledon starch forming pastes with the highest viscosity, hull starch the second highest viscosity and wheat starch the lowest viscosity. The pasting curves in Fig. 8b and c had the same heating rate of 1.5 °C/min whilst the pasting curve in (Fig. 8a) was the fastest with 12 °C/min. The cotyledon starch began to paste first, at around 77 °C, followed by

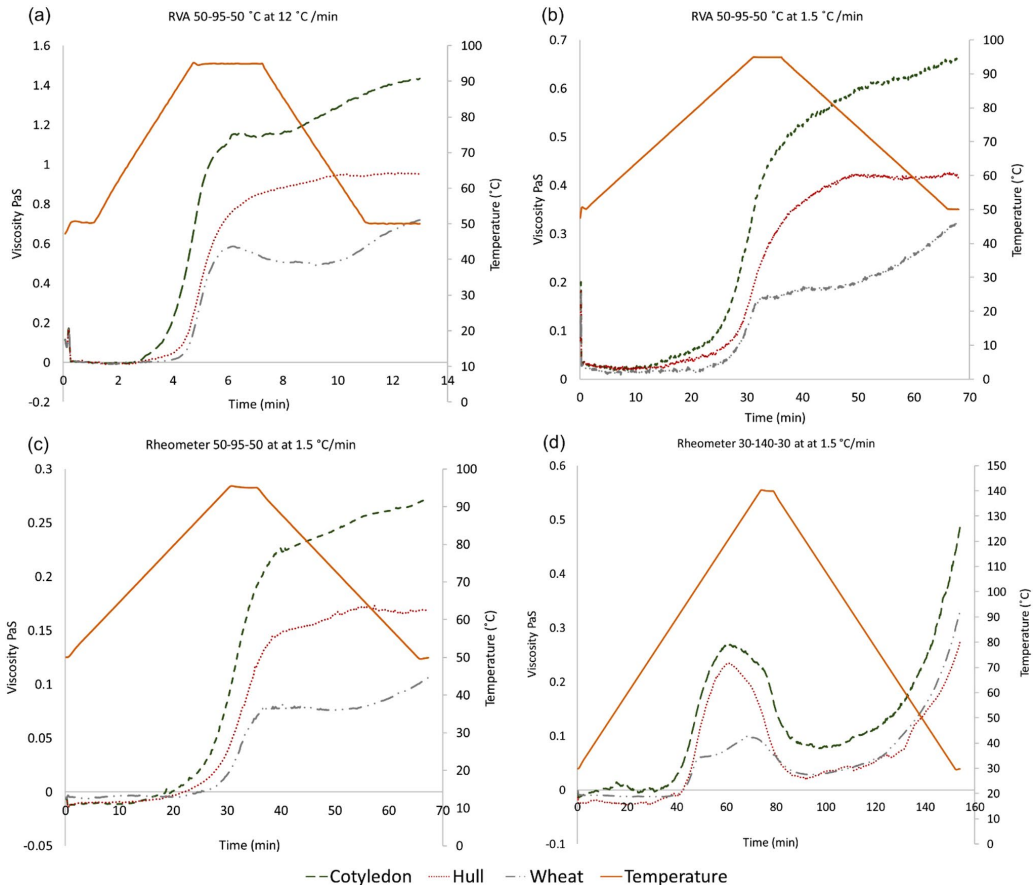


Fig. 8 Pasting curves of faba bean cotyledon starch, faba bean hull starch and wheat starch; **a** Rapid viscosity analysis (RVA) heating profile 50–95–50 at heating rate 12 °C/min; **b** RVA heating profile 50–95–50 at heating rate 1.5 °C/min; **c** rheometer heating profile 50–95–50 at heating rate 1.5 °C/min; **d** Rheometer heating cycle

30–140–30 °C at heating rate 1.5 °C/min. Please note the different viscosity ranges (Pa S) for each pasting graph. In the supplementary material pasting graphs of the same data can be found, only difference is that the Viscosity ranges (Pa S) are the same for all graphs

hull starch (85 °C) and wheat starch (94 °C). The cotyledon and hull starches both displayed the common characteristics of legume starches, i.e. high pasting temperature, absence of peak viscosity, increasing viscosity during the holding period and high set-back (Fig. 8a–c). This in agreement with previous findings for pulse starches [17].

Higher prevalence of longer amylopectin chains and amylose chains was correlated with higher pasting viscosity ($r = 0.99$; $p = 0.001$). The abundance of amylopectin chain with $DP < 6$ in the wheat starch may have further lowered the relative viscosity ($r = -0.97$; $p = 0.008$). The theory is that longer amylopectin chains have the ability to interact with the amylose chains, increasing the aggregation viscosity [44].

The final viscosity for the RVA with a heating rate at 12 °C/min was on average 2.2 times higher than the final viscosity for the same starch when the heating rate was 1.5 °C/min in the RVA and 5.9 times higher than the values measured with the rheometer. A correlation between swollen granular size and peak viscosity after heating cycle 50–95–50 °C was observed ($r = 0.73$; $p < 0.025$). The swollen starch granules in the smear micrographs (see Fig. 9) with heating rate 12 °C/min (Fig. 9a1–c1) were on average 1.3 times larger than when the heating rate was 1.5 °C/min for both the RVA (Fig. 9a2–c2) and the rheometer (Fig. 9a3–c3). Suspensions with larger starch granules have

previously been reported to exhibit higher viscosities [45, 61, 62].

As the RVA consistently measured higher viscosities than the rheometer, possibly due to water evaporation because the RVA is not a fully sealed system, shows that the instruments are not interchangeable.

When using instruments for estimating rheological properties of different food products produced at an industrial scale, an important consideration will be how much material is heated, at what pace and how sealed the heating vessels are.

Heating the samples to 140 °C, which is a much higher temperature than the standard 95 °C, was sufficient for the faba bean starches to achieve peak viscosity, at 119 °C for cotyledon starch and 121 °C for hull starch, followed by an evident viscosity break-down (Fig. 8d). For the wheat starch there appeared to be two peaks, a first smaller peak at 104 °C and a second more pronounced peak at 132 °C, with the first peak presumably reflecting amylopectin melting and the second peak reflecting melting of amylose lipid complexes [63, 64]. Peak viscosity reflects the swelling intensity [65]. Breakdown viscosity occurs because of granule rupture, which induces loss of paste viscosity [66]. In terms of final viscosity, the cotyledon paste was significantly more viscous ($p = 0.003$) than the hull and the wheat starch pastes, while the hull paste was slightly less viscous than the wheat paste, possibly because of disintegration of the granules (Fig. 9a4–c4).

Interestingly, at lower heating temperatures, the hull starch appeared most heat-stable but at very high temperatures, the hull starch produced the softest gels. Comparing the smears from all heating cycles (Fig. 9) the starch granules heated to 95 °C (a1–c3) appear much more intact with low leakage of amylose compared to the smears after heating samples to 140 °C (a4–c4). A negative correlation was found between the pasting set-back after heating the samples to 140 °C and proportion of other components (lipids $r = -0.96$; $p = 0.024$, ash $r = -0.98$; $p = 0.002$). The hull starch was the least pure starch and produced the weakest gels. In the presence of amylose, addition of lipids has been found to reduce paste viscosities because of formation of short pastes [67]. Richardson et al. [63, 68] have also shown that amylose gels with emulsifiers produce weaker gels because the amylose aggregates into clusters, not into networks. For some starches these types of aggregates are only induced after high temperatures, possibly because of the amylose melting [63]. When heating starch to 140 °C, increasing amylose content had a significant effect in increasing the breakdown viscosity ($r = 0.97$; $p = 0.013$). In previous studies [13, 14, 66,] when heating of samples was just to 95 °C, a negative correlation has been observed. A correlation between higher amylose molecular weight (mw) and higher pasting temperature was also observed ($r = 0.97$;

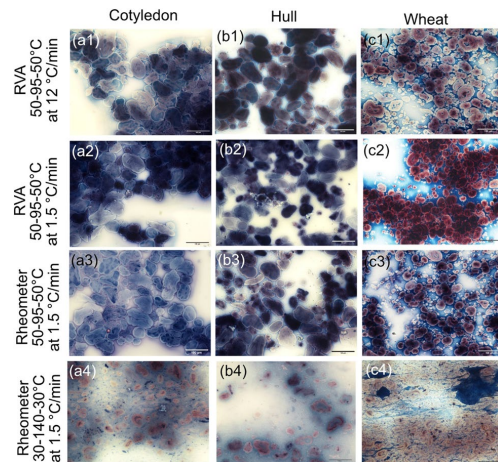


Fig. 9 Smears of starch pastes at the end of rheological heating cycles. The blue areas are amylose and the pink/brown amylopectin. **a** Faba bean cotyledon starch; **b** faba bean hull starch; **c** wheat starch; **(1)** Rapid viscosity analysis (RVA) heating profile 50–95–50 at heating rate 12 °C/min; **(2)** RVA heating profile 50–95–50 at heating rate 1.5 °C/min; **(3)** rheometer heating profile 50–95–50 at heating rate 1.5 °C/min; **(4)** Rheometer heating cycle 30–140–30 °C at heating rate 1.5 °C/min; Scale bar = 100 μm

$p=0.016$) whilst negative correlation was found with amylose molecular weight (mw) and breakdown viscosity after heating the samples to 140 °C ($r = -0.96$; $p= 0.04$). These correlations indicate that larger amylose molecules required more energy to melt and are more difficult to breakdown; however, more research is necessary to validate this theory.

To our knowledge, this is the first time faba bean starch has studied at temperatures up to 140 °C by using rheometry and microscopy. The research results revealed that by altering the heating rate, temperature ranges and instruments, different starch paste textures can be achieved. This research is relevant for many food processes.

Conclusions

In comparison to wheat, faba bean starch produced more viscous pastes attributed to the larger granules and a higher degree of polymerization. The significantly higher amylose content of the faba bean starch to wheat starch, augmented the gelatinisation temperatures. The cotyledon and hull starch from the same botanical origin were more similar to each other, than to the wheat, however, some differences were noted. Compared with the cotyledon starch, the hull starch displayed higher gelatinisation temperature and lower pasting viscosity, possibly due to a higher lipid and resistant starch content creating short pastes.

For all starches, the apparent viscosity was higher when the heating rate was higher (12 °C/min compared to 1.5 °C/min) because of increased granular swelling. Paste viscosities were higher in the RVA than in the fully sealed rheometer, presumably because of a higher water evaporation during the heating. Peak viscosity and breakdown viscosity were achieved at a high temperature cycle (30–140–30 °C), causing substantial breakdown of the swollen granules, which reduced the final viscosities of the starch gels after cooling.

From the results, it can be speculated that food products containing faba bean starch will gelatinise at higher temperature and be more viscous, both during and after heating, than products with wheat starch. Firmness of the food products can also be tailored by controlling heating rate, type of heating vessel and temperature ranges.

Supplementary Information The online version contains supplementary material available at <https://doi.org/10.1007/s11694-022-01543-7>.

Acknowledgements The authors gratefully acknowledge Galia Zamaratskaia for reviewing the paper and Astrid Gumucio and Anna-Greta Haglund efforts in protein and fat analysis.

Author Contributions “Conceptualization, KN and ML.; methodology, KN and ML.; validation, KN and ML; formal analysis, KN.; investigation, KN, HDÖ, FV and CS ; resources, MHe and ML ;

writing—original draft preparation, KN; writing—review and editing, HDÖ, FV , CS, MH and ML; visualization, KN.; supervision, Corine Sandström. MH and ML.; funding acquisition, ML. All authors commented on previous versions of the manuscript. All authors read and approved the final manuscript.”

Funding Open access funding provided by Swedish University of Agricultural Sciences. Svenska Forskningsrådet Formas (2018-018699), Lantmännen Research Foundation (2017F003), and Trees and Crops for the Future (TC4F).

Declarations

Conflict of interest “The authors declare no conflict of interest.” “The funders had no role in the design of the study; in the collection, analyses, or interpretation of data; in the writing of the manuscript, or in the decision to publish the results”.

Open Access This article is licensed under a Creative Commons Attribution 4.0 International License, which permits use, sharing, adaptation, distribution and reproduction in any medium or format, as long as you give appropriate credit to the original author(s) and the source, provide a link to the Creative Commons licence, and indicate if changes were made. The images or other third party material in this article are included in the article's Creative Commons licence, unless indicated otherwise in a credit line to the material. If material is not included in the article's Creative Commons licence and your intended use is not permitted by statutory regulation or exceeds the permitted use, you will need to obtain permission directly from the copyright holder. To view a copy of this licence, visit <http://creativecommons.org/licenses/by/4.0/>.

References

1. R.E.H. Sims, *Energy-Smart Food for People and Climate - Issue Paper* (FAO, Rome, 2011)
2. EAT-Lancet Commission: Summary Report of the EAT-Lancet Commission. (2019)
3. E. Rööf, G. Carlsson, F. Ferawati, M. Hefni, A. Stephan, P. Tidåker, C. Witthöft, Less meat, more legumes: prospects and challenges in the transition toward sustainable diets in Sweden. *Renew. Agric. Food Syst.* **35**, 192–205 (2018)
4. Jordbruksverket; Statistiska centralbyrån: Skörd av spannmål, trindsäd, oljeväxter, potatis och slättervall 2019. SCB (2020)
5. Hellsten, S.A., Hann, S., Johansson, M.E.: Åtgärder och väg framåt för att minska kväve- och fosforanvändningen i samhället. IVL Svenska Miljöinstitutet (2019)
6. M. Fouad, N. Mohammed, H. Aladdin, A. Ahmed, Z. Xuxiao, B. Shiyang, Y. Tao, Faba bean, in *Genetic and Genomic Resources of Grain Legumes Improvement*. ed. by S. Mohar et al. (Elsevier, Amsterdam, 2013), pp. 113–136
7. M.J. Messina, Legumes and soybeans: overview of their nutritional profiles and health effects. *Am. J. Clin. Nutr.* **70**, 439S–450S (1999)
8. F. Guillon, M.M. Champ, Carbohydrate fractions of legumes: uses in human nutrition and potential for health. *Br J Nutr* **88**(Suppl 3), S293–306 (2002)
9. Y. Ren, T.Z. Yuar, C.M. Chigwedere, Y. Ai, A current review of structure, functional properties and industrial applications of pulse starches for value-added utilization. *Compr. Rev. Food Sci. Food Saf.* **20**, 3061–3092 (2021)

10. I.A. Wani, D.S. Sogi, A.M. Hamdani, A. Gani, N.A. Bhat, A. Shah, Isolation, composition, and physicochemical properties of starch from legumes: a review. *Starch - Stärke* **68**, 834–845 (2016)
11. S. Punia, S.B. Dhull, K.S. Sandhu, M. Kaur, Faba bean (*Vicia faba*) starch: structure, properties, and in vitro digestibility: a review. *Legume Sci.* **1**, e18 (2019)
12. N. Singh, Functional and physicochemical properties of pulse starch, in *Pulse Foods Processing, Quality and Nutraceutical Applications*. ed. by B.K. Tiwari, A. Gowen, B. McKenna (Academic Press, London, 2021), pp. 87–112
13. F.L. Stoddard, Starch chemistry, in *Reference Module in Food Science*. ed. by G. Smithers (Elsevier, Amsterdam, 2016), pp. 1–7
14. P. Ambigaipalan, R. Hoover, E. Donner, S. Liu, Q. Jaiswal, R. Chibbar, K.K.M. Nantanga, K. Seetharama, Structure of faba bean, black bean and pinto bean starches at different levels of granule organization and their physicochemical properties. *Food Res. Int.* **44**, 2962–2974 (2011)
15. Z. Zhang, X. Tian, P. Wang, H. Jiang, W. Li, Compositional, morphological, and physicochemical properties of starches from red azuki bean, chickpea, faba bean, and baiyue bean grown in China. *Food Sci. Nutr.* **7**, 2485–2494 (2019)
16. L. Li, T.Z. Yuan, R. Setia, R.B. Raja, B. Zhang, Y. Ai, Characteristics of pea, lentil and faba bean starches isolated from air-classified flours in comparison with commercial starches. *Food Chem.* **276**, 599–607 (2019)
17. R. Hoover, T. Hughes, H.J. Chung, Q. Liu, Composition, molecular structure, properties, and modification of pulse starches: a review. *Food Res. Int.* **43**, 399–413 (2010)
18. E. Bertoft, Understanding starch structure: recent progress. *Agronomy* **7**, 56 (2017)
19. M.A. Glaring, C.B. Koch, A. Blennow, Genotype-specific spatial distribution of starch molecules in the starch granule: a combined CLSM and SEM approach. *Biomacromolecules* **7**, 2310–2320 (2006)
20. C. Gernat, S. Radosta, D. Damaschun, Supramolecular structure of legume starches revealed by X-Ray scattering. *Starch/Stärke* **42**, 175–178 (1990)
21. Y. Ai, J.-L. Jane, Gelatinization and rheological properties of starch. *Starch - Stärke* **67**, 213–224 (2015)
22. N.U. Haase, H.L. Shi, A characterization of Faba Bean starch (*Vicia faba* L.). *Starch/Stärke* **43**, 205–208 (1991)
23. S. Balet, A. Guelpa, G. Fox, M. Manley, Rapid Visco Analyser (RVA) as a tool for measuring starch-related physicochemical properties in cereals: a review. *Food Anal. Methods* **12**, 2344–2360 (2019)
24. R. Tester, W. Morrison, Swelling and gelatinization of cereal starches. I. Effects of amylopectin, amylose and lipids. *Cereal Chem.* **67**, 551–557 (1990)
25. P. Ambigaipalan, R. Hoover, E. Donner, Q. Liu, Retrogradation characteristics of pulse starches. *Food Res. Int.* **54**, 203–212 (2013)
26. M. Kaur, K.S. Sandhu, S.-T. Lim, Microstructure, physicochemical properties and in vitro digestibility of starches from different Indian lentil (*Lens culinaris*) cultivars. *Carbohydr. Polym.* **79**, 349–355 (2010)
27. A.P. Nugent, Health properties of resistant starch. *Br. Nutr. Found.* **30**, 27–54 (2005)
28. Sverigeförsöken: Sverigeförsöken Trial report 2012 Middle Sweden. (2012)
29. H.J. Lee, *The isolation and characterisation of starches from legume grains and their application in food formulations* (RMIT University, Melbourne, 2007), p. 197
30. AOAC International, *Official Methods of Analysis*, 17th edn. (AOAC International, Rockville, 2000)
31. S.H. Yun, N.K. Matheson, Estimation of amylose content of starches after precipitation of amylopectin by concanavalin-A. *Starch/Stärke* **42**, 302–305 (1990)
32. Nordic Committee on Food Analysis, *Nitrogen. Determination in food and feed according to Kjeldahl* (Nordic Committee on Food Analysis, Bergen, 1976), p. 6
33. European Commission: Determination of crude oils and fat. Official Journal of the European Communities, (2009)
34. L. Dunn Jr., W. Krueger, Branching ratios of starch via proton nuclear magnetic resonance and their use in determining amylose/amylopectin content: evidence for three types of amylopectin. *Macromol. Symp.* **140**, 179–186 (1999)
35. M. Gidley, Quantification of the structural features of starch polysaccharides by NMR spectroscopy. *Carbohydr. Res.* **139**, 85–93 (1985)
36. G. Nilsson, K. Bergquist, U. Nilsson, L. Gorton, Determination of the degree of branching in normal and amylopectin type potato starch with ¹H-NMR spectroscopy. Improved resolution and two-dimensional spectroscopy. *Starch/Stärke* **48**, 352–357 (1996)
37. F. Vilaplana, R.G. Gilbert, Two-dimensional size/branch length distributions of a branched polymer. *Macromolecules* **43**, 7321–7329 (2010)
38. H.M. Rietveld, A profile refinement method for nuclear and magnetic structures. *J. Appl. Crystallogr.* **2**, 65–71 (1969)
39. H.D. Özeren, R.T. Olsson, F. Nilsson, M.S. Hedenqvist, Prediction of plasticization in a real biopolymer system (starch) using molecular dynamics simulations. *Mater. Des.* **187**, 108387 (2019)
40. P.H. Hermans, A. Weidinger, Quantitative X-ray investigations on the crystallinity of cellulose fibers. A background analysis. *J. Appl. Phys.* **19**, 491–506 (1948)
41. M. Johansson, D. Johansson, A. Ström, J. Rydén, K. Nilsson, J. Karlsson, R. Moriana, M. Langton, Effect of starch and fibre on faba bean protein gel characteristics. *Food Hydrocolloids* **131**, 107741 (2022)
42. H.N. Englyst, S.M. Kingman, J.H. Cummings, Resistant starch: Measurement in foods and physiological role in man, in *Plant Polymeric Carbohydrates*, vol. 134, ed. by F. Meuser, D.J. Manners, W. Seibel (The Royal Society of Chemistry, Cambridge, 1993), pp. 137–146
43. R. Hoover, Y. Zhou, In vitro and in vivo hydrolysis of legume starches by α -amylase and resistant starch formation in legumes—a review. *Carbohydr. Polym.* **54**, 401–417 (2003)
44. C. Li, A. Wu, W. Yu, Y. Hu, E. Li, C. Zhang, Q. Liu, Parameterizing starch chain-length distributions for structure-property relations. *Carbohydr. Polym.* **241**, 116390 (2020)
45. R. Bajaj, N. Singh, A. Kaur, N. Inouchi, Structural, morphological, functional and digestibility properties of starches from cereals, tubers and legumes: a comparative study. *J. Food Sci. Technol.* **55**, 3799–3808 (2018)
46. K. Dome, E. Podgorbunskikh, A. Bychkov, O. Lomovsky, Changes in the crystallinity degree of starch having different types of crystal structure after mechanical pretreatment. *Polymers* **12**, 641 (2020)
47. V. Vamadevan, E. Bertoft, Structure-function relationships of starch components. *Starch - Stärke* **67**, 55–68 (2015)
48. S. Pérez, E. Bertoft, The molecular structures of starch components and their contribution to the architecture of starch granules: a comprehensive review. *Starch - Stärke* **62**, 389–420 (2010)
49. W. He, C. Wei, Progress in C-type starches from different plant sources. *Food Hydrocolloids* **73**, 162–175 (2017)
50. S. Hizukuri, X-ray diffractometric studies on starches. *Agric. Biol. Chem.* **25**, 45–49 (1961)
51. M.J. Gidley, S.M. Bociek, Organization in starches. *J. Am. Chem. Soc.* **107**, 7040–7044 (1985)

52. H. Tang, B. Hills, Use of ^{13}C MAS NMR to study domain structure and dynamics of polysaccharides in the native starch granules. *Biomacromolecules* **4**, 1269–1276 (2003)
53. K. Morgan, R. Furneaux, N. Larsen, Solid-state NMR studies on the structure of starch granules. *Carbohydr. Res.* **276**, 387–399 (1995)
54. F. Zhu, NMR spectroscopy of starch systems. *Food Hydrocolloids* **63**, 611–624 (2017)
55. J. Cai, C. Cai, J. Man, W. Zhou, C. Wei, Structural and functional properties of C-type starches. *Carbohydr. Polym.* **101**, 289–300 (2014)
56. M. Paris, H. Bizot, J. Emery, J.Y. Buzare, A. Buleon, NMR local range investigations in amorphous starchy substrates I. Structural heterogeneity probed by ^{13}C CP–MAS NMR. *Int. J. Biol. Macromol.* **29**, 127–136 (2001)
57. E.A. Meireles, C.N. Carneiro, R.A. DaMatta, R.I. Samuels, C.P. Silva, Digestion of starch granules from maize, potato and wheat by larvae of the the yellow mealworm, *Tenebrio molitor* and the Mexican bean weevil, *Zabrotes subfasciatus*. *J. Insect. Sci.* **9**, 43 (2009)
58. A. Blennow, M. Hansen, A. Schulz, K. Jorgensen, A.M. Donald, J. Sanderson, The molecular deposition of transgenically modified starch in the starch granule as imaged by functional microscopy. *J. Struct. Biol.* **143**, 229–241 (2003)
59. V. Vamadevan, E. Bertoft, Observations on the impact of amylopectin and amylose structure on the swelling of starch granules. *Food Hydrocolloids* **103**, 105663 (2020)
60. N. Singh, J. Singh, L. Kaur, N. Singh Sodhi, B. Singh Gill, Morphological, thermal and rheological properties of starches from different botanical sources. *Food Chem.* **81**, 219–231 (2003)
61. S. Singh, N. Singh, N. Isono, T. Noda, Relationship of granule size distribution and amylopectin structure with pasting, thermal, and retrogradation properties in wheat starch. *J. Agric. Food Chem.* **58**, 1180–1188 (2010)
62. Y.I. Cornejo-Ramírez, O. Martínez-Cruz, C.L. Del Toro-Sánchez, F.J. Wong-Corral, J. Borboa-Flores, F.J. Cinco-Moroyoqui, The structural characteristics of starches and their functional properties. *CyTA J. Food* **16**, 1003–1017 (2018)
63. G. Richardson, S. Kidman, M. Langton, A.-M. Hermansson, Differences in amylose aggregation and starch gel formation with emulsifiers. *Carbohydr. Polym.* **58**, 7–13 (2004)
64. A. Ahuja, R. Lee, A. Latshaw, P. Foster, Rheology of starch dispersions at high temperatures. *J. Texture Stud.* **51**, 575–584 (2020)
65. M. Schirmer, M. Jekle, T. Becker, Starch gelatinization and its complexity for analysis. *Starch Stärke* **67**, 30–41 (2015)
66. M. Schirmer, A. Höchstötter, M. Jekle, E. Arendt, T. Becker, Physicochemical and morphological characterization of different starches with variable amylose/amylopectin ratio. *Food Hydrocolloids* **32**, 52–63 (2013)
67. Y. Ai, J. Hasjim, J.L. Jane, Effects of lipids on enzymatic hydrolysis and physical properties of starch. *Carbohydr. Polym.* **92**, 120–127 (2013)
68. G. Richardson, Y. Sun, M. Langton, A.-M. Hermansson, Effects of Ca- and Na-lignosulfonate on starch gelatinization and network formation. *Carbohydr. Polym.* **57**, 369–377 (2004)

Publisher's Note Springer Nature remains neutral with regard to jurisdictional claims in published maps and institutional affiliations.

Authors and Affiliations

Klara Nilsson¹  · Corine Sandström¹ · Hüsametlin Deniz Özeren^{2,3}  · Francisco Vilaplana³  · Mikael Hedenqvist²  · Maud Langton¹ 

Corine Sandström
corine.sandstrom@slu.se

Hüsametlin Deniz Özeren
ozeren@kth.se

Francisco Vilaplana
franvila@kth.se

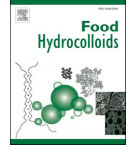
Mikael Hedenqvist
mikaelhe@kth.se

Maud Langton
maud.langton@slu.se

¹ Department of Molecular Sciences, SLU - Swedish University of Agricultural Sciences, Box 7015, 750 07 Uppsala, Sweden

² Division of Polymeric Materials, Department of Fibre and Polymer Technology, KTH- Royal Institute of Technology, 10044 Stockholm, Sweden

³ Division of Glycoscience, Department of Chemistry, KTH- Royal Institute of Technology, 10621 Stockholm, Sweden



Pasting and gelation of faba bean starch-protein mixtures

Klara Nilsson^{a,*,1}, Mathias Johansson^{a,*,1}, Corine Sandström^a, Hanna Eriksson Röhnisch^a, Mikael S. Hedenqvist^b, Maud Langton^a

^a Department of Molecular Sciences, Swedish University of Agricultural Sciences, Box 7015, SE-750 07, Uppsala, Sweden

^b Division of Polymeric Materials, Department of Fibre and Polymer Technology, KTH-Royal Institute of Technology, 10044, Stockholm, Sweden

ARTICLE INFO

Keywords:

Faba bean
Protein
Starch
Texture
Microstructure
Gelation

ABSTRACT

Starch and protein are major components in many foods, contributing to nutritional and textural properties. Understanding how the behaviour and interactions of these components contribute to different textures is important. In this study, mixed gel systems were created with different ratios of starch to protein (constant solid content 12%) extracted from faba bean, a promising crop for locally produced plant-based foods in cold climate regions. The mixed starch-protein gels were characterised in terms of pasting, texture and microstructure. Starch-rich mixtures showed higher water binding and water absorption than samples with higher protein content. A tendency for more efficient hydration in starch-rich samples was confirmed by NMR. Iodine affinity appeared to be lower for high-protein samples, particularly at higher temperatures. Mixtures with high starch content also showed higher viscosity during pasting, higher storage modulus throughout gelation, lower $\tan \delta$ and lower frequency dependence of the final gel. Characterisation by compression tests showed stronger and more elastic gels with increasing starch content. Light microscopy revealed that starch granules were tightly packed, especially at higher starch content, with protein filling the spaces between starch granules. SEM micrographs revealed a network structure with larger pores and thicker strands in samples with higher starch content. Overall, increasing protein content reduced viscosity during pasting and caused softer gels, likely owing to different gelation and hydration properties of starch and protein.

1. Introduction

Transitioning to more plant-based diets is suggested to have nutritional and environmental benefits (Röös et al., 2020; Willett et al., 2019). Across Europe, a trend for greater interest in plant-based foods is emerging (Aschemann-Witzel, Gantriis, & Fraga, 2021). There are many reasons why consumers opt for plant-based foods, including health, sustainability and animal welfare (Aschemann-Witzel et al., 2021). Consumers are now demanding a greater array of plant-based products using simple ingredients with good organoleptic properties. Faba bean already has an established market for animal feed and an emerging market for human consumption, and is a high-protein crop that can be grown in Northern Europe. With increased research and technological innovation, faba bean has the potential to be used in locally produced and sustainable plant-based foods (Multari, Stewart, & Russell, 2015).

Under appropriate processing conditions, faba bean starch and faba

bean protein can both act as a gelling agent, but with different gelling abilities and properties. In real food matrices, starch and protein are likely to be blended and interactions between the biopolymers will influence the formation and texture of the final gel. Depending on the final food product, different gel textures and structures will be acceptable. The gelling properties and mixability of starch and protein are among the most important features in food formulation (Onwulata, Tunick, & Thomas-Gahring, 2014; Schorsch, Wilkins, Jones, & Norton, 2001).

Gelatinisation is a process whereby starch granules swell and leach out amylose during heating in excess water. According to Walstra (2002), as the system cools a gel can develop through the formation of microcrystallites between the amylose chains and/or as a closely packed system of granules, with the amylose layer acting as glue between the granules. Faba bean starch gels are reported to be strong and firm (Li et al., 2019). Faba bean also has high final viscosity during pasting, which has been attributed to the relatively high amylose content

* Corresponding author.

** Corresponding author.

E-mail addresses: klara.nilsson@slu.se (K. Nilsson), mathias.johansson@slu.se (M. Johansson).

¹ These authors contributed equally.

(Ambigaipalan et al., 2011; Li et al., 2019; Punia, Dhull, Sandhu, & Kaur, 2019; Zhang, Tian, Wang, Jiang, & Li, 2019) that aggregates to form a gel network upon cooling. High amylose content has also been related to retarded swelling of starch granules (Nilsson et al., 2022; Sasaki & Matsuki, 1998; Tester & Morrison, 1990; Vamadevan & Bertoft, 2020). Faba bean starch has been found to leach out more amylose than other bean varieties with similar amylose content, contributing to a rise in viscosity (Ambigaipalan et al., 2011; Ambigaipalan, Hoover, Donner, & Liu, 2013). Two other factors that result in faba bean starch gels having higher viscosity than e.g. wheat starch gels are larger size of the swollen granules and higher prevalence of larger polymer chains (Nilsson et al., 2022). Amylose and amylopectin molecular weight in faba bean starch is reported to be 10–20 MDA and 60–100 MDA, respectively, and heating the starch at a higher rate (12 °C/min vs 1.5 °C/min) to temperatures below peak viscosity (119 °C for faba bean) has been found to produce the most viscous gels (Nilsson et al., 2022). The temperature range for gelatinisation of faba bean starch has been shown to be 59–75 °C (Ambigaipalan et al., 2011; Li et al., 2019; Nilsson et al., 2022; Punia et al., 2019; Zhang et al., 2019), with pasting commencing at around 77 °C.

Similarly to starch gelatinisation, protein gelation is an essential process in the production of many foods. Most legumes, including faba bean, contain mainly globular proteins (Kimura et al., 2008; Nicolai & Chassenieux, 2019). The globular proteins in faba bean can be divided into two major fractions, hexameric legumin-type (11S) and trimeric vicilin-type (7S) globulins, with an approximate size of 330 and 150 kDa, respectively (Sharan et al., 2021; Warsame, O'Sullivan, & Tosi, 2018). Gelation of globular proteins occurs by complete or partial denaturation of the protein, exposing hydrophobic residues and other interaction sites (Zha, Rao, & Chen, 2021). The newly exposed parts of the protein interact and aggregate to form a network if the protein concentration is sufficiently high (Zha et al., 2021). The gelation process and gel properties of proteins are affected by multiple factors, such as pH, presence of salt, extraction method and protein source (Langton et al., 2020; Ma et al., 2022; Nicolai & Chassenieux, 2019). A denaturation point within the range 75–95 °C, depending on the ionic strength of the environment, has been reported for the 7S and 11S fractions in faba bean protein (Kimura et al., 2008). Gelation of faba bean protein and the effects of salt, pH and extraction method have been studied previously (Langton et al., 2020). The effect of partly replacing faba bean protein with starch and/or fibre has been investigated previously, resulting in an increased storage modulus of gels whilst the fracture stress was simultaneously reduced (Johansson, Johansson, et al., 2022).

In brief, concentrated starch gels can be described as a composite system consisting of swollen granules embedded in a three-dimensional network of aggregated amylose chains (Yang, Irudayaraj, Otgonchimeg, & Walsh, 2004), while globular proteins form fine-stranded gel networks at high repulsion or a coarse-stranded network of colloidal particles as the isoelectric point is approached (Langton et al., 2020; Langton & Hermansson, 1992). Depending on the ratio of starch to protein, gel formation and properties may differ, with e.g. higher protein content in starch-protein composite gels being associated with augmented pasting temperature and reduced gel firmness (Bravo-Núñez, Garzón, Rosell, & Gómez, 2019; Joshi, Aldred, Panozzo, Kasapis, & Adhikari, 2014; Núñez-Santiago, Bello-Pérez, & Tecante, 2004; Oñate Narciso & Brennan, 2018; Onwulata et al., 2014; Ribotta, Colombo, León, & Añón, 2007; Yang et al., 2004). According to Eliasson (1983), higher protein content alters the water retention capacity of the system because the proteins compete with starch for available water, thereby causing an increase in pasting temperature. Protein adsorption to granule surfaces during pasting could explain both the reduced pasting viscosity and increased pasting temperature, as the adsorbed proteins would restrict water diffusion and thus reduce and delay granule swelling (Bravo-Núñez et al., 2019; Bravo-Núñez & Gómez, 2019; Oñate Narciso & Brennan, 2018). Joshi et al. (2014) found that the pasting temperature increased from 73.5 °C in 100% starch systems to 82.4 °C in

50:50 lentil starch/lentil protein systems, and attributed this to the characteristically high denaturation temperature (118 °C) of lentil protein isolate. The decrease in pasting viscosity with increasing protein content may also be partly due to an overall reduction in the starch fraction, as starch tends to form more viscous pastes. However, the apparent viscosities of blends were reported to be higher in the corresponding diluted starch systems, indicating that protein-starch interactions also alter the gelatinisation and gelling properties (Bravo-Núñez et al., 2019; Bravo-Núñez & Gómez, 2019).

Breakdown viscosity has also been found to be lower for starch-protein mixtures compared to that of the corresponding sample containing only starch (Oñate Narciso & Brennan, 2018; Onwulata et al., 2014). In a study adding 10% extra protein, breakdown of starch-protein mixed pastes was no longer detected, suggesting that the protein gel network increased the resistance to mechanical shearing (Joshi et al., 2014). During cooling of starch dispersions, gelation occurs as amylose and amylopectin aggregate to form a gel network, but higher protein content has been found to correlate with a reduction in final viscosity (Bravo-Núñez et al., 2019; Bravo-Núñez & Gómez, 2019; Joshi et al., 2014; Oñate Narciso & Brennan, 2018; Onwulata et al., 2014; Ribotta et al., 2007). The amylose:amylopectin ratio in starch has been shown to have an effect on the viscosity and gel strength of composite gels, with the reduced viscosities associated with incorporation of protein being more pronounced for high-amylose starches (Joshi et al., 2014; Oñate Narciso & Brennan, 2018). Studies by Oñate Narciso and Brennan (2018) and Onwulata et al. (2014) revealed that proteins appeared to prevent molecular rearrangement of amylose, resulting in weaker gels. In contrast, the rigidity of high-amylopectin starch gel has been shown to increase with additional protein, as the protein acts as a filler (Onwulata et al., 2014).

Gels with higher solids content tend to be firmer and stronger, e.g. Yang et al. (2004) found that the reducing effect of protein on gel firmness became less marked as the solids content increased. Shim and Mulvaney (2001) observed a similar effect in gels with 15% solids content, where addition of whey protein isolate had a diluting effect on corn starch (Shim & Mulvaney, 2001). As the solids content increased to 30% in that study, separate phases in the mixtures were still present but the complex modulus (G^*) increased, suggesting that the gel structure was maintained by the higher solids content.

The aim of the present study was to evaluate gel formation and pasting properties of different faba bean starch-protein gel mixtures. Gel microstructures were evaluated and continuous and discrete phases in the gels were identified. The gel structures observed were then compared against physical and textural attributes of the gels. By understanding the role of protein and starch in composite gel systems, products with tailored textures and functionality can be developed.

2. Materials and methods

To assess gel formation and properties, different analytical techniques were applied at different stages of gel production. The key steps in gel production are summarised, together with the analytical techniques applied during the different steps of gel formation, in Fig. S1 in Supplementary Information (SI).

2.1. Materials

The protein and starch fractions used in this study were isolated from dehulled and finely milled faba beans (*Vicia faba* var. Gloria) grown in central Sweden, harvested and dried in 2016. The beans were kindly provided by RISE (Research Institutes of Sweden). Based on previous characterisations by Johansson, Johansson, et al. (2022), the composition of the protein fraction was: protein 77.3%, starch 0.3%, fibre 1.0%, fat 3.4% and ash 8%, while that of the starch fraction was: protein 0.5%, starch 94.5%, fibre 2.2%, fat 0.3% and ash 0.2%.

Hydrochloric acid (HCl) and sodium hydroxide (NaOH) were

purchased from Merck, ethanol from Solveco, osmium tetroxide and glutaraldehyde from Ted Pella, ruthenium red and light green from Sigma-Aldrich, Technovit 7100 from Kulzer and iodine from Fluka.

2.2. Extraction

Extraction of the protein and starch fractions was performed using methodology described previously (Johansson, Nilsson, Knab, & Langton, 2022). In brief, dehulled and milled faba beans were dispersed in de-ionised water with pH adjusted to 9. Protein was separated from starch and fibre by centrifugation and precipitated from the supernatant by adjusting the pH to 4. The mixture was further centrifuged and washed once before adjusting the pH back to 7 and freeze-drying. The pellet from the initial centrifugation was used to extract starch. First, the pellet was re-dispersed in de-ionised water and the pH was adjusted to 9.5. The mixture was then stirred for 24 h at room temperature and left to stand without agitation for an additional 24 h at 4 °C, followed by centrifugation and washing until pH 7 was reached. Finally, the starch was separated by filtering through a 70 µm nylon filter and dried at 40 °C.

2.3. Gel formation

Starch and protein flours were mixed well and then dispersed in distilled water to obtain a final concentration of 12% (g flour/g sample). The following starch:protein (S%P%) ratios were produced (values in brackets are percentage starch or protein in the total sample):

S100P0: Starch 100% (12%), protein 0% (0%)
 S90P10: Starch 90% (10.8%), protein 10% (1.2%)
 S80P20: Starch 80% (9.6%), protein 20% (2.4%)
 S70P30: Starch 70% (8.4%), protein 30% (3.6%)
 S60P40: Starch 60% (7.2%), protein 40% (4.8%)
 S0P100: Starch 0% (0%), protein 100% (12%)

Initial trials conducted to identify the ideal solids content for the gels revealed that 12% solids content was a good intermediate concentration, as S60P40 samples were able to form freestanding gels and S90P10 samples did not form too viscous pastes for handling during the gel-making process.

To make the gels, the dispersions were stirred at 500 rpm at room temperature for 40 min and then stirred in a water bath at 65 °C for an additional 20 min, with the aim of avoiding sedimentation of the starch and maintaining a homogenous mixture for gelation. To produce gels of suitable size for compression tests and microscopy, 3-mL samples were loaded into hollow glass tubes with inner diameter 12 mm. The bottom of each glass tube was closed with a rubber lid and the top with thread tape punctured with a small hole to prevent pressure build-up. The samples were heated in a water bath (DYNEO DD-1000F Refrigerated/heating circulator, Julabo, Seelbach, Germany) from 65 to 95 °C at a rate of 1.5 °C/min. After a 30-min holding time at 95 °C, the samples were cooled to 25 °C at a rate of 1.5 °C/min. The gels were then left at room temperature for approximately 30 min before being stored at 4 °C overnight.

2.4. Hydration and water binding properties by centrifugation

Hydration and water binding properties were analysed before and after heat treatment, following the methodology of Bravo-Núñez and Gómez (2019) with some slight modifications. The hydration properties were assessed by measuring water binding capacity (WBC), i.e. the amount of water retained by samples before heating, which was determined by making 12% (w/v) flour mixture-water solutions. To ensure complete dispersion, the samples were quickly vortexed before being magnetically stirred for 40 min at 500 rpm. The samples were then centrifuged at 580×g for 10 min, the excess water was removed and the

remaining hydrated solids were weighed. WBC was calculated as grams of water retained per gram of dry sample.

For further assessment of the water binding properties after heat treatment, water absorption index (WAI), swelling power (SP) and water solubility index (WSI) were determined (Bravo-Núñez & Gómez, 2019). For analysis, 120 mg of sample (W_i) were dispersed in 1 mL of de-ionised water and the samples were prepared in the same manner as described in section 2.3 until cooling to 25 °C. The samples were then left to stand overnight at 4 °C, prior to being centrifuged at 3000×g at 4 °C for 10 min. The supernatant was decanted and dried at 105 °C for 8 h, giving the dry solids weight (W_s). The remaining pellet was also weighed (W_r). WAI, WSI and SP were calculated using the following equations:

$$\text{Water Absorption Index} \left(\frac{\text{g}}{\text{g}} \right) = \frac{W_r}{W_i} \quad (1)$$

$$\text{Water Solubility Index} \left(\frac{\text{g}}{100\text{g}} \right) = \frac{W_s}{W_i} \times 100 \quad (2)$$

$$\text{Swelling Power} \left(\frac{\text{g}}{\text{g}} \right) = \frac{W_r}{W_i - W_s} \quad (3)$$

2.5. NMR spectroscopy

Sample preparation for nuclear magnetic resonance (NMR) spectroscopy followed the method described by Larsen et al. (2013) with slight modification. For this, 50 µg of flour or flour mixtures with starch: protein ratio 60:40 and 90:10 were weighed out and packed into 4 mm ZrO₂ rotors. The moisture content in the flours was 4.0% (starch) and 6.4% (protein). Then 50 µL of D₂O were inserted into the rotor using a Hamilton Microliter® #810 syringe. To equilibrate the D₂O within the rotor, the samples were left to stand for 1 h prior to spinning at 9 kHz for 1 h to ensure proper mixing of flour and D₂O.

NMR spectra (carbon-13 (¹³C) cross-polarisation magic angle spinning (CPMAS) and single-pulse excitation magic angle spinning (SPMAS) were obtained using a Bruker Avance III 600 MHz spectrometer equipped with a double-resonance 4 mm (1H&19F)/(15N-31P) CPMAS probe. The CPMAS spectra were recorded with a contact time of 1–2 ms and a repetition delay of 2.5–5 s. The NMR measurements were performed at a spinning frequency of 8 kHz and at three different temperatures; first at 25 °C before heating, then at 85 °C and finally at 25 °C after cooling. The maximum temperature was set to 85 °C, due to the limits of the instrument. All samples were analysed in triplicate.

2.6. Hot-stage microscopy

Swelling of the starch granules was visualised following the method described by Nilsson et al. (2022). Suspensions with starch-protein mixtures of 10 mg/mL were mixed for 40 min and then 80 µL of sample were pipetted onto a cover slip and 15 µL of diluted Lugol's stock solution were added to dye the starch. The samples were covered with a slightly smaller coverslip and sealed using nail polish. A tensile strength test stage (model TST350, Linkam Scientific Instruments, Surrey, UK) with heating capacity was attached to the light microscope (Nikon Eclipse Ni-U microscope, Tokyo, Japan) for temperature control. The heating rate was 5 °C/min within the range 30–95 °C. Samples were observed under bright-field light using a Plan Fluor 10 × (0.30 N.A.) objective. For observations under polarised light, samples were prepared in the same manner, with the exception of iodine staining. Micrographs were captured with a Nikon Digital Sight DS-Fi2 camera (Nikon, Tokyo, Japan) every 12 s. Captured micrographs had a pixel size of 1.21 µm (data size: 2560 × 1920 pixels). All micrographs acquired were analysed and compared visually, to pinpoint the temperature at which major changes in granules occurred.

2.7. Effect of heating on iodine dyeing of starch

To test the effect of heating on iodine dyeing, 200 mg flour were dispersed in 20 mL distilled water in capped heat-proof glass test tubes, 2 mL of Lugol's solution were added to each sample and the samples were heated in a water bath from 20 to 95 °C at 1.5 °C/min. Starting at 20 °C and at 10 °C intervals up to the final temperature (90–95 °C), the test tubes were shaken to ensure that flour and iodine were dispersed in the mixtures and 1-mL aliquots of each solution were collected in separate Eppendorf tubes and immediately placed on ice to cool. Duplicate 200 µL aliquots were then pipetted onto a 96-well plate. The samples were shaken for 2 min and absorbance was measured at 510 nm. Distilled water with iodine subjected to the same heat treatment was used as a control. All samples were analysed in duplicate.

2.8. Rheology

2.8.1. Pasting (95 °C)

Pasting data were obtained using a Discovery HR-3 rheometer (TA Instruments, New Castle, DE, USA) equipped with a Peltier pressure cell and steel starch paddle. Starch-protein mixtures with a solids content of 12% in solution were mixed at 20 °C for 40 min at the instrument maximum of 50 rad/s. For the remainder of the experiment the stirring rate was set to 16.75 rad/s, which is equivalent to the standard rotational rate of 160 rpm used in the rapid visco-analyser. As in the gelation process, samples were heated to 95 °C at a heating rate of 1.5 °C/min and kept at 95 °C for 30 min under constant stirring. Samples were cooled to 25 °C at a cooling rate of 1.5 °C/min and then kept for 30 min at 25 °C under constant stirring. All samples were analysed in duplicate.

2.8.2. High-temperature pasting (150 °C)

To investigate how the starch:protein ratio influenced peak viscosity, high-temperature pasting measurements were performed. Previous work has reported that peak viscosity of (pure) faba bean starch occurs at 119 °C (Nilsson et al., 2022). However, initial high-temperature pasting trials on the starch-protein mixtures in the present study revealed that the samples needed to be heated to 150 °C to guarantee that peak viscosity was achieved for all samples.

As in the lower-temperature pasting experiments (section 2.8.1), the flour solutions were mixed in the instrument for 40 min at 50 rad/s at 20 °C. During the pasting analysis, the heating cycle used was 20–150–25 °C with a heating and cooling rate of 5 °C/min and a constant stirring rate of 16.75 rad/s. The samples were kept for 5 min at the maximum temperature (150 °C) and 5 min at the end-set (25 °C) temperature. The main aim of the high-temperature pasting analysis was to determine how peak viscosity differed between the samples and identify any behavioural pattern present depending on the starch:protein ratio. The higher heating/cooling rate was applied to improve experimental efficiency, by reducing the time required for each trial, as overall relative pasting behaviour of the samples did not appear to change. Samples were analysed in duplicate.

2.8.3. Oscillatory rheology

The gelation process and viscoelastic properties of the gels were evaluated using a Discovery HR-3 rheometer (TA Instruments, New Castle, DE, USA) equipped with a 40-mm aluminium plate. Samples were prepared as described in section 2.3, excluding the final gelation step in the glass tubes. Paraffin oil, covering the exposed parts of the sample, was combined with a custom-made solvent trap to limit evaporation. The gelation process was monitored at 0.5% strain during a temperature ramp consisting of heating from 65 °C to 95 °C at a rate of 1.5 °C/min and 30 min holding time at 95 °C before cooling at 1.5 °C/min to 25 °C, followed by an additional holding time of 30 min. After the temperature ramp, a frequency sweep was run from 0.628 to 100 rad/s at 0.5% strain and 25 °C. Finally, an amplitude sweep was performed from 0.01 to 100% at 1 Hz and 25 °C to determine the linear viscoelastic

region (LVR) and ensure that all measurements were performed within this region. The LVR was defined as the strain at which a 5% loss in storage modulus was observed. All oscillatory rheology measurements were performed in triplicate.

2.9. Compression tests

Gels prepared as described in section 2.3 were allowed to equilibrate to room temperature for 1 h before being cut into cylindrical pieces with height 14 mm and diameter 12 mm. The samples were compressed to 70% of their original height at a rate of 1 mm/s using a texture analyser (Stable Micro Systems, TA-HDi, Surrey, UK) equipped with a 500 N load cell and a 36 mm cylindrical aluminium probe. A trigger force of 0.05 N was used to initiate measurement and data collection. Due to the weak nature of the 60:40 gels, a trigger force of 0.01 N was used to reduce the compression of these gels occurring before data collection started. To account for changes in cross-section during compression, true stress and true strain were calculated as described previously (Munialo, van der Linden, & de Jongh, 2014). True fracture stress and true fracture strain (hereafter referred to simply as fracture stress and fracture strain) were defined as the maximum true stress and corresponding true strain at the first clear peak before fracture. Young's modulus was calculated as the slope of the true stress-true strain curve during the initial 1–5% of deformation. This specific region (1–5%) was chosen to be within the initial linear region of the curve without including the potentially noisy first few measurements. Compression tests were performed for each sample, in three batches of 4–8 gels each. Statistical analysis was performed on the mean value obtained for each batch.

2.10. Microstructural characterisation of gels

Gels for both light microscopy and scanning electron microscopy (SEM) were prepared similarly as described previously (Johansson, Johansson, et al., 2022).

2.10.1. Light microscopy

Gels were cut into approximately $2 \times 2 \times 2 \text{ mm}^3$ cubes and fixed overnight in 2.5% glutaraldehyde and 0.1% ruthenium red. The gels were then further fixed in 1% osmium tetroxide for 2 h, followed by dehydration in a series of solutions with increasing ethanol concentration. Thereafter, the gels were embedded using Technovit 7100 and sectioned (Leica Microsystems GmbH, Leica EM UC6, Wetzlar, Germany) into 1 µm thick sections. The light microscope (Nikon, Eclipse Ni-U microscope, Tokyo, Japan) was equipped with a 60 × (1.4 N.A.) plan apochromatic objective and micrographs were captured using a Nikon Digital Sight DS-F12 camera (Nikon, Tokyo, Japan) with 0.08 µm/pixel (data size: 2560 × 1920 pixels).

2.10.2. Scanning electron microscopy

For SEM, samples were prepared as for light microscopy up to dehydration in ethanol. After dehydration, the samples were critical point-dried (Quorum Technologies Ltd, K850 Critical Point Dryer, East Sussex, UK), fractured and sputter-coated with gold (Cressington Scientific Instruments, Sputtercoater-108 auto, Watford, UK). Samples were then examined in the SEM device (Hitachi, FlexSEM 1000II, Tokyo, Japan) at 5 kV and micrographs were digitally recorded at two different magnifications (9.92 and 4.96 nm/pixel, data size: 2560 × 1920 pixels).

2.11. Statistical analyses

Data on hydration and water binding properties, rheological measurements and results of compression tests were analysed by analysis of variance (ANOVA) and pairwise comparison (Tukey) with a significance level of 95% ($p < 0.05$), using R studio (Version 1.2.5033, RStudio Inc., MA, USA). After evaluation of the residuals, G' , end of LVR, n -values and

fracture stress values were log-transformed to obtain normally distributed residuals before statistical analysis (ANOVA and pairwise comparison (Tukey)). Similarly, the inverse of $\tan \delta$ values was used in statistical analysis. Pearson correlation coefficients were calculated to gain an overall understanding of parameters affected by the starch:protein ratio and to determine whether correlations between the parameters were significant.

3. Results and discussion

3.1. Hydration and water binding properties

The water binding capacity (WBC) increased with increasing starch content (Table 1). A negative WBC was observed for the sample containing only protein (SOP100), presumably because the protein dissolved in the water and was decanted with the supernatant.

The water absorption index (WAI) values of all samples increased dramatically after heat treatment but the gels with higher starch content still had higher water absorption, indicating that starch had a higher affinity for water than protein. The swelling power (SP) value also increased with increasing starch content and the correlation between WAI and SP was high ($r = 0.86$; $p = 0.002$). The swelling power of starch granules has previously been found to correlate with amylopectin content and faster heating rate (Nilsson et al., 2022; Tester & Morrison, 1990).

The WSI value of the samples increased with increasing protein content. The supernatant from both the hydration and gelation analysis was much clearer for the composite mixtures with higher starch content, corresponding to lower WSI.

3.2. NMR results

The ^{13}C -CPMAS NMR spectra at 25 °C of powder of starch, protein and a 50:50 starch-protein mixture are shown in Fig. 1, with assignments of the C1 to C6 resonances of the glucose-repeating unit in the starch indicated on top of the spectra. Assignments of the major protein signals are also shown.

Hydration often leads to large changes in the molecular mobility of starch. ^{13}C solid-state NMR has been used in a number of studies to follow hydration of the polysaccharide (Garbow & Schaefer, 1991; Larsen, Blennow, & Engelsen, 2008; Larsen et al., 2013; Morgan, Furseaux, & Larsen, 1995; Tang & Hills, 2003; Zhu, 2017). Two types of ^{13}C NMR spectroscopy, CPMAS and SPMAS, were used to monitor hydration in this study. Cross-polarisation (CP) depends on heteronuclear dipolar couplings between the ^1H and ^{13}C nuclei and if these couplings are averaged because of rapid molecular motion due to hydration, then CP will not occur. NMR signals from mobile components can be observed instead by a single pulse NMR experiment as performed in the solution-state. The CPMAS signals are interpreted as "rigid" carbons and SPMAS signals as "mobile" carbons. Thus, in CPMAS spectra, resonances

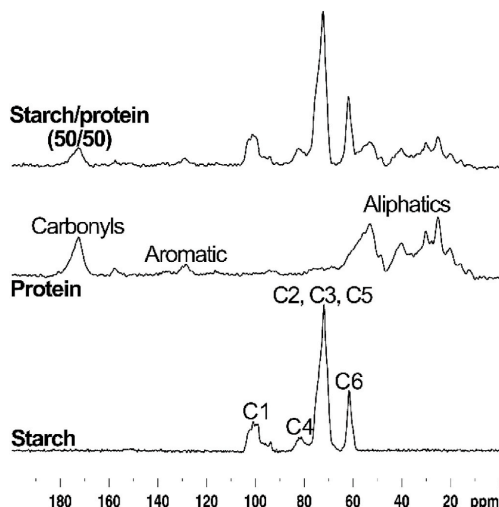


Fig. 1. Nuclear magnetic resonance ^{13}C -CPMAS spectra of powder of (top) 50:50 (w/w) starch-protein mixture, (middle) protein and (bottom) starch.

from carbons originating from immobile regions are enhanced, while in SPMAS spectra carbon resonances from immobile and mobile regions are enhanced.

Addition of water to starch resulted in attenuation of signal intensities in the amorphous region. After addition of water, the signals around 80–84 ppm, corresponding to C4, almost completely disappeared (Figs. 1 and 2). This is consistent with previous findings and derives from hydration-induced mobilisation of the amorphous starch, leading to reduced cross-polarisation efficiency. Hydration also resulted in an increase in spectral resolution for the ordered polysaccharide, due to reduced conformational distribution and substantial decreases in the signals from the amorphous region. The signals in the SPMAS spectra were sharp and the spectra were similar, although with broader resonances, to the solution-state spectra of soluble starch (Fig. 2). The increase in temperature to 85 °C led to a strong decrease in signal to noise ratio in the CPMAS spectra, but to a significant increase in spectral resolution in the SPMAS spectra. This indicates, as shown previously by others, that gelatinisation reduced the amount of immobile fraction of starch. Lowering the temperature back to 25 °C led to NMR spectra similar to those obtained before the temperature increase.

Addition of water to the S90P10 and S60P40 samples gave CPMAS and SPMAS spectra for starch that were similar to those obtained for starch alone (Figs. 2 and 3). However, closer inspection showed some small differences between the S90P10 and S60P40 samples, e.g. the C4 resonances at 80–84 ppm were not completely eliminated in the CPMAS spectra of the S60P40 samples at 25 °C. Narrower lines in the SPMAS NMR spectra are indicative of more efficient hydration and higher mobility. Thus, the narrower line width of the resonance in the SPMAS spectra of the S90P10 samples (60–90 Hz) compared with the S60P40 samples (130–140 Hz) suggests that hydration of starch was slightly more efficient in the S90P10 samples at 25 °C.

The differences between the S90P10 and S60P40 samples became more clear upon heating to 85 °C. The S90P10 samples showed results similar to that of pure starch, with a clear decrease in the signal to noise ratio in the CPMAS spectra and a significant increase in spectral resolution in the SPMAS spectra (Fig. 3). In contrast, only a slight decrease in the signal to noise ratio in the CPMAS spectra was observed for the S60P40 samples upon heating. Furthermore, the increase in spectral

Table 1

Hydration and water binding properties of the starch-protein (S%P%) mixtures. Values shown are mean \pm 1 st.dev. Different superscript letters indicate significant differences ($p < 0.05$).

	Water binding capacity (WBC)	Water absorption index (WAI)	Water solubility index (WSI)	Swelling power (SP)
S100P0	1.4 \pm 0.0 ^a	11.7 \pm 0.4 ^a	2.5 \pm 0.1 ^f	12.0 \pm 0.4 ^a
S90P10	1.2 \pm 0.0 ^b	10.3 \pm 0.2 ^b	5.7 \pm 0.4 ^e	10.9 \pm 0.2 ^b
S80P20	1.1 \pm 0.0 ^c	9.5 \pm 0.0 ^c	12.5 \pm 0.5 ^d	10.8 \pm 0.03 ^b
S70P30	0.9 \pm 0.1 ^d	8.1 \pm 0.1 ^d	20.0 \pm 0.6 ^c	10.2 \pm 0.1 ^{b,c}
S60P40	0.8 \pm 0.0 ^e	7.0 \pm 0.3 ^e	29.7 \pm 2.6 ^b	9.9 \pm 0.1 ^c
SOP100	-0.4 \pm 0.1 ^f	2.5 \pm 0.2 ^f	73.6 \pm 1.8 ^a	9.6 \pm 0.4 ^c

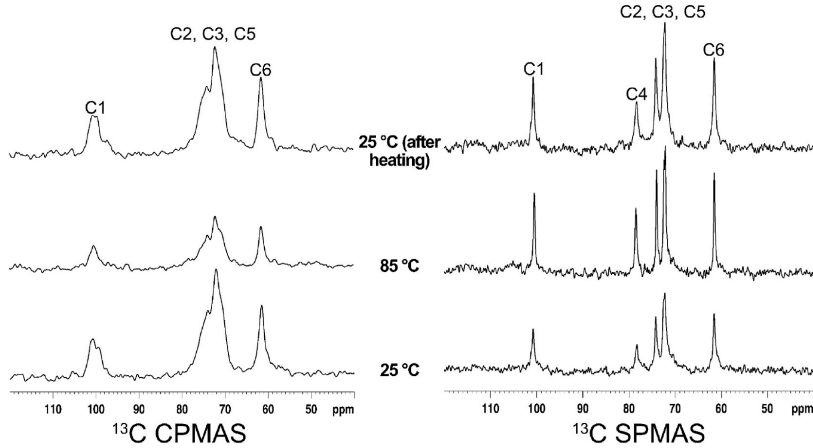


Fig. 2. Nuclear magnetic resonance ^{13}C CPMAS spectra (left) and SPMAS spectra (right) of hydrated starch (top) at 25 °C after heating to and cooling from 85 °C, (middle) at 85 °C and (bottom) at 25 °C. CPMAS signals interpreted as “rigid” carbons and SPMAS signals as “mobile” carbons.

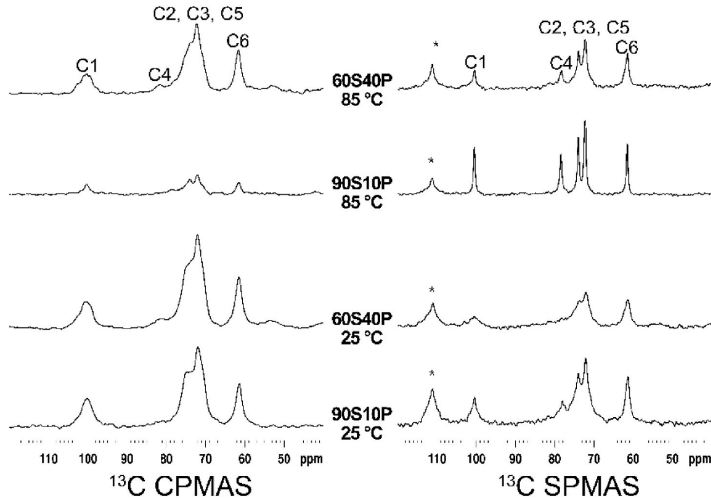


Fig. 3. Nuclear magnetic resonance ^{13}C CPMAS spectra (left) and ^{13}C SPMAS spectra (right) of (top to bottom) the samples S60P40 at 85 °C, S90P10 at 85 °C, 60S40P at 25 °C and 90S10P at 25 °C. *Background signal.

resolution was less pronounced for the S60P40 samples compared to the S90P10 samples. This indicates that the amount of immobile fraction was reduced less upon heating when more protein was present in the system. I.e. the hydration of starch seemed to be hampered by the addition of protein, which in turn could potentially influence the physicochemical properties of the starch. It is possible that, due to the relatively high solid to liquid ratio used for NMR experiments, the observed difference is simply a result of the protein absorbing water and reducing the water availability for the starch. However, further studies would be needed to clarify the mechanism behind this effect.

The assessments of water binding properties (Table 1) showed that WBC, WAI and SP of the mixtures increased as starch content increased, which may be because of increased starch content but also, as indicated

by the NMR results, because of differences in hydration efficiency between the starch and protein. Addition of gluten (Eliasson, 1983), soy (Ribotta et al., 2007) and whey (Onate Narciso & Brennan, 2018) protein has been shown to delay diffusion of water into starch due to its presence on the surface of starch granules. The decrease in hydration efficiency with increasing content of faba bean protein may have been the result of limited water diffusion.

3.3. Hot stage microscopy

Micrographs of the different starch-protein samples at 30, 67, 73 and 90 °C are shown in Fig. 4. At 30 °C, the colour intensity, size and shape of the starch granules were similar for all samples. As the temperature

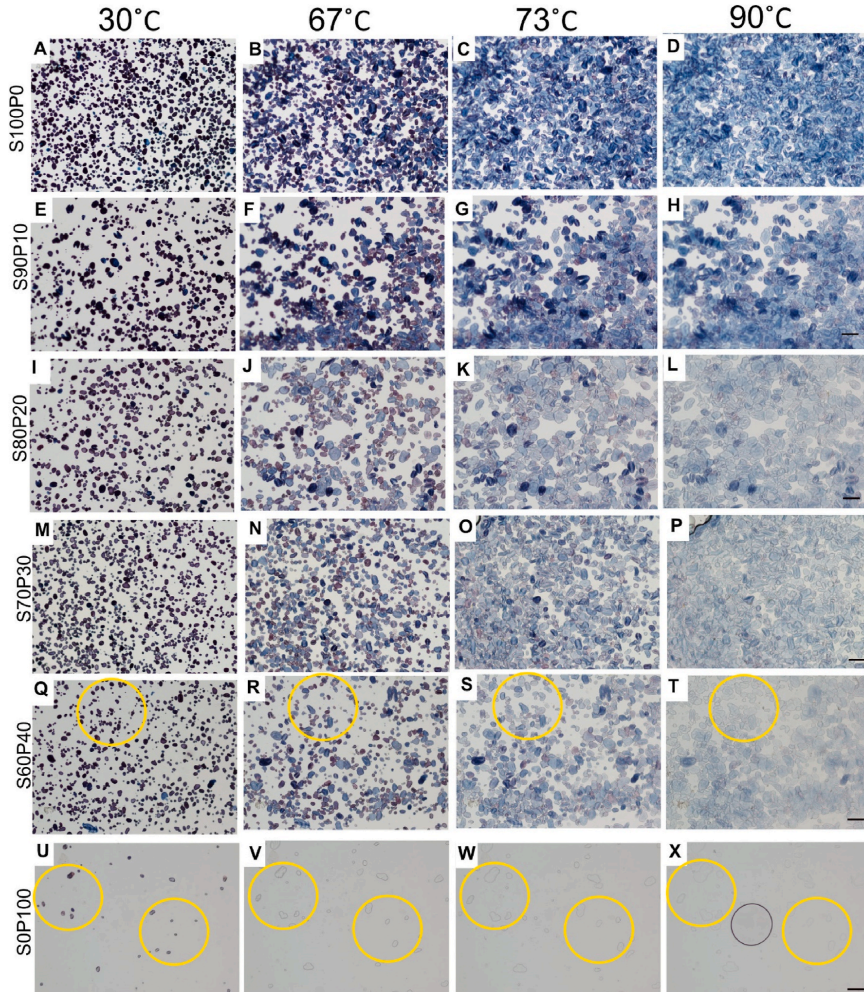


Fig. 4. Micrographs of samples S100P0 (A–D), S90P10 (E–H), S80P20 (I–L), S70P30 (M–P), S60P40 (Q–T) and S0P100 (U–X) under hot-stage microscopy at a temperature of 30 °C (first column A–U), 67 °C (second column B–V), 73 °C (third column C–W) and 90 °C (fourth column D–X). Scale bar = 100 μ m. The starch granules were stained purple/blue by iodine, with the colour intensity decreasing for each sample as the temperature increased. The yellow circles for samples S60P40 and S0P100 indicate areas where starch granules had completely lost their colour. The grey circle, as seen in figure X, indicate air bubbles.

increased the starch granules began to swell, with swelling initiating at around 63 °C and the most pronounced swelling at 70 °C. There was a gradual increase in granule size as the temperature increased to 67 °C, 73 °C and 90 °C (Fig. 4). The gradual increase in the size of the starch granules during heating is also evident in Fig. S2 in SI. From the granule size distribution, the protein-rich sample S60P40 appeared to have the smallest granules at both 30 and 67 °C, which may tie in with the NMR observation that mixture S60P40 showed slightly less efficient starch hydration. There was a tendency for the largest starch granules to be found in samples S90P10 and S80P20, indicating that addition of protein may have had a small effect in delaying granule swelling. However, this tendency was very weak overall, with no distinct difference between the populations, making it challenging to draw any direct conclusions on

whether starch swelling was delayed by the presence of protein. Furthermore, faba bean starch has a relatively high amylose content compared to many other starches (Nilsson et al., 2022). High amylose content has previously been related to retarded swelling of starch granules (Nilsson et al., 2022; Sasaki & Matsuki, 1998; Vamadevan & Bertoft, 2020). It is possible that the effect of amylose on granule swelling was affected by the presence of protein and difference in starch content between samples.

Examination under polarised light revealed that samples with starch content $\geq 60\%$ completely lost their birefringence at temperatures similar to that at which swelling occurred (around 70 °C). In the sample with no added protein (S0P100), birefringence was completely lost already at around 63 °C. Starch birefringence under polarised light is

caused by radial alignment of the crystalline amylopectin and is lost as the granules swell and lose their crystalline structure (Ambigaipalan et al., 2011; Li et al., 2019).

As the granules swelled, they became lighter and less intensely coloured. The loss of colour under progressive heating was more noticeable for the samples with higher protein content, indicating that the protein somehow interfered with or altered iodine dyeing of the starch, or that it interacted with the starch, inhibiting the formation of starch-iodine complexes. A possible explanation is that iodine formerly bound to and staining the starch granules bound to the protein instead at higher temperatures. At 95 °C, the S60P40 sample had completely lost its colour, with some of the starch granules in this sample losing their colour already at 90 °C (Fig. 4T). Areas where the starch granules in samples S0P100 and S60P40 lost their colour completely are indicated with yellow circles in the micrographs in Fig. 4. For the samples with starch content $\geq 70\%$, complete loss of colour of all granules was not observed. Samples S100P0 and S90P10 retained their colour relatively well throughout the heating (Fig. 4D and H). For sample S0P100 (Fig. 4U–X), where no starch was added to the mixture, any starch present was residual starch from protein isolation, which started to lose colour at 57 °C and lost its colour completely at around 60 °C in all micrographs.

3.4. Iodine binding capacity during heating

Fig. 5A shows the colouration of iodine staining in the different samples at different temperature intervals from 20 to 95 °C, while Fig. 5B shows the corresponding absorbance measured at 510 nm. For samples S90P10, S80P20, S70P30 and S60P40, the absorbance and observed colour intensity of the iodine staining decreased as the temperature of the mixture increased. As already observed in the hot-stage micrographs, the loss of colour was more prominent in the samples with higher protein content, with complete loss of colouration occurring at lower temperatures (50 °C for S60P40, 60 °C for S70P30, 70 °C for S80P20 and 80 °C for S90P10). For the pure starch sample S100P0, the measured absorbance remained constant up to and including 60 °C, while at 70 °C the absorbance peaked before decreasing. In a previous study, we found that gelatinisation of faba bean starch extracted from the same batch of raw beans occurred between 67 and 73 °C (Nilsson et al., 2022), so increased granule size might explain the observed peak in absorbance. As the temperature continued to increase measured absorbance decreased but, unlike in the other samples, there was no complete loss of colour for sample S100P0.

To verify that the loss in colour in the protein-rich samples was not due solely to the lower concentration of starch, a new sample S60P0 was prepared containing the same quantity of starch as the S60P40 sample but without any added protein (i.e. the overall solids content was lower). Sample S60P0 showed similar behaviour to the pure starch sample

S100P0, with iodine colouration better maintained and not completely lost at higher temperatures. Hence, the loss in colour was not simply a consequence of the reduced starch content in the mixed samples.

Unheated starch in contact with iodine turns into a characteristic blue-black colour, as the iodine forms complexes inside the long helical chains of linear amylose. The highly branched amylopectin, with much shorter but more numerous chains, turns into a reddish-brown colour upon contact with iodine (Holló & Szejtli, 1958; Huber & Bemiller, 2017). Loss of colour of starch-iodine mixtures upon heating is a well-known phenomenon believed to be caused by the complex decomposing at elevated temperatures (Fonslick & Khan, 1989). The starch-iodine reaction has an exothermic equilibrium, with the iodine colouration recovering upon cooling. However, for the starch-protein mixtures in this study, the discolouration caused by heating did not recover after the samples were cooled, indicating that some interaction between protein-iodine and/or protein-starch prevented the reaction from returning to its original equilibrium. There was also no recovery of colour for the pure starch sample when tested at a lower iodine concentration (200 μ L Lugol's solution instead of 2 mL) (Fig. S3 in SI). On adding iodine to the cooled samples, the mixtures turned blue-black again.

One possible explanation for the observed loss of colour is that the protein in the samples had a higher affinity for iodine than the starch, resulting in less iodine binding to starch in the presence of protein. The lower iodine concentration tested here resulted in loss of colour upon heating that was relatively similar to that seen for S60P40 (Fig. S3). Other possible explanations are complex formation between the starch and protein or protein adsorption on the surface of starch granules, preventing the iodine from binding to amylose. Encapsulation of corn starch granules by whey protein has been reported (Yang, Zhong, Goff, & Li, 2019). The iodine dyeing intensity may also be reduced if the amylose spiral cavity is occupied by guest molecules, thus hindering amylose-iodine complex formation. Further tests involving mixing the starch and Lugol's solution before addition of protein, compared with mixing the starch and protein before addition of Lugol's solution, resulted in a delay in observed colour loss as the temperature increased (Fig. S3). This indicates that competition for iodine is the more likely explanation for the observed loss of colour, with iodine previously complexed with starch instead bonding with the protein as the complex decomposed because of heating, and remaining bound to protein and no longer available to form a complex with starch again after cooling, resulting in the cooled mixture remaining discoloured. However, further studies are needed to fully identify the mechanism behind the observed loss in colour.

3.5. Pasting

Fig. 6 shows the pasting curves of the starch-protein mixtures during

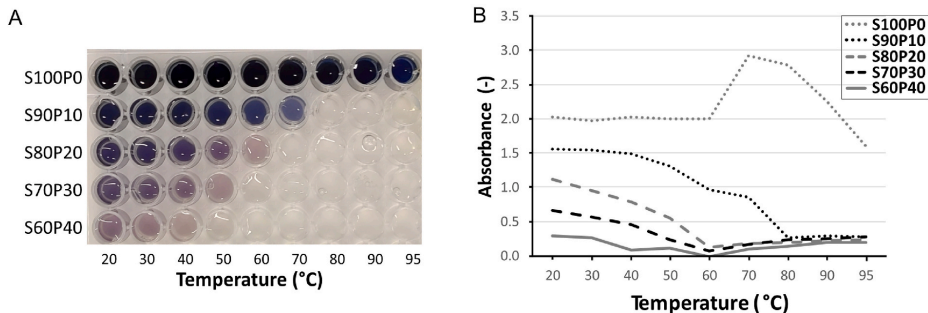


Fig. 5. (A) Image of iodine-stained starch-protein (S:P) mixtures at different temperatures and (B) corresponding absorbance measured at 510 nm.

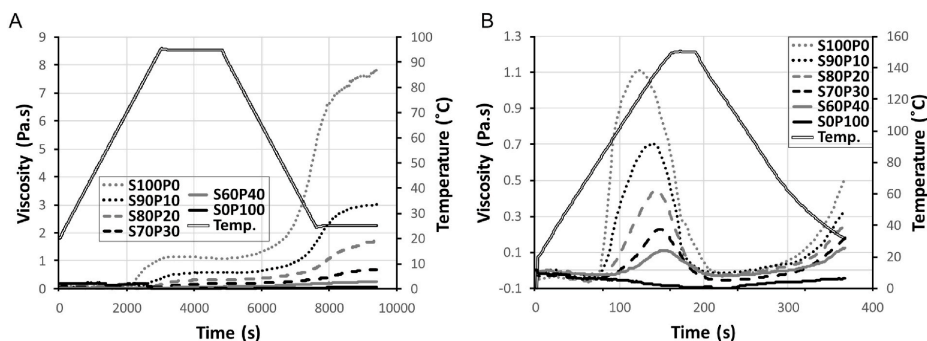


Fig. 6. Pasting curves of the starch-protein (S%P%) mixtures on heating to (A) maximum temperature 95 °C and (B) maximum temperature 150 °C.

heating to 95 °C and 150 °C. Although the shape of the curves differed, both graphs show that apparent pasting viscosities increased with higher starch content. This was observed from the thickness of the pastes already during analysis in the laboratory. At both temperatures, the S0P100 sample had the lowest final viscosity and did not form a gel in the pressure cell. Samples S60P40 and S70P30 formed viscous soft gels, while samples with starch content $\geq 80\%$ formed cohesive gels. Another observation from the pasting analyses was that pasting was initiated at lower temperatures when the sample contained more starch.

In the pasting curves for heating to 95 °C (Fig. 6A), pasting commenced at around 73.2 °C for sample S100P0. For sample S90P10, the pasting temperature increased to 78.3 °C and for sample S60P40 it was 89.9 °C. For the pure protein sample S0P100, the pasting temperature could not be determined, as no pasting occurred. An absence of peak viscosity was observed during pasting experiments with heating to 95 °C. This is in line with previous results on faba bean starch and could possibly be related to the high amylose content which could help maintain the granular integrity (Hoover, Hughes, Chung, & Liu, 2010; Nilsson et al., 2022). Samples with a starch content of $\geq 70\%$ showed a plateau during the holding time after the initial viscosity increase in the cooling phase (Fig. 6, Fig. S4 in SI). For sample S60P40, the viscosity increased steadily throughout the experiment. Increased protein content in the samples delayed the onset time for the second increase in viscosity in the samples. The second onset temperature, when the viscosity increased again during the cooling phase in the pasting analysis, was 31.6 °C for sample S70P30 and 42.1 °C for sample S100P0. From these results, it is not possible to conclude whether the difference in pasting temperature between the starch-rich and protein-rich samples was a result of the two components interacting or an effect of the starch-rich gels having overall higher viscosity.

Heating the samples to 150 °C was sufficient to achieve peak viscosity, followed by breakdown of the paste (Fig. 6B). The final viscosities in the 150 °C measurements were much lower than those in the 95 °C measurements (Table S1 in SI). The lower final viscosities in the high-temperature pasting analysis were presumably because of substantial granule breakdown on heating to 150 °C compared with 95 °C (Nilsson et al., 2022). However, the difference in heating/cooling rates and holding time at 25 °C limited comparison of the results of the different pasting experiments.

As the protein content increased, the temperature at which peak viscosity occurred also increased and the peak viscosity decreased (Fig. 6B, Table S1). The peak viscosity was highest (1.11 Pa s) for the pure starch sample S100P0 and was reached at 121 °C, while for sample S60P40 peak viscosity was 0.11 Pa s and was reached at 145 °C. Moreover, the breakdown viscosity of the samples increased with increasing starch content, most likely due to the higher peak viscosities of the more starch-rich samples. However, well-maintained viscosity

during the heating and cooling may also suggest molecular entanglement between starch and/or protein molecules in the paste (Onwulata et al., 2014).

3.6. Oscillatory rheology

Storage modulus (G') was monitored during gel formation (Fig. 7). The increase in G' seen during initial heating seemed to occur earlier as the starch content increased. At a starch content of 80% (of total flour added) or higher, the gels showed a peak in G' during heating and changes during cooling more similar to those in the pure starch gels. At lower starch contents, the peak observed during heating was not visible, and the changes in G' were more similar to those in the pure protein gels.

The loss modulus (G'') showed a similar pattern to G' (Fig. S5 in SI). Except in the pure protein gels, G'' was lower than G' throughout the whole gelation process. In the pure protein gels, G'' exceeded G' during the initial part of the measurement, before gelation of the sample occurred. G' , G'' , $\tan \delta$ and end of LVR of the final gels are summarised in Fig. 7B–E and Table S2 in SI.

Both G' and G'' decreased with increasing protein content. $\tan \delta$ of the final gels increased with increasing protein content, indicating less solid-like behaviour of the gels. Except for the pure protein gels, the amplitude sweep showed a decrease in LVR with increasing protein content. Large deformation properties, such as the structural breakdown occurring at high amplitudes during an amplitude sweep, may be affected by inhomogeneities and structural defects (Dille, Draget, & Hattrem, 2015; Muniolo et al., 2014). Hence, the reduced LVR for the mixed systems could be related to inhomogeneities in the gel network created by either the starch, the protein or both. The amplitude sweep also showed a more distinct breaking point at the end of LVR with increasing starch content (Fig. S6 in SI), indicating more clear and brittle fracturing of the starch-rich gels. In contrast, the samples with higher protein content showed a more gradual decay in G' as the strain increased, indicating more creamy behaviour.

The changes in G' during gelation showed a relatively similar pattern to those of the pasting curves at 95 °C. However, the peak observed during heating of the starch-rich samples in the oscillatory measurements (highlighted with arrows in Fig. 7A) was not observed during pasting at 95 °C, which may be attributable to the continuous shearing occurring for the pasting measurements potentially being more disruptive for gel formation. The differences between pasting and oscillatory rheology data observed in the initial part of the measurements, as well as any potential differences between the pure protein gels, should be interpreted with caution, due to the erratic data obtained at low torques.

The changes in G' observed for the pure protein gel were similar, but lower in absolute terms, to those previously reported for faba bean protein at higher protein concentrations (Johansson, Johansson, et al.,

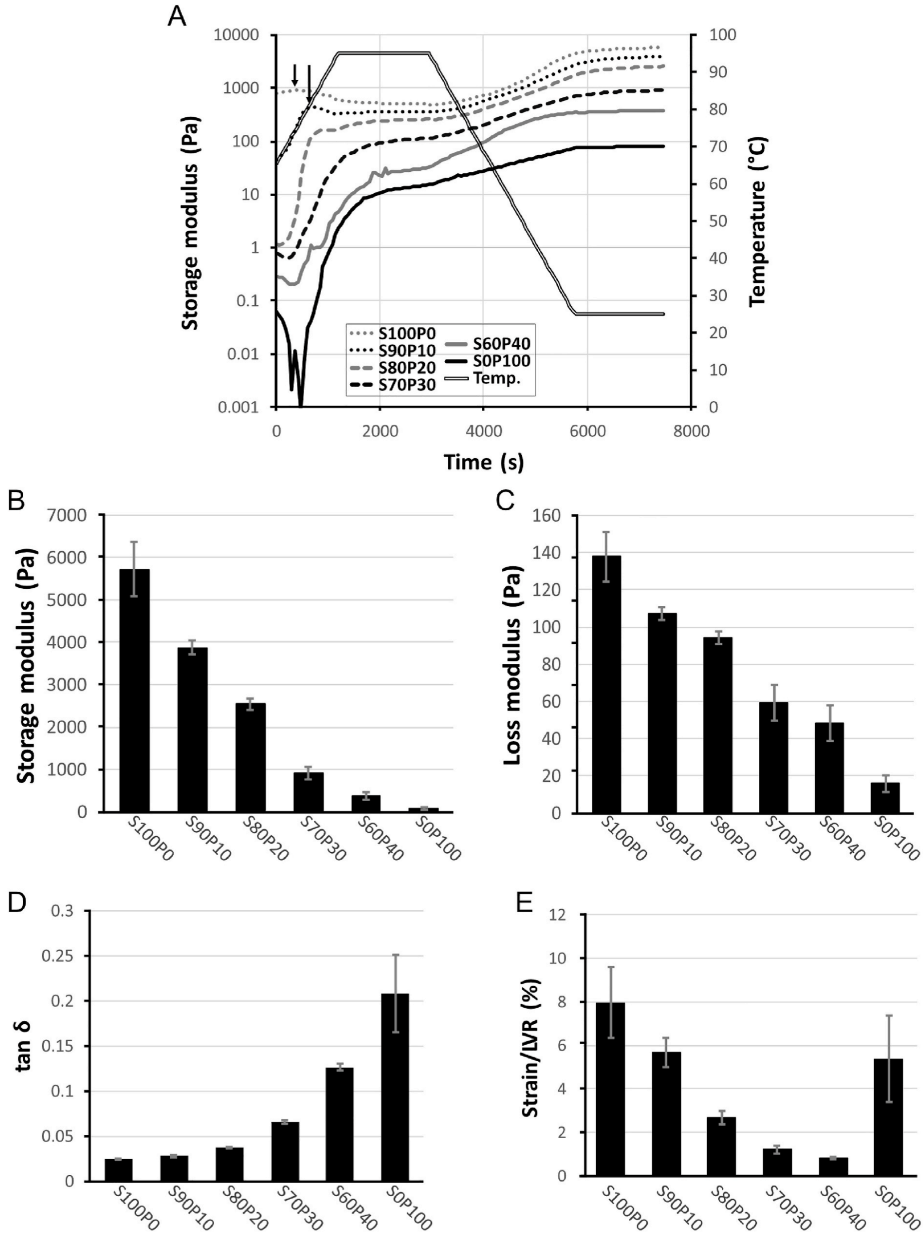


Fig. 7. (A) Storage modulus during temperature ramp for the different starch-protein (S%P%) composites. (B–D) Storage modulus, loss modulus and tan δ obtained from the final time point of the temperature ramp in A. (E) End of the linear viscoelastic region (LVR) measured on the final gels after the temperature ramp. Error bars represent ± 1 s.d.e.v.

2022; Langton et al., 2020). As the starch content in the mixtures here increased, G' also increased and a gradual shift towards the behaviour of the pure starch sample was observed (Fig. 7A). A similar increase in G' throughout the gelation process has been observed previously for faba bean starch-protein systems, although at higher total solids content and lower proportions of starch (Johansson et al., 2022a).

An increase in G' with increasing starch:protein ratio has previously been reported for lentil starch:protein gels (Joshi et al., 2014). However, the opposite has been observed for potato protein:potato starch gels, with an increase in the proportion of starch reducing the G' value of the gels (Zhang, Mu, & Sun, 2017). These results indicate that the properties and behaviour of starch-protein gel systems depend on the source and properties of the starch and protein used.

A study by Muhrbeck and Eliasson (1991) on the rheological properties of starch-protein mixtures from different sources revealed that the transition temperature and gelation rate of the two components were critical for the behaviour of the mixed system. In brief, it was shown here, that if the starch gelled before the protein, the rheological properties of the mixed gel system could be predicted by simple addition of the modulus values of its individual components. If the protein gelled before the starch, the system showed higher modulus values than predicted by simple addition of its components. The faba bean starch used in the present study has a gelatinisation temperature below the denaturation temperature of the protein (75–95 °C) (Kimura et al., 2008), and can be assumed to gel first. This assumption was supported by laboratory observations that gels with a higher fraction of starch were noticeably more viscous after the pre-heating step at 65 °C. Hence, the decrease in G' in the gels as the starch content decreased seems to be in line with observations by Muhrbeck and Eliasson (1991), i.e. that increased protein concentration leads to lower G' of the mixed system, since protein forms weaker gels than starch, and that G' of the mixed system can be predicted by adding together the modulus values for its individual components.

The gels were further characterised by a frequency sweep (Fig. 8). The dependence of G' on frequency was evaluated by calculating the relaxation exponent (n) after fitting the data to a power law equation, $G' = S\omega^n$, where S and n are constants and ω is the angular frequency (Chambon & Winter 1987; Tanger, Müller, Andlinger, & Kulozik, 2022; Winter & Chambon, 1986). A purely elastic material is frequency-independent, with $n = 0$ (Alting, Hamer, De Kruijff, & Visschers, 2003), and gel networks formed by mainly chemical cross-links will have a relaxation exponent close to zero (Tanger et al., 2022). A gel network formed by mainly secondary bonds (e.g. hydrogen bonding and hydrophobic interactions) will have a slightly higher frequency dependence (Tanger et al., 2022). A small contribution from the viscous component (G'') is typical for food gels. This contribution results in a frequency dependence of G' reflecting relaxation of the viscous components (Alting et al., 2003).

In this study, G' was higher than G'' for all samples over the full frequency range analysed (Fig. 8A and B), indicating mainly elastic deformations (Zhang et al., 2017). The n -values of the gels indicated that interactions within the gel network were mainly of a physical nature. The n -values increased with increasing protein content. This increased frequency dependence is in agreement with the increase in $\tan \delta$, reflecting the more viscous behaviour of the protein-rich gels, indicating weaker gel structure (Vogelsang-O'Dwyer et al., 2020).

The G'' values indicated stronger frequency dependence compared with G' , as evidenced by the higher n -values (Table 2). Overall, similar trends were observed for n -values calculated for both G' and G'' . As found for G' , both similar and opposing trends in n -values with increasing starch:protein ratio have been observed for other starch-protein sources (Gui et al., 2022; Joshi et al., 2014; Zhang et al., 2017). However, it could be noted that for all these cases, the gels with the highest G' gave the lowest n -values. This is in line with the lower frequency dependence typically observed for stronger and less fluid like gels (Vogelsang-O'Dwyer et al., 2020).

3.7. Compression tests

Compression tests were used to investigate the textural properties of the gels. All characteristics evaluated (fracture stress, fracture strain, Young's modulus) showed a decrease with increasing protein content (Fig. 9, Table S3). The gels with 60% starch and 40% protein (S60P40) were not completely homogenous, with more solid-like behaviour towards the lower part of the gel due to partial sedimentation of the starch, so the middle part of these gels was used for compression tests. The gels containing only protein were not self-standing and could therefore not be analysed by compression tests.

Fracture stress, fracture strain and Young's modulus decreased with increasing protein content. The fracture and fracture point were more distinct for the gels with higher starch content, showing a clear drop in force as the gels fractured (Fig. S7 in SI). The gels with higher protein

Table 2

n -values (mean \pm 1 st.dev.) for the different starch-protein (S%P%) gels. Values obtained after fitting frequency sweep data (storage (G') and loss modulus (G'')) to the equation: Storage/loss modulus = $S\omega^n$, where S and n are constants and ω is the angular frequency. Different superscript letters indicate significant differences within columns ($p < 0.05$).

Sample	n (G')	n (G'')
S100P0	0.016 \pm 0.000 ^a	0.197 \pm 0.004 ^a
S90P10	0.019 \pm 0.001 ^a	0.198 \pm 0.003 ^a
S80P20	0.024 \pm 0.001 ^b	0.200 \pm 0.005 ^a
S70P30	0.038 \pm 0.001 ^c	0.234 \pm 0.023 ^a
S60P40	0.069 \pm 0.002 ^d	0.249 \pm 0.032 ^a
S0P100	0.134 \pm 0.022 ^e	0.291 \pm 0.054 ^a

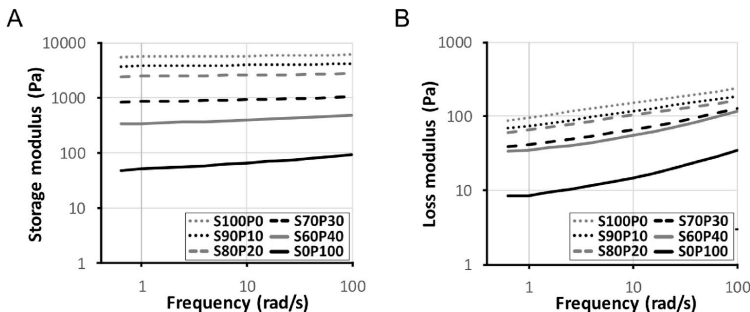


Fig. 8. (A) Storage modulus and (B) loss modulus as a function of frequency for the different starch-protein (S%P%) gels.

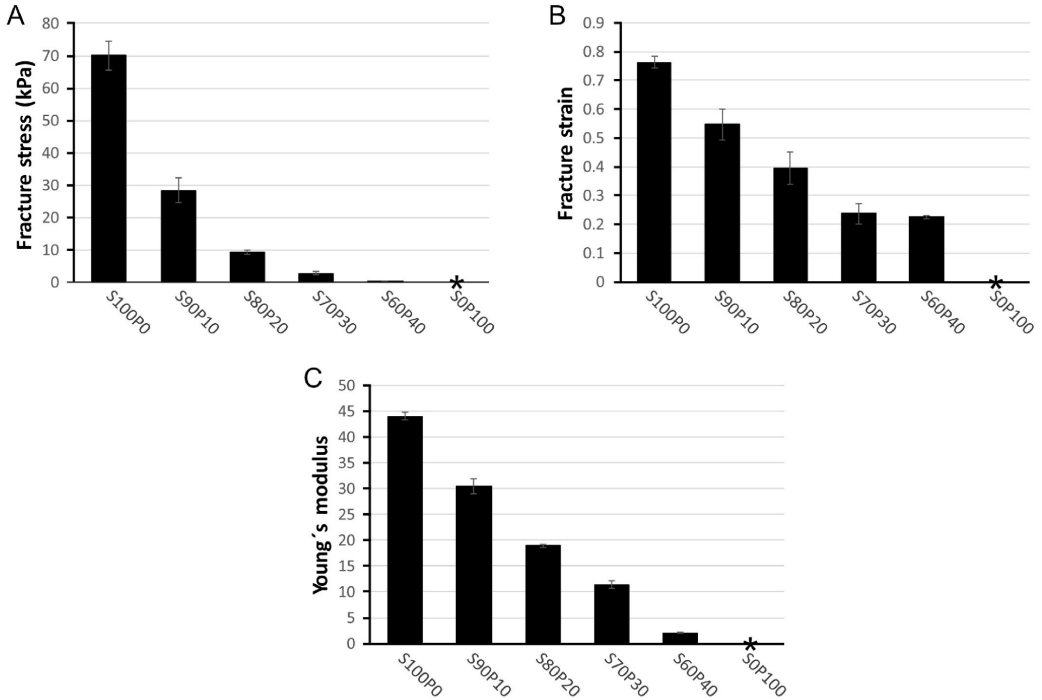


Fig. 9. (A) Fracture stress, (B) fracture strain and (C) Young's modulus of the different starch-protein (S%P%) gels analysed by compression tests. Error bars represent ± 1 st.dev. *Sample did not form self-standing gels and could not be measured.

content showed more ductile behaviour and less clear fracture. The more distinct fracture of the starch-rich gels was also observed visually during compression tests, where starch-rich samples ($\geq 80\%$ starch) fractured into well-defined/separate pieces, whereas gels with $\leq 70\%$

starch did not break into separate pieces and showed more paste-like behaviour upon fracture.

As expected, the Young's modulus and fracture strain values from compression tests showed similar trends to those observed for G' and

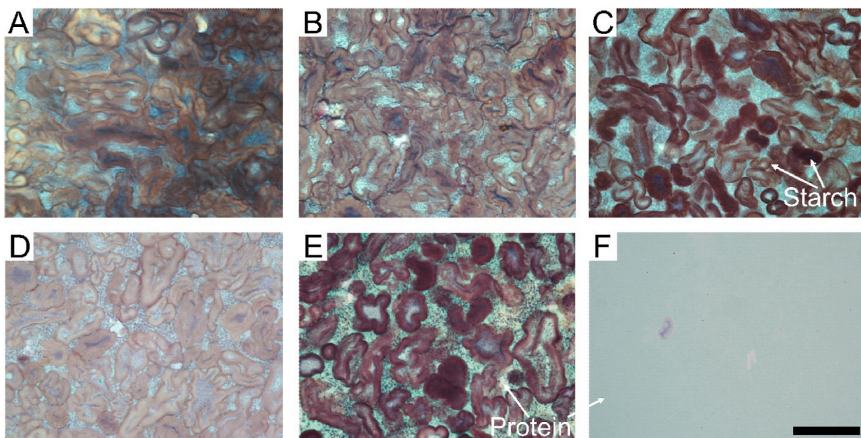


Fig. 10. Light microscopy micrographs of the starch-protein (S%P%) gels. (A) S100P0, (B) S90P10, (C) S80P20, (D) S70P30, (E) S60P40 and (F) S0P100. Scale bar = 50 μm .

LVR during oscillatory rheology measurements. The more clear and distinct fracture observed during compression of starch-rich gels (Fig. S7) was in agreement with the clearer drop in G' at higher strains observed in the strain sweep (Fig. S6).

Previous studies on faba bean starch-protein gels have reported lower fracture stress and fracture strain with increasing starch content (Johansson, Johansson, et al., 2022). However, those gels contained mainly protein, with a maximum starch:protein ratio of 35:65, and had a higher solids content (20%) than in this study (12%). Firmer gel consistency with increasing starch:protein ratio has previously been reported for lentil starch:lentil protein gels (Joshi et al., 2014).

3.8. Microstructural characterisation of gels

3.8.1. Light microscopy

Gel microstructure was characterised by light microscopy with protein stained in blue/green and starch in brown/purple (Fig. 10). The micrographs indicated that starch-rich gels were more densely packed with starch, which could explain the observed firmness of starch-rich gels during compression tests, higher elastic modulus in oscillatory rheology and higher viscosity development in pasting analysis. The protein fraction was more evident in gels with higher protein content. The starch granules appeared to be the continuous phase for all gels with starch content $\geq 70\%$. For the S60P40 gel samples, the continuous phase was more difficult to define (Fig. 10E), with the starch and protein potentially forming two separate bicontinuous networks.

For the gels with higher protein content, the leaked amylose seemed to aggregate into more amylose-dense regions (darker blue spots) within the protein network (Fig. 11). Amylose aggregates within a continuous protein network have been observed previously in mixed faba bean protein:starch gels with higher protein content (protein $\geq 65\%$) and solids content (20%) (Johansson, Johansson, et al., 2022). For the gels with starch content $\geq 90\%$, the amylose seemed to form a gradually finer network, rather than the larger aggregates observed in the gels with higher protein content (Fig. 11). This amylose aggregation into clusters rather than a network could relate to the observed reduction in storage modulus, fracture stress and fracture strain with increasing protein content. Aggregation of amylose has been shown to occur in other mixed systems (starch-emulsifier), indicating that it is due to phase separation rather than amylose-protein complex formation (Richardson, Kidman, Langton, & Hermansson, 2004). The phase separation occurring

between the amylose and protein might be related to differences in their hydrophobicity. Most plant proteins, including the majority of faba bean proteins, are globular proteins and tend to become more hydrophobic upon denaturation (Kim, Wang, & Selomulya, 2020). However, upon denaturation, the protein gel network will also start to form and mobility within the system will be reduced. Hence, any phase separation occurring before gelation might be permanently captured within the gelled structure (Yang, Liu, Ashton, Gorczyca, & Kasapis, 2013).

Previous studies have suggested that protein in mixture gels may perturb starch network formation, thereby weakening the gel (Bravo-Núñez et al., 2019; Bravo-Núñez & Gómez, 2019; Joshi et al., 2014; Oñate Narciso & Brennan, 2018; Onwulata et al., 2014). The compression test results here showed a strong correlation between high starch content and increased firmness, which could be explained by higher protein content disrupting the starch gel network and producing a heterogeneous and weaker gel. The sequence of gel formation has been found to influence the microstructure of lentil starch-protein mixed gels, with the starch becoming more viscous than the protein at lower temperatures (Joshi et al., 2014). Similar behaviour could be expected for faba bean gels, as faba bean starch has a lower gelatinisation temperature than the denaturation temperature of faba bean protein.

3.8.2. SEM

Gel microstructure characterisation by SEM revealed that gels with $\geq 80\%$ starch had regions with a more porous network structure than gels with less starch (Fig. 12, Fig. S8 in SI). In general, the continuous network of these gels showed a structure more similar to the pure starch gels, while the network of gels with $\leq 70\%$ starch showed a denser structure more similar to that of the pure protein gels. Examples of regions with porous and dense network structures are highlighted with arrows in Fig. 12. For gels containing starch, starch granules and cavities where starch granules had been present were evident throughout the structure. In general, a denser and finer network structure was observed around these cavities.

In the LM micrographs, starch was the most visible and dominant component of all samples except the pure protein gels. Despite this, the microstructure of S70P30 and S60P40 gels showed a greater resemblance to the pure protein gels when observed by SEM. The gels with $\geq 30\%$ protein largely lacked the less dense and more fibrous and stranded structure observed in the starch-rich gels. This was possibly due to the fracturing of samples performed before analysis to expose the

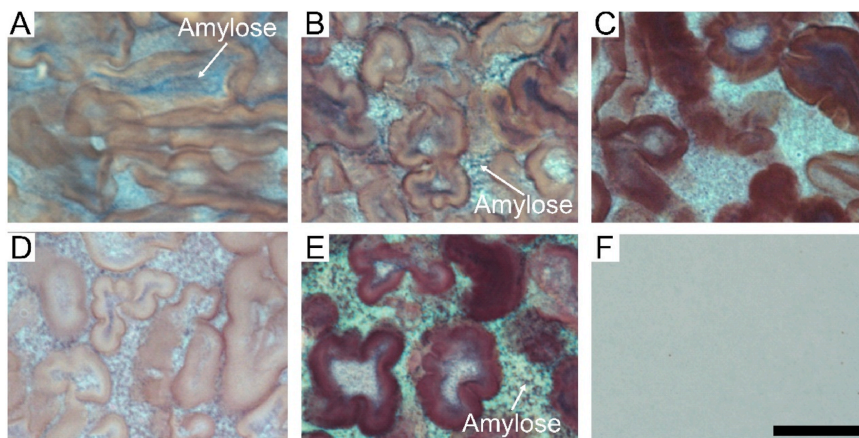


Fig. 11. Magnified views of the micrographs in Fig. 10. (A) S100P0, (B) S90P10, (C) S80P20, (D) S70P30, (E) S60P40 and (F) S0P100. Scale bar = 25 μm . Data size: 975 \times 731 pixels.

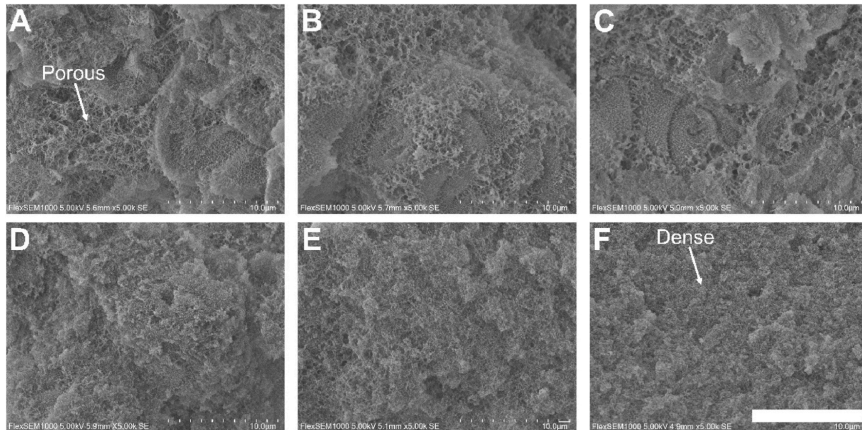


Fig. 12. Scanning electron microscopy (SEM) micrographs of the starch-protein (S%P%) gels. Examples of regions with porous or dense network structures are highlighted with arrows. (A) S100P0, (B) S90P10, (C) S80P20, (D) S70P30, (E) S60P40 and (F) S0P100. Scale bar: 10 μ m.

inner part of the fixed gel, with fractures propagating mainly through the weakest regions of the structure. Since the protein-rich regions were likely to be weaker than the network formed by the starch, fracturing was more likely to occur through these regions. This could explain why the samples with $\geq 30\%$ protein showed such high similarity to the pure protein gels despite their high starch content and why the starch was clearly evident in the LM micrographs of corresponding gel samples.

3.9. Overall trends and correlations

Overall, the results showed that gel morphology/structure and properties were highly dependent on the starch:protein ratio in the mixture. A comprehensive overview of the relationships between morphology/structure and properties of starch-protein mixtures is provided by Zhang et al. (2021). To summarise, higher protein content in the faba bean starch-protein samples resulted in lower pasting viscosities, less firm gels and a more compact and less fibrous gel structure, with the starch appearing to aggregate into clusters. Hydration was also less efficient for the high-protein mixtures. These effects became more pronounced as the protein content of the samples increased.

Apparent viscosity and firmness were strongly positively correlated for high-starch samples, e.g. there was a strong correlation ($r = 0.98$, $p < 0.001$) between peak pasting viscosity and elastic modulus in the rheological temperature ramp. Gels with a higher proportion of protein were also more frequency-dependent, which indicates a weakened gel structure (Joshi et al., 2014).

More efficient hydration and higher iodine absorbance were also positively correlated with higher paste viscosity and firmer gel ($r = 0.97$; $p < 0.001$ for the correlation between WAI and peak viscosity, $r = 0.85$; $p = 0.003$ for that between WAI and elastic modulus). The less efficient hydration properties of the gels containing protein could have affected the distribution of water within the starch-protein matrix and affected molecular interactions. A lower water holding capacity, as observed for the gels containing protein, can lead to lower textural stability (Boye, Zare, & Pletch, 2010). Proteins competing with starch for water may limit granule swelling by restricting water absorption, thereby reducing apparent viscosity (Eliasson, 1983; Onate Narciso & Brennan, 2018; Ribotta et al., 2007). As indicated by the hot-stage microscopy micrographs (see Fig. 4 and Fig. S2), there was a tendency for slightly less intense swelling in the high-protein samples. The NMR results (Fig. 3) confirmed that hydration was slightly less efficient for sample S60P40

compared with S90P10. Slower absorption of water may also lead to delayed pasting because of retarded swelling of the starch granules causing less granule contact.

The more prevalent iodine colour loss associated with higher protein content (see Figs. 4 and 5) indicates that the protein formed a complex with the starch or bound the iodine, rendering it unavailable to form complexes with the starch. If protein-starch complexes are formed, consequences could be delayed granule hydration and swelling and a reduction or perturbation in starch-starch network development.

Another plausible explanation for higher protein content resulting in reduced paste viscosity (Fig. 6) and less firm gels (Fig. 9) is dilution of the starch by the protein, as starch often has better gelling properties, forming stronger gels, than protein (Bravo-Núñez et al., 2019; Bravo-Núñez & Gómez, 2019). The LM micrographs (Figs. 10 and 11) showed that starch granules were more tightly packed in the high-starch gels. However, viscosity differences exceeded actual starch dilution, suggesting that the protein somehow interfered with viscosity development of the starch.

In the SEM micrographs (Fig. 12), the starch-rich gels displayed regions with a more porous and fibrous network. The oscillating frequency results, with higher calculated n -value for samples with higher protein content, indicated greater presence of secondary bonds (Tanger et al., 2022), which in turn could lead to denser network structure because of less bonding between the starch chains. Starch gel matrices consist of swollen granules, entangled polymer chains and non-covalent interactions (Larrea-Wachtendorf, Del Grosso, & Ferrari, 2022; Walstra, 2002). Ribotta et al. (2007) concluded that soy protein can interact readily with amylose and exposed branches of amylopectin through non-covalent bonding, especially hydrogen bonds, causing further gel matrix weakening.

Proteins may act as an inert filler, hindering realignment of the starch chains during gelation. An effect of protein addition in altering microstructure and reducing viscosity and/or gel strength has been reported for numerous starch-protein mixtures, such as wheat starch-soy protein (Ribotta et al., 2007), starch-dairy (Yang et al., 2004) and various starch-plant/animal-based proteins (Bravo-Núñez et al., 2019; Bravo-Núñez & Gómez, 2019). A previous study analysing the same starch as used in this study revealed that the amylose content was 32.2% (Nilsson et al., 2022). The effect of protein in decreasing viscosity and gel strength has been shown to be greater for amylose-rich starches, as the proteins are more likely to interfere with re-ordering of the amylose

(Bravo-Núñez et al., 2019; Joshi et al., 2014; Oñate Narciso & Brennan, 2018). Amylose re-ordering into clusters, rather than developing into a network, in the presence of emulsifiers has also been found to have a weakening effect (Richardson, Kidman, et al., 2004; Richardson, Sun, Langton, & Hermansson, 2004). As observed from the LM micrographs (Figs. 10 and 11), similar re-ordering into clusters rather than a network seemed to occur for the gels in this study as the protein content increased.

The overall effect on pasting and gel structure matrix is also dependent on the type of protein incorporated (Zhang et al., 2021). The pure protein mixtures (SOP100) in this study formed very weak gels, as indicated by the rheological results (Figs. 6 and 7), compression results (Fig. 9) and LM micrographs (Figs. 10 and 11), so the protein in the mixed systems likely did not create any strong network contributing to the overall strength of the mixed systems. The lowest gelling concentration of faba bean protein is reported to be around 13–14% (Fernández-Quintela, Macarulla, del Barrio, & Martínez, 1997; Langton et al., 2020), which is higher than in the mixtures here (12% solids).

4. Conclusions

A decrease in the proportion of starch in faba bean starch-gel mixtures, while keeping the solids content (starch + protein) constant, resulted in lower measured viscosities during pasting. Gels with decreased starch content (and increasing protein content) also showed a decrease in storage modulus, fracture stress, fracture strain and Young's modulus. The water binding and hydration properties of the starch-protein mixtures improved with higher starch content, suggesting that water binding and gel rheological values may be related. Changes in textural and rheological properties appeared to occur gradually over the starch:protein ratios tested. Light microscopy indicated that starch was the continuous phase, consisting of swollen granules, for gels with starch content $\geq 70\%$ of total solids and that starch and protein potentially formed two bicontinuous networks at a starch content of 60%. Scanning electron microscopy revealed a more porous starch network, with thicker strands than in the protein network. In general terms, it can be stated that the textural properties, and in turn also the mouthfeel and perception, of starch-protein gels depend largely on the starch to protein ratio in the system. To produce a stable and brittle gel a higher starch content may be desirable, while to produce a softer and perhaps pourable gel a higher proportion of protein may be preferred. However, if the solids content in the gels (12%) had exceeded the lowest gelling concentration of faba bean protein (14%), their properties may have been different.

CRedit authorship contribution statement

Klara Nilsson: Conceptualization, Formal analysis, Investigation, Methodology, Validation, Visualization, Writing – original draft, Writing – review & editing. **Mathias Johansson:** Conceptualization, Formal analysis, Investigation, Methodology, Validation, Visualization, Writing – original draft, Writing – review & editing. **Corine Sandström:** Investigation, Methodology, Writing – review & editing. **Hanna Eriksson Röhnisch:** Investigation, Writing – review & editing. **Mikael S. Hedenqvist:** Writing – review & editing. **Maud Langton:** Conceptualization, Funding acquisition, Methodology, Supervision, Writing – review & editing.

Declaration of competing interest

None.

Data availability

Data will be made available on request.

Acknowledgements

This work was supported by the FORMAS [grant numbers 2018–01869, 2017–00426]; and Trees and Crops for the Future (TC4F), a Strategic Research Area at SLU, supported by the Swedish Government.

Appendix A. Supplementary data

Supplementary data to this article can be found online at <https://doi.org/10.1016/j.foodhyd.2023.108494>.




References

- Alting, A. C., Hamer, R. J., De Kruijff, C. G., & Visschers, R. W. (2003). Cold-set globular protein gels: Interactions, structure and rheology as a function of protein concentration. *Journal of Agricultural and Food Chemistry*, 51(10), 3150–3156. <https://doi.org/10.1021/jf0209342>
- Ambigaipalan, P., Hoover, R., Donner, E., & Liu, Q. (2013). Retrogradation characteristics of pulse starches. *Food Research International*, 54(1), 203–212. <https://doi.org/10.1016/j.foodres.2013.06.012>
- Ambigaipalan, P., Hoover, R., Donner, E., Liu, Q., Jaiswal, S., Chibbar, R., et al. (2011). Structure of faba bean, black bean and pinto bean starches at different levels of granule organization and their physicochemical properties. *Food Research International*, 44(9), 2962–2974. <https://doi.org/10.1016/j.foodres.2011.07.006>
- Aschemann-Witzel, J., Gantriis, R. F., & Fraga, P. (2021). Plant-based food and protein trend from a business perspective : Markets , consumers , and the challenges and opportunities in the future. *Critical Reviews in Food Science and Nutrition*, 61(18), 3119–3128. <https://doi.org/10.1080/10408398.2020.1793730>
- Boye, J., Zare, F., & Pletch, A. (2010). Pulse proteins: Processing, characterization, functional properties and applications in food and feed. *Food Research International*, 43(2), 414–431. <https://doi.org/10.1016/j.foodres.2009.09.003>
- Bravo-Núñez, A., Garzón, R., Rosell, C. M., & Gómez, M. (2019). Evaluation of starch-protein interactions as a function of pH. *Foods*, 8(5), 155. <https://doi.org/10.3390/foods8050155>
- Bravo-Núñez, A., & Gómez, M. (2019). Physicochemical properties of native and extruded maize flours in the presence of animal proteins. *Journal of Food Engineering*, 243(August 2018), 49–56. <https://doi.org/10.1016/j.jfoodeng.2018.09.005>
- Chambon, F., & Winter, H. H. (1987). Linear viscoelasticity at the gel point of a crosslinking PDMS with imbalanced stoichiometry. *Journal of Rheology*, 31(8), 683–697. <https://doi.org/10.1122/1.549955>
- Dille, M. J., Drager, K. L., & Hattrem, M. N. (2015). 9 - the effect of filler particles on the texture of food gels. In J. Chen, & A. Rosenthal (Eds.), *Modifying food texture* (pp. 183–200). Woodhead Publishing. <https://doi.org/10.1016/B978-1-78242-333-1.00009-7>
- Eliasson, A. C. (1983). Differential scanning calorimetry studies on wheat starch–gluten mixtures: I. Effect of gluten on the gelatinization of wheat starch. *Journal of Cereal Science*, 1(3), 199–205. [https://doi.org/10.1016/S0733-5210\(83\)80021-6](https://doi.org/10.1016/S0733-5210(83)80021-6)
- Fernández-Quintela, A., Macarulla, M. T., del Barrio, A. S., & Martínez, J. A. (1997). Composition and functional properties of protein isolates obtained from commercial legumes grown in northern Spain. *Plant Foods for Human Nutrition*, 51(4), 331–341. <https://doi.org/10.1023/A:1007936930354>
- Fonslick, J., & Khan, A. (1989). Thermal stability and composition of the amylose-iodine complex. *Journal of Polymer Science*, 27, 4161–4167.
- Garbow, J. R., & Schaefer, J. (1991). Magic-angle 13c nmr study of wheat flours and doughs. *Journal of Agricultural and Food Chemistry*, 39(5), 877–880. <https://doi.org/10.1021/jf00005a013>
- Gui, Y., Zou, F., Zhu, Y., Li, J., Wang, N., Guo, L., et al. (2022). The structural, thermal, pasting and gel properties of the mixtures of enzyme-treated potato protein and potato starch. *LWT*, 154, Article 112882. <https://doi.org/10.1016/j.lwt.2021.112882>
- Holló, J., & Szejtli, J. (1958). The mechanism of starch-iodine reaction. *Periodica Polytechnica, Chemical Engineering*, 2(1), 25–37.
- Hoover, R., Hughes, T., Chung, H. J., & Liu, Q. (2010). Composition, molecular structure, properties, and modification of pulse starches: A review. *Food Research International*, 43(2), 399–413. <https://doi.org/10.1016/j.foodres.2009.09.001>
- Huber, K. C., & Bemiller, J. N. (2017). 3.3.6.8 starch complexes. In S. Damodaran, & K. L. Parkin (Eds.), *Fennema's food chemistry* (5th ed., pp. 140–141). CRC Press.
- Johansson, M., Johansson, D., Ström, A., Rydén, J., Nilsson, K., Karlsson, J., et al. (2022). Effect of starch and fibre on faba bean protein gel characteristics. *Food Hydrocolloids*, 131, Article 107741. <https://doi.org/10.1016/j.foodhyd.2022.107741>
- Johansson, M., Nilsson, K., Knab, F., & Langton, M. (2022). Faba bean fractions for 3D printing of protein-, starch- and fibre-rich foods. *Processes*, 10(3). <https://doi.org/10.3390/pr10030466>
- Joshi, M., Aldred, P., Panozzo, J. F., Kasapis, S., & Adhikari, B. (2014). Rheological and microstructural characteristics of lentil starch–lentil protein composite pastes and gels. *Food Hydrocolloids*, 35, 226–237. <https://doi.org/10.1016/j.foodhyd.2013.05.016>
- Kimura, A., Fukuda, T., Zhang, M., Motoyama, S., Maruyama, N., & Utsumi, S. (2008). Comparison of physicochemical properties of 7S and 11S globulins from pea, faba bean, cowpea, and French bean with those of soybean—French bean 7S globulin

- exhibits excellent properties. *Journal of Agricultural and Food Chemistry*, 56(21), 10273–10279. <https://doi.org/10.1021/jf801721b>
- Kim, W., Wang, Y., & Selomulya, C. (2020). Dairy and plant proteins as natural food emulsifiers. *Trends in Food Science & Technology*, 105, 261–272. <https://doi.org/10.1016/j.tifs.2020.09.012>
- Langton, M., Ehsanzamir, S., Karkehbabadi, S., Feng, X., Johansson, M., & Johansson, D. P. (2020). Gelation of faba bean proteins - effect of extraction method, pH and NaCl. *Food Hydrocolloids*, 103, Article 105622. <https://doi.org/10.1016/j.foodhyd.2019.105622>
- Langton, M., & Hermansson, A.-M. (1992). Fine-stranded and particulate gels of β -lactoglobulin and whey protein at varying pH. *Food Hydrocolloids*, 5(6), 523–539. [https://doi.org/10.1016/S0268-005X\(09\)80122-7](https://doi.org/10.1016/S0268-005X(09)80122-7)
- Larrea-Wachtendorf, D., Del Grosso, V., & Ferrari, G. (2022). Evaluation of the physical stability of starch-based hydrogels produced by high-pressure processing (HPP). *Gels*, 8(3), 152. <https://doi.org/10.3390/gels8030152>
- Larsen, F. H., Blennow, A., & Engelsen, S. B. (2008). Starch granule hydration-A MAS NMR investigation. *Food Biophysics*, 3(1), 25–32. <https://doi.org/10.1007/s11483-007-9045-4>
- Larsen, F. H., Kasprzak, M. M., Larke, H. N., Knudsen, K. E. B., Pedersen, S., Jorgensen, A. S., et al. (2013). Hydration properties and phosphorus speciation in native, gelatinized and enzymatically modified potato starch analyzed by solid-state MAS NMR. *Carbohydrate Polymers*, 97(2), 502–511. <https://doi.org/10.1016/j.carbpol.2013.05.014>
- Li, L., Yuan, T. Z., Setia, R., Raja, R. B., Zhang, B., & Ai, Y. (2019). Characteristics of pea, lentil and faba bean starches isolated from air-classified flours in comparison with commercial starches. *Food Chemistry*, 276(October 2018), 599–607. <https://doi.org/10.1016/j.foodchem.2018.10.064>
- Ma, K. K., Greis, M., Lu, J., Nolden, A. A., McClements, D. J., & Kinchla, A. J. (2022). Functional performance of plant proteins. *Foods*, 11(4), 594. <https://doi.org/10.3390/foods11040594>
- Morgan, K. R., Furneaux, R. H., & Larsen, N. G. (1995). Solid-state NMR studies on the structure of starch granules. *Carbohydrate Research*, 276(2), 387–399. [https://doi.org/10.1016/0008-6215\(95\)00173-Q](https://doi.org/10.1016/0008-6215(95)00173-Q)
- Muhrbeck, P., & Eliasson, A. (1991). Rheological properties of protein/starch mixed gels. *Journal of Texture Studies*, 22(3), 317–332.
- Multari, S., Stewart, D., & Russell, W. R. (2015). Potential of faba bean as future protein supply to partially replace meat intake in the human diet. *Comprehensive Reviews in Food Science and Food Safety*, 14(5), 511–522. <https://doi.org/10.1111/1541-4337.12146>
- Munialo, C. D., van der Linden, E., & de Jongh, H. H. J. (2014). The ability to store energy in pea protein gels is set by network dimensions smaller than 50nm. *Food Research International*, 64, 482–491. <https://doi.org/10.1016/j.foodres.2014.07.038>
- Nicolai, T., & Chassenieux, C. (2019). Heat-induced gelation of plant globulins. *Current Opinion in Food Science*, 27, 18–22. <https://doi.org/10.1016/j.cofs.2019.04.005>
- Nilsson, K., Sandström, C., Özeren, H. D., Vilaplana, F., Hedenvist, M., & Langton, M. (2022). Physicochemical and thermal characterisation of faba bean starch. *Journal of Food Measurement and Characterization*, 16(6), 4470–4485. <https://doi.org/10.1007/s11694-022-01543-7>
- Núñez-Santiago, M. C., Bello-Pérez, L. A., & Tecante, A. (2004). Swelling-solubility characteristics, granule size distribution and rheological behavior of banana (*Musa paradisica*) starch. *Carbohydrate Polymers*, 56(1), 65–75. <https://doi.org/10.1016/j.carbpol.2003.12.003>
- Onate Narciso, J., & Brennan, C. (2018). Whey and pea protein fortification of rice starches: Effects on protein and starch digestibility and starch pasting properties. *Starch/Stärke*, 70(9–10), 1–6. <https://doi.org/10.1002/star.201700315>
- Onwulata, C. L., Tuminck, M. H., & Thomas-Gahring, A. E. (2014). Pasting and extrusion properties of mixed carbohydrate and whey protein isolate matrices. *Journal of Food Processing and Preservation*, 38(4), 1577–1591. <https://doi.org/10.1111/jfpp.12118>
- Punia, S., Dhull, S. B., Sandhu, K. S., & Kaur, M. (2019). Faba bean (*Vicia faba*) starch: Structure, properties, and in vitro digestibility—a review. *Legume Science*, 1(1), 3–7. <https://doi.org/10.1002/leg3.18>
- Ribotta, P. D., Colombo, A., León, A. E., & Anón, M. C. (2007). Effects of soy protein on physical and rheological properties of wheat starch. *Starch - Stärke*, 59(12), 614–623. <https://doi.org/10.1002/star.200700650>
- Richardson, G., Kidman, S., Langton, M., & Hermansson, A. M. (2004). Differences in amylose aggregation and starch gel formation with emulsifiers. *Carbohydrate Polymers*, 58(1), 7–13. <https://doi.org/10.1016/j.carbpol.2004.06.013>
- Richardson, G., Sun, Y., Langton, M., & Hermansson, A. M. (2004). Effects of Ca- and Na-lignosulfonate on starch gelatinization and network formation. *Carbohydrate Polymers*, 57(4), 369–377. <https://doi.org/10.1016/j.carbpol.2004.04.023>
- Röös, E., Carlsson, G., Ferawati, F., Hefni, M., Stephan, A., Tidåker, P., et al. (2020). Less meat, more legumes: Prospects and challenges in the transition toward sustainable diets in Sweden. *Renewable Agriculture and Food Systems*, 35(2), 192–205. <https://doi.org/10.1017/S1742170518000443>
- Sasaki, T., & Matsuki, G. (1998). Effect of wheat starch structure on swelling power. *Cereal Chemistry*, 75(4), 525–529. <https://doi.org/10.1094/CHEM.1998.75.4.525>
- Schorch, C., Wilkins, D. K., Jones, M. G., & Norton, I. T. (2001). Gelation of casein-whey mixtures: Effects of heating whey proteins alone or in the presence of casein micelles. *Journal of Dairy Research*, 68(3), 471–481. <https://doi.org/10.1017/S0022029901004915>
- Sharan, S., Zanghelini, G., Zotzel, J., Bonerz, D., Aschoff, J., Saint-Eve, A., et al. (2021). Fava bean (*Vicia faba* L.) for food applications: From seed to ingredient processing and its effect on functional properties, antinutritional factors, flavor, and color. *Comprehensive Reviews in Food Science and Food Safety*, 20(1), 401–428. <https://doi.org/10.1111/1541-4337.12687>
- Shim, J., & Mulvaney, S. J. (2001). Effect of heating temperature, pH, concentration and starch/whey protein ratio on the viscoelastic properties of corn starch/whey protein mixed gels. *Journal of the Science of Food and Agriculture*, 81(8), 706–717. <https://doi.org/10.1002/jsfa.869>
- Tanger, C., Müller, M., Andlinger, D., & Kulozik, U. (2022). Influence of pH and ionic strength on the thermal gelation behaviour of pea protein. *Food Hydrocolloids*, 123, Article 106903. <https://doi.org/10.1016/j.foodhyd.2021.106903>
- Tang, H., & Hills, B. P. (2003). Use of ¹³C MAS NMR to study domain structure and dynamics of polysaccharides in the native starch granules. *Biomacromolecules*, 4(5), 1269–1276.
- Tester, R. F., & Morrison, W. R. (1990). Swelling and gelatinisation of cereal starches I. Effect of amylopectin, amylose and lipids. *Cereal Chemistry*, 65(6), 551–557.
- Vamadevan, V., & Bertoft, E. (2020). Observations on the impact of amylopectin and amylose structure on the swelling of starch granules. *Food Hydrocolloids*, 103, Article 105663. <https://doi.org/10.1016/j.foodhyd.2020.105663>
- Vogelsang-O'Dwyer, M., Petersen, L. L., Joehnk, M. S., Sørensen, J. C., Bez, J., Detzel, A., et al. (2020). Comparison of faba bean protein ingredients produced using dry fractionation and isoelectric precipitation: Techno-functional, nutritional and environmental performance. *Foods*, 9(3), 322. <https://doi.org/10.3390/foods9030322>
- Walstra, P. (2002). Physical chemistry of foods. In O. R. Fennema, Y. H. Hui, M. K. Rutgers, P. Walstra, & J. R. Whitaker (Eds.), *Physical chemistry of foods*. Marcel Dekker inc. <https://doi.org/10.1201/9780203910436>
- Warsame, A. O., O'Sullivan, D. M., & Tosi, P. (2018). Seed storage proteins of faba bean (*Vicia faba* L.): Current status and prospects for genetic improvement. *Journal of Agricultural and Food Chemistry*, 66(48), 12617–12626. <https://doi.org/10.1021/acs.jafc.8b04992>
- Willett, W., Rockström, J., Loken, B., Springmann, M., Lang, T., Vermeulen, S., et al. (2019). Food in the anthropocene: The EAT–lanet commission on healthy diets from sustainable food systems. *The Lancet*, 393(10170), 447–492. [https://doi.org/10.1016/S0140-6736\(18\)31788-4](https://doi.org/10.1016/S0140-6736(18)31788-4)
- Winter, H. H., & Chambon, F. (1986). Analysis of linear viscoelasticity of a crosslinking polymer at the gel point. *Journal of Rheology*, 30(2), 367–382. <https://doi.org/10.1122/1.549853>
- Yang, H., Irudayaraj, J., Otgonchimeg, S., & Walsh, M. (2004). Rheological study of starch and dairy ingredient-based food systems. *Food Chemistry*, 86(4), 571–578. <https://doi.org/10.1016/j.foodchem.2003.10.004>
- Yang, N., Liu, Y., Ashton, J., Gorczyca, E., & Kasapis, S. (2013). Phase behaviour and in vitro hydrolysis of wheat starch in mixture with whey protein. *Food Chemistry*, 137(1), 76–82. <https://doi.org/10.1016/j.foodchem.2012.10.004>
- Yang, C., Zhong, F., Goff, H. D., & Li, Y. (2019). Study on starch-protein interactions and their effects on physicochemical and digestive properties of the blends. *Food Chemistry*, 280, 51–58. <https://doi.org/10.1016/j.foodchem.2018.12.028>
- Zhang, D., Mu, T., & Sun, H. (2017). Calorimetric, rheological, and structural properties of potato protein and potato starch composites and gels. *Starch - Stärke*, 69(7–8), Article 1600329. <https://doi.org/10.1002/star.201600329>
- Zhang, B., Qiao, D., Zhao, S., Lin, Q., Wang, J., & Xie, F. (2021). Starch-based food matrices containing protein: Recent understanding of morphology, structure, and properties. *Trends in Food Science & Technology*, 114, 212–231. <https://doi.org/10.1016/j.tifs.2021.05.033>
- Zhang, Z., Tian, X., Wang, P., Jiang, H., & Li, W. (2019). Compositional, morphological, and physicochemical properties of starches from red adzuki bean, chickpea, faba bean, and baiyeu bean grown in China. *Food Sciences and Nutrition*, 7(8), 2485–2494. <https://doi.org/10.1002/fsn3.865>
- Zha, F., Rao, J., & Chen, B. (2021). Plant-based food hydrogels: Constitutive characteristics, formation, and modulation. *Current Opinion in Colloid & Interface Science*, 56, Article 101505. <https://doi.org/10.1016/j.cocis.2021.101505>
- Zhu, F. (2017). NMR spectroscopy of starch systems. *Food Hydrocolloids*, 63, 611–624. <https://doi.org/10.1016/j.foodhyd.2016.10.015>

Article

Faba Bean Fractions for 3D Printing of Protein-, Starch- and Fibre-Rich Foods

Mathias Johansson ^{*,†}, Klara Nilsson ^{*,†}, Fanny Knab and Maud Langton 

Department of Molecular Sciences, Swedish University of Agricultural Sciences, SE-750 07 Uppsala, Sweden; fanny.knabb@gmail.com (F.K.); maud.langton@slu.se (M.L.)

* Correspondence: mathias.johansson@slu.se (M.J.); klara.nilsson@slu.se (K.N.)

† These authors contributed equally to this work.

Abstract: Food 3D printing allows for the production of personalised foods in terms of shape and nutrition. In this study, we examined whether protein-, starch- and fibre-rich fractions extracted from faba beans can be combined to produce fibre- and protein-rich printable food inks for extrusion-based 3D printing. Small amplitude oscillatory shear measurements were used to characterise the inks while compression tests and scanning electron microscopy were used to characterise the freeze-dried samples. We found that rheological parameters such as storage modulus, loss tangent and yield stress were related to ink printability and shape stability. Investigations on the effect of ink composition, infill pattern (honeycomb/grid) and direction of compression on textural and microstructural properties of freeze-dried 3D-printed objects revealed no clear effect of infill pattern, but a strong effect of direction of compression. Microstructure heterogeneity seemed to be correlated with the textural properties of the printed objects.

Keywords: 3D printing; faba bean; starch; protein; fibre; rheology; texture; microstructure; infill pattern



Citation: Johansson, M.; Nilsson, K.; Knab, F.; Langton, M. Faba Bean Fractions for 3D Printing of Protein-, Starch- and Fibre-Rich Foods.

Processes **2022**, *10*, 466. <https://doi.org/10.3390/pr10030466>

Academic Editors: Vlad Mureşan and Adriana Paucean

Received: 19 January 2022

Accepted: 21 February 2022

Published: 25 February 2022

Publisher's Note: MDPI stays neutral with regard to jurisdictional claims in published maps and institutional affiliations.



Copyright: © 2022 by the authors. Licensee MDPI, Basel, Switzerland. This article is an open access article distributed under the terms and conditions of the Creative Commons Attribution (CC BY) license (<https://creativecommons.org/licenses/by/4.0/>).

1. Introduction

There are multiple advantages and possible applications of food 3D printing. Beyond the possibility of creating complex structures, the technique can also be used to supply personalised nutrition and food formulations for consumers with different preferences and needs [1]. It can be used to enhance children's curiosity towards vegetable-based foods, supply more appealing foods for the elderly and people with swallowing difficulties and produce delivery systems for the controllable release of nutrients and medication [2]. One example of a nutritious and healthy 3D-printed food that has been studied is fibre- and/or protein-rich snacks [3]. The 3D printing technique could also be used to create novel textures, such as plant-based steaks with textural properties resembling those of meat [4].

One of the greatest challenges in food 3D printing is finding inks that have good printing precision and shape stability [5,6]. Inks used for extrusion-based 3D printing must be able to flow through a nozzle and retain their shape after printing. Rheological characterisation of inks for 3D printing has been used in efforts to predict the printability of a material and its dimensional stability after printing [3,7,8]. Examples of parameters investigated include storage modulus (G'), loss modulus (G''), $\tan(\delta)$ and yield stress. Storage modulus is a measure of the elasticity of a material and its ability to store deformational energy and can be seen as a measure of the structural strength and mechanical rigidity of a material at rest [9]. Loss modulus represents the viscous response of the material and is a measure of the energy dissipated as heat during deformation [9]. $\tan(\delta)$, or loss tangent, is the ratio between G'' and G' , i.e., the ratio of energy lost to energy stored during cyclic deformation. Yield stress relates to the force that can be applied before the structure of the material starts to break and flow is initiated [3].

A correlation between shear modulus and the deformation behaviour of methylcellulose gels has been reported [10], indicating that this parameter can be used to predict printability. Multiple studies have observed a correlation between storage modulus and/or yield stress of the ink with the degree of deformation after printing [5,11,12]. Furthermore, it has been shown that the loss modulus value can supply additional information important for predicting the dimensional stability of 3D-printed food structures [8].

One advantage of 3D food printing compared with the use of moulds or forms is the possibility of using different infill patterns for the interior of the printed object in order to alter its textural properties. The effect of the infill pattern of 3D-printed foods such as air-fried potato snacks and chocolate has been investigated in two previous studies, both of which showed that the infill pattern can influence the texture of printed foods [13,14].

Few studies have so far investigated the possibility of using plant-based materials for food printing without the inclusion of thickeners such as sodium alginate, xanthan gum or methylcellulose. Chen et al. [15] found that not including thickeners for samples 3D-printed using soy protein isolates reduced the objects' shape stability and hardness. Another study showed that 3D printing quality was satisfactory, although the samples tended to swell, when using either oat or faba bean protein concentrates without additional thickeners at solid contents of 45% and 35%, respectively [5]. In the same study, 3D objects were produced from rye bran inks with a solid content of 30%. The starch present in the plant materials was assumed to act as a natural thickening agent through gelatinisation. Other factors affecting the viscosity and printability of the inks include composition, size and shape of insoluble particles and response to heating and shear between the materials [5].

In this study, the following two current trends—3D printing and plant-based foods—are combined. The objective was to produce 100% faba bean-based 3D-printed food prototypes. Edible inks composed of different fractions (faba bean fractions rich in protein, starch or fibre) will be compared on rheological properties and printability. The influence of the composition and infill pattern on the texture and microstructure of the 3D-printed samples will also be investigated. This study provides new insight into how the proportion of faba bean fractions influences the properties of 3D-printed foods.

2. Materials and Methods

The protein-, starch- and fibre-rich fractions used in this study were extracted from dehulled and milled faba beans (*Vicia faba* var. Gloria) kindly provided by RISE (Research Institutes of Sweden). A complete characterisation of the fractions can be found in [16]. A brief summary of the composition of the fractions are the following protein-(protein 77.3%; starch 0.3%; fibre 2.3%; fat 3.4%; ash 8%), starch-(protein 0.5%; starch 94.5%; fibre 3.6%; fat 0.3%; ash 0.2%), and fibre-rich (protein 5.3%; starch 22.5%; fibre 73.1%; fat 0.4%; ash 3.5%). The beans were grown in central Sweden, harvested and dried in 2016. Sodium hydroxide (NaOH) and hydrochloric acid (HCl), purchased from Merck KGaA (Darmstadt, Germany), were used for extraction.

2.1. Extraction

To separate the cotyledon and hull, the faba beans were dehulled (Hi-Tech Machinery Manufacturing Co. Ltd., Heze, Shandong, China) and then milled (Ultra-Centrifugal Mill ZM-1, Retsch, Haan, Germany) into flours with a mesh size of 0.5 mm. Only the cotyledon flour was used for further extraction. The extraction was performed as described previously, with some slight modifications [16]. In brief, faba bean flour was dispersed at a distilled water:flour ratio of 10:1 (*v/w*) and the pH was adjusted to 9.0 using 2 M NaOH. The protein was separated by centrifugation (Thermo Scientific, Sorvall Lynx 4000, Waltham, MA, USA) at $3700 \times g$ (20 °C, 30 min) and precipitated at pH 4 using 1 M HCl. The protein was then washed once, the pH adjusted to 7 and the protein freeze-dried (Martin Christ, Epsilon 2-6D LSC Plus, Osterode am Harz, Germany). For starch and fibre extraction, the pellet from the first centrifugation step was re-dispersed in distilled water, the pH adjusted to 9.5 and the mixture stirred at room temperature for 24 h. Thereafter, the mixture was

left to stand without stirring at 4 °C for 24 h before being centrifuged ($3700 \times g$, 20 °C, 5 min). The supernatant was discarded and the pellet re-dispersed in distilled water. This centrifugation step was repeated until pH 7 was reached. To separate the starch from the fibre, the final pellet was dispersed in distilled water and filtered through a 70 µm nylon filter. This filtration step was repeated 12 times, followed by drying of the starch-rich filtrate at 40 °C for 48 h and freeze-drying of the fibre-rich filter cake. After drying, all fractions were sieved (Retsch, AS200 basic, Haan, Germany) through a 150 µm (protein and starch) or 250 µm (fibre) mesh (Retsch, Testsieve, Haan, Germany).

2.2. Swelling Power and Water Soluble Index

The swelling power (SP) of the samples was determined in triplicate following a modified version of existing methods by Muñoz et al. and Schoch [17,18]. In brief, 0.5 g of sample was weighed into a 15 mL centrifuge tube with a screw cap and 10 mL of distilled water was added. The tubes were placed in a shaking water bath at 60 °C for 10 min. The tubes were removed and left to cool to room temperature in an ice water bath before centrifugation at 7000 g for 20 min. The supernatant was decanted and left to dry at 105 °C overnight. The dried sample was used to calculate the water soluble index (WSI) and the mass of the sediment was used to determine the swelling power. These were calculated using the following equations:

$$\text{WSI}(\%) = \frac{\text{Mass dried supernatant}}{\text{Mass of dry fraction}} \times 100 \quad (1)$$

$$\text{SP}\left(\frac{\text{g}}{\text{g}}\right) = \frac{\text{Mass sediment}}{\text{Mass of dry fraction}} \quad (2)$$

2.3. Preparation of Inks

The composition of the different inks (fibre-rich, protein-rich, starch-rich, protein- and starch-rich; see Table 1) were chosen based on a pre-study, providing printable inks covering a relatively wide range of composition. The mixture of flours to water ratio was adjusted for each ink. The criteria for the inks were that they should be printable and produce a standing object. The pastes used for 3D printing and stress sweep measurements were prepared by first mixing the starch with 70% of the total amount of diH₂O used. The starch dispersion was then heated in a water bath at 60 °C for 10 min. Thereafter, the mixture was removed from the water bath, the fibre and protein added and the mixture mixed thoroughly by hand using a spatula. For rheological characterisation, the fibre was added and the sample mixed before addition of the protein and additional mixing. After the addition of fibre and protein, the final 30% of diH₂O was added before mixing to a homogenous paste. To further homogenise the sample and eliminate larger air bubbles, the paste was extruded three times through a 5-mL Luer syringe without a needle before being added to the 3-mL cartridges used for printing. The cartridges were sealed and left at room temperature for 1 h before printing and rheological measurements.

Table 1. Composition of the different inks used for 3D printing.

Ink	Protein Fraction (%)	Starch Fraction (%)	Fibre Fraction (%)	Water (%)
Fibre-rich	7.8	7.8	7.8	76.7
Starch-rich	4.5	18.2	4.5	72.8
Protein-rich	21.7	5.4	5.4	67.5
Protein- & starch-rich	25.0	12.5	0	62.5

2.4. Rheological Characterisation of Inks

The viscoelastic properties of the inks were analysed by stress sweep measurements using a Discovery HR-3 rheometer (TA Instruments, New Castle, DE, USA) equipped with a 40 mm aluminium plate. The stress was increased logarithmically from 0.001 to 10,000 Pa at a frequency of 0.1 Hz and a temperature of 22 °C. The edges of the sample were covered with paraffin oil to limit evaporation and a 300 s resting time was applied before starting the measurements. The yield stress was defined as the stress at which 5% loss of the original storage modulus was observed. The analysis was performed in duplicate.

2.5. 3-D Printing

The model of the cube (14 × 14 × 14 mm) used for printing was created using the digital design tool Tinkercad (Autodesk Inc., San Rafael, CA, USA) and exported as an STL file to the bioprinter. The cubes were printed at room temperature using two different infill patterns (honeycomb, grid). For the cubes with a honeycomb pattern, the pattern available in the bioprinter software was used. The grid pattern was created using Cellink Heartware (Version 2.1.6, Cellink, Gothenburg, Sweden, 2021) combined with the open source slicing software Slic3r (Version 1.3.0, 2021).

Samples were printed on petri dishes using a BIO X bioprinter (Cellink, Gothenburg, Sweden). Pressure and pre-flow were adjusted for each ink individually. The number of layers was 24, the infill density was 25% and the tip diameter of the nozzle was 580 µm. After printing, the samples were left for 5 min at room temperature and then stored at −18 °C until freeze-drying.

2.6. Freeze Drying

Frozen 3D-printed objects were further frozen at −50 °C for 48 h, followed by freeze-drying (Martin Christ, Epsilon 2-6D LSC Plus, Osterode am Harz, Germany).

2.7. Visual Inspection

The freeze-dried cubes were evaluated and compared using six criteria; colour, infill pattern, wall straightness, wall texture, layer distinction and uniformity.

2.8. Colour Measurements

Cube colour was measured with L*a*b colour space using a colorimeter (CR-300, Minolta, Japan). The built-in light source was carefully placed on the wall of the cube, on the side without the infill pattern, until the end of measurements.

2.9. Texture Analysis

Compression tests were performed on the freeze-dried samples using a texture analyser (Stable Micro Systems, TA-HDi, Surrey, UK) equipped with a 500 N load cell and a 36 mm cylindrical aluminium probe. The samples were compressed to 60% at a rate of 1 mm/s. The compression tests were performed in two directions, from the top (infill pattern facing the direction of compression) and from the side (infill pattern facing 90° from the direction of compression). The compression tests were performed in triplicate.

2.10. Image Analysis for Particle Size after Compression

Compressed matter collected from the texture analysis was spread out on a black background to emphasise contrast and images (1800 × 4000 pixels) of the compressed cube particles were taken at a height of 30 cm. Fiji-Image J was used for image analysis. Using the software, the individual crushed pieces were counted and measured in terms of length, width and area. A ruler was used to standardise the scale bar (0.095 mm per pixel).

2.11. Scanning Electron Microscopy

Freeze-dried samples were fractured, sputter-coated with gold (Au) (Cressington Scientific Instruments, Sputter coater-108 auto, Watford, UK) and examined using a scanning elec-

tron microscope (Hitachi, FlexSEM 1000II, Tokyo, Japan) at 5 kV. Images (1280 × 960 pixels) were recorded digitally at two different magnifications, giving a pixel size of 0.992 µm/pixel and 0.198 µm/pixel.

2.12. Statistical Analysis

Results from the rheology and texture analysis were analysed by analysis of variance (ANOVA) and pairwise comparison (Tukey) using R studio (Version 1.2.5033, RStudio Inc., MA, USA). The size distribution of the fragments after compression in the texture analysis was visualised with ggplot2, with geometry density and log scale, using R studio (Version 1.2.5033, RStudio Inc., Boston, MA, USA). Principal component analysis (PCA), loading and score plot, were created using Simca17, Satorious Stedim Data Analytics AB.

3. Results

3.1. Characterisation of Isolated Fractions

The extraction method and raw material have been used in a previous study. Hence, the composition of the extracted fractions (starch, protein and fibre) and original flour was assumed to be similar to that reported in that study [16]. Starch displayed the highest yield in terms of both quantity and proportion obtained, meaning that starch was the fraction with the smallest losses during extraction (Table 2). The swelling power was negatively correlated with WSI. Under heating, fibre swelled the most, followed by starch, original flour and protein (Table 2).

Table 2. Properties of faba bean cotyledon flour and isolated fractions; starch, protein and fibre.

	Extracted Yield (%) *	Moisture Content (%)	Water Soluble Index (%)	Swelling Power (g/g)
Original flour	NA	10.9 ± 0.2 ^d	31.6 ± 0.1 ^c	2.4 ± 0.0 ^{a,b}
Protein	55.5 ± 3.7 ^b	6.4 ± 0.1 ^b	84.1 ± 0.4 ^d	1.1 ± 0.1 ^a
Starch	82.6 ± 0.1 ^c	4.0 ± 0.3 ^a	2.0 ± 0.1 ^b	3.7 ± 0.0 ^b
Fibre	30.1 ± 1.3 ^a	7.4 ± 0.1 ^c	0.5 ± 0.1 ^a	12.1 ± 0.8 ^c

* Proportion of fraction isolated from the original flour. NA—not applicable. Different letters (a, b, c, d) within columns indicate significant differences ($p < 0.05$).

3.2. Rheological Characterisation of Inks

The inks used for 3D printing were characterised by stress sweeps (Table 3). The G' value in the linear viscoelastic region ranged between 2 and 30 kPa. It was highest for the starch-rich sample and lowest for the protein- and starch-rich sample containing no fibre. The G'' value was lowest for the protein- and starch-rich sample, whereas no significant difference was observed between the other samples. All samples showed $\tan(\delta) \ll 1$, indicating elasticity-dominating behaviour. The lowest loss tangent value was observed for the starch-rich sample and the highest for the protein- and starch-rich sample. Yield stress was highest for the starch-rich sample while all the other samples showed significantly lower values. The air pressure used for printing the different inks was highest for the starch-rich sample.

3.3. Printability

Twenty-five percent of the cubes printed using the protein and starch rich inks had to be discarded because of 'ink-fail', i.e., unstable flow resulting in poor infill pattern or low shape stability. The other inks produced more stable and uniform cubes, and ink-fails occurred at similar frequency (fibre-rich 0%, starch-rich 5.9%, protein-rich 5.3%). Around 80% of the printer fails caused by the ink were with the honeycomb infill pattern. The protein- and starch-rich cubes were the most troublesome to print and only produced "satisfactory" cubes.

Table 3. Results of stress sweep measurements and printing pressure for each ink. The storage modulus (G'), loss modulus (G'') and $\tan(\delta)$ values were calculated as averages over the linear viscoelastic region. The apparent yield stress was defined as the stress at 5% loss in G' .

Sample	G' (kPa)	G'' (kPa)	Tan (δ)	Apparent Yield Stress (Pa)	Printing Pressure (kPa)
Fibre-rich	17.37 ± 0.81^b	1.48 ± 0.06^a	0.085 ± 0.000^c	27.6 ± 2.9^b	69 ± 2^c
Starch-rich	29.48 ± 1.03^a	1.68 ± 0.08^a	0.057 ± 0.001^d	130.2 ± 5.2^a	183 ± 9^a
Protein-rich	7.51 ± 0.47^c	1.63 ± 0.08^a	0.218 ± 0.001^b	17.9 ± 2.4^b	85 ± 7^b
Protein- & starch-rich	2.12 ± 0.21^d	0.61 ± 0.04^b	0.284 ± 0.008^a	18.6 ± 3.2^b	86 ± 11^b

Different letters (a, b, c, d) within columns indicate significant differences ($p < 0.05$).

3.4. Visual Inspection of 3D-Printed Samples

The 3D-printed samples were examined visually after freeze-drying (Figure 1). For texture analysis, a requirement was that all samples retained their shape and infill pattern after printing and drying. The different recipes produced different looking cubes that could be distinguished from each other. The cubes produced with the fibre-rich and starch-rich inks were light in colour, with very straight cube walls, distinct layers and a very sharp and defined infill pattern. The cubes from the protein-rich and protein- & starch-rich inks were darker in colour, with wall surfaces that were smooth and glossy. The printed layers were more distinct for the cubes with lower protein content and higher starch and/or fibre, indicating the structural role of fibre and starch. The protein- and starch-rich cubes (no fibre) showed a slight tendency to collapse due to gravitational forces and the stress build-up from deposition of additional layers on top of the lower ink filaments. This resulted in slightly curved walls of the cube. Samples containing fibre showed better shape stability, which was reflected in the sharpness of the infill pattern. The infill pattern was least sharp for the protein- & starch-rich cubes, followed by the protein-rich cubes, where swelling of the filaments was evident. The holes in the infill pattern, particularly at the corners and along the edges, were much smaller in the protein- & starch-rich and protein-rich prototypes than in the fibre-rich and starch-rich prototypes.

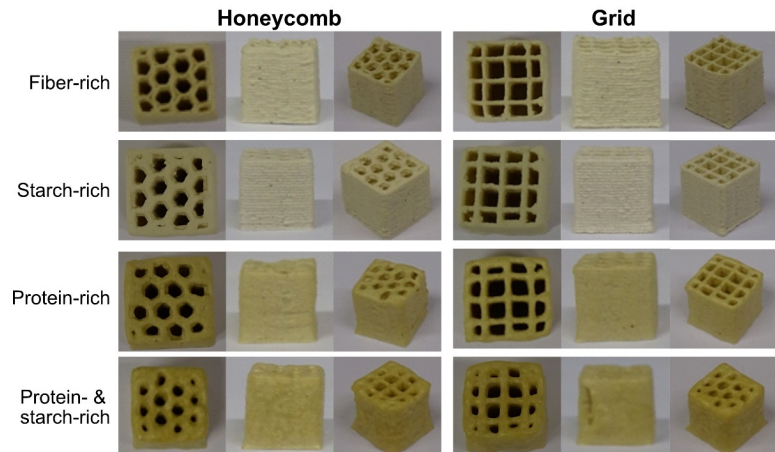


Figure 1. 3D printed cubes ($14 \times 14 \times 14$ mm) after freeze-drying.

3.5. Colour Measurements

The colorimeter measurements confirmed the findings of the visual inspections that increased proportion of starch and decreased protein content caused a lighter cube (higher

L), whereas higher protein content caused the cubes to be more yellow (higher b value) (Table 4).

Table 4. L*a*b* colour values of cubes made from the different inks (L: lightness; a: red/green value; b: blue/yellow value).

Sample	L	a	B
Fibre-rich	83.9 ± 0.5 ^c	−9.4 ± 0.1 ^b	42.2 ± 0.3 ^b
Starch-rich	85.1 ± 0.5 ^c	−10.5 ± 0.2 ^a	40.0 ± 0.2 ^a
Protein-rich	79.1 ± 0.6 ^b	−7.2 ± 0.3 ^c	46.1 ± 0.3 ^c
Protein- & starch-rich	75.4 ± 1.1 ^a	−6.1 ± 0.4 ^d	47.9 ± 0.3 ^d

Different letters (a, b, c, d) within columns indicate significant differences ($p < 0.05$).

3.6. Texture Analysis

Differences in peak force and peak strain based on recipe, infill pattern and direction of compression were analysed (Figure 2). The freeze-dried cubes were compressed from above, either with the infill pattern facing upwards towards the probe (from the top) or with the infill pattern facing towards the side (from the side). The peak force was significantly larger (3–5 times larger) when compressing from the top compared with from the side.

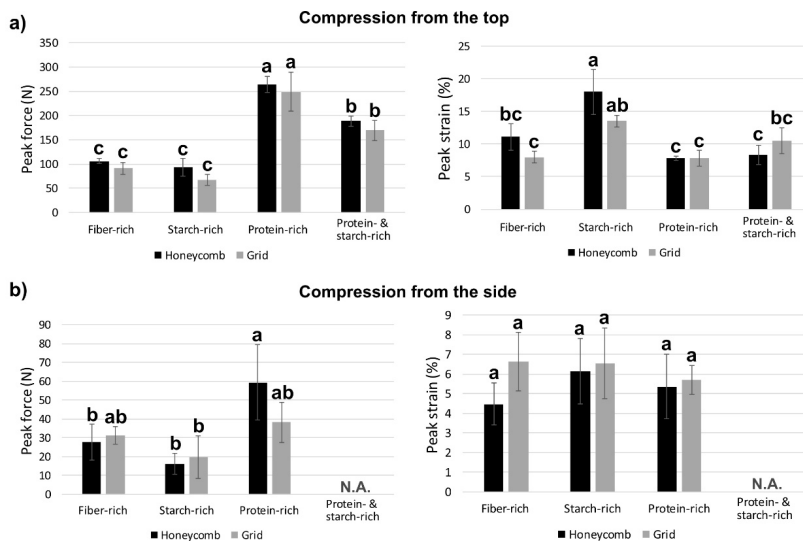


Figure 2. Peak force and corresponding strain (peak strain) from compression tests on 3D-printed samples (a) compressed from above with the infill pattern facing upwards and (b) compressed from above with the infill pattern facing sideways. Different letters (a, b, c) within panels indicate significant differences ($p < 0.05$). N.A.—not applicable.

The general shape of the force vs. strain curve for most samples was similar to that of crispy foods (See Supplementary Materials, Figures S1 and S2) [19]. A clear peak with an abrupt drop in force was observed for all recipes of cubes compressed from the side. When compressed from the top, the starch-rich and fibre-rich cubes had a broader peak, with a less abrupt decrease in force during fracture. Because of the infill pattern and the resulting porous cell structure, most samples compressed from the side showed multiple peaks, with the first peak being the largest. These multiple peaks were a result of the cube breaking layer by layer, rather than in one large fracture as when compressed from the top. When compressed from the top, the peak force was highest for the protein-rich sample, followed by the protein- and starch-rich, fibre-rich and starch-rich samples, respectively. A similar trend was observed for cubes compressed from the side. Due to the curvature of the side of the cubes, the protein- and starch-rich samples were compressed only from the top. No clear differences in peak force were observed between infill patterns (honeycomb/grid).

When compressed from the top, the highest peak strain was observed for the starch-rich samples. No significant differences in peak strain were observed for cubes compressed from the side.

From ANOVA analysis of the compression test data, it was found that the infill pattern did not have a significant effect ($p > 0.05$) on peak force or peak strain, regardless of the direction of compression (Table 5). Recipe was significant for all variables except for the strain of samples compressed from the side. A significant interaction effect (infill \times recipe) for peak force and peak strain was found for samples compressed from the top.

Table 5. p -values from ANOVA analysis of compression tests investigating the effect of recipe, infill pattern and their interaction. Significant values ($p < 0.05$) are highlighted in bold.

	Peak Force		Peak Strain	
	Top	Side	Top	Side
Infill	0.96	0.41	0.080	0.18
Recipe	<0.0001	0.0019	<0.0001	0.57
Infill \times Recipe	0.032	0.14	0.021	0.48

3.7. Analysis of Fragments after Compression

Compressing the cubes from the side produced noticeably fewer and larger fragments than compressing the cubes from the top. When compression was from the side, there were gaps between the layers because of the infill pattern, which caused fragments to break off into larger pieces. Figure 3 shows the size distribution of the fragments after compressing the cube from either the top or the side, which confirmed the observation that top compression produced smaller fragments than side compression. The size of the fragments compressed from the top followed a general trend with three peaks. At fragment size $>0.1 \text{ mm}^2$, a general decrease in the proportion of fragments was seen as the curve approached zero at particle size $>10 \text{ mm}^2$. For top compression, the distribution of fragments with area $>100 \text{ mm}^2$ was close to zero, while for side compression the geometry density for fragments $>100 \text{ mm}^2$ was between 0.03–0.08. Compression from the side produced larger variation in the size of the particles between the different recipes (see Figure 3b), where it appears that the average fragment size was the largest for the starch rich samples. For fibre-rich samples there were two peaks in the size distribution, a stronger peak at 0.05 mm^2 and a second weaker peak at 30 mm^2 , showing a tendency for the absolute largest fragments. The higher force required for compression was negatively correlated with particle size ($r = -0.623$; $p = 0.002$) and positively correlated with the number of particles ($r = 0.716$; $p < 0.001$).

Figure 4 shows the platform of the Textural analyser (TA) with the cubes requiring the highest and the lowest force for compression, i.e., protein-rich samples with top compression and starch-rich samples with side compression, respectively. Compression from the top resulted in finer and more numerous particles that were evenly spread out on the

platform, whereas compression from the side produced fewer and larger particles that were spread out in a linear fashion on the platform (Figure 4).

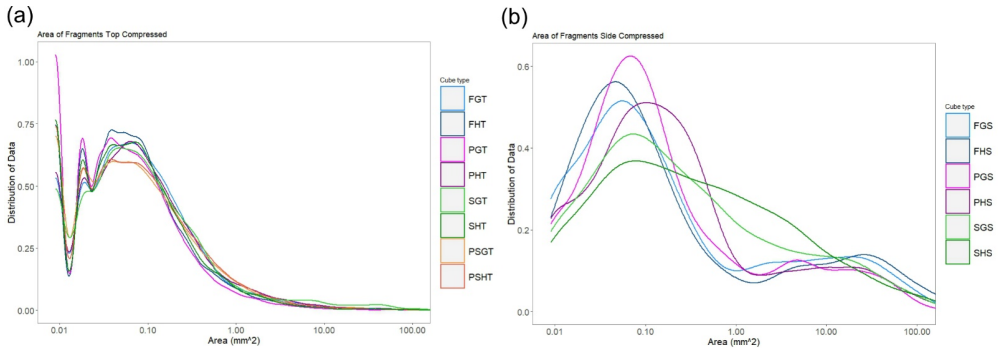


Figure 3. Density diagrams showing size distribution of areal size of fragments after Textural analyser (TA) (a) from the top and (b) from the side. F Fibre-rich, P Protein-rich, S Starch-rich, PS protein- and starch-rich, G Grid, H honeycomb, T Top, S side.

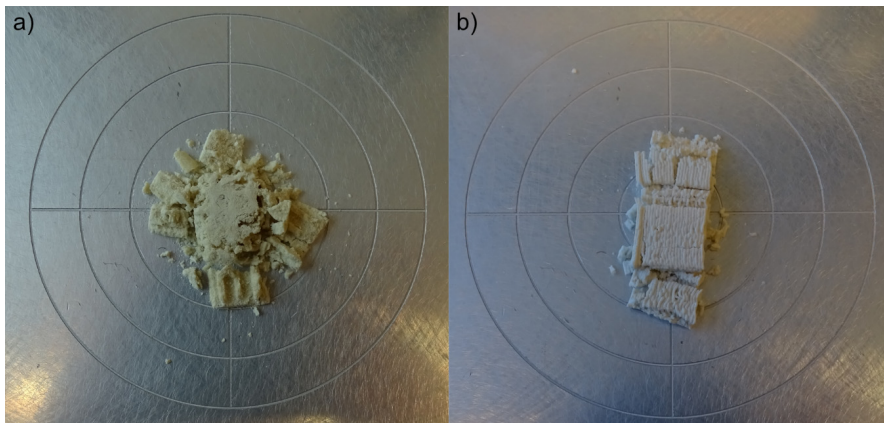


Figure 4. Images of the two samples that differed most after compression: (a) protein-rich recipe with grid infill pattern compressed from the top (PGT) and (b) starch-rich recipe with honeycomb infill pattern compressed from the side (SHS).

3.8. Scanning Electron Microscopy

The scanning electron microscopy (SEM) micrographs revealed that for all samples, the microstructure was strongly affected by freezing and freeze-drying. This could be seen from the porous structure created by ice crystals formed during freezing. At low magnification (Figure 5a), the microstructure was relatively similar between recipes. At higher magnification (Figure 5b), the protein-rich samples showed smoother surfaces and rounded shapes/edges of the pores and cavities in the microstructure. In samples with more carbohydrates (fibre-rich, starch-rich), the structure became more irregular and the almost perforated-like structure observed for the protein-rich samples was less distinct. Starch granules were visible on and inside the surfaces of the samples containing starch.

The walls around the air bubbles seemed potentially thicker for the protein- and starch-rich and protein-rich recipes than for the fibre-rich and starch-rich recipes.

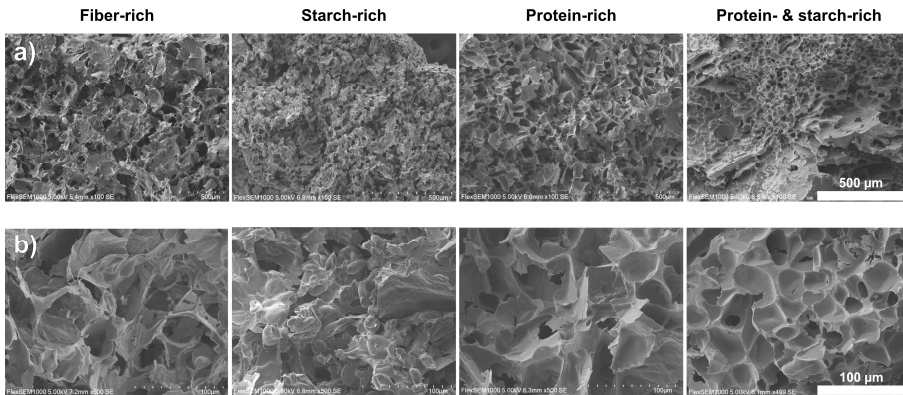


Figure 5. SEM micrographs of the fracture surface of freeze-dried printed samples at different magnification (a,b). Scale bar (a): 500 µm (0.992 µm/pixel), (b): 100 µm (0.198 µm/pixel).

3.9. Principal Component Analysis (PCA)

Figure 6 shows the first two principal components (PC), which together explained 74.5% of the total variance (PC1 53%, PC2 21.5%). Protein content and variables directly associated with protein content were correlated with PC1, while variables associated with fibre and starch content were correlated with PC2. The PCA results confirmed some of the observations and correlations seen in the empirical results. In Figure 6b, the samples are grouped by their recipe and divided further within the groupings by compression direction (side or top). Higher protein content was correlated with increased compression force and loss factor (tan δ). The protein-rich and protein- and starch-rich samples represented one side of the PC1, and the fibre-rich and starch-rich samples represented the other side. The fibre-rich and starch-rich samples were associated with higher water content in ink, lighter colour, more distinct layers, straight walls and higher G' . At higher force, a greater number of fragments was observed, which was inversely correlated to the area of particles. Fibre content was correlated with larger fragments, very well-defined and uniform cubes and increased G'' . Thus, higher elastic modulus may be a determining factor for wall straightness and 3D printed cube stability.

Higher strain and higher yield stress were both associated with higher starch content. As already mentioned, the starch-rich inks required the highest pressure to flow during printing.

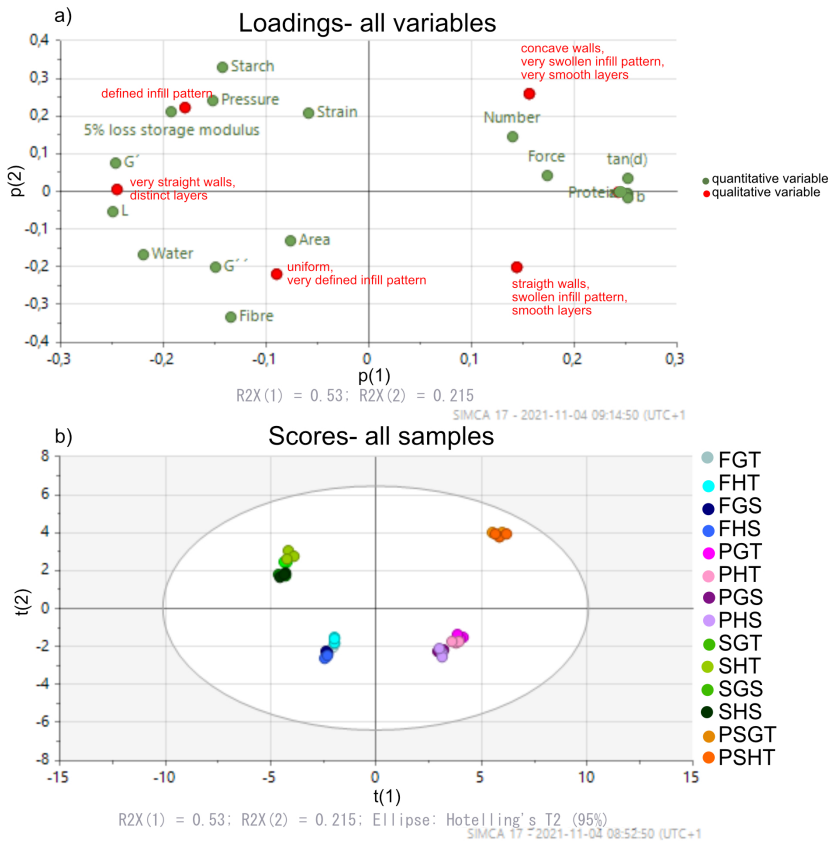


Figure 6. Principal component (PC) analysis (a) component plot and (b) samples in PC plot. F Fibre-rich, P Protein-rich, S Starch-rich, PS protein- and starch-rich, G Grid, H honeycomb, T Top, S side.

4. Discussion

The different compositions of inks were adjusted to create printable inks with good flow and shape stability properties. The water content of the inks was increased with fibre and starch content, which correlated well with the swelling power of the fractions. Based on visual inspection, the infill pattern was least distinct for the protein- and starch-rich samples, with irregular size and shape of the holes within the pattern. The protein- and starch-rich sample also had the highest percentage of ink-failure due to unstable flow and low shape stability. This suggests that the fibre might have a stabilising effect, contributing to the shape stability of the cubes. During ink production, the starch is heated to 60 °C, which is below the gelatinisation temperature of faba bean starch (67–72 °C [20]). Heating the starch to gelatinisation has been found to enhance the structural function of starch in cookie systems [21]. Structure and shape instability, particularly for the protein- and starch-rich cubes (with no fibre), may have been caused by the starch not fully gelatinising because of insufficient heating temperature during the production of the bio-inks.

Due to difficulties such as wall slip and material escaping the gap during viscosity measurements of highly viscous or semi-solid materials, oscillatory tests at small deforma-

tions were used rather than a rotational rheometer [22]. All inks showed predominantly solid-like behaviour ($G' > G''$), with G' values in the approximate range 2–30 kPa. A similar range of G' values has previously been reported for printable pastes, and significantly lower G' values (down to 10 Pa) for pastes forming self-standing cylinders [5,8]. The filaments of the samples with the lowest G' (protein- and starch-rich, protein-rich) seemed to swell more and showed a slight tendency to collapse. These two samples also had the highest loss tangent values, which could potentially explain their lower dimensional stability. The starch-rich samples showed higher yield stress than the other inks. Similarly, the pressure needed to print the starch-rich cubes was significantly higher than for the other inks. A correlation between high yield stress and high printing pressure has been observed by others [5].

High yield stress or high storage modulus alone is not always sufficient to create a good ink, e.g., a previous study found that two inks with similar G' and phase angles showed different shape stability after printing [5]. Hence, G' and phase angle alone are not always sufficient to determine the suitability of a material for 3D printing. Combining these results with the rheological characterisation of our inks, it appears that a combination of high G' , high yield stress and low phase angle is required to provide an ink with good shape stability after printing.

After printing and freeze-drying, the texture of the cubes was analysed by compression tests performed along two different axes of the cubes. The effect of orientation was investigated on the cubes standing, with the infill pattern facing upwards (compressed from the top), and lying on their side, with the infill pattern facing 90° from the axis of compression (compressed from the side). A significantly higher peak force (3- to 7-fold higher) was recorded as the cubes were compressed from the top compared with from the side. The higher force required for top compression is likely due to the wall layers being stacked directly on top of each other, creating a denser wall structure that requires more force to compress. For compression from the side, there are gaps between the layers because of the infill pattern, which will reduce the force required for compression until fracture. The multiple peaks observed from the force vs. strain graphs for samples compressed from the side, but not the top, was a result of the infill pattern. The multiple peaks also related to the size and spreading of pieces after compression, as seen in Figure 3. The samples compressed from the side spread out in a linear fashion as multiple larger pieces that likely relate to the multiple peaks observed in the force vs. strain graphs (Figures S1 and S2).

Scanning electron microscopy of the freeze-dried samples revealed that microstructure was strongly affected by the freezing and freeze-drying. The microstructure consisted of cavities with an approximate diameter of 30–70 μm . A similar microstructure in freeze-dried gelatin products has been observed by others [23]. The porous structure was more irregular for the samples with more fibre and less protein and these samples also had less smooth surfaces. The more irregular structure could potentially explain the lower peak force seen for the starch-rich and fibre-rich samples. Fracture is generally believed to occur by the propagation of cracks, which form at or close to defects and weak spots acting as stress concentrators during deformation [19,24]. Hence, it could be hypothesised that the increased heterogeneity of the starch-rich and fibre-rich samples contributed to their lower peak force.

The SEM micrographs also indicated that pore walls were thicker for the protein-rich and protein- and starch-rich samples than for the starch-rich and fibre-rich samples. Further studies, e.g., by X-ray tomography, would have been needed to confirm this. Nonetheless, increased cell diameter and cell wall thickness have previously been correlated to reduced crushing/breaking stress and compression modulus of cellular corn starch and corn-based extrudates [25–27].

Crispiness and crunchiness are textural properties directly related to microstructure and macrostructure that influence the mechanical and fracture properties of solid food [19]. A higher force was required for compression from the top in this study, indicating that the cubes would be perceived as harder. A previous combination of sensory evaluation and

texture analysis of almonds showed that almonds perceived as more brittle and less hard by sensory evaluation required less force for compression and displayed more deformation peaks in the textural analysis [28]. In this study, the cubes compressed from the side required less force, with more deformation peaks present, indicating that side compression of the cube may enhance the perceived crispness and brittleness of the products and perhaps be a preferred characteristic in a future food product.

In a laboratory taste test on the cubes of the four different recipes, the fibre-rich and starch-rich samples were perceived as more neutral in flavour and with a crispier texture. The protein-rich and protein- and starch-rich samples were rated similar to each other and were less preferred than the other samples, both in terms of flavour and texture. The protein-rich cubes were perceived by the tasters to have a hard texture that became clayey after chewing. None of the different recipes produced cubes that were perceived as beany in flavour.

5. Conclusions

This study showed that protein-, starch- and fibre-rich fractions extracted from faba beans can be successfully combined to create nutritious printable inks for extrusion-based 3D printing. Inks with lower loss tangent values showed higher shape stability. Ink composition had a clear effect on textural properties of the freeze-dried 3D-printed objects, while infill pattern (honeycomb/grid) had no effect. Increased heterogeneity of microstructure seemed to be associated with decreased peak force during compression. Further research is needed to evaluate the shape stability during other post-treatment steps, such as oven baking or frying. Sensory and consumer testing will also be necessary to optimise the product.

Supplementary Materials: The following are available online at <https://www.mdpi.com/article/10.3390/pr10030466/s1>, Figure S1: Force vs. Strain graphs from compression tests on freeze-dried samples compressed from the top, Figure S2: Force vs. Strain graphs from compression tests on freeze-dried samples compressed from the side.

Author Contributions: Conceptualization, K.N., M.J. and M.L.; validation, K.N. and M.J.; formal analysis, K.N. and M.J.; investigation, K.N., M.J. and F.K.; resources, M.L.; writing—original draft preparation, K.N. and M.J.; writing—review and editing, K.N., M.J. and M.L.; visualization, K.N. and M.J.; supervision, M.L.; funding acquisition, M.L. All authors have read and agreed to the published version of the manuscript.

Funding: This research was funded by FORMAS Texturized legume-based food product by recombining fractions (2018-01869) and FORMAS Gelation properties of protein from Swedish legumes (2017-00426); and Trees and Crops for the Future (TC4F).

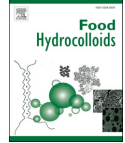
Data Availability Statement: Data is contained within the article.

Conflicts of Interest: The authors declare no conflict of interest. The funders had no role in the design of the study; in the collection, analyses or interpretation of data; in the writing of the manuscript or in the decision to publish the results.

References

1. Zhao, L.; Zhang, M.; Chitrakar, B.; Adhikari, B. Recent advances in functional 3D printing of foods: A review of functions of ingredients and internal structures. *Crit. Rev. Food Sci. Nutr.* **2020**, *61*, 3489–3503. [CrossRef]
2. Godoi, F.C.; Bhandari, B.; Prakash, S.; Zhang, M. *Fundamentals of 3D Food Printing and Applications*; Academic Press: Cambridge, MA, USA, 2018; ISBN 012814565X.
3. Lille, M.; Kortekangas, A.; Heiniö, R.-L.; Sozer, N. Structural and Textural Characteristics of 3D-Printed Protein- and Dietary Fibre-Rich Snacks Made of Milk Powder and Wholegrain Rye Flour. *Foods* **2020**, *9*, 1527. [CrossRef] [PubMed]
4. Meisenzahl, M. A Startup is 3D Printing Plant-Based Steaks to Recreate the Taste and Texture of the Real Thing—See How They Do It. Available online: <https://www.businessinsider.com/define-meat-3d-printed-plant-based-faux-steaks-in-photos-2020-9?r=US&IR=T> (accessed on 20 September 2021).
5. Lille, M.; Nurmela, A.; Nordlund, E.; Metsä-Kortelainen, S.; Sozer, N. Applicability of protein and fiber-rich food materials in extrusion-based 3D printing. *J. Food Eng.* **2018**, *220*, 20–27. [CrossRef]

6. Guo, C.; Zhang, M.; Bhandari, B. Model Building and Slicing in Food 3D Printing Processes: A Review. *Compr. Rev. Food Sci. Food Saf.* **2019**, *18*, 1052–1069. [CrossRef] [PubMed]
7. Zhu, S.; Stieger, M.A.; van der Goot, A.J.; Schutyser, M.A.I. Extrusion-based 3D printing of food pastes: Correlating rheological properties with printing behaviour. *Innov. Food Sci. Emerg. Technol.* **2019**, *58*, 102214. [CrossRef]
8. Nijdam, J.J.; LeCorre-Bordes, D.; Delvart, A.; Schon, B.S. A rheological test to assess the ability of food inks to form dimensionally stable 3D food structures. *J. Food Eng.* **2021**, *291*, 110235. [CrossRef]
9. Mezger, T. *The Rheology Handbook*, 4th ed.; Vincentz Network: Hanover, Germany, 2014; ISBN 3748603703.
10. Kim, H.W.; Bae, H.; Park, H.J. Classification of the printability of selected food for 3D printing: Development of an assessment method using hydrocolloids as reference material. *J. Food Eng.* **2017**, *215*, 23–32. [CrossRef]
11. Liu, Z.; Bhandari, B.; Prakash, S.; Mantihal, S.; Zhang, M. Linking rheology and printability of a multicomponent gel system of carrageenan-xanthan-starch in extrusion based additive manufacturing. *Food Hydrocoll.* **2019**, *87*, 413–424. [CrossRef]
12. Liu, Z.; Zhang, M.; Bhandari, B.; Yang, C. Impact of rheological properties of mashed potatoes on 3D printing. *J. Food Eng.* **2018**, *220*, 76–82. [CrossRef]
13. Mantihal, S.; Prakash, S.; Bhandari, B. Textural modification of 3D printed dark chocolate by varying internal infill structure. *Food Res. Int.* **2019**, *121*, 648–657. [CrossRef]
14. Liu, Z.; Dick, A.; Prakash, S.; Bhandari, B.; Zhang, M. Texture Modification of 3D Printed Air-Fried Potato Snack by Varying Its Internal Structure with the Potential to Reduce Oil Content. *Food Bioprocess Technol.* **2020**, *13*, 564–576. [CrossRef]
15. Chen, J.; Mu, T.; Goffin, D.; Blecker, C.; Richard, G.; Richel, A.; Haubruge, E. Application of soy protein isolate and hydrocolloids based mixtures as promising food material in 3D food printing. *J. Food Eng.* **2019**, *261*, 76–86. [CrossRef]
16. Johansson, M.; Johansson, D.; Ström, A.; Ryden, J.; Nilsson, K.; Karlsson, J.; Moriana, R.; Langton, M. *Effect of Starch and Fibre on Faba Bean Protein Gel Characteristics*; Swedish University of Agricultural Sciences: Uppsala, Sweden, 2022; status (manuscript submitted).
17. Schoch, T.J. Measuring the useful properties of starch. *Starch-Stärke* **1959**, *11*, 156–162. [CrossRef]
18. Muñoz, L.A.; Pedreschi, F.; Leiva, A.; Aguilera, J.M. Loss of birefringence and swelling behavior in native starch granules: Microstructural and thermal properties. *J. Food Eng.* **2015**, *152*, 65–71. [CrossRef]
19. Luyten, H.; Plijter, J.J.; Van Vliet, T.O.N. Crispy/crunch crust of cellular solid foods: A literature review with discussion. *J. Texture Stud.* **2004**, *35*, 445–492. [CrossRef]
20. Nilsson, K.; Sandström, C.; Özeren, H.; Vilaplana, F.; Hedenqvist, M.; Langton, M. *Physicochemical and Thermal Characterisation of Faba Bean Starch*; Swedish University of Agricultural Sciences: Uppsala, Sweden, 2022; status (manuscript submitted).
21. Kulp, K.; Olewnik, M.; Lorenz, K.; Collins, F. Starch Functionality in Cookie Systems. *Starch-Stärke* **1991**, *43*, 53–57. [CrossRef]
22. Rheological Techniques for Yield Stress Analysis. Available online: <http://www.tainstruments.com/pdf/literature/RH025.pdf> (accessed on 19 February 2022).
23. Stevenson, M.; Long, J.; Guerrero, P.; de la Caba, K.; Seyfoddin, A.; Etxabide, A. Development and characterization of ribose-crosslinked gelatin products prepared by indirect 3D printing. *Food Hydrocoll.* **2019**, *96*, 65–71. [CrossRef]
24. Dille, M.J.; Draget, K.I.; Hattrem, M.N. 9—The effect of filler particles on the texture of food gels. In *Modifying Food Texture*; Chen, J., Rosenthal, A., Eds.; Woodhead Publishing Series in Food Science, Technology and Nutrition; Woodhead Publishing: Sawston, UK, 2015; pp. 183–200. ISBN 978-1-78242-333-1.
25. Agbisit, R.; Alavi, S.; Cheng, E.; Herald, T.; Trater, A. Relationships between microstructure and mechanical properties of cellular cornstarch extrudates. *J. Texture Stud.* **2007**, *38*, 199–219. [CrossRef]
26. Barrett, A.H.; Peleg, M. Extrudate Cell Structure-Texture Relationships. *J. Food Sci.* **1992**, *57*, 1253–1257. [CrossRef]
27. Chanvrier, H.; Jakubczyk, E.; Gondek, E.; Gumy, J.-C. Insights into the texture of extruded cereals: Structure and acoustic properties. *Innov. Food Sci. Emerg. Technol.* **2014**, *24*, 61–68. [CrossRef]
28. Varela, P.; Salvador, A.; Fiszman, S. On the assessment of fracture in brittle foods: The case of roasted almonds. *Food Res. Int.* **2008**, *41*, 544–555. [CrossRef]



“Faba bean protein films reinforced with cellulose nanocrystals as edible food packaging material”

Sandra Rojas-Lema^a, Klara Nilsson^b, Jon Trifol^c, Maud Langton^b, Jaume Gomez-Caturla^a, Rafael Balart^a, Daniel Garcia-Garcia^{a,*}, Rosana Moriana^{b,c,d}

^a Instituto de Tecnología de Materiales (ITM), Universitat Politècnica de València (UPV), Plaza Ferrándiz y Carbonell 1, 03801, Alcoy, Alicante, Spain

^b Department of Molecular Sciences, Swedish University of Agricultural Sciences (SLU), Box 7051, SE-750 07, Uppsala, Sweden

^c Department of Fibre and Polymer Technology, School of Engineering Sciences in Chemistry, Biotechnology and Health. Royal Institute of Technology (KTH), SE-100 44, Stockholm, Sweden

^d RISE Bioeconomy and Health, Research Institute of Sweden (RISE), Drottning Kristinas Väg 61, SE-114 28, Stockholm, Sweden

ARTICLE INFO

Keywords:

Faba beans
Proteins films
Cellulose nanocrystals (CNCs)
Food packaging
Pine cone

ABSTRACT

In the present work, transparent films were obtained by the solution casting method from faba bean protein isolate (FBP), reinforced with different cellulose nanocrystals (CNCs) content (1, 3, 5 and 7 wt%), obtained by acid hydrolysis of pine cone, and using glycerol as plasticizer. The influence of different CNCs loadings on the mechanical, thermal, barrier, optical, and morphological properties was discussed. Microstructurally, the FTIR and FESEM results corroborated the formation of intramolecular interactions between the CNCs and proteins that lead to more compact and homogeneous films. These interactions had a positive influence on the mechanical strength properties, which is reflected in higher tensile strength and Young's modulus in reinforced films with respect to the control film, resulting in stiffer films as the CNCs content increases. Thermal stability of the FBP films was also improved with the presence of CNCs, by increasing the characteristic onset degradation temperature. In addition, the linkages formed between the CNCs, and proteins reduced the water affinity of the reinforced films, leading to a reduction in their moisture content and water solubility, and an increase in their water contact angle, obtaining more hydrophobic films as the CNCs content in the matrix increased. The addition of CNCs in the FBP film also considerably improved its barrier properties, reducing its water vapour transmission rate (WVTR) and oxygen transmission rate (OTR). The present work shows the possibility of obtaining biobased and biodegradable films of CNC-reinforced FBP with improved mechanical, thermal and barrier properties, and low water susceptibility, which can be of great interest in the food packaging sector as edible food packaging material.

1. Introduction

In recent years, the worldwide consumption of plastics has increased in a remarkable way, mainly due to its high versatility and low price. Only in Europe there was a total production of 57.9 million tonnes in 2019, with the packaging industry being the main consumer with a 39.6% of the total (Plastics Europe, 2020). The high consumption of plastics generates a large amount of waste that causes serious environmental problems, especially when used as single-use packaging materials. This has led to an increase in environmental concern in society which, together with petroleum depletion, has led to a considerable increase in the research and development of new, more environmentally

friendly materials capable of replacing traditional synthetic plastics (Liminana, Garcia-Sanoguera, Quiles-Carrillo, Balart, & Montanes, 2018). Among the sustainable materials that have received the most attention, biodegradable polymeric films from renewable sources that are abundant in nature such as proteins, lipids and polysaccharides, have positioned as an actual alternative to synthetic polymer films, and are characterized by their biodegradability, wide availability, and low cost (Zhang et al., 2016). Protein films are characterized by their non-toxicity, biodegradability and good barrier properties to oxygen, lipids and flavourings (Reddy, Jiang, & Yang, 2012). However, they have a number of drawbacks compared to synthetic polymers that limit their massive use in sectors such as packaging. Among these

* Corresponding author.

E-mail address: dagarga4@epsa.upv.es (D. Garcia-Garcia).

<https://doi.org/10.1016/j.foodhyd.2021.107019>

Received 4 February 2021; Received in revised form 5 July 2021; Accepted 6 July 2021

Available online 10 July 2021

0268-005X/© 2021 Elsevier Ltd. All rights reserved.

disadvantages, it is worthy to note their low mechanical strength, poor water vapour barrier properties and high water sensitivity due to the highly hydrophilic nature of the proteins (Bourtoom, 2009). Although these properties highly depend on the protein structure and the method of film preparation (Salgado, Ortiz, Petruccielli, & Mauri, 2010).

Legume seeds are a cheap source of protein with high nutritional value, which makes them an interesting raw material for use in the manufacture of bio-based materials for the packaging sector due to their sustainability (Makri, Papalamprou, & Doxastakis, 2005). One of the most consumed legumes worldwide is faba bean (*Vicia Faba* L.), which is characterized by its low cost and high quality protein content, which can contain up to 27.34% protein (dry weight), depending on the cultivation conditions and the variety. (Samaei et al., 2020). Faba bean has long been a basic food staple in Middle Eastern and Southeast Asian countries, however, its main use has been as a livestock feed, although it has also been used as a cover crop to restore nitrogen content and prevent soil erosion (Nivala, Nordlund, Kruus, & Erçili-Cura, 2020; Vioque, Alaiz, & Giron-Calle, 2012). This makes it an excellent raw material for protein extraction for use as films in the food packaging industry. However, currently, the use of faba bean proteins to produce biodegradable films is still very limited. Some works such as those carried out by Saremnezhad et al. (Saremnezhad, Azizi, Barzegar, Abbasi, & Ahmadi, 2011) and Montalvo-Paquini et al. (Montalvo-Paquini, Rangel-Marrón, Palou, & López-Malo, 2014) analyzed the effect of different pH values, and plasticizer content of film forming solution on the physical and chemical properties of faba bean protein films. On the other hand, Hopkins et al. (Hopkins, Stone, Wang, Korber, & Nickerson, 2019) observed that faba bean protein films with 50% glycerol content, had better tensile strength and opacity and lower water permeability than protein films obtained from other legumes such as peas, lupins, lentils, and soybeans.

On the other hand, the formulation of protein films requires the use of plasticizers to reduce their brittleness and increase their functionality. The plasticizer molecules interact by hydrogen bonding with amino-acid groups in protein chains, thus reducing the intermolecular forces between them, resulting in an increase in their mobility, which translates into an increase in the flexibility, toughness and tear strength of the films (Aguirre, Borneo, & León, 2013; Tian, Guo, Xiang, & Zhong, 2018). Some of the most commonly used plasticizers for the manufacture of protein films are sorbitol, polyethylene glycol and glycerol, being glycerol one of the most effective for the production of stable, flexible and less brittle films (Pérez, Piccirilli, Delorenzi, & Verdini, 2016; Ramos et al., 2013). Glycerol is one of the most important by-products of biodiesel production, which is generated in large amounts due to the remarkable increase in biodiesel production, becoming a waste product with an associated economic and environmental cost (Rosa et al., 2010; Tong, Luo, & Li, 2015). Glycerol represents approximately 10 wt% of total biodiesel production (Yang, Hanna, & Sun, 2012). Therefore, the use of glycerol as plasticizers in protein films, in addition to increasing the ductile mechanical properties of the films, can be an effective alternative to convert a by-product of the biodiesel industry into a high value-added product (Ye, Xiu, Shahbazi, & Zhu, 2012).

One of the approaches to overcome the above-mentioned drawbacks of protein films is the use of nanoparticles. The use of small amounts of nanoparticles has shown good potential to improve the mechanical and barrier properties of protein films (Calva-Estrada, Jiménez-Fernández, & Lugo-Cervantes, 2019). Inorganic nanoparticles such as montmorillonite (Azevedo et al., 2018; Azevedo, Silva, Pereira, da Costa, & Borges, 2015; Kumar, Sandeep, Alavi, Truong, & Gorga, 2010; Pereira, Carneiro, Assis, & Borges, 2017), TiO₂ (Fathi, Almasi, & Pirouzifard, 2019; Li et al., 2011; Y.; Liu et al., 2019), halloysite nanotubes (Kang, Liu, Zhang, & Li, 2017; X.; Liu et al., 2017), or carbon nanotubes (Xiang, Guo, & Tian, 2017) have been successfully employed to reduce the drawbacks of protein films. However, the use of renewable and biodegradable nanoparticles has gained relevance in recent years due to their greater environmental friendliness. In this way, cellulose nanocrystals (CNCs)

obtained from agroforestry residues are considered one of the most promising reinforcing agents due to their biodegradability, abundance, variety, chemical modification capacity and price (García-García, Lopez-Martinez, Balart, Strömberg, & Moriana, 2018). Cellulose nanocrystals consist of highly crystalline rod-like particles, obtained from biomass, usually by acid hydrolysis, with dimensions of around 10–20 nm in width and several hundred nanometers in length, giving rise to high aspect ratios (Xu et al., 2013). CNCs are characterized by high strength, high elastic modulus and low density (Moriana, Vilaplana, & Ek, 2016), despite their physico-chemical properties depend on the cellulose source, and on synthesis process conditions (Silvério, Neto, Dantas, & Pasquini, 2013; Slavutsky & Bertuzzi, 2014). CNCs are also characterized by good compatibility with hydrophilic polymers (Han, Yu, & Wang, 2018). The effect of CNC incorporation has been previously studied in soy (González & Igarzabal, 2015; Han et al., 2018; Yu et al., 2018; Zhang et al., 2016), whey (Qazanfarzadeh & Kadivar, 2016), amaranth (Condés, Anón, Mauri, & Dufresne, 2015), or canola (Osorio-Ruiz, Avena-Bustillos, Chiou, Rodríguez-González, & Martínez-Ayala, 2019) protein films, showing that the presence of nanoparticles in the protein matrix leads to intramolecular interactions between both phases, resulting in more compact films with better mechanical properties and better barrier properties.

The main objective of the present work is to evaluate the effect of the incorporation of different CNC content extracted from pine cone (1, 3, 5 and 7 wt%) on the mechanical properties, thermal stability, barrier properties, optical properties, water susceptibility (moisture content, contact angle and water solubility) and the microstructure on glycerol-plasticized faba bean protein-based biodegradable films.

2. Experimental

2.1. Materials

Faba beans used in this work (*Gloria variety*) were supplied by RISE (Research Institutes of Sweden). Pine cones (*Pinus Pinea*) were collected from a local pine forest in Alicante (Spain). Sodium hydroxide (NaOH, 99.0% purity) and hydrochloric acid (HCl, 36% purity) were supplied by VWR (Darmstadt, Germany). Glycerol was purchased from POCH S.A. (Gliwice, Poland).

2.2. Faba bean protein isolation

The faba bean protein (FBP) isolation was done following the method described by Langton et al. (Langton et al., 2020) with some modifications. First, the faba beans were dehulled with a dehuller, and the beans were milled in a rotary mill from Brabender (Duisburg, Germany) with a 1.5 mm mesh screen. Subsequently, faba bean flour was mixed in distilled water at a ratio 1:10 (w/v) and the pH of the obtained solution was adjusted to 9.0 using 2 M NaOH to increase solubility of the protein. The suspension was stirred at room temperature for 1 h, and then was centrifuged in a Sorvall Lynx 6000 centrifuge from Thermo Scientific (Langensfeld, Germany) at 3700 G for 30 min and 18 °C. The pH of supernatant was adjusted to 4.0 using 1 M HCl to precipitate the protein, stirred at room temperature for 1.5 h and centrifuged at 3700 G for 30 min and 18 °C. The precipitates were collected and re-dispersed in distilled water at a ratio 1:10 (w/v). The suspension was adjusted to pH 4 and centrifuged again with the same described conditions. Finally, the precipitate protein was frozen and lyophilized to obtain FBP.

2.3. Preparation of pine cone nanocrystals

Pine cone nanocrystals were obtained by acid hydrolysis according to our previous work (García-García, Balart, Lopez-Martinez, Ek, & Moriana, 2018). Briefly, grinded pine cone particles were first subjected to an alkaline treatment in a 4.5% NaOH solution for 2 h at 80 °C followed by bleaching process using a solution made up of 1.7 wt%

aqueous sodium hypochlorite, acetate buffer (0.2 M, pH 4.8) and water (1:1:1) for 4 h at 80 °C, in order to remove extractives, hemicellulose and lignin of the raw material. Subsequently, the bleached fibres were hydrolysed with sulfuric acid (65 wt%) for 45 min at 45 °C. The excess acid was then removed from the solution by washing with Milli-Q water by repetitive centrifugation and finally by dialysis. The resulting suspension was sonicated to promote CNCs dispersion and then centrifuged to remove the remaining unhydrolyzed fibres. The collected suspension was then stored in a refrigerator for further use.

2.4. Preparation of reinforced protein films

Preparation of FBP films was done by solution casting process. Control protein films were prepared dissolving FBP (5% w/v), glycerol (50% w/w based on the dry weight of FBP) and distilled water. The pH of the solution was adjusted to 10.5 using a 1M NaOH solution and was mechanically stirred for 1 h. After this, the solution was denatured by heating at 85 °C for 30 min in a water bath and cooled down at room temperature. For the CNCs-reinforced films, the same procedure was followed as for the control film, however in this case the appropriate amounts of CNCs were incorporated (1, 3, 5 and 7 wt% on the dry weight of FBP) after the denaturation process, keeping the solution in a stirrer for 30 min. The resulting solutions were casted into a polystyrene Petri dish and dried at 40 °C for 24 h. Then, the dried films were peeled off and conditioned at 52% relative humidity (RH) and 25 °C for 48 h prior to testing. All films were prepared in triplicate. Table 1 summarizes the composition of all the developed films.

2.5. Characterization techniques

2.5.1. Film thickness

The thickness of the FBP films was determined at ten random points around each film sample using a manual micrometer Mitutoyo No. 2109S-10 (Tokyo, Japan) with 0.001 mm sensitivity. The average value of each film was determined and used in calculations for mechanical properties, oxygen transmission rate, water vapour transmission rate and transparency.

2.5.2. Mechanical properties

The mechanical tensile properties, namely the tensile strength (TS), the Young's modulus (E) and the elongation at break (ϵ) of FBP films were determined following the standard method ASTM D882-02, using a Linkam TST-350 tensile stage (Linkam Scientific Instruments, Ltd., U.K.) with a 20 N load cell. Preconditioned FBP films were cut into rectangular strips (30 × 4 mm²) and placed between the tensile grips. The initial grip distance was set at 15 mm and the crosshead speed at 5 mm min⁻¹. At least five specimens from each film were tested at room temperature and the average results were obtained.

Table 1
Composition and codes for faba beans proteins (FBP) films with different pine cone cellulose nanocrystals content.

Samples	Content			
	Proteins (g)	Glycerol (g)	Water (g)	CNC (wt% on dry proteins)
FBP	5	2.5	100	0
FBP.CNC-1	5	2.5	100	1
FBP.CNC-3	5	2.5	100	3
FBP.CNC-5	5	2.5	100	5
FBP.CNC-7	5	2.5	100	7

2.5.3. Thermogravimetric analysis (TGA)

Thermal behaviour of different FBP films obtained was analyzed by thermogravimetric analysis using a Mettler-Toledo TGA/DSC 1 thermobalance (Schwerzenbach, Switzerland). Samples with a total weight between 8 and 10 mg were placed in an alumina crucible (70 µL) and heated from 30 to 800 °C at a constant heating rate of 10 °C min⁻¹ under nitrogen atmosphere (flow rate 50 mL min⁻¹). All samples were analyzed in triplicate to ensure reproducibility.

2.5.4. Moisture content

Moisture content of FBP films samples was determined gravimetrically by measuring the weight loss of films, with a size of 1 × 1 cm², before and after drying in an oven at 105 °C for 24 h, to attain a constant weight. The moisture content of each film was calculated according to the following Equation (1):

$$\text{Moisture content (\%)} = 100 \times \left[\frac{W_i - W_f}{W_i} \right] \quad (1)$$

where W_i and W_f are the initial and dried weight of the samples respectively. Three replications of each film were used for calculating the moisture content average.

2.5.5. Solubility

The solubility of FBP films in water was determined according to the method proposed by K. Masamba et al. (Masamba et al., 2016) with minor modifications. Rectangular pieces of films (10 × 10 mm²) were dried in an oven at 105 °C for 24 h, until constant weight. The weight of the dried films was measured, and then the films were placed into a test tube with 10 mL of distilled water. The tubes were slowly and periodically stirred for 24 h at 25 °C. After that period, the non-solubilized fraction was dried in the oven at 105 °C for 24 h in order to determine the weight of dry matter not dissolved in water. The % solubility of each film was determined using the following equation (2):

$$\text{Solubility (\%)} = 100 \times \left[\frac{W_i - W_f}{W_i} \right] \quad (2)$$

where W_i is the initial weight of the sample and W_f is the sample weight after drying. The measurements were made in triplicate.

2.5.6. Static contact angle measurements

The static contact angle (θ) of each preconditioned FBP films was measured by an optical goniometer model FM140 (110/220 V, 50/60 Hz) from KRÜSS GmbH (Hamburg, Germany) at room temperature. This goniometer is equipped with a video capture kit and analysis software (Drop Shape Analysis SW21; DSA1). Five different water droplets, using distilled water as contact liquid, were deposited onto the film surface with a micro syringe and ten measurements were obtained for each drop and averaged. The contact angle was measured 30 s after depositing the drop to obtain stabilized values.

2.5.7. Transparency

FBP films transparency was determined using a UV-Vis spectrophotometer Perkin Elmer model Lambda 2 (Massachusetts, EEUU) according to ASTM D1746. Preconditioned film specimens were cut into rectangle shape and directly placed in the spectrophotometer cell. The percent transmittance of light at 600 nm in each film was measured by triplicate, and the transparency value was calculated by the following equation (3):

$$\text{Transparency} = \left[\frac{\text{Log} T_{600}}{x} \right] \quad (3)$$

where T_{600} is the transmittance at 600 nm of each film and x is the film thickness (mm).

2.5.8. Colour of films

The effect of CNCs in the colour properties of FBP films was studied in a colorimeter model KONICA CM-3600d COLORFLEX-DIFF2 from Hunter Associates Laboratory (Virginia, EEUU) calibrated using a white standard. The CIELAB colour space was used to measure the degree of L^* (lightness), a^* (red-green) and b^* (yellow-blue) of each film. Five measurements were made at random positions over each film surface and average values were calculated. Total colour difference (ΔE) was calculated using the following equation (4):

$$\Delta E = \sqrt{(\Delta L^*)^2 + (\Delta a^*)^2 + (\Delta b^*)^2} \quad (4)$$

where ΔL^* , Δa^* and Δb^* are the differences between the corresponding colour parameters of the samples and the colour parameter values of the control film ($L^* = 66.6$, $a^* = 5.5$, $b^* = 37.0$).

2.5.9. Oxygen transmission rate (OTR)

The oxygen transmission rate (OTR) of the FBP films was obtained using an OTR Permeation Analyzer Mocon OX-TRAN model 2/20 from Modern Controls Inc. (Minneapolis, USA) equipped with a coulometric oxygen sensor in accordance with ASTM D3985-95. The area of measurement of the samples was 5 cm^2 and the OTR measurements were performed at 23°C and 50% RH. Before the analysis, the samples were conditioned for 2 days at 23°C and 50% RH. At least two samples of each film were tested.

2.5.10. Water vapour permeability (WVP)

The WVP test was conducted gravimetrically in triplicate following ASTM E96-95. Conditioned circular films were sealed on permeability cups TQC Sheen B.V. model VF2200 (Capelle aan den IJssel, Netherlands) containing 2 g of CaCl_2 (0% RH) with an exposed area of 10 cm^2 . Later, the cups were placed in a desiccator at $25 \pm 1^\circ \text{C}$ containing a saturated $\text{Mg}(\text{NO}_3)_2 \cdot 6\text{H}_2\text{O}$ solution to reach a relative humidity of $54\% \pm 3\%$. The cups were weighed each hour for a total period of 8 h using an analytical balance. The changes in cup weight were plotted as a function of time and the slope was calculated by linear regression. Finally, the WVTR was calculated according to the following equation (5) (Trifol et al., 2016):

$$\text{WVTR} = \frac{n \times l}{S} \quad (5)$$

where n is the slope of the straight line, l is the thickness of the film and S is the exposed area of the film.

2.5.11. Field emission scanning electron microscopy (FESEM)

The morphology of the cross section of nitrogen cryofractured films was studied in a field emission scanning electron microscope (FESEM) ZEISS model ULTRA55 (Eindhoven, The Netherlands) with an operating voltage of 1 kV. Prior to the morphological characterization, the cryofracture surface of films were coated with a thin layer of platinum in a high vacuum sputter coater EM MED20 from Leica Microsystems (Millton Keynes, United Kingdom).

2.5.12. Attenuated total reflection-Fourier transform infrared (ATR-FTIR) spectroscopy

The FBP films spectra were recorded by attenuated total reflection method (ATR) in an infrared spectrometer Perkin-Elmer Spectrum BX (Perkin-Elmer Spain S.L., Madrid, Spain). Each sample was subjected to 20 scans between 4000 and 600 cm^{-1} with a resolution of 4 cm^{-1} . After attenuation of total reflectance and baseline correction, spectra were normalized with a limit ordinate of 1.5 absorbance units.

3. Results and discussion

3.1. Mechanical properties

The mechanical properties of the control film (FBP) and films reinforced with different CNCs content are shown in Fig. 1. As can be seen, the incorporation of low CNCs content (1 and 3 wt%) to the FBP film hardly affects the strength and tensile modulus, obtaining values very similar to those of the unreinforced FBP film. However, it is observed that the addition of higher CNCs amounts (5 and 7 wt%) results in a considerable increase in tensile strength, with values of 5.3 MPa and 6.5 MPa for the films reinforced with 5 and 7 wt% of CNCs respectively, which represents a percentage increase of 22.3% and 50.5% respectively, with respect to the unreinforced film (4.3 MPa). The tensile strength values obtained with the film reinforced with 7 wt% CNCs are higher than those obtained with other protein films reinforced with similar or higher amounts of CNCs (González et al., 2015; Osorio-Ruiz et al., 2019; Sukyai et al., 2018). This tendency is also observed in Young's modulus, where it can be seen that the addition of 5 and 7 wt% of CNCs into the FBP film resulted in an increase of 43.7% and 76.1% respectively with respect to the unreinforced protein film (67.1 MPa). Therefore, the incorporation of CNCs into the FBP film resulted in an increase in its stiffness, which increases with the amount of reinforcement in the matrix. This is due to the increased hydrogen bonds formed between the protein matrix and the reinforcement as CNCs loading increases, thus increasing the cohesion of the films and reducing their flexibility (González et al., 2015; Sukyai et al., 2018). This same trend with respect to mechanical strength properties was observed by Sukyai et al. (Sukyai et al., 2018) who studied the effect of different content of cellulose nanocrystals from sugarcane bagasse (0, 2, 5 and 8 wt%) in whey protein films. In this case, the authors observed that the addition of 8 wt% CNCs to the whey protein film resulted in an increase in tensile strength from 2.30 MPa to 4.93 MPa and Young's modulus from 57.56 MPa to 187.42 MPa with respect to the unreinforced whey protein film.

With respect to the elongation at break, Fig. 1 shows how the addition of CNCs results in a decrease of ductile mechanical properties of the FBP film. In this case, it is observed that the control film shows an elongation at break of about 105%. This elongation at break is significantly higher than the elongation at break obtained in other protein films with similar plasticizer content, such as soy protein films (González, Gastelú, Barrera, Ribotta, & Igarzabal, 2019) or whey protein films (Galus & Kadzińska, 2016). The addition of 1 wt% of CNCs considerably reduces the elongation at break of the control film, changing from 104.4% in FBP film to 63.9%. For higher amounts of CNCs (3 and 5 wt%) the elongation at break decreases to around 54%, while for films reinforced with 7 wt% CNCs the elongation decreases to 48.9%, which represents a decrease of around 53.1% with respect to the elongation at break of the control film. This decrease in elongation at break is typical of protein films reinforced with cellulose nanocrystals, since the interactions of the CNCs with the proteins lead to a reduction in the polymer chains' mobility, thus reducing their ductility (Shabanpour, Kazemi, Ojagh, & Pourashouri, 2018).

Comparing the mechanical properties of unreinforced FBP films and films reinforced with different CNCs content with those of synthetic films used in the food packaging sector, it can be observed that the elongation at break obtained in the control film is higher than that of widely used materials such as PET (70%) or HDPE (20–50%). However, these materials have higher tensile strength values than FBP films. On the other hand, it is observed that the tensile strength achieved by the FBP film reinforced with 7 wt% CNCs has a tensile strength value similar to that of LDPE (7–25 MPa) and EVA (6–19 MPa) (Bastarrachea, Dhawan, & Sablani, 2011).

3.2. Thermal properties

The thermal stability of unreinforced FBP film and films reinforced

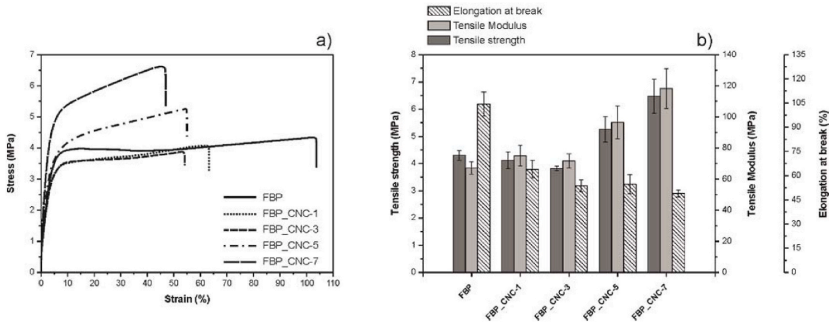


Fig. 1. Tensile properties of unreinforced (control) FBP film and FBP film reinforced with different CNCs content: a) stress-strain curves and b) tensile properties.

with different CNCs content was studied by thermogravimetric analysis. Fig. 2 shows the mass loss curves of the FBP films with respect to temperature and their corresponding first derivative curves (DTG). Additionally, Table 2 gathers the most relevant thermal degradation properties, namely the onset degradation temperature of each film and the maximum degradation temperatures in each of the different degradation stages, as well as the percentage of mass loss obtained in each of them. As can be seen in all the curves, three main stages can be identified. The weight loss that occurs at low temperatures (30–125 °C) is related to the moisture loss absorbed by the films. The second degradation stage (125–280 °C) is attributed to the loss of low molecular weight protein fractions and glycerol evaporation. Finally, the third stage (280–500 °C), is related to the protein and CNCs degradation (Osorio-Ruiz et al., 2019). As shown in Table 2, the control film (FBP) has a higher moisture content than the CNCs-reinforced films. This is a clear evidence of the increased hydrophobicity of the film due to the presence of the CNCs, as their interaction with the proteins reduces the number of active sites capable of reacting with the water molecules, thus reducing the moisture content of the film. It can also be observed that the FBP film onset degradation temperature increases with the presence of CNCs, with higher values as the CNCs content increases. In this case, the highest onset degradation temperature is obtained for the film reinforced with 7 wt% CNCs, with an increase of about 15 °C with respect to the control film. On the other hand, if the third degradation stage is observed, related to the degradation of the proteins and CNCs, it can be seen that the reinforced films present higher thermal stability with increasing CNCs content. This increase in degradation temperature in reinforced films may be due to the higher thermal stability of CNCs

compared to proteins, as well as the formation of strong intermolecular bonds between CNCs and the matrix phase resulting in improved thermal stability compared to the control film (Chang, Jian, Zheng, Yu, & Ma, 2010; Osorio-Ruiz et al., 2019). In this case, the highest degradation temperature (T_{max3}) was obtained in the film reinforced with 7 wt% of CNCs, with a value of 318.9 °C. This is due to the higher number of interactions established between the proteins and CNCs, resulting in an increase in their thermal stability.

3.3. Water susceptibility

Moisture content, water solubility and contact angle values of different FBP films are shown in Table 3. As can be seen, the addition of CNCs to the protein film results in a slight reduction in the moisture content of the films, being this reduction greater for higher CNCs contents (5 and 7%). This decrease in the moisture content of the reinforced films may be due to the interactions formed between the hydroxyl groups of the CNCs and the free functional groups of the proteins, which reduce the number of available active sites capable of interacting with the water molecules, resulting in an increase in the hydrophobicity (Qazanfarzadeh et al., 2016). This reduction of hydrophilic groups in the protein film due to interactions with CNCs also leads to an increase in the surface hydrophobicity. As can be seen in Table 3, the contact angle of the control film (56.7°) increases after the addition of CNCs, being higher as the CNCs concentration in the film increases. In this case, the maximum contact angle is obtained for the FBP film reinforced with 7 wt % CNCs, with a contact angle of 66.7°, which represents an increase of 21.4% with respect to the control film (Condés et al., 2015). This

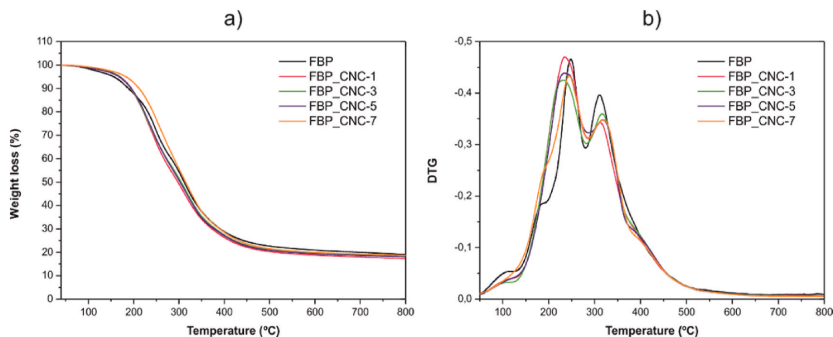


Fig. 2. a) TGA curves and b) DTGA curves of unreinforced (control) FBP film and FBP film reinforced with different CNCs content.

Table 2

Thermal parameters of unreinforced (control) FBP film and FBP film reinforced with different CNCs content.

Samples	T_0^a (°C)	Stage 1		Stage 2		Stage 3		Residue Mass (%)
		30 - 125 °C		125-280 °C		280-500 °C		
		Mass loss (%)	Mass loss (%)	T_{max2} (°C)	Mass loss (%)	T_{max3} (°C)		
FBP	155.9 ± 0.1	2.8 ± 0.2	34.2 ± 2.9	245.9 ± 1.2	44.1 ± 3.3	311.9 ± 1.5	18.9 ± 0.3	
FBP_CNC-1	165.4 ± 1.9	2.1 ± 0.0	45.6 ± 1.6	237.9 ± 1.7	35.3 ± 1.3	311.7 ± 0.7	17.1 ± 0.3	
FBP_CNC-3	166.7 ± 1.4	2.0 ± 0.1	39.6 ± 1.6	235.0 ± 2.7	40.0 ± 1.2	316.4 ± 0.4	18.4 ± 0.3	
FBP_CNC-5	167.1 ± 1.0	2.1 ± 0.0	43.7 ± 1.2	232.8 ± 1.9	36.3 ± 0.9	318.5 ± 0.5	17.9 ± 0.3	
FBP_CNC-7	170.8 ± 2.1	1.9 ± 0.2	43.2 ± 3.4	243.7 ± 3.7	36.3 ± 3.0	318.9 ± 0.6	18.6 ± 0.1	

^a T_0 is calculated at 5% weight loss.**Table 3**

Moisture content, water solubility and contact angle for unreinforced (control) FBP film and FBP film reinforced with different CNCs content.

Samples	Sample				
	FBP	FBP_CNC-1	FBP_CNC-3	FBP_CNC-5	FBP_CNC-7
Moisture content (%)	15.9 ± 0.5	15.4 ± 0.6	15.3 ± 0.7	14.2 ± 0.3	14.3 ± 0.9
Water solubility (%)	34.6 ± 0.5	33.6 ± 0.2	31.7 ± 0.5	31.1 ± 1.1	31.5 ± 0.8
Contact angle (°)	56.7 ± 1.3	57.4 ± 2.1	61.6 ± 1.4	64.6 ± 3.1	66.7 ± 1.0

increase in FBP film hydrophobicity after CNCs incorporation is of great interest for food packaging applications. However, the contact angle is still lower than that of materials used as food packaging such as LDPE (100.2°), HDPE (92.4°) or PP (90°), which is evidence of their hydrophilic nature (Fávaro, Rubira, Muniz, & Radovanovic, 2007; Karbowiak, Debeaufort, Champion, & Voilley, 2006).

Table 3 shows the water solubility values of the different films. Water solubility is an important property to be considered in food packaging applications where the film has to be in contact with food that contains a large amount of water. In this case it is observed that the unreinforced FBP film shows a low water solubility compared to other protein films, such as soy protein films (González et al., 2019; González et al., 2015), whey protein (Sukyai et al., 2018) or Amaranth protein films (Condés et al., 2015). This low solubility of the films was evidenced by the good structural integrity obtained after 24 h of immersion in water, which showed that only small amounts of low molecular weight peptides and plasticizer were dissolved in the water during the test (Wang et al., 2017). In this case, it is observed that the incorporation of CNCs in the FBP film decreases its water solubility, obtaining a reduction in solubility of around 10% for films with CNCs contents of 3, 5 and 7 wt% compared to the control film. This reduction in solubility is due to the strong hydrogen bonding interactions established between the hydroxyl groups of CNCs and the carboxyl and amino groups of proteins, which improve their cohesion and reduce their susceptibility to water molecules (Abdollahi, Alboofetileh, Behrooz, Rezaei, & Miraki, 2013; Shabanpour et al., 2018). Some authors have reported that this reduction in water solubility may also be influenced by the high crystallinity of the CNCs (Deepa et al., 2016).

3.4. Chemical structural properties

The chemical interactions between CNCs and the proteins during film production were assessed by ATR-FTIR. Fig. 3 shows the FTIR spectra of the unreinforced FBP film and the films reinforced with different CNCs content. As can be seen, the control film spectra (FBP) shows the main absorption bands of the peptide linkage which are the peak at 1630 cm^{-1} corresponding to the amide I band (C=O stretching), the peak at 1538 cm^{-1} attributed to the amide II band (N-H bending and

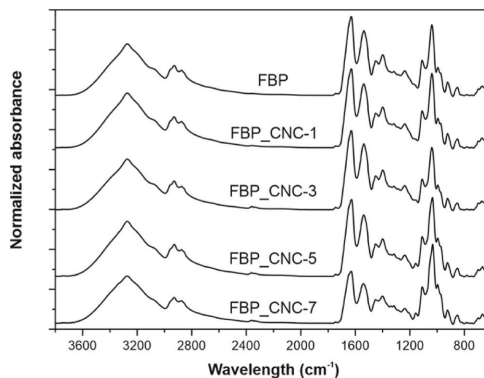


Fig. 3. FTIR spectra of unreinforced (control) FBP film and FBP film reinforced with different CNCs content.

C-N stretching) and the peak at 1238 cm^{-1} corresponding to the amide III band (N-H bending and C-N stretching) (Montalvo-Paquini et al., 2014). Other characteristic peaks appearing in the spectra are the peak at 3272 cm^{-1} related to the N-H and O-H groups of the proteins, and the peak at 1038 cm^{-1} associated with C-C and C-O stretching vibrations. On the other hand, the peaks located in the range between 800 and 1150 cm^{-1} are attributed to the glycerol used as a film plasticizer (Shabanpour et al., 2018; Sogut, 2020; Sukyai et al., 2018). After the incorporation of CNCs, no significant changes in the spectra were observed. However, it is observed that in the reinforced films a new peak appears at 1158 cm^{-1} related to the saccharide structures of CNCs (Yu et al., 2018), as well as a change in the intensity of the bands associated to the amide I, II, and III compared to the control film. These differences are most evident in the case of the film reinforced with 7 wt% CNCs. This suggests the formation of interactions between the main polypeptide chains of proteins and the CNCs, consisting mainly of hydrogen bonds between the amino and carboxyl groups of the proteins and the hydroxyl groups of the CNCs (Martelli-Tosi et al., 2018; Shabanpour et al., 2018).

3.5. Morphological properties

The FESEM images of the cryofractured cross section of the different films are gathered in Fig. 4. As can be seen, the control film has a smooth and homogeneous surface, with the presence of small microcracks and numerous surface pores. After the CNCs incorporation, a modification of the fracture surface is observed. In this case, CNCs-reinforced films have a higher cross-section roughness, which increases as the CNCs content in the film increases. Furthermore, it is observed that the CNCs incorporation in the film leads to a reduction in the size and pore number on the surface, resulting in a more homogeneous and uniform surface. This is

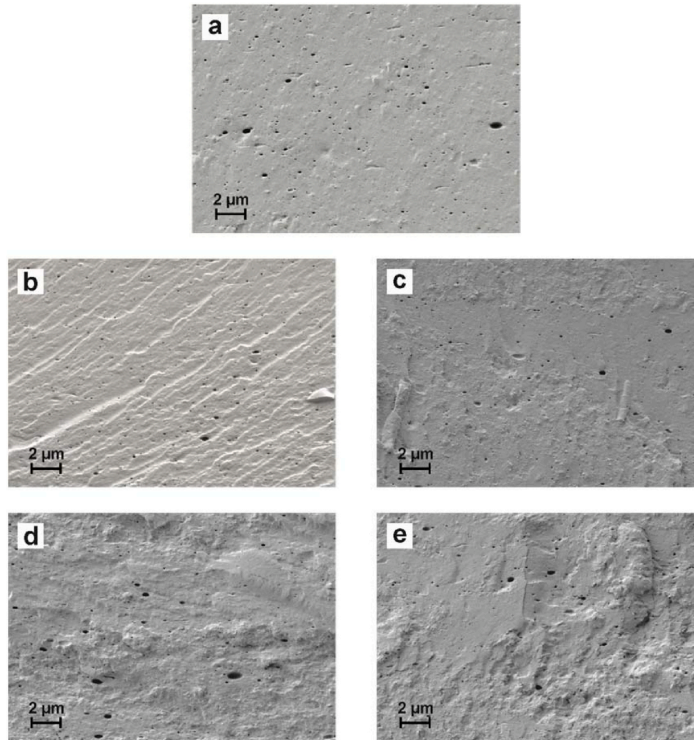


Fig. 4. Field emission scanning electron microscopy (FESEM) images at $5000\times$ of cryofractured cross section of FBP-based films: (a) FBP (control); (b) FBP_CNC-1; (c) FBP_CNC-3; (d) FBP_CNC-5 and (e) FBP_CNC-7.

most noticeable in samples reinforced with small CNCs content (1% and 3%). This reduction in the size and number of pores on the surface evidences the good interaction between the functional groups of the proteins, the glycerol and the CNCs, which results in more compact and resistant films, but with a lower molecular mobility, which is reflected in the mechanical properties with an increase in the tensile strength and a decrease in the elongation at break (Mirpoor et al., 2020; Osorio-Ruiz et al., 2019; Yu et al., 2018).

3.6. Barrier properties

Fig. 5 shows the OTR and WVTR values of unreinforced FBP film (control), and films reinforced with different CNCs content. As can be seen in Fig. 5a, the CNCs addition to the control FBP film results in a reduction of the OTR values, being this reduction greater as the CNCs content in the film increases. In this case, the lowest OTR value was obtained in the film with a CNCs content of 7 wt% (3.67×10^3 mL μm^2 day^{-1}).

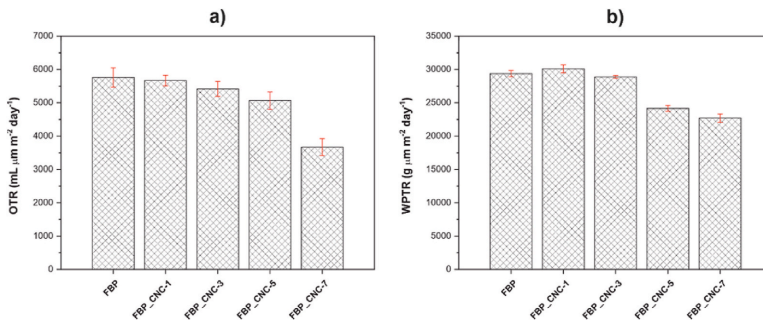


Fig. 5. a) OTR and b) WVTR of unreinforcing (control) FBP film and FBP film reinforcing with different CNCs content.

$\text{m}^{-2} \text{day}^{-1}$), obtaining an OTR value 36.2% lower than the control film ($5.75 \times 10^3 \text{ mL } \mu\text{m}^{-2} \text{day}^{-1}$). This OTR decrease is due to the formation of a dense network structure by the interaction between proteins and CNCs which results in an increase in the tortuosity of the diffusion pathway of the oxygen molecules, hindering their transfer through the film and thus increasing its oxygen barrier property (Xie et al., 2020). This reduction of oxygen permeability is of great importance in the food packaging sector, as it allows to increase the product's shelf life.

In the same way, it can be seen in Fig. 5b that the WVTR is also reduced by the presence of CNCs, improving the water barrier property of the FBP films. In this case, the addition of 1 wt% CNCs hardly affects the water vapour permeability. However, higher CNCs content results in a decrease in WVTR with respect to the control film, leading to a greater decrease as the CNC content in the film increases. The WVTR of the control film was $2.93 \times 10^4 \text{ g } \mu\text{m}^{-2} \text{day}^{-1}$, reducing to $2.27 \times 10^4 \text{ g } \mu\text{m}^{-2} \text{day}^{-1}$ after incorporating 7 wt% CNCs, a decrease of about 22.7%. This improvement of the water vapour barrier property of the reinforced films can be influenced by several aspects, such as the decrease of the films' hydrophilicity due to the presence of CNCs, or the increase of the tortuosity of the diffusion path of water molecules due to the presence of highly crystalline CNCs. In addition, the restricted polymer chain mobility and the higher matrix structure density obtained due to the strong interactions of the functional groups of proteins and CNCs also contribute to the reduction of the water vapour permeability of CNC-reinforced films. (Azevedo et al., 2020; Rafeian, Shahedi, Keramat, & Simonsen, 2014).

3.7. Colour and transparency properties

Fig. 6 shows the light transmission in the UV and visible ranges and the transparency of unreinforced FBP film and films reinforced with different CNCs content. As can be seen, all films show a good ability to absorb UV light at wavelengths between 250 and 300 nm, while for wavelengths between 300 and 400 nm, the CNCs addition to the FBP film reduces the UV light absorption, which is of interest in the food preservation packaging sector. In the visible range region (400–700 nm), the FBP film shows a high transmittance percentage, which is reduced after the CNCs incorporation. As can be seen in Fig. 6a, the transmittance decreases as the CNC content of the film increases.

The films' transparency is one of the most important properties to be considered for their use in the food packaging industry. Fig. 6b shows that the control film has a high transparency, however, after CNCs addition, this transparency is slightly reduced, obtaining a higher opacity as the CNCs content in the film increases. The decrease in transparency of the reinforced films may be related to light scattering caused by the dispersed CNCs in the matrix which leads to a reduction of light passing through the film. The increased opacity of reinforced films may also be due to the formation of CNCs aggregates during film fabrication, which cause a slight darkening and make it difficult for light to pass through the matrix (Qazanfarzadeh et al., 2016; Shabanpour et al., 2018). This loss of transparency in CNCs-reinforced protein films has also been observed by several authors such as Sukyai et al. (Sukyai et al., 2018), Han et al. (Han et al., 2018) or Huang et al. (Huang, Tao, Ismail, & Wang, 2020). In this case, FBP films are less transparent than

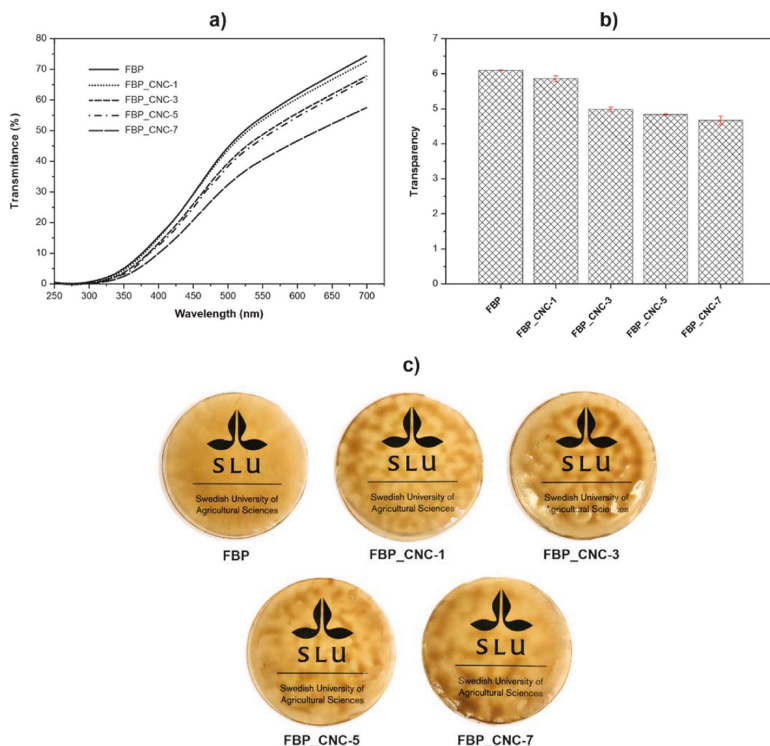


Fig. 6. a) transmittance, b) transparency and c) macroscopic aspect of unreinforced (control) FBP film and FBP film reinforced with different CNCs content.

other CNCs-reinforced films, such as CNCs-reinforced whey protein films from sugar cane bagasse. (Sukyai et al., 2018). However, it is worth noting that the control film and the FBP film reinforced with 1 wt% of CNCs show higher transparency than the commercial LDPE film used for food packaging, 4.26 A/mm, being this very similar to that obtained in the FBP films reinforced with 3, 5 and 7 wt% of CNCs (Guerrero, Hanani, Kerry, & De La Caba, 2011).

Table 4 shows the surface colour values of unreinforced film and films reinforced with different CNCs content. As can be seen, the incorporation of CNCs into the FBP films results in a slight increase in L^* and a decrease in the a^* and b^* coordinate values, which is representative for a slight increase of the brown colour in the samples, probably due to the formation of CNC aggregates in the film. However, the ΔE values of the CNC-reinforced films show that the reinforcement addition into the FBP film hardly alters its colour properties.

4. Conclusions

In the present work, the effect of the incorporation of different CNCs content (1, 3, 5 and 7 wt%) synthesized from pine cone on the mechanical, thermal, barrier, water susceptibility, optical and morphological properties of faba bean protein (FBP) films has been evaluated. The CNCs addition to the FBP film resulted in the formation of intramolecular interactions between the hydroxyl groups of the CNCs and the amino and carboxyl groups of the proteins, mainly through hydrogen bonds. This chemical affinity resulted in more compact films with lower chain mobility, which was reflected in the mechanical properties of the reinforced films through an increase in tensile strength and Young's modulus and a decrease in the elongation at break compared to the unreinforced FBP film. In this case, the incorporation of 7 wt% CNC in the FBP film resulted in an increase in tensile strength and Young's modulus of 50.5 and 76.1% respectively with respect to the control film, as well as a decrease in elongation at break of about 53.1%. The thermal stability of the FBP film was also affected by the presence of CNCs, increasing the onset degradation temperature as the CNC content in the film increases. In this case, an increase of 15 °C was obtained in the onset degradation temperature of the film reinforced with 7 wt% of CNCs compared to the control film. A slight increase in the maximum degradation temperature was also observed in the reinforced films with respect to the FBP film. The interactions formed between the CNCs and the proteins also reduced the amount of active sites able to react with the water molecules in the proteins, which resulted in an increase in the hydrophobicity of the CNC-reinforced films, as evidenced by a reduction in moisture content and water solubility and an increase in their contact angles. The CNCs addition to the FBP film also significantly improved its barrier properties, reducing its WVTR and OTR as the CNC content in the matrix increased. In this case, the film reinforced with 7 wt% CNC obtained 36.2 and 22.7% lower OTR and WVTR values, respectively, compared to the unreinforced FBP film. Finally, it was observed that the presence of CNCs in the FBP film led to an increase in its opacity as the CNCs content increases. This work has shown that CNCs obtained from pine cone are of great interest to improve some physical and mechanical properties of FBP films, obtaining biobased and biodegradable materials that could present attracting potential for use in the food packaging sector as edible food packaging material. These films could be a potential solution to reduce the amount of non-degradable food packaging waste of petrochemical origin.

Author statement

Sandra Rojas-Lema: Data Curation, Software, Formal analysis, Writing - Original Draft, Klara Nilsson: Investigation, Validation, Data Curation, Jon Trifol: Investigation, Validation, Data Curation, Maud Langton: Resources, Project administration, Funding acquisition, Jaume Gomez-Caturla: Data Curation, Software, Formal analysis, Writing - Original Draft, Rafael Balart: Conceptualization, Supervision, Project

Table 4

Colour parameters from CIELab space of unreinforced (control) FBP films and FBP film reinforced with different CNCs content.

Parameter	FBP	FBP CNC-1	FBP CNC-3	FBP CNC-5	FBP CNC-7
L^*	66.6 ± 0.4	68.0 ± 0.7	69.8 ± 1.3	68.6 ± 1.6	69.4 ± 1.4
a^*	5.5 ± 0.3	4.3 ± 0.3	3.9 ± 0.6	5.1 ± 0.7	4.0 ± 0.5
b^*	37.0 ± 0.5	34.5 ± 0.8	35.6 ± 1.2	35.1 ± 1.3	34.2 ± 1.2
ΔE	-	3.1	3.8	2.7	4.2
(Control) ^a					

^a ΔE is calculated from the colour difference between FBP film and each FBP/CNC film.

administration, Funding acquisition, Daniel Garcia-Garcia: Methodology, Investigation, Validation, Writing - Review & Editing, Visualization, Rosana Moriana: Conceptualization, Supervision, Project administration.

Declaration of competing interest

The authors declare that they have no known competing financial interests or personal relationships that could have appeared to influence the work reported in this paper.

Acknowledgements

This research was supported by the Ministry of Science and Innovation (MICI) [MAT2017-84909-C2-2-R]. S. Rojas-Lema thanks the Generalitat Valenciana (GVA) for the financial support through a Santiago Grisolia grant (GRISOLIAP/2019/132). D. Garcia-Garcia wants to thank the Ministry of Science, Innovation and Universities for their financial support through the "José Castillejo" mobility grant (CAS19/00332).

References

- Abdollahi, M., Alboofeteleh, M., Behrooz, R., Rezaei, M., & Miraki, R. (2013). Reducing water sensitivity of alginate bio-nanocomposite film using cellulose nanoparticles. *International Journal of Biological Macromolecules*, 54, 166–173.
- Aguirre, A., Borneo, R., & León, A. E. (2013). Properties of triticale protein films and their relation to plasticizing–antiplasticizing effects of glycerol and sorbitol. *Industrial Crops and Products*, 50, 297–303.
- Azevedo, V. M., de Oliveira, A. C. S., Borges, S. V., Raguzzoni, J. C., Dias, M. V., & Costa, A. L. R. (2020). Pea protein isolate nanocomposite films for packaging applications: Effect of starch nanocrystals on the structural, morphological, thermal, mechanical and barrier properties. *Emirates Journal of Food and Agriculture*, 32(7), 495–504.
- Azevedo, V. M., Dias, M. V., de Siqueira Elias, H. H., Fukushima, K. L., Silva, E. K., Carneiro, J. d. D. S., et al. (2018). Effect of whey protein isolate films incorporated with montmorillonite and citric acid on the preservation of fresh-cut apples. *Food Research International*, 107, 306–313.
- Azevedo, V. M., Silva, E. K., Pereira, C. F. G., da Costa, J. M. G., & Borges, S. V. (2015). Whey protein isolate biodegradable films: Influence of the citric acid and montmorillonite clay nanoparticles on the physical properties. *Food Hydrocolloids*, 43, 252–258.
- Bastarrachea, L., Dhawan, S., & Sablani, S. S. (2011). Engineering properties of polymeric-based antimicrobial films for food packaging: A review. *Food Engineering Reviews*, 3(2), 79–93.
- Bourtoom, T. (2009). Edible protein films: Properties enhancement. *International Food Research Journal*, 16(1), 1–9.
- Calva-Estrada, S. J., Jiménez-Fernández, M., & Lugo-Cervantes, E. (2019). Protein-based films: Advances in the development of biomaterials applicable to food packaging. *Food Engineering Reviews*, 11(2), 78–92.
- Chang, P. R., Jian, R., Zheng, P., Yu, J., & Ma, X. (2010). Preparation and properties of glycerol plasticized-starch (GPS)/cellulose nanoparticle (CN) composites. *Carbohydrate Polymers*, 79(2), 301–305.
- Condés, M. C., Anón, M. C., Mauri, A. N., & Dufresne, A. (2015). Amaranth protein films reinforced with maize starch nanocrystals. *Food Hydrocolloids*, 47, 146–157.
- Deepa, B., Abraham, E., Pothan, L. A., Cordeiro, N., Faria, M., & Thomas, S. (2016). Biodegradable nanocomposite films based on sodium alginate and cellulose nanofibrils. *Materials*, 9(1), 50.
- Fathi, N., Almasi, H., & Pirouzfard, M. K. (2019). Sesame protein isolate based bionanocomposite films incorporated with TiO2 nanoparticles: Study on

- morphological, physical and photocatalytic properties. *Polymer Testing*, 77, Article 105919.
- Fávoro, S., Rubira, A. M., Muniz, E., & Radovanovic, E. (2007). Surface modification of HDPE, PP, and PET films with KMnO_4/HCl solutions. *Polymer Degradation and Stability*, 92(7), 1219–1226.
- Galus, S., & Kadzińska, J. (2016). Whey protein edible films modified with almond and walnut oils. *Food Hydrocolloids*, 52, 78–86.
- García-García, D., Balart, R., Lopez-Martinez, J., Ek, M., & Moriana, R. (2018). Optimizing the yield and physico-chemical properties of pine cone cellulose nanocrystals by different hydrolysis time. *Cellulose*, 25(5), 2925–2938.
- García-García, D., Lopez-Martinez, J., Balart, R., Strömberg, E., & Moriana, R. (2018). Reinforcing capability of cellulose nanocrystals obtained from pine cones in a biodegradable poly(3-hydroxybutyrate)/poly(ϵ -caprolactone)(PHB/PCL) thermoplastic blend. *European Polymer Journal*, 104, 10–18.
- González, A., Gastelú, G., Barrera, G. N., Ribotta, P. D., & Igarzabal, C. I.Á. (2019). Preparation and characterization of soy protein films reinforced with cellulose nanofibers obtained from soybean by-products. *Food Hydrocolloids*, 89, 758–764.
- González, A., & Igarzabal, C. I. A. (2015). Nanocrystal-reinforced soy protein films and their application as active packaging. *Food Hydrocolloids*, 43, 777–784.
- Guerrero, P., Hanani, Z. N., Kerry, J., & De La Caba, K. (2011). Characterization of soy protein-based films prepared with acids and oils by compression. *Journal of Food Engineering*, 107(1), 41–49.
- Han, Y., Yu, M., & Wang, L. (2018). Soy protein isolate nanocomposites reinforced with nanocellulose isolated from licorice residue: Water sensitivity and mechanical strength. *Industrial Crops and Products*, 117, 252–259.
- Hopkins, E. J., Stone, A. K., Wang, J., Korber, D. R., & Nickerson, M. T. (2019). Effect of glycerol on the physicochemical properties of films based on legume protein concentrates: A comparative study. *Journal of Texture Studies*, 50(6), 539–546.
- Huang, S., Tao, R., Ismail, A., & Wang, Y. (2020). Cellulose nanocrystals derived from textile waste through acid hydrolysis and oxidation as reinforcing agent of soy protein film. *Polymers*, 12(4), 958.
- Kang, H., Liu, X., Zhang, S., & Li, J. (2017). Functionalization of halloysite nanotubes (HNTs) via mussel-inspired surface modification and silane grafting for HNTs/soy protein isolate nanocomposite film preparation. *RSC Advances*, 7(39), 24140–24148.
- Karbowiak, T., Debeaufort, F., Champdon, D., & Volleey, A. (2006). Wetting properties at the surface of iota-carrageenan-based edible films. *Journal of Colloid Interface Science*, 294(2), 400–410.
- Kumar, P., Sandeep, K., Alavi, S., Truong, V., & Gorga, R. (2010). Preparation and characterization of bio-nanocomposite films based on soy protein isolate and montmorillonite using melt extrusion. *Journal of Food Engineering*, 100(3), 480–489.
- Langton, M., Ehsanzamir, S., Kärkehabadi, S., Feng, X., Johansson, M., & Johansson, D. P. (2020). Gelation of faba bean proteins—Effect of extraction method, pH and NaCl. *Food Hydrocolloids*, 103, Article 105622.
- Li, Y., Jiang, Y., Liu, F., Ren, F., Zhao, G., & Leng, X. (2011). Fabrication and characterization of TiO₂/whey protein isolate nanocomposite film. *Food Hydrocolloids*, 25(5), 1098–1104.
- Liminana, P., Garcia-Sanoguera, D., Quiles-Carrillo, L., Balart, R., & Montanes, N. (2018). Development and characterization of environmentally friendly composites from poly(butylene succinate)(PBS) and almond shell flour with different compatibilizers. *Composites Part B: Engineering*, 144, 153–162.
- Liu, X., Kang, H., Wang, Z., Zhang, W., Li, J., & Zhang, S. (2017). Simultaneously toughening and strengthening soy protein isolate-based composites via carboxymethylated chitosan and halloysite nanotube hybridization. *Materials*, 10(6), 653.
- Liu, Y., Xu, L., Li, R., Zhang, H., Cao, W., Li, T., et al. (2019). Preparation and characterization of soy protein isolate films incorporating modified nano-TiO₂. *International Journal of Food Engineering*, 15(7).
- Makri, E., Papanalmprou, E., & Doxastakis, G. (2005). Study of functional properties of seed storage proteins from indigenous European legume crops (lupin, pea, broad bean) in admixture with polysaccharides. *Food Hydrocolloids*, 19(3), 583–594.
- Martelli-Tosi, M., Masson, M. M., Silva, N. C., Esposito, B. S., Barros, T. T., Assis, O. B., et al. (2018). Soybean straw nanocellulose produced by enzymatic or acid treatment as a reinforcing filler in soy protein isolate films. *Carbohydrate Polymers*, 198, 61–68.
- Masamba, K., Li, Y., Hategeskimana, J., Liu, F., Ma, J., & Zhong, F. (2016). Effect of Gallie acid on mechanical and water barrier properties of zein-oleic acid composite films. *Journal of Food Science and Technology*, 53(5), 2227–2235.
- Mirpoor, S. F., Gioiafatto, C. V. L., Di Pietro, P., Di Girolamo, R., Regalado-González, C., & Porta, R. (2020). Valorisation of posidonia oceanica sea balls (Egagropilli) as a potential source of reinforcement agents in protein-based biocomposites. *Polymers*, 12(12), 2788.
- Montalvo-Paquini, C., Rangel-Marrón, M., Palou, E., & López-Malo, A. (2014). Physical and chemical properties of edible films from faba bean protein. *Cellulose*, 8, 125–131.
- Moriana, R., Vilaplana, F., & Ek, M. (2016). Cellulose nanocrystals from forest residues as reinforcing agents for composites: A study from macro- to nano-dimensions. *Carbohydrate Polymers*, 139, 139–149.
- Nivala, O., Nordlund, E., Kruss, K., & Ercil-Cura, D. (2020). The effect of heat and transglutaminase treatment on emulsifying and gelling properties of faba bean protein isolate. *Lebensmittel-Wissenschaft und -Technologie: Food Science and Technology*, Article 110517.
- Osoerio-Ruiz, A., Avena-Bustillos, R. J., Chiu, B.-S., Rodríguez-González, F., & Martínez-Ayala, A.-L. (2019). Mechanical and thermal behavior of canola protein isolate films as improved by cellulose nanocrystals. *ACS Omega*, 4(21), 19172–19176.
- Pereira, R. C., Carneiro, J. d. D. S., Assis, O. B., & Borges, S. V. (2017). Mechanical and structural characterization of whey protein concentrate/montmorillonite/lycopene films. *Journal of the Science of Food and Agriculture*, 97(14), 4978–4986.
- Pérez, L. M., Piccirilli, G. N., Delorenzi, N. J., & Verdini, R. A. (2016). Effect of different combinations of glycerol and/or trehalose on physical and structural properties of whey protein concentrate-based edible films. *Food Hydrocolloids*, 56, 352–359.
- Plastics Europe. (2020). An analysis of European plastics production, demand and waste data. <https://www.plasticseurope.org/en/resources/market-data>. (Accessed 5 July 2021).
- Qazanfarzadeh, Z., & Kadivar, M. (2016). Properties of whey protein isolate nanocomposite films reinforced with nanocellulose isolated from oat husk. *International Journal of Biological Macromolecules*, 91, 1134–1140.
- Rafieian, F., Shahedi, M., Keramat, J., & Simonsen, J. (2014). Mechanical, thermal and barrier properties of nano-biocomposite based on gluten and carboxylated cellulose nanocrystals. *Industrial Crops and Products*, 53, 282–288.
- Ramos, Ó. L., Reinas, I., Silva, S. I., Fernandes, J. C., Cerqueira, M. A., Pereira, R. N., et al. (2013). Effect of whey protein purify and glycerol content upon physical properties of edible films manufactured therefrom. *Food Hydrocolloids*, 30(1), 110–122.
- Reddy, N., Jiang, Q., & Yang, Y. (2012). Preparation and properties of peanut protein films crosslinked with citric acid. *Industrial Crops and Products*, 39, 26–30.
- Rosa, D., Bardí, M., Machado, L., Dias, D., Silva, L., & Kodama, Y. (2010). Starch plasticized with glycerol from biodiesel and polypropylene blends: Mechanical and thermal properties. *Journal of Thermal Analysis and Calorimetry*, 102(1), 181–186.
- Salgado, P. R., Ortiz, S. E. M., Petruccielli, S., & Mauri, A. N. (2010). Biodegradable sunflower protein films naturally activated with antioxidant compounds. *Food Hydrocolloids*, 24(5), 525–533.
- Samaei, S. P., Ghorbani, M., Taghizadeh, D., Martini, S., Gotti, R., Themelis, T., et al. (2020). Functional, nutritional, antioxidant, sensory properties and comparative peptidomic profile of faba bean (Vicia faba, L.) seed protein hydrolysates and fortified apple juice. *Food Chemistry*, 330, Article 127120.
- Saremnezhad, S., Azizi, M., Barzegar, M., Abbasi, S., & Ahmadi, E. (2011). Properties of a new edible film made of faba bean protein isolate. *Journal of Agricultural Science and Technology A*, 13(2), 181–192.
- Shabanpour, B., Kazemi, M., Ojagh, S. M., & Pourashouri, P. (2018). Bacterial cellulose nanofibers as reinforce in edible fish myofibrillar protein nanocomposite films. *International Journal of Biological Macromolecules*, 117, 742–751.
- Silvério, H. A., Neto, W. P. F., Dantas, N. O., & Pasquini, D. (2013). Extraction and characterization of cellulose nanocrystals from corn cob for application as reinforcing agent in nanocomposites. *Industrial Crops and Products*, 44, 427–436.
- Slavutsky, A. M., & Bertuzzi, M. A. (2014). Water barrier properties of starch films reinforced with cellulose nanocrystals obtained from sugarcane bagasse. *Carbohydrate Polymers*, 110, 53–61.
- Sogut, E. (2020). Active whey protein isolate films including bergamot oil emulsion stabilized by nanocellulose. *Food Packaging and Shelf Life*, 23, Article 100430.
- Sukyai, P., Amongjaya, P., Bunyahwuthakul, N., Kongsin, K., Harnkarnsujarit, N., Sukatta, U., et al. (2018). Effect of cellulose nanocrystals from sugarcane bagasse on whey protein isolate-based films. *Food Research International*, 107, 528–535.
- Tian, H., Guo, G., Xiang, A., & Zhong, W.-H. (2018). Intermolecular interactions and microstructure of glycerol-plasticized soy protein materials at molecular and nanometer levels. *Polymer Testing*, 67, 197–204.
- Tong, X., Luo, X., & Li, Y. (2015). Development of blend films from soy meal protein and crude glycerol-based waterborne polyurethane. *Industrial Crops and Products*, 67, 11–17.
- Trifol, J., Plackett, D., Sillard, C., Szabo, P., Bras, J., & Daugaard, A. E. (2016). Hybrid poly(lactic acid)/nanocellulose/nanoclay composites with synergistically enhanced barrier properties and improved thermomechanical resistance. *Polymer International*, 65(8), 988–995.
- Vioque, J., Alaiz, M., & Girón-Calle, J. (2012). Nutritional and functional properties of Vicia faba protein isolates and related fractions. *Food Chemistry*, 132(1), 67–72.
- Wang, X., Ullah, N., Sun, X., Guo, Y., Chen, L., Li, Z., et al. (2017). Development and characterization of bacterial cellulose reinforced biocomposite films based on protein from buckwheat distiller's dried grains. *International Journal of Biological Macromolecules*, 96, 353–360.
- Xiang, A., Guo, G., & Tian, H. (2017). Fabrication and properties of acid treated carbon nanotubes reinforced soy protein nanocomposites. *Journal of Polymers and the Environment*, 25(3), 519–525.
- Xie, Y., Niu, X., Yang, J., Fan, R., Shi, J., Ullah, N., et al. (2020). Active biodegradable films based on the whole potato peel incorporated with bacterial cellulose and curcumin. *International Journal of Biological Macromolecules*, 150, 480–491.
- Xu, X., Liu, F., Jiang, L., Zhu, J., Haagenborn, D., Wiesenborn, D. P., et al. (2013). Cellulose nanocrystals vs. cellulose nanofibers: A comparative study on their microstructures and effects as polymer reinforcing agents. *ACS applied materials*, 5(8), 2999–3009.
- Yang, F., Hanna, M. A., & Sun, R. (2012). Value-added uses for crude glycerol—a byproduct of biodiesel production. *Biotechnology for Biofuels*, 5(1), 1–10.
- Ye, Z., Xiu, S., Shahbazi, A., & Zhu, S. (2012). Co-liquefaction of swine manure and crude glycerol to bio-oil: Model compound studies and reaction pathways. *Bioresource Technology*, 104, 783–787.
- Yu, Z., Sun, L., Wang, W., Zeng, W., Mustapha, A., & Lin, M. (2018). Soy protein-based films incorporated with cellulose nanocrystals and pine needle extract for active packaging. *Industrial Crops and Products*, 112, 412–419.
- Zhang, S., Xia, C., Dong, Y., Yan, Y., Li, J., Shi, S. Q., et al. (2016). Soy protein isolate-based films reinforced by surface modified cellulose nanocrystal. *Industrial Crops and Products*, 80, 207–213.

ACTA UNIVERSITATIS AGRICULTURAE SUECIAE

DOCTORAL THESIS NO. 2023:48

This thesis characterised the functionality of faba bean components (starch, protein and fibre) and their effect on structure and texture in different food matrices. First, the samples were chemically, structurally and physically characterised. Next, ingredient functionalities were analysed and the data were compared against the molecular properties. Finally, the food-model-systems were assessed to evaluate the suitability of these potential prototype products for their end-use.

Klara Nilsson received her graduate education at the Department of Molecular Sciences, SLU, Uppsala, She attained her B.Sc. degree in Nutrition and Food Science at the University of Nottingham, England and M.Sc. in Food Innovation and Health at the University of Copenhagen, Denmark.

Acta Universitatis Agriculturae Sueciae presents doctoral theses from the Swedish University of Agricultural Sciences (SLU).

SLU generates knowledge for the sustainable use of biological natural resources. Research, education, extension, as well as environmental monitoring and assessment are used to achieve this goal.

ISSN 1652-6880

ISBN (print version) 978-91-8046-148-1

ISBN (electronic version) 978-91-8046-149-8